University of Bath

UNIVERSITY OF BATH

PHD

Active sites, agglomerates or increased cohesion? Investigations into the mechanism of how lactose fines improve dry powder inhaler performance

Kinnunen, Hanne

Award date:
2012

Awarding institution:
University of Bath

[Link to publication](#)

Active sites, agglomerates or increased cohesion? Investigations into the mechanism of how lactose fines improve dry powder inhaler performance

Hanne Maarit Kinnunen
A thesis submitted for the degree of Doctor of Philosophy
University of Bath
Department of Pharmacy and Pharmacology
June 2012

TABLE OF CONTENTS

LIST OF FIGURES

emitted dose (FPF$_{ED}$) from formulations prepared with different fines and aerosolised with different devices. The data represents mean ± standard deviation, n=3.

LIST OF TABLES

fines below 4.5, 15 and 30 µm and the 10th percentile of density distribution (d10). The values shown are averages from five repeated measurements.

Table 5.3   Flow and fluidisation properties of the carrier pre-blends in terms of bulk and tapped densities, Hausner ration, Basic flow energy (BFE$_{NORM}$), dynamic flow index (DFI), flow rate indes (FRI), normalised fluidisation energy (FE$_{NORM}$) and specific energy (SE). The values shown are averages from three repeated measurements

Table 5.4   Summary of *in vitro* performance of the formulations prepared with the lactose pre-blends as the carrier in terms of fine particle fraction of emitted dose (FPF$_{ED}$), mean mass aerodynamic diameter (MMAD) and the proportion of total recovered budesonide that was deposited in the pre-separator (PS of RD). The results shown are averages from three repeated *in vitro* assessments.

Table 5.5   Coefficient of correlation for linear relationships between the different DPI performance measures and the properties of the lactose pre-blends used as the carriers in the formulations. The correlations are based on the average values reported in tables 5.2, 5.3 and 5.4.

Table 5.6   The standardised coefficients for the different physical parameters describing the lactose carriers in the partial least squares model defining DPI performance. The parameters describing how well the data is fitted within the model are also tabulated (x-variance and R^2). The correlations were established using the average values reported in tables 5.2, 5.3 and 5.4.

Table 5.7   The connection weights for the different inputs parameters in the neural networks describing DPI performance. The networks were based on the average values reported in tables 5.2, 5.3 and 5.4.

Table 6.1   Proportion of fine particles in the carrier blend as measured by laser diffraction and the *in vitro* performance of the formulations in terms of fine particle fraction of emitted dose (FPF$_{ED}$) and the mean mass aerodynamic diameter (MMAD) of the drug aerosolised from the formulations. The data for % < 4.5 µm represents an average of five repeated measurements. The data for FPFED and MMAD represents mean ± standard deviation, n=3.

ACKNOWLEDGEMENTS

ABSTRACT

Dry powder inhalers (DPIs) are used for delivering drugs to the airways. In addition to the drug, the formulations often contain a coarse carrier, most commonly alpha lactose monohydrate. The presence of fine lactose particles in the formulation is known to improve the formulation performance. The active site, drug-fines agglomeration and increased cohesion theories have been suggested to explain improved DPI performance upon addition of fine excipient particles. This project aimed to investigate the validity of those theories.

The viability of the active sites theory in explaining the improved DPI performance was investigated by studying the impact of loaded drug dose on the *in vitro* performance for formulation series prepared with coarse carriers with different surface characteristics. The formulations prepared with the rougher lactose carrier were seen to outperform the formulations prepared with the smoother carrier at all drug concentrations. These findings were concluded to be non-compatible with the active sites theory.

The impact of addition of lactose fines with different size distributions on powder flow and fluidisation properties and *in vitro* performance was studied. Powder cohesion increased independent of size distribution of the fines, but did not necessarily correspond to improved performance. Therefore, the increased cohesion theory was concluded not to be the sole explanation for the improvement in DPI performance in the presence of lactose fines. Instead, the increase in performance could be preliminarily attributed to the formation of agglomerated systems. The formation and co-deposition of drug-fines agglomerates, and consequential improvement in the DPI performance was proved using morphologically directed Raman spectroscopy.

The project also aimed to develop a universal model for predicting DPI performance based on the lactose properties for a wide range of carriers with different properties. No simple linear correlations between any the lactose properties and the final DPI performance were found. Therefore no single parameter can be used as a universal predictor for DPI performance. To establish more complex relationships, artificial neural networks were used for modelling the importance of different lactose properties in determining DPI performance. The proportion of fine lactose particles (<4.5 µm) was identified as the most important parameter. However, this parameter was capable of explaining only approximately half of the variation seen in the formulation performance. The current study showed that to obtain more accurate predictions for the purposes of quality-by-design approach, also other lactose properties need to be characterised.

24

LIST OF ABBREVIATIONS AND SYMBOLS

A	Hamaker constant
A_m	Affinity of an analyte to the mobile phase
A_s	Affinity of an analyte to the stationary phase
a	Separation distance between bodies
ACU	Aeration control unit of FT4
ANN	Artificial neural network
ANOVA	Analysis of variance
API	Active pharmaceutical ingredient
BFE_{Norm}	Normalised basic flow energy
BSA	Bovine serum albumin
CAB	Cohesive-adhesive balance
CCD	Charge coupled device
CE	Circular equivalent
CI	Carr's index
C_{Drag}	Drag coefficient
CFCs	Chlorofluorocarbons
COPD	Chronic obstructive pulmonary disease
d	Particle diameter
dn	Particle size below which n % of the particles are (n=10, 50 or 90)
d_{50}	Mean particle size
D	Distribution coefficient in chromatography
d'	Airway diameter
d''	Diameter of a tube
Dif	Diffusion constant
DFI	Dynamic flow index
DPI	Dry powder inhaler
E_{Kin}	Kinetic energy of an agglomerate formed upon fluidisation
F	Downward force
F_c	Capillary force
F_{Drag}	Drag force
F_{vdW}	Van der Waals force
f(Σ)	Threshold function
FDA	United States Food and drug administration
ff_c	Flow function
FE_{Norm}	Normalised fluidisation energy
FPF_{ED}	Fine particle fraction of emitted dose

FPF$_{RD}$	Fine particle fraction of recovered dose
FPM	Fine particle mass
FRI	Flow rate index
g	Acceleration due to gravity (9.81 m/s^2)
GSD	Geometric standard deviation
h	Height of a powder bed
H/D	Height to diameter ratio of a powder bed
HFAs	Hydrofluoroalkanes
HPLC	High performance liquid chromatography
HPMC	Hydroxypropylmethylcellulose
HR	Hausner ratio
HRLD	High resolution laser diffraction
HS	High sensitivity
I_0	Intensity of light
I_s	Intensity of scattered light
ISM	Impactor stage mass
k	Boltzmann constant (1.3806503 × 10^{-23} J/K)
LH	Lactohale$^®$
m	Mass of a particle or a powder bed
MHz	Megahertz
MLR	Multiple linear regression
MMAD	Mean mass aerodynamic diameter
n	Number of nozzles
NGI	Next generation impactor
ODS	Octadecyl siloxane
PAT	Process analytical technologies
PLS	Partial least squares
pMDI	Pressurised metered dose inhaler
PS of RD	Proportion of the total recovered drug deposited in the pre-separator
Q	Air flow rate
QbD	Quality by design
R	Radius of the airway
R_e	Reynold's number
R_s	Radius of a sphere
R^2	Regression coefficent
S	Distance between a nozzle orifice and the impaction surface
SE	Specific energy
SEM	Scanning electron microscopy
Stk	Stokes' number

T	Absolute temperature
u	Velocity of fluid
U_{mf}	Minimum fluidisation velocity
USP	United States Pharmacopoeia
UV	Ultraviolet
V	Air velocity
V_0	Air velocity through a nozzle
VMD	Volume mean diameter
V_{ts}	Terminal settling velocity of a particle
v/v-%	Volume percentage
W	Diameter of a nozzle
w	Connection weight
WHO	World Health Organisation
wt-%	Weight-to-weight percent
α	Shear plane angle (Schulze), helical angle of the blade movement (FT4)
γ	Surface tension of liquid
η	Viscosity of air, or learning rate for
θ	Angle of scattered light
μ	Viscosity of fluid, or momentum for artificial neural networks
ρ	Density of fluid
ρ_a	Density of air
ρ_{Agg}	Density of an agglomerate
ρ_B	Bulk density of a powder
ρ_p	Density of a particle
ρ_T	Tapped density of a powder
Σ	Activation function
σ	Tensile strength
σ_1	Vertical consolidation stress obtained from the yield locus measurement
σ_α	Consolidation stress for a shear plane defined by shear plane angle α
σ_c	Unconfined yield strength
σ_h	Horizontal consolidation stress
σ_{Pre}	Pre-shear consolidation stress
σ_{Shear}	Consolidation stress for measuring a point on the yield locus
σ_v	Vertical consolidation stress
τ	Shear stress (Schulze), Torque (FT4)
τ_{Pre}	Shear stress at steady state flow
Φ_{Agg}	Diameter of an agglomerate

CHAPTER 1 INTRODUCTION

OVERVIEW

Dry powder inhaler (DPI) formulations are used for delivering drugs to the lungs for the treatment of respiratory diseases. This thesis concentrates on understanding how the properties of lactose used as an excipient in carrier based DPI formulations govern the performance of the final product. The introduction can be roughly divided into three parts. During the first part, to appreciate the requirements of successful pulmonary drug delivery, the anatomy of the respiratory tract, the pharmacokinetic properties of the lung as a port of entry for the drug, the target diseases for respiratory drug delivery, the mechanisms of particle deposition in the lungs and the dosage forms currently available for delivering drugs to the lungs are introduced. To understand the physical phenomena governing dry powder inhaler formulation performance, the second part of the introduction covers the general properties of powders, interparticulate interactions, powder fluidisation and deagglomeration. The last part of the introduction is more specific to dry powder inhaler formulations. The available formulation strategies will be discussed. This is followed by an introduction to lactose and a review of literature on the relationship between lactose properties and the final formulation performance.

1.1 DRUG DELIVERY TO THE LUNGS

1.1.1 Anatomy of the respiratory tract

The human upper airways consist of oral and nasal cavities, pharynx and larynx (Stevens *et al.* 1995). With regards to the delivery of orally inhaled drug products, the anatomy of the upper airways is dominated by a major change of direction in the pharynx, where the oral and nasal cavities are joined together.

The structure of the lower airways is often referred to as the tracheobronchial tree (Newell 2003). This is because the airways form a tree like structure with each of the parent airways splitting into two daughter airways for an average of 23 generations (Weibel *et al.* 2005). A 3D visualisation of the tracheobronchial tree based on high resolution computerised tomography is shown in Figure 1.1 (Schmidt *et al.* 2004). The uppermost part of the lower airways is the trachea, analogous to the trunk of the tree. The next few generations are the bronchi and the deepest airways are the bronchioles. Bronchi and

bronchioles form the branches of the tree. The last seven generations of the airways are covered by alveoli, which are responsible for the large surface area of the lungs. The peripheral regions of the airways, covered by the alveoli, form the respiratory zone of the lung where the gas exchange takes place (Patton *et al.* 2007). Within the respiratory zone, the air flow is governed by diffusion. The airways above the respiratory airways are the conducting airways. The air flow in the conductive airways is convective (Weibel *et al.* 2005).

An important feature of the respiratory tract with regards to pulmonary drug delivery is that the more peripheral the airway within the tracheobronchial tree, the smaller the diameter. Trachea has a diameter of approximately 18 mm, the primary bronchi 12 mm and the first generation of bronchioles approximately 4 mm. The diameter of the airways connected to the alveoli is approximately 0.5 mm or less (Tsuda *et al.* 2008). The decrease in the airway diameter as the airways reach the peripheral lung regions is also visible in Figure 1.1.
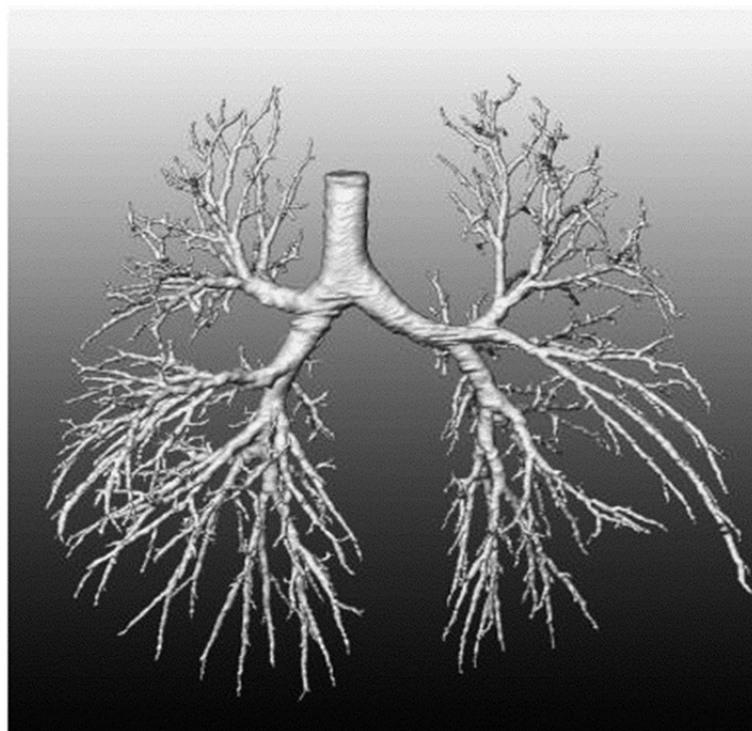
FIGURE 1.1 3D VISUALISATION OF THE TRACHEOBRONCHIAL TREE OBTAINED FROM HIGH RESOLUTION COMPUTERISED TOMOGRAPHY MEASUREMENTS. REPRINTED FROM COMPUTERIZED MEDICAL IMAGING AND GRAPHICS, 28, SCHMIDT, A. *et al.*, A DIGITAL REFERENCE MODEL OF THE HUMAN BRONCHIAL TREE, 203-211, COPYRIGHT (2004), WITH PERMISSION FROM ELSEVIER

1.1.2 Pharmacokinetics of respiratory drug delivery

The lungs are an appealing route for topical, and increasingly also for systemic, drug delivery. There are various reasons for this, all deriving from the favourable pharmacokinetics of pulmonary drug delivery. The large surface area of the lungs means that the drug delivered as an aerosol via the pulmonary route is dispersed sparsely on the epithelial surfaces available. This may result in rapid dissolution and absorption of the drug. The rapid absorption of the drug via the pulmonary route makes the lung an excellent route for administering drugs for symptoms where a quick onset of action is required, such as asthma exacerbations (Patton *et al.* 2004).

Additionally, the first pass metabolic effect is avoided when the drugs are delivered via the pulmonary route, resulting in good bioavailability (Patton *et al.* 2004). Lungs also have very low enzymatic activity (Patton *et al.* 2007). Therefore, molecules that might be digested in the gastrointestinal tract before absorption can often successfully be delivered via the pulmonary route. Systemic side effects can also often be avoided when drugs are delivered via the lungs (Lipworth 1996).

1.1.3 Traditional target diseases for respiratory drug delivery and inhaled drug therapies available for managing the diseases

1.1.3.1 Asthma

Asthma is a chronic disease affecting the airways. The patients often have a genetic tendency towards asthma. However, exposure to environmental factors, such as allergens and air pollutants, is also known to significantly contribute to the development of the disease by inducing irritation of the airways (Welte *et al.* 2006). According to the World Health Organization (WHO), approximately 235 million people worldwide suffer from the disease (WHO 2012). The symptoms of asthma include coughing, wheezing, tightness of the chest and shortness of breath. These symptoms are caused by two main mechanisms, bronchoconstriction and inflammation (Welte *et al.* 2006). In an asthmatic lung, bronchoconstriction and inflammation are expressed both in the conducting and peripheral airways (Hyde *et al.* 2009).

Asthma can be controlled by a combination of long term control and quick-relief inhaled medication (Fanta 2009). The purpose of the long term control medication is mainly to reduce inflammation. The drugs used for this purpose are corticosteroids. However, the long term control of asthma can also include long term bronchodilation using long acting

β$_2$-agonists (Fanta 2009). Quick relief medication on the other hand aims to relieve exacerbations caused by acute bronchoconstriction. Short acting β$_2$-agonists are the most effective drugs for this purpose (Fanta 2009).

1.1.3.2   *Chronic obstructive pulmonary disease*

Chronic obstructive pulmonary disease (COPD) is an irreversible condition where the airways are progressively obstructed. The airway obstruction in COPD is caused by inflammation, structural changes within the airways and mucociliary dysfunction (Agusti 2005). The airway obstruction results in a gradual decrease in lung function and worsening of the symptoms over time (William 2003). COPD mainly affects the small airways (Cazzola *et al.* 2007). The disease is aggravated by air pollutant particles, the greatest cause for the disease being cigarette smoke (William 2003). It has been estimated that by year 2020 COPD will be the third most common cause of death in the world (Welte *et al.* 2006).

At present, the only effective treatment for COPD is smoking cessation. However, the symptoms, which include chronic cough and abnormal sputum excretion, can be relieved by medication. The inhaled drugs used for relieving symptoms of COPD include bronchodilators for relieving the airway obstruction and corticosteroids for controlling inflammation (Hanania *et al.* 2005). The combination of long acting β$_2$-agonist and inhaled corticosteroids has been shown to be beneficial for regulating the mucus hypersecretion (Hanania *et al.* 2005).

1.1.4 Mechanisms of particle deposition in the lungs

1.1.4.1   *Inertial impaction*

Inertial impaction is the most important mechanism in determining the drug deposition in the lungs (Zeng *et al.* 2001a). Inertial impaction of the drug particles takes place when the momentum of the particles carried in the inspiratory air flow is too large to negotiate a change of direction in the airflow, for example when the respiratory tract branches to the next generation. As a consequence, the particles with too high a momentum will deposit in the respiratory tract by inertial impaction (Zeng *et al.* 2001a). Stokes' number, *Stk*, is a dimensionless parameter and describes the likelihood of particle deposition in the respiratory tract by impaction according to Equation 1.1, where ρ_p is particle density, *d* is

the particle diameter, V is air velocity, η is the viscosity of air and R is the radius of the airway.

$$Stk = \frac{\rho_p d^2 V}{18\eta R}$$

The larger the Stokes' number for a particle, the more likely it is it will be deposited by inertial impaction (Zeng *et al.* 2001a). According to Equation 1.1, the particle deposition in the deeper regions of the lungs by inertial impaction can be improved by decreasing the particle size, density or air flow rate.

1.1.4.2   Sedimentation

Sedimentation of the particles in the airways is a time dependent process and maximising the drug deposition in the smaller airways and alveolar region by sedimentation is the reason patients are commonly instructed to hold breath after inhalation (Zeng *et al.* 2001a). During sedimentation, particles settle in the airways under the influence of gravity as determined by their terminal settling velocity, V_{ts}, as defined by the Stokes' law (Zeng *et al.* 2001a). V_{ts} of a particle is defined by Equation 1.2, where ρ_p is the density of a particle, ρ_a is the density of air ($\rho_p > \rho_a$), d is the particle diameter, g is the acceleration due to gravity and η is the viscosity of air.

$$V_{ts} = \frac{(\rho_p - \rho_a)d^2 g}{18\eta}$$

Particles smaller than 10 µm sediment easier than predicted by the Stokes' law (Zeng *et al.* 2001a). This is because slipping of the particles between each other may take place. Therefore, the Cunningham slip factor is applied for particles smaller than 10 µm (Zeng *et al.* 2001a). Stokes' law is also valid only when the air flow is laminar (Zeng *et al.* 2001a). Reynold's number, R_e determines whether air flow is laminar ($R_e < 2000$) or turbulent ($R_e > 4000$) according to Equation 1.3, where ρ_a is the density of air, V is the air velocity, d' is the diameter of the airway and η is the viscosity of air.

$$R_e = \frac{\rho_a V d'}{\eta}$$

Turbulent airflow is characterised by fluctuations in the direction of the air flow. Consequentially, if the air flow in the respiratory tract is turbulent, inertial impaction becomes the prevalent mechanism of particle deposition instead of sedimentation (Zeng *et al.* 2001a).

1.1.4.3 Diffusion

Deposition of particles smaller than 1 µm in the airways takes place by diffusion. This form of deposition is a result of random movement of the particles, the Brownian motion. Brownian motion is caused by bombardment of the particles by surrounding gas molecules (Brown 1828). The phenomena is related to the size of the particles according to the diffusion constant, *Dif*, determined by Stokes-Einstein equation (Equation 1.4), where *k* is the Boltzmann constant, *T* is the absolute temperature, *η* is the viscosity of air and *d* is the diameter of the particle.

$$Dif = \frac{kT}{3\pi\eta d}$$

EQUATION 1.4

Brownian motion is inversely proportional to the particle size. Therefore, the smaller the particle size, the more likely the particles are to behave in a similar way to gas molecules, and will be exhaled before deposition (Ariyananda *et al.* 1996). To avoid exhalation of the drug particles, the particle size for inhalable drugs is generally recommended to be larger than 1 µm.

1.1.4.4 Interception

Particle deposition by interception takes place in the airways when the particle shape differs from a perfect sphere (Zeng *et al.* 2001a). The centre of gravity of an irregularly shaped particle may be within the streamlines of the air flow. However, owing to the irregular shape, the distal end of a non-spherical particle may be touching the walls of the airways earlier than determined by the impaction, sedimentation or diffusion for a spherical particle, thus resulting in particle deposition in a different region in the airways (Cai *et al.* 1988). In practice, for inhalation formulations, interception is not an important mechanism because the particle diameter is generally much smaller than the diameter of the airways. However, if the formulation contained elongated drug particles, the mechanism would become more important in determining the regional drug deposition in the lungs (Zeng *et al.* 2001a).

1.1.4.5   Electrostatic precipitation

Upon inhalation, drug particles may develop a charge that is unlikely to dissipate between the inhalation event and the drug deposition in the respiratory tract (Zeng *et al.* 2001a). Two different mechanisms for particle deposition by electrostatic precipitation exist (Heyder 2004). The charged particles from the inhalation bolus can create an image charge on the grounded surface of the respiratory tract that attracts the particles. A less important mechanism is repulsion between particles with a charge of the same sign that results in particle deposition in the respiratory tract (Heyder 2004).

1.1.5   Dosage forms for respiratory drug delivery

1.1.5.1   Pressurised metered dose inhalers

Worldwide, pressurised metered dose inhalers (pMDIs) are the most prescribed drug delivery systems for asthma and COPD (Dolovich *et al.* 2011). In a pMDI formulation the drug particles within the respirable range are suspended or solubilised in a propellant with the aid of a surfactant. The suspension/solution formulation is contained within a canister that holds multiple doses of the drug. The dose of the drug delivered by a single actuation is controlled by a metering valve. Upon actuation, the dose metered in the holding chamber is released and a jet of droplets containing the propellant and the drug is formed. The propellant then evaporates leaving behind drug particles or droplets within the respirable range (Ariyananda *et al.* 1996). Traditionally the propellants used in the pMDI products were chlorofluorocarbons (CFCs). However, due to environmental concerns related to ozone depletion, the use of CFCs was banned in the Montreal protocol set out in 1987 (McDonald *et al.* 2000). The propellants that have replaced CFCs in the pMDIs are hydrofluoroalkanes (HFAs).

The advantages of pMDIs over other pulmonary drug delivery platforms are related to the formulation stability, device portability and cost effectiveness (Keller 1999). The main drawback of pMDIs is the requirement for co-ordination between the actuation of the dose and inspiration. Correct timing of the actuation and inhalation is essential to ensure that the high velocity aerosol jet exiting the device will be entrained in the inhaled air flow rather than impacted in the pharynx. However, drug deposition at the back of the throat due to the lack of co-ordination between the actuation and the inhalation can be reduced by using add-on devices, such as spacers or holding chambers (Keller 1999).

1.1.5.2   Nebulisers

With nebulisers, respirable droplets of the drug are produced from solution or suspension formulations. Traditionally, two different technologies for forming the droplets from the liquid have been available, namely jet nebulisers and ultrasonic nebulisers (Dalby *et al.* 2003). With jet nebulisers, a pressure differential between the liquid reservoir and the orifice of the liquid feed tube is created by using compressed gas. The pressure differential results in the liquid from the reservoir being drawn up the feed tube following Bernoulli's principle. The liquid is then broken in to a fine mist of droplets at the outlet of the feed tube (Labiris *et al.* 2003). With ultrasonic nebulisers, the droplets are generated by a piezoelectric crystal that is vibrating at a high frequency (1-3 MHz). As a result, a standing wave is formed on the surface of the liquid reservoir. A fountain of droplets is formed at the crest of the standing wave by cavitation and capillary wave formation (Dalby *et al.* 2003). The higher the frequency of the piezoelectric crystal, the smaller the resulting droplet size (Labiris *et al.* 2003).

Due to the large size of the compressors and the nebulising masks, the use of nebulisers has mainly been restricted to hospital and ambulatory settings. The proportion of drug deposited from the nebulisers has also traditionally been low because of the lack of control over the aerosol formation relative to the patient's breathing patterns. This has resulted not only in a large proportion of the drug being wasted but also in relatively long inhalation times for gaining the therapeutic dose, a factor that has also restricted the use of nebulisers in chronic disease management. However, the most recent developments in nebuliser technology in the form of multidose liquid inhalers and vibrating mesh nebulisers have resulted in more portable devices, shorter inhalation times and more efficient drug delivery (Dolovich *et al.* 2011).

1.1.5.3   Dry powder inhalers

Unlike pMDIs and nebulisers, DPI formulations do not contain a liquid phase. The drug is delivered to the patient's lungs from a static powder bed instead. The current section will concentrate on the different devices available for delivering the dose from dry powder inhalers and the general mechanisms involved in delivering the dose to the patient's lungs. The formulation aspects are central to the thesis and therefore will be discussed in more detail later on in the introduction.

The first commercial DPI product, Aerohalor, was introduced in 1948 for the pulmonary delivery of penicillin (Sanders 2007). Since then, a variety of different device types has

been developed. Nowadays, the devices on the market can be classified according to the number of doses held within the device (single dose vs. multidose), the storage mechanism of the formulation in the device (capsule vs. blister vs. reservoir) and the fluidisation mechanism (active vs. passive). These forms of devices will be briefly introduced in the following.

A DPI device can either hold a single or multiple doses of the drug (Smith *et al.* 2003). With single dose devices, the patient loads a capsule containing the dose into the device and primes the capsule before every inhalation. With multiple dose devices, the doses of drug are either held in a reservoir where the drug dose is metered upon priming the device, or in a blister strip where a single dose of the drug is exposed upon priming the device (Smith *et al.* 2003). The drug delivery mechanism of the device can be either passive or active. In traditional, passive DPI devices the drug delivery to the lungs relies on the patient's inspiratory effort for delivering the dose of the drug from a static powder bed. In active DPIs, mechanical aids such as piezoelectric crystals or compressed air are used for delivering the dose of drug (Tobyn *et al.* 2004).

With all these devices, three steps are required to achieve successful drug delivery to the lungs from the formulation contained within the device. Firstly, the powder containing the dose of the drug has to be fluidised. Secondly, the particles have to be deagglomerated to achieve drug particles within the respirable size range. Thirdly, the particles within the respirable range have to be entrained in the inspiratory airflow to be deposited in the site of action in the lungs (Telko *et al.* 2005). The significance of fluidisation of the dose in the drug delivery from DPIs is a relatively newly realised concept and was first mentioned as a requirement for successful drug delivery from DPIs by Telko *et al.* (2005). The importance of deagglomeration and entrainment has been recognised in the literature for longer (Ganderton 1997).

The process of fluidising a static powder bed followed by simultaneous entrainment and deagglomeration of the formulation is illustrated in Figure 1.2. Deagglomeration and entrainment are presented as simultaneous processes in the schematic. This is because the proportion of the respirable fraction of drug from DPI formulations is often relatively low, between 20 and 30% of the loaded dose (Steckel *et al.* 1997). It is therefore reasonable to assume that some of the formulation will be entrained before deagglomeration and thus never reach the respirable particle size range. However, it is also known that powder deagglomeration takes place due to particle-particle and particle-device impactions and turbulences in the inspiratory flow (Voss *et al.* 2002). Therefore, due to turbulences in the inspiratory air flow, some deagglomeration may also take place after the formulation has been entrained.
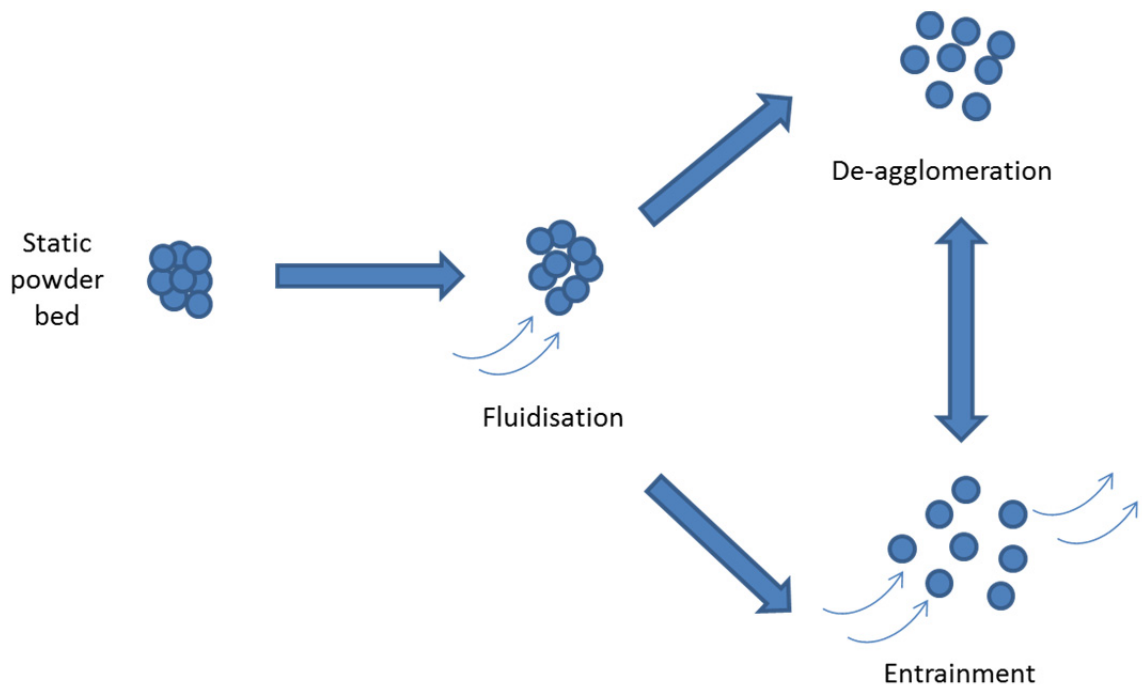
FIGURE 1.2 A SCHEMATIC SHOWING THE PROCESSES INVOLVED WITH DELIVERING THE DRUG FROM A STATIC POWDER BED CONTAINED IN A DPI PRODUCT. THE POWDER BED IS FLUIDISED AND THE DRUG IS THEN SIMULTANEOUSLY DEAGGLOMERATED AND ENTRAINED

The main advantage of DPIs compared to the pMDIs is that the delivery of the dose is breath actuated. Therefore, the issue of co-ordinating the inhalation with the actuation of the dose is avoided. However, the extent of drug delivery also relies on the inspiratory effort. Therefore, the delivered dose may be compromised, especially with patients with severe constriction in pulmonary capacity. In addition, the production of DPIs is relatively expensive compared to the production of pMDIs (Ariyananda *et al.* 1996).

1.2   CHARACTERISTICS OF POWDERS

1.2.1   The fourth phase of matter?

Powders are granular materials consisting of solid particles of different sizes. In a dry powder, interstitial gas fills the voids between the particles (Rietema 1984). Powders exhibit properties of all the other three phases and under certain circumstances they can be compressed like gases, poured like liquids or deformed both plastically or elastically like solids (Rietema 1984). However, unlike gases, liquids and solids, powders are temperature independent (Heinrich *et al.* 1996). This is because the potential energy for a particle with a mass of m and diameter of d, is of the order of mgd, where g is the acceleration due to gravity. For a typical grain of sand, this value will be 10^{12} higher than

the thermal constant kT, where k is Avogadro's constant and T the absolute temperature (Heinrich *et al.* 1996). The driving force of gravitation over the thermal effects explains, for example, how cereal segregates in a container as a result of the vibrations induced by transport despite the lower entropy of the system in the segregated state (Heinrich *et al.* 1996).

Powders also have a memory of past process history. The memory effect affects the properties of powders down the line (Valverde *et al.* 2003). For example, after segregation, the powder does not spontaneously return to its initial state after the factor that caused the segregation has been eliminated.

Cohesion is a property of bulk powders that is defined as the powder's resistance to flow (Geldart *et al.* 2007). Cohesion of a powder is determined by the magnitude of the interparticulate forces within the powder bulk. The major interparticulate forces contributing to the general powder flow and handling properties are introduced in the following.

1.2.2 Particle-particle interactions in powders

1.2.2.1   *Van der Waals interactions*

Van der Waals interactions are named after a Dutch physicist who discovered that the attractive forces between molecules were responsible for the deviation of the behaviour of real gases from the ideal gas law. These interactions are a consequence of the attraction between molecules due to momentary changes in their electron densities exhibited even by molecules that do not carry a charge. In general, van der Waals interactions can be classified as dipole/dipole, dipole/non-polar and non-polar/non-polar interactions (Valderrama 2010). The van der Waals force, F_{vdW}, between two identical spheres of radius R_s is defined by Equation 1.5, where A is the Hamaker constant and a is the separation distance between the bodies (Seville *et al.* 2000).

$$F_{vdW} = \frac{AR_s}{12a^2}$$

EQUATION 1.5

The contact between two spherical particles is illustrated in Figure 1.3A. Generally, the separation distance between particles becomes smaller as the particle size is diminished. In addition, the gravitational force becomes negligible compared to the van der Waals

interaction as particle size decreases (Visser 1989). As a result, van der Waals forces are very significant in fine powders.

In reality, particles are seldom perfect spheres but exhibit surface roughness or irregular shapes instead. The van der Waals interactions will be significantly altered as a result of the changes in the surface morphology and contact geometry of the particles (Visser 1989). Figure 1.3B illustrates a case of reduced van der Waals interaction due to decreased contact area derived from small scale surface roughness. Figure 1.3C and Figure 1.3D on the other hand illustrate cases of increased van der Waals interactions originating from increased contact area due to large scale surface roughness and non-spherical contact geometry, respectively.
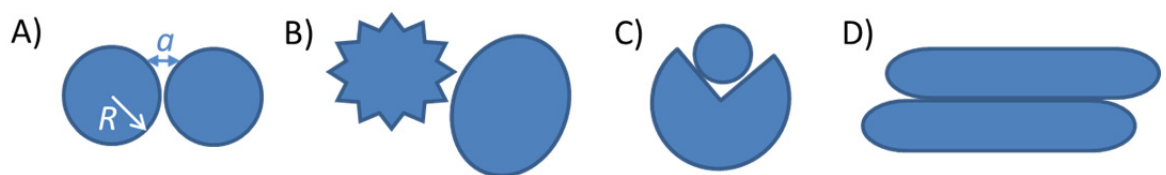
FIGURE 1.3 SCHEMATICS OF VAN DER WAALS INTERACTION BETWEEN A) TWO IDEAL SPHERES WITH RADIUS OF *R* AND SEPARATION DISTANCE OF *a*, B) REDUCED VAN DER WAALS INTERACTION DUE TO DECREASED CONTACT AREA AND C) AND D) INCREASED VAN DER WAALS INTERACTION DUE TO INCREASED CONTACT AREA

1.2.2.2   Electrostatic interactions

In dry, gaseous environments particles of insulating material can accumulate electric charge due to contact charging, also known as triboelectrification (Bailey 1984). The process of triboelectrification includes charge transfer between insulating bodies carrying different potential to compensate for the potential difference. If the bodies are then separated before the charge can flow back, the bodies will remain charged (Karner *et al.* 2011). Electrostatic charging of powders is often associated with pharmaceutical blending and powder transport during manufacturing, but also, importantly, with powder discharge from a dry powder inhaler device. This is due to the collisions between particles and different surfaces taking place during these processes, resulting in triboelectrification (Karner *et al.* 2011). The potential difference, and thus the magnitude of triboelectric charging, between two bodies is affected by the positions of the materials within the triboelectric series, which is a ranking of different materials according to their charge transfer properties (Shaw 1917). However, also surface roughness, particle size, mechanics of particle movement, mixing ratio of different components within the powder, speed of mixing, relative humidity, amorphous content of the materials and charge

dissipation properties of the materials, all of which are relevant variables for dry powder inhaler formulations, influence the magnitude of electrostatic charging (Karner *et al.* 2011). Charge accumulation influences the cohesion of powders because opposite charges will attract each other, thus increasing the strength of the interparticulate contacts (Visser 1989).

1.2.2.3 Capillary interactions

Capillary interactions arise from condensation of liquid in the void spaces between the particles within a bulk powder (Seville *et al.* 2000). These interactions become significant at relative humidity of higher than 65% (Visser 1989). The maximum capillary force, F_c, between two spheres of radius R_s, both completely wetted by liquid with a surface tension of γ is defined by Equation 1.6.

$$\boldsymbol{F_c = 2\pi R \gamma}$$

<div align="right">**EQUATION 1.6**</div>

A schematic of a liquid bridge formed as a result of capillary condensation is presented in Figure 1.4. Capillary interactions have practical applications for example in granulation processes. This is because the magnitude of the capillary forces, and thus the strength of the granules, can be engineered by changing the amount, viscosity and surface tension of the liquid (Seville *et al.* 2000).
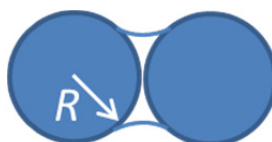
FIGURE 1.4 SCHEMATIC OF A LIQUID BRIDGE FORMED AS A RESULT OF CAPILLARY CONDENSATION WITHIN THE VOID SPACE BETWEEN TWO SPHERICAL PARTICLES OF RADIUS R

1.2.3 Powder fluidisation

1.2.3.1 Definition

Fluidisation is a phenomenon where particles within a powder bed are made free of internal friction by a counter force. As a result, the powder bed will enter a fluid-like regime (Horio 2010). In this regime the powder behaves like a fluid. Therefore, for example, less dense objects would float on the surface of a fluidised powder bed, the surface of the bed would stay horizontal even if the container was tilted and the particles would pour out of a

hole in the side of the vessel (Holdich 2002). In the fully fluidised state, bubbling on the surface of the powder bed is often observed.

1.2.3.2   Fluidising a single particle

A static particle of mass *m* experiences a downward force *F* due to the earth's gravitation. The force experienced by a particle can be written as per Equation 1.7, where *g* is the acceleration due to gravity.

$$F = mg$$

<div align="right">EQUATION 1.7</div>

If a fluid or gas flow is passed through the powder, the drag forces, F_{Drag}, exerted by the fluid flow may exceed the weight of the particle. The excess of the upward component in the force balance means that the particle will become fully supported by the fluid flow, i.e. fluidised (Holdich 2002). This situation is illustrated in Figure 1.5. The statistical mechanics of a single fluidised particle are well understood and it is known that a single spherical fluidised particle undergoes Brownian motion whilst suspended in the gas flow (Ojha *et al.* 2004).
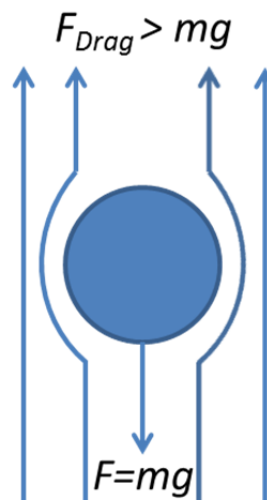
FIGURE **1.5 A** SCHEMATIC OF A SINGLE, SPHERICAL PARTICLE OF MASS *m* SUSPENDED IN AIR FLOW DUE TO A DRAG FORCE (F_{Drag}) THAT IS LARGER THAN THE GRAVITATIONAL FORCE (*F*) EXPERIENCED BY THE PARTICLE. **g** IS THE ACCELERATION DUE TO GRAVITY

1.2.3.3   Fluidising bulk powders

In a free flowing bulk powder system where interparticulate forces are negligible, the drag force created by the flow of the fluidising gas has to overcome the gravitational downward

force experienced by the powder bed to initiate fluidisation (Holdich 2002). Therefore, the force balance for a single spherical particle presented in Figure 1.5 is also valid for a cohesionless powder bed of mass of *m*. However, powders often exhibit interparticulate contact forces. Therefore, for a cohesive powder, the strength of the interparticulate contacts within the powder bulk has to be taken into account in the force balance for fluidisation. In the presence of interparticulate contact forces, the downward force component can be written as per Equation 1.8, where σ is the strength of the interparticulate contacts within the bulk powder, also known as the tensile strength.

$$F = mg + \sigma$$ **EQUATION 1.8**

It follows from Equation 1.8 that when a cohesive powder is being fluidised, the drag force exerted by the fluidising gas has to be greater than the gravitational and cohesive forces within the powder bed before fluidisation takes place.

1.2.3.4   Classifying powders according to their fluidisation properties

Geldart (1973) introduced a classification system for powders according to their fluidisation properties. The Geldart classification system is based on the particle size of the material to be fluidised and the density difference between the fluidising gas and the powder. Fluidised bed technology is a significant industrial application. The uses of the process range from catalytic conversion reactions to the food and agricultural industries (Horio 2010). To cater for all the different industrial applications of fluidised bed technology, Geldart's classification covers particle sizes between 10 µm and 10 mm.

The Geldart's classification chart is presented in Figure 1.6. Powders consisting of fine particles belong to group C, which is a group for cohesive, difficult to fluidise powders. When these powders are fluidised, the fluidising gas cannot be evenly distributed throughout the powder bed. This is because the interparticulate forces within the powder are of much greater magnitude than the drag forces exerted by the fluidising gas (Molerus 1982). Therefore, group C powders often exhibit channelling upon fluidisation or lift as a plug in a small diameter fluidisation vessel. Consequentially, group C powders have sometimes been allocated as being outside the applicability of fluidisation-based technologies (Molerus 1982). The classification chart shown in Figure 1.6 indicates that, independent of the density difference between the particles and the fluidising gas, powders consisting of particles finer than 20 µm always fall in this category. However, if

the density difference between the particles and the fluidising gas becomes smaller, also larger particles will exhibit poor fluidisation behaviour.

Aeratable powders on the other hand belong to group A. Powders in this group are easily fluidised. Upon fluidisation, powders belonging to this group demonstrate bed expansion before entering the bubbling regime. In addition, if the fluidising gas supply is suddenly cut off, the bed collapse is slow (Geldart 1973). According to the original classification by Geldart (1973), the boundary between groups C and A is not definitive. However, a few years later Molerus (1982) was able to explain the border between groups A and C by the force balance between the drag forces caused by the fluidising gas and the interparticulate forces within the powder bed.

Group B powders exhibit bubbling behaviour upon fluidisation. In contrast to group A powders, the bed collapses rapidly when the fluidising gas supply is cut off. According to Molerus (1982), group B powders are separated from group A powders because the magnitude of the interparticulate contacts in group B is negligible compared to the drag caused by the fluidising gas. Group D powders, in turn, form spouting beds (Geldart 1973). The particles belonging to this group have a large particle size and possibly also a high density. The spouting behaviour of group D particles has been explained by the dominance of inertial forces acting on the fluidised particles over the drag forces induced by the fluidising gas (Molerus 1982).
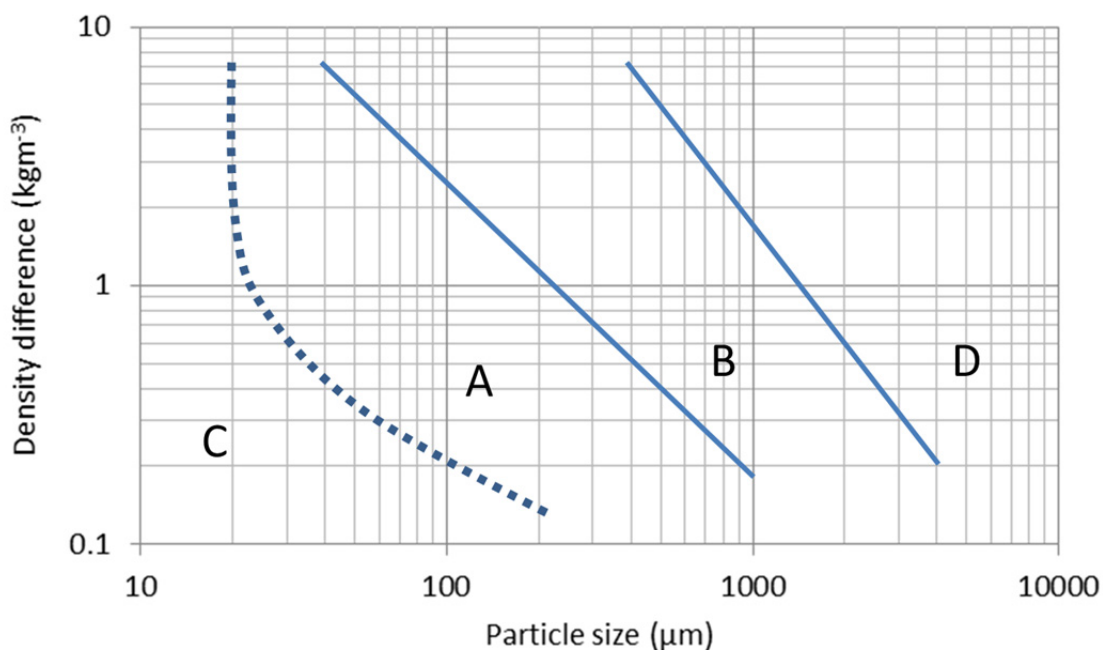
FIGURE 1.6 GELDART CLASSIFICATION OF POWDERS ACCORDING TO THEIR FLUIDISATION PROPERTIES BASED ON PARTICLE SIZE AND THE DENSITY DIFFERENTIAL BETWEEN THE PARTICLES AND THE FLUIDISING MEDIUM. C=COHESIVE, A=AERATABLE, B=BUBBLING AND D = SPOUTING. ADAPTED FROM GELDART (1973)

1.2.3.5   Particulate vs. aggregative fluidisation

Powder fluidisation can also be classified as particulate or aggregative (Kwauk *et al.* 2000). In particulate fluidisation, particles are homogeneously suspended within the fluid with the bed voidage between the particles remaining constant throughout the powder bed. Particulate fluidisation is usually only achieved if the fluid used as the fluidisation medium is a liquid. Aggregative fluidisation on the other hand is characterised by uneven voidage between unevenly sized agglomerates of powder. However, particulate and aggregative fluidisation are not two distinct classes, but end points for a continuous spectra of different behaviour of a fluidised powder bed (Kwauk *et al.* 2000).

Following on from the fact that particulate fluidisation can only take place when the fluidisation media is a liquid, only aggregative fluidisation is relevant for DPI formulations. To understand the implications of aggregative fluidisation on the DPI performance, the following section of the introduction will discuss agglomeration and agglomerate breakage.

1.2.4 Agglomerates and deagglomeration

Agglomerate and aggregate are terms often used in parallel for describing loose assemblages of powders. As recommended by Nichols *et al.* (2002), the term agglomerate is used throughout the current thesis. Agglomerates are defined as systems where primary particles of different sizes are held together by interparticulate contact forces. Furthermore, each particle within an agglomerate has at least one point of contact with a neighbouring particle (Bika *et al.* 2001).

Agglomeration has many applications, for example in the food, pharmaceutical, cement, mining and chemical industries (Mishra *et al.* 2001). In most of these applications, a delicate balance between stability and ease of disintegration of the agglomerate has to be achieved. This balance is especially important for dry powder inhaler formulations. Stability is required to avoid segregation of the formulation during storage and transport. Simultaneously, the contact forces have to be weak enough achieve deagglomeration upon inhalation (Boerefijn *et al.* 1998). In dry powder agglomerates, the void spaces between the particles are filled with interstitial gas. The proportion of interstitial gas within an agglomerate, defined as the porosity of an agglomerate, is an important property in determining the breakage properties of an agglomerate (Bika *et al.* 2001).

If the network of contact forces within a powder agglomerate is disturbed by mechanical impaction or turbulence, agglomerate breakage, also known as deagglomeration, will take place. However, this only happens if the energy of the impaction is sufficient to overcome the magnitude of the contact forces within the agglomerate. For agglomerates with strong interparticulate forces, such as liquid bridges in wet agglomerates, fracture planes are often observed across the agglomerate upon impaction. The size of the fragments is known to depend on the porosity of the agglomerate and the velocity of the impact (Subero *et al.* 2001). The mechanism of dispersion for weak agglomerates, which are often dry agglomerates held together by van der Waals forces, is less well described in the literature. Boerefijn *et al.* (1998) suggested that upon impaction, dry powder agglomerates disintegrated to primary particles and small clusters. Simulation results by Mishra *et al.* (2001) indicated that dry powder agglomerates with high porosity disintegrate and agglomerates with low porosity fracture upon impaction. The relationship between the agglomerate properties and the breakage pattern is relevant to DPI formulations, because the extent of deagglomeration, and thus drug delivery, can be changed by altering the powder properties.

1.3 FORMULATION CHALLENGE AND STRATEGIES FOR DPI FORMULATIONS

1.3.1 The challenge

To summarise what has been discussed in the introduction so far, a schematic presenting the requirements for successful drug delivery to the lungs and the consequential challenges faced by a DPI formulator is shown in Figure 1.7. Ultimately, the requirements derive from the anatomy of the lungs. Asthma and COPD affect the bronchi and bronchioles. Therefore, the drug delivery is targeted in those regions of the lung. Due to the diameter of these peripheral airways and the particle deposition mechanisms within the lung, a particle size between 1 and 5 µm is required if drug delivery to the bronchi and bronchioles is to be achieved. Additionally, due to the favourable pharmacokinetic properties of the lung as the route of entry for drugs, only small doses of the drug are needed to obtain the required therapeutic effect.

As outlined in Figure 1.7, the fine particle size and the small doses of drug required pose challenges for both the manufacturing process and the optimisation of DPI formulation performance. Fine powders exhibit high interparticulate contact forces and

consequentially, poor flow properties. Therefore, drug powders within the respirable range are difficult to handle during the manufacturing process. Additionally, the small doses required are difficult to weigh accurately and reproducibly.

More importantly, from the formulation point of view, the drug delivery from DPIs relies on fluidising the dose. Particles within the respirable range belong to Geldart group C and cannot be fluidised. Therefore, the first challenge for a DPI formulator is to engineer the interparticulate contact forces within the formulation so that fluidisation can be achieved. Additionally, particulate fluidisation can only be achieved when a liquid is used as the fluidisation medium. Therefore only aggregative fluidisation is relevant for DPI formulations. Consequentially, the formulator has to also make sure that efficient powder deagglomeration takes place after fluidisation, so that a particle size of the drug within the respirable range is achieved.

The formulation strategies available to a DPI formulator for achieving favourable powder properties for manufacturing the formulations and for fluidising and deagglomerating the dose of the drug will be introduced in the following.
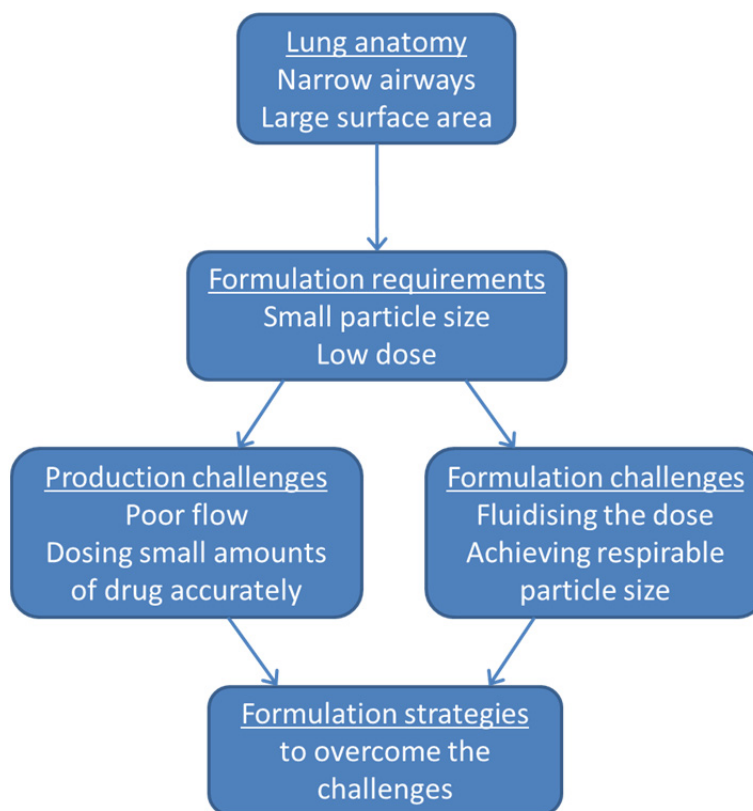
FIGURE 1.7 A SCHEMATIC ILLUSTRATING THE FORMULATION REQUIREMENTS FOR PULMONARY DRUG DELIVERY DERIVING FROM THE LUNG ANATOMY AND THE CONSEQUENTIAL CHALLENGES FOR FORMULATION AND PRODUCTION OF DPI PRODUCTS

1.3.2 Formulation strategies

1.3.2.1   Carrier free formulations

The simplest of the formulation strategies available to a DPI formulator is to alter the interparticulate contact forces of the drug powder so that the powder can be easily handled during processing and the dose can be fluidised upon inhalation. There are various options for achieving this. For example, larger, loosely bound agglomerates of the drug can be formed (Edwards *et al.* 1989). These agglomerates act as larger particles due to the increased significance of gravitational forces and relative decrease in the contact surface area between the agglomerates. This in turn will reduce the magnitude of the interparticulate forces within the bulk powder. Therefore, these agglomerated powders exhibit better flow properties, thus facilitating the manufacturing process and dose fluidisation. Providing the agglomerates are weak enough, they can be deagglomerated upon inhalation to achieve a particle size suitable for pulmonary drug delivery (Edwards *et al.* 1989; Hino *et al.* 1998). Turbuhaler Pulmicort is a commercially available product utilising this formulation approach.

Another approach for preparing free flowing and easily fluidisable drug powders for DPIs is to use spray drying (Nolan *et al.* 2009; Steckel *et al.* 2004a) or spray freeze drying (Mueannoom *et al.* 2012) to produce hollow particles. The hollow particles have a low density. It follows from Equation 1.1 that the diameter of a low density particle can be larger than the diameter of a higher density particle to deposit at a similar site in the lungs. Therefore, respirable low density particles can be manufactured at larger particle sizes. Consequentially, the interparticulate forces within these powders are smaller and therefore manufacturing and fluidisation issues are somewhat solved.

The surface properties of the drug particles can also be modified so that the interparticulate forces within the bulk powder are decreased. In practice, this often means producing small scale surface roughness on the surface of the drug particles. As a result of the decreased interparticulate forces, powders will exhibit improved flow and fluidisation properties. Surface modifications have been performed for example by crystallising vaporised solution of L-leucine on to the surface of drug particles (Raula *et al.* 2009).

1.3.2.2   Binary formulations

One of the formulation approaches widely used in DPI production is blending the cohesive Geldart group C drug powder with a Geldart group A powder that can be easily fluidised.

This results in interactive mixtures (Egermann *et al.* 1983), where the cohesive drug particles adhere on the surfaces of the easily fluidised large carrier crystals that act as the binary component in the formulation. The coarse carrier particles make up the bulk of the formulation allowing the resulting formulation to be fluidised upon inhalation. Bell *et al.* (1971) were the first to report the use of a coarse carrier for improving the flow properties of the cohesive drug. The most commonly used carrier in DPI formulations is α-lactose monohydrate, although studies where other sugars, such as mannitol, xylitol and glucose have been used as carriers have been published (Hamishehkar *et al.* 2010; Harjunen *et al.* 2003; Hooton *et al.* 2006).

The approach of engineering the fluidisation properties of Geldart Group C powders by adding easy-to-fluidise particles is widely used within fluidisation science (Alavi *et al.* 2005; Zhou *et al.* 1999). However, although the fluidisation properties of the drug delivered with DPIs can be adjusted by adding easy-to-fluidise coarse carrier particles, the challenge of detaching the drug particles from the surfaces of the coarse carrier and de-agglomerating the drug upon inhalation remains somewhat unsolved. Consequentially, the respirable fraction delivered from these formulations is often only 20% or less of the drug dose (Steckel *et al.* 1997). The drug particles still remaining attached to the coarse carrier particles will deposit at the back of the throat. Therefore, optimising the drug delivery from DPI formulations would be advantageous for avoiding ingestion, rather than inhalation, of the drug. This would reduce potential systemic side effects caused by the absorption of the drug via the digestive system. Additionally, if the drug delivery from the DPI formulations was optimised, the loaded drug dose in the formulations could be lower whilst still delivering the same therapeutic dose of the drug. This would make the manufacturing of DPI formulations more economic.

1.3.2.3   Ternary formulations

To optimise the drug detachment from the surfaces of the coarse carrier, and thus improve the respirable fraction of the drug delivered from DPIs, ternary components can be added to the formulation. The ternary component can for example be either a force control agent or fine particle excipient.

The exact mechanisms for how the ternary components alter the formulation performance remain unclear. However, it has been hypothesised that the force control agents, such as magnesium stearate, modify the surface energies of the large lactose carrier particles so that drug detachment becomes favourable (Begat *et al.* 2005). This is especially the case if the force control agent particles are dispersed on the surfaces of the large carrier

particles as a thin monolayer. Other mechanisms, such as the force control agent particles acting as micro-carriers or altering the powder structure to be more favourable for drug detachment and deagglomeration, have also been suggested (Tay *et al.* 2010).

Similarly, the mechanism of action of the fine excipient particles is not currently fully understood. However, by the inclusion of fine excipient particles, a significant increase in the respirable fraction of the drug can be achieved compared to a binary formulation (Louey *et al.* 2003). The hypotheses for the mechanism accounting for the improved formulation performance include the active site, agglomerate formation and increased cohesion theories. The current thesis focuses on the role of lactose fines in regulating DPI formulation performance. Therefore, a thorough summary of these mechanisms will be given later in the introduction, after a general introduction to lactose and a review of all the research that has led to the development of these theories.

1.4 LACTOSE AS A CARRIER IN DPI FORMULATIONS

1.4.1 General introduction to lactose

1.4.1.1 Chemistry

Lactose is a naturally occurring disaccharide consisting of galactose and glucose moieties linked together with a glycosidic bond. The chemical structure of lactose is shown in Figure 1.8. In solution, the conformation of the hydroxyl group linked to C1 of the glucose ring can be either in α or β anomeric form. The position of this hydroxyl group is highlighted in Figure 1.8, with the hydroxyl group shown in α conformation. Mutarotation between the conformations takes place, and in the equilibrium, the proportion of α form is 37.3% and β form 62.7 (Gänzle *et al.* 2008). Due to the hydroxyl group in the C1 position in the glucose ring, lactose is a reducing sugar. Consequentially, in the presence of water, Maillard reaction between lactose and molecules containing amino groups can take place over time (Narang *et al.* 2009).
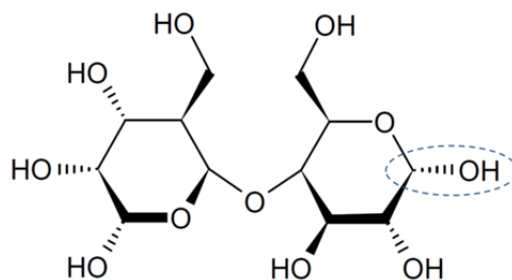
FIGURE 1.8 THE CHEMICAL STRUCTURE OF THE α ANOMERIC FORM OF LACTOSE WITH THE ANOMERIC HYDROXYL GROUP HIGHLIGHTED

1.4.1.2 Production

Lactose is crystallised out from whey that is a by-product of cheese manufacturing. If the crystallisation is performed below 93.5 °C, the crystalline form of α-lactose, α-lactose monohydrate, is obtained. If the crystallisation is performed above 93.5 °C, the lactose will crystallise in the β-anhydrous form (Gänzle *et al.* 2008). The most common crystal shapes of lactose are tomahawks, pyramids and prisms (Clydesdale *et al.* 1997). However, the crystal habit of lactose depends on the crystallisation conditions, especially the rate of crystal growth. Therefore, also other morphologies of lactose crystals can be obtained (Gänzle *et al.* 2008). Amorphous, non-crystalline lactose can also be obtained for example by spray, freeze or roller drying of the solution containing the lactose. The resulting proportions of α-lactose monohydrate and β-anhydrous lactose within the amorphous lactose glass are identical to the solution from which the crystallisation was performed (Gänzle *et al.* 2008).

After crystallisation, lactose can be further processed for example by sieving, milling, air classification or micronisation to produce lactose with desirable physicochemical and physical attributes. Therefore, there are various commercial grades of lactose on the market, some of which have been specifically designed for inhalation purposes (Pilcer *et al.* 2012).

1.4.1.3 Lactose as an excipient in DPI formulations

Traditionally excipients have been defined as ingredients present in pharmaceutical formulations that do not provide the patient with direct therapeutic value. Excipients are added to drug products mainly for two reasons. The first one is to facilitate the manufacturing of the drug product. The second objective of the use of excipients is to increase the patient compliance to the treatment by making the dosage forms more pleasant. This includes for example increasing the size of a tablet so that it can be easily handled or coating tablets so that they will be easier to swallow (Parker 2009). However, in some cases, rather than defining excipients as inert materials present in the formulations, it has been realised that the excipients also exhibit functionality, often altering the pharmacological properties of the final products (Pifferi *et al.* 1999).

Lactose has traditionally been used as filler, binding agent and diluent in tablet and capsule based formulations (Edge *et al.* 2006). In the advent of the era of DPIs, the excipient was adopted for use in inhalation formulations. This was mainly due to the good availability, inexpensive price and compatibility with most of the inhaled therapy small

molecules (Telko *et al.* 2005). The α-monohydrate form is the most commonly used lactose in inhalation formulations. The only restriction on the use of lactose in inhalation formulations is the reducing properties of the molecule. Therefore, lactose cannot be used as an excipient in formulations containing peptides, proteins or other molecules containing amino groups (Edge *et al.* 2006).

Favourable toxicological properties also contributed towards the adoption of lactose as an excipient for DPI formulations. The pulmonary deposition of lactose in humans has been proven to be non-toxic, although in some cases mild irritation of the airways and non-severe bronchoconstriction have been reported (Thoren *et al.* 2001). The lactose that is small enough to be deposited in the lungs has been shown to be rapidly absorbed and excreted in urine (Baldrick *et al.* 1997). Upon inhalation, the lactose particles outside the respirable range are deposited in the oropharynx, and consequentially ingested. However, the amounts of lactose typically contained within a dose of DPI formulation are not sufficient for triggering the symptoms of lactose intolerance. This is because grams of ingested lactose are needed for the symptoms to appear (Baldrick *et al.* 1997).

The pharmacopoeial requirements for inhalation grade lactose are summarised in the lactose monograph of the Handbook of Pharmaceutical Excipients (Edge *et al.* 2006). All the parameters specified, such as specific optical rotation, heavy metal content and microbial content, are related to ensuring the chemical identity and purity of the lactose. However, the physical and physicochemical properties, such as particle size, have not been strictly specified. Therefore, a wide range of different lactose grades are commercially available. The lactose monograph of the Handbook of Pharmaceutical Excipients highlights the variety of the marketed grades in terms of particle size distributions (Edge *et al.* 2006). The differences in the physical and physicochemical properties of the commercially available lactose grades result in a wide variation in the functionality of lactose sourced from different manufacturers or processed in different ways. In fact, some studies have even addressed the issue of batch-to-batch variability of the carrier lactose affecting the final performance of the DPI formulations, especially at low drug loadings (Steckel *et al.* 2004b). The following sections of the introduction aim to summarise how the different physical and physicochemical properties of the lactose carrier influence the performance of DPI formulations.

1.4.2 The link between the properties of the coarse lactose carrier and the DPI performance

1.4.2.1 Crystalline form

An early study reported that the crystalline form of coarse lactose did not have an impact on the *in vitro* performance of a steroid formulation. Similar performances were obtained from formulations prepared with α-lactose monohydrate, chemically dehydrated α-anhydrous lactose and β-anhydrous lactose (Robertson *et al.* 1996). Larhrib *et al.* (1999) reported that the 63-90 μm sieved fraction of anhydrous lactose outperformed equivalent sieved fractions of α-lactose monohydrate as the carrier for salbutamol sulphate. However, the fine lactose content and surface roughness of the anhydrous form of the lactose used in the study were significantly different from the monohydrate carriers. Therefore, the findings of the study are somewhat inconclusive with regards to the role of the crystalline form of the lactose carrier. Subsequently, Pitchayajittipong *et al.* (2010) studied the impact of the crystalline form of lactose sourced from different manufacturers on the formulation performance of budesonide. The study indicated that the source of lactose was more important in regulating the performance than the crystalline form. This finding was attributed to the powder bulk properties, such as fluidisation properties, dominating over the chemical identity of the lactose carrier in determining the DPI performance.

Traini *et al.* (2008) reported differences in the delivery of salbutamol sulphate from formulations prepared with different polymorphic forms of lactose. The α-monohydrate form produced the highest performance. The findings of this study were attributed to the surface energies of the carrier particles with the α-monohydrate having the lowest surface energy, resulting in lower drug-excipient interactions and thus greater drug detachment.

1.4.2.2 Moisture content

The water loss on drying has been shown to contribute to the *in vitro* performance of salmeterol xinafoate. The effect of increasing moisture content of the carrier on the formulation performance was shown to be two-fold. Firstly, the drug losses in the device were increased. Secondly, the amount of drug lost due to adhesion to the large carrier particles was reduced. The former finding was attributed to the increased adhesive forces upon increasing water content preventing a complete emptying of the device. The latter observation on the other hand was attributed to the water molecules acting as lubricant on

the surface as long as the relative humidity was kept at too low a level for capillary interactions to take place (Podczeck 1998)

1.4.2.3   Surface morphology

Several studies have reported the impact of the surface roughness of the coarse lactose carrier on the DPI formulation performance. Kawashima *et al.* (1998) found that microscale roughness on the surface of the lactose carrier was advantageous for the detachment of pranlukast hydrate from DPI formulations. The study also reported that both large scale surface roughness and smooth surfaces of the carrier lactose crystals had a negative effect on the formulation performance. The decrease in performance in the latter two cases was attributed to the increased interparticulate forces due to increased contact area between the drug particles and the carrier lactose (Kawashima *et al.* 1998). Similar conclusions were made by Young *et al.* (2009), who prepared lactose composite carriers with different degrees of surface roughness. The study reported an improvement in the delivery of salbutamol sulphate upon increasing microscale surface roughness of the carrier. The differences in the resulting contact geometry between the carrier surface and the drug particles were concluded to affect the drug detachment from the carrier surfaces. Similarly, Kaialy *et al.* (2012a) reported an increased delivery of salbutamol sulphate upon increasing surface roughness of the carrier. In this study different commercial, 63-90 µm sieved grades of lactose were used as the carriers.

In contrast, studies by Zeng and co-workers indicated that smoother lactose carriers produced higher *in vitro* performance for salbutamol sulphate, also known as albuterol sulphate (Zeng *et al.* 2000a; Zeng *et al.* 2001b; Zeng *et al.* 2001c). A study by de Boer *et al.* (2003) on the other hand concluded that small scale surface roughness on the surface of commercial coarse grade lactose carriers had very negligible effect on the detachment of budesonide from the carrier surfaces.

1.4.2.4   Particle shape

Kaialy *et al.* (2012a) have reported that the more irregular the shape of the coarse carrier, the better the *in vitro* performance of salbutamol sulphate from commercial, 63-90 µm sieved fractions of lactose. Numerous studies have also shown that increasing the elongation of the coarse carrier particles improved the respirable fraction of salbutamol sulphate (Dhumal *et al.* 2008; Kaialy *et al.* 2012a; Larhrib *et al.* 2003a; Larhrib *et al.* 2003b; Zeng *et al.* 2000a). The authors of most of these studies unanimously concluded

that the elongated shape of the carrier crystals was aerodynamically favourable. As a result, elongated carrier particles would stay suspended in the air flow for a longer period of time. Consequentially, the drag forces had more time to act to detach the drug particles from the surfaces of the carrier particles.

To investigate the impact of extremely elongated particles, lactose and different crystal forms of mannitol were used as the carriers for salbutamol sulphate in a study by Kaialy *et al.* (2011). Depending on the crystallisation conditions, the particle shape of mannitol was greatly altered. Needle like mannitol particles with an elongation ratio of approximately 6 were obtained when crystallisation was performed in ethanol. The study demonstrated that even in extreme cases, the more elongated the carrier particles, the better the fine particle dose from the formulations. However, it was also demonstrated that the drug emission and powder flow properties were adversely affected as a result of increasing elongation.

1.4.2.5   Particle size

A study by Zeng and co-workers showed that the emission of salbutamol sulphate from DPI formulations improved upon increasing the particle size of the coarse carrier. However, in the same study it was shown that the drug deagglomeration efficiency decreased simultaneously with the increase in the carrier particle size. The different size fractions of lactose used in that study were recrystallized from Carbopol gel and therefore exhibited smooth carrier surfaces (Zeng *et al.* 2001c). However, in a later study, similar results were reported for commercial grades of coarse lactose carriers with a decrease in the *in vitro* delivery of salbutamol sulphate upon increasing median particle size (Louey *et al.* 2003).

Le *et al.* (2012a) fractionated a commercial grade of coarse lactose to different size fractions by sieving. The different sieve fractions were then used as carriers for fluticasone propionate. It was demonstrated that the smaller size fractions produced a higher *in vitro* performance than the larger size fractions. The finding was attributed to lower adhesion energy between the smaller size fractions of lactose and the drug particles.

1.4.2.6   Complications

A complication in establishing the link between the coarse lactose properties and the formulation performance is that the effects of the various properties of the lactose

discussed above are not independent of each other. For example, Donovan *et al.* (2010) compared the formulation performance of budesonide prepared with sieved fractions of anhydrous and granular tablet grades of lactose. The former had a smooth surface and the latter exhibited large scale surface roughness. It was found that the anhydrous, smooth carrier outperformed the granular carrier with the rough surface when the carrier size was small. However, the opposite was observed for the coarser sieve fractions with the rough carrier outperforming the smooth carrier. The findings were attributed to the different drug detachment mechanisms, drag forces or impaction, prevailing for different carrier systems. According to the authors, detachment by drag forces is the most important mechanism in conventional DPI formulations. However, impaction became an important mechanism upon increasing the particle size of the carrier. Consequentially, the drug particles that were accommodated by the surface roughness of the granular carriers were dislodged more efficiently from the larger size fractions of the carrier upon impaction (Donovan *et al.* 2010).

A further complication in gaining an understanding between the lactose carrier properties and DPI performance is that studying the impact of an isolated variable with lactose carriers is difficult. This is because lactose is a natural product and altering one parameter, such as particle surface roughness, will very likely also change the overall particle morphology and particle size. Therefore, another approach recently used for collecting the pieces for the bigger picture is developing model systems where the different variables can be independently isolated. Ooi *et al.* (2011) used three different monodisperse size fractions of spherical polystyrene beads with similar surface characteristics as the carrier for salbutamol sulphate. The results of the study indicated that smaller carriers outperformed the larger size carriers. The finding was attributed to the higher number of collisions taking place in the formulations prepared with smaller carriers upon aerosolisation, leading to a greater extent of drug detachment from the surfaces.

1.4.3   Influence of lactose fines

The relationship between the different properties of the coarse carrier and the performance of binary DPI formulations was discussed above. Clearly, the interplay between the different physical and chemical properties of the coarse carrier and the drug detachment is complex. As was discussed earlier in the introduction, one of the formulation strategies to improve the drug detachment from the surface of the coarse carrier is to add a ternary component, such as fine particle lactose, to the formulation. The following sections of the introduction aim to summarise the research that has been

conducted on the impact of adding lactose fines as the ternary component on the DPI performance.

1.4.3.1 Intrinsic fines

Some coarse carriers contain a small proportion of lactose fines. These fines are termed intrinsic fines. The role of intrinsic lactose fines in regulating DPI performance has been shown in numerous studies. Zeng *et al.* (1998) showed that the *in vitro* performance of salmeterol xinafoate could be reduced by removing intrinsic fine lactose particles from the coarse carrier by air sieving. The reduction in the performance was shown to be reversible by the addition of a fine lactose component to the formulation after air jet sieving. Similarly, Islam *et al.* (2004) reported a decrease in the *in vitro* performance of salmeterol xinafoate after surface smoothing a coarse lactose using wet decantation. However, the impact of surface modification was concluded to have a much less significant impact on the *in vitro* performance than the removal of intrinsic fines, which also took place during the wet decantation. Again, the performance was found to be reversible to the original level by the addition of fine particle lactose to the surface smoothed carriers (Islam *et al.* 2004). A decrease in the performance of budesonide (Dickhoff *et al.* 2006) and salbutamol sulphate (Boshhiha *et al.* 2009) formulations has also been reported after surface smoothing by removing the intrinsic lactose fines by wet decantation. Le *et al.* (2012b) showed a decrease in the *in vitro* performance of fluticasone propionate and terbutaline sulphate upon the removal of intrinsic lactose fines by air jet sieving.

Steckel *et al.* (2006) used a different approach of creating intrinsic fines by milling commercial grade lactose carriers. The commercial and milled products were sieved to produce identical size fractions. The fractions of the milled carriers outperformed the equivalent fractions of commercial grades as carriers for bechlometasone dipropionate and salbutamol sulphate, proving the role of intrinsic fines in improving the DPI performance. Xu *et al.* (2010) used milled and sieved grades of α-lactose monohydrate as the carriers for salbutamol sulphate and disodium cromoglycate. The upper ends of the particle size distributions of the lactose carriers were similar. However, the proportion of intrinsic fines within the milled grade carriers was higher than in the sieved grades. The milled grades of lactose were seen to outperform the sieved grade of lactose as a carrier for both the drugs, once again addressing the importance of the intrinsic fines.

1.4.3.2   Particle size of the fines

Zeng *et al.* (1999) reported that micronised lactose fines were more efficient in improving the *in vitro* performance of salbutamol sulphate than intermediate size lactose fines. A few years later, the same research group concluded that it was the presence of micronised lactose fines (<10 µm) that was ruling the DPI performance of salbutamol sulphate formulations, not the properties of the coarse lactose carrier (Zeng *et al.* 2001b). Harjunen *et al.* (2002) showed that the presence of crystalline, micronised lactose fines improved the formulation performance of budesonide. However, in the same study, it was shown that the performance of a formulation containing the micronised lactose fines was greatly decreased upon storage (Harjunen *et al.* 2002). Similarly, a study by Guenette *et al.* (2009) showed that the lactose fines below 10 µm had the greatest positive effect on the *in vitro* delivery of salbutamol sulphate. However, again, the formulations prepared with this fraction of fines were the most affected upon storage.

A study by Adi *et al.* (2006) specified the optimum size of the fines more accurately by showing that an added fine fraction with a volume median diameter (VMD) of 7.9 µm was the most effective in improving the delivery of salmeterol xinafoate. Fines with a VMD of 3.3 µm were shown to be less efficient as were larger fines with VMD of 17.7 and 33.3 µm. The two largest fractions were in fact suggested to act as secondary carriers (Adi *et al.* 2006). Following on from this study, the impact of the polydispersity of the fine fractions with similar VMDs was investigated (Adi *et al.* 2009). The study concluded that the optimum particle size of the fines was between 5 and 10 µm. The finding was attributed to fines between these sizes forming agglomerates with favourable deagglomeration properties (Adi *et al.* 2009).

1.4.3.3   Adding sequence of the fines

Zeng *et al.* (1999) found that the *in vitro* performance of salbutamol sulphate was better from a formulation where the lactose fines were added to the formulation before salbutamol sulphate compared to a formulation prepared with an opposite mixing order. The same observation was made in a different study for a hydrophobic drug, bechlometasone dipropionate (Zeng *et al.* 2000b). However, the optimum mixing order for bechlometasone dipropionate was shown to be initially mixing the lactose fines and the drug, followed by blending the resulting pre-blend with the coarse lactose carrier (Zeng *et al.* 2000b). In contrast, Louey *et al.* (2002) found that the mixing order of the fine ternary component and salbutamol sulphate did not have an impact on the performance of the final formulation.

A study by Jones *et al.* (2010) pointed out that the mixing process and the drug concentration played a role in the results of blending order studies for salbutamol sulphate. It was reported that with short mixing times (15 min), neither the mixing order nor the drug concentration had an impact on the formulation performance. With longer mixing times (30 min), formulations with low drug contents produced better performance by adding the fines before the drug. The performance at high drug concentrations on the other hand was not affected by the mixing order. The authors concluded that the different drug concentrations used in the previous studies by Zeng *et al.* (1999) and Louey *et al.* (2002) were likely to explain the discrepancies between the studies, which both used mixing time of 30 minutes.

1.4.3.4   Concentration of the fines

A study by Guchardi *et al.* (2008) indicated that the optimum concentration of fine particle lactose <10 µm was 5% for formoterol fumarate. Louey *et al.* (2003) concluded that, for salbutamol sulphate, the optimum concentration of micronised lactose fines was approximately 10 wt-%. At higher concentrations than this, a decrease in the formulation performance was reported.

1.4.3.5   Addition of non-lactose fines

Sorbitol and mannitol fines have been employed as the fine particle component. However, the chemical identity of the fines has been shown to be insignificant for determining the performance of salbutamol sulphate formulations for inhalation (Tee *et al.* 2000).

1.4.4 Mechanisms for lactose fines improving the DPI performance

1.4.4.1   Active sites theory

The active site theory was originally proposed by Ganderton (1991; 1992) based on the concept of ordered mixing introduced by Hersey (1975). According to the theory, the surfaces of the coarse lactose crystals contain highly energetic spots where the drug particles strongly adhere (Staniforth 2000). These spots, termed the active sites, have been suggested to be regions with morphological defects such as asperities on clefts, chemical impurities or amorphous material on the surface of the large lactose crystals (Pilcer *et al.* 2011). According to the theory, upon the addition of the ternary component,

the fine excipient particles occupy these active sites. When the drug is added to the formulation, the drug particles attach to the surfaces with lower interaction energy. Due to the lower energy, the drug particles are easily detached from the surface upon inhalation. The active sites theory is illustrated in Figure 1.9.
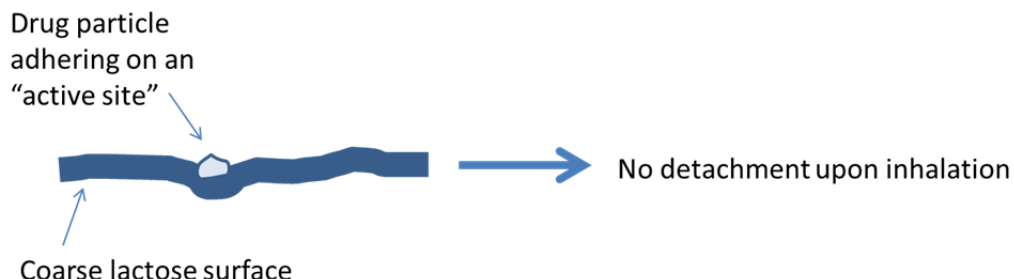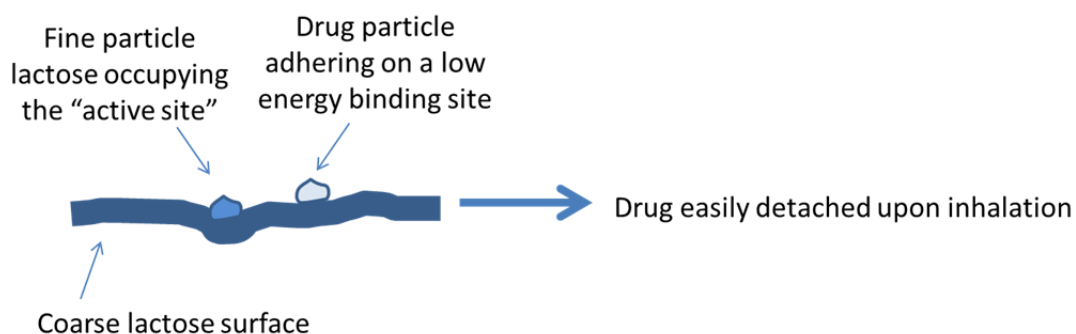
FIGURE 1.9 A SCHEMATIC ILLUSTRATING THE ACTIVE SITE THEORY AND THE IMPACT OF THE ACTIVE SITES ON THE DRUG DETACHMENT FROM THE CARRIER IN BINARY AND TERNARY DPI FORMULATIONS

Since the introduction of the active sites theory, numerous studies have found supporting evidence in favour of the hypothesis. The authors of the studies where the DPI formulation performance was reduced upon the removal of intrinsic fines and reversed back to the original level by adding fines have explained the findings with the active site theory (Steckel *et al.* 2006; Zeng *et al.* 1998).

Parallel studies by Young *et al.* (2005) and El-Sabawi *et al.* (2006) used a commercial and a surface smoothed grade of lactose as the carriers for salbutamol sulphate. By dose titration for the drug it was shown that initially, at low drug concentrations, no improvement in the formulation performance was achieved upon increasing the drug concentration. This was attributed to the continuous process of filling the active sites below the saturation concentration. However, at higher drug concentrations, once all the active sites had been filled and the excess drug was binding to the low energy binding sites, an improving trend in the formulation performance was apparent. The concentration where the improvement started was termed as the critical concentration. It was shown that the critical

concentration was lower for the surface smoothed lactose than for the commercial grade of lactose. This was explained by the lower number of active sites on the surface of the smoothed lactose (El-Sabawi *et al.* 2006; Young *et al.* 2005).

The active site theory was also supported by a study, where in addition to the *in vitro* deposition of formoterol fumarate, the deposition profile for lactose was determined. The results of the study indicated that the amount of lactose fines associated with the coarse lactose did not change after approximately 4 wt-% fines concentration. This was attributed to lactose fines having saturated the active sites at this concentration. Any fines added above this concentration were attached to the low energy binding sites and therefore were detached upon dose fluidisation (Guchardi *et al.* 2008).

However, although many studies have supported the active sites theory, other studies have reported opposite findings. Louey *et al.* (2002) investigated the role of lactose and glucose fines on the *in vitro* performance of salbutamol sulphate. The results of the study were concluded to be inconsistent with the active site theory for two reasons. Firstly, if the active sites theory was true, the mixing order of the drug and fines should have an impact on the performance, because the component that was added first would occupy the active sites. However, the mixing order of the fines and the drug had no impact on the performance. Secondly, the active sites are defined as high energy binding sites. However, using AFM, the addition of fines was found to increase the surface energy of the lactose carrier. The increase in the surface energy of the carrier system upon the addition of fine excipient particles has also been reported based on inverse gas chromatography measurements by Ho *et al.* (2010).

1.4.4.2   *Drug-fines agglomeration theory*

The drug-fines agglomeration theory is another traditional view for the mechanism for the improvement in DPI performance in the presence of a ternary component. This theory was originally proposed by Lucas *et al.* (1998), who found that the performance of a carrier based bovine serum albumin (BSA) formulation improved in the presence of fine particle lactose. According to the theory, the improved DPI performance in the presence of excipient fines can be explained by agglomerate formation between the drug and the fine particle excipient. Upon inhalation, these agglomerates are more likely to detach from the carrier surfaces. The theory can be verified by calculating the drag force (F_{Drag}) experienced by a particle or an agglomerate on a surface of a coarse carrier crystal as per Equation 1.9 (Begat *et al.* 2004a), where C_{Drag} is drag coefficient, ρ_a is the density of air, Φ_{Agg} the diameter of the agglomerate and V the air velocity.

$$F_{Drag} = C_{Drag} \frac{\pi}{8} \rho_a \Phi_{Agg}^2 V^2$$

EQUATION 1.9

It follows on from Equation 1.9 that the drag force experienced by any particle or an agglomerate is directly proportional to the square of its diameter. Therefore, the detachment of the agglomerates from the surfaces is more likely than the detachment of primary drug particles. The detached agglomerates may be of respirable size, or may deagglomerate to produce a respirable particle size. The drug fines agglomeration theory is illustrated in Figure 1.10.

Binary formulation:

Drug particle

Drag force inadequate to detach the drug particles from the surfaces

Ternary formulation:

Agglomerates of the drug and the fines

Drag force adequate to detach the agglomerates from the surface. The agglomerates may be of respirable size, or may go through deagglomeration
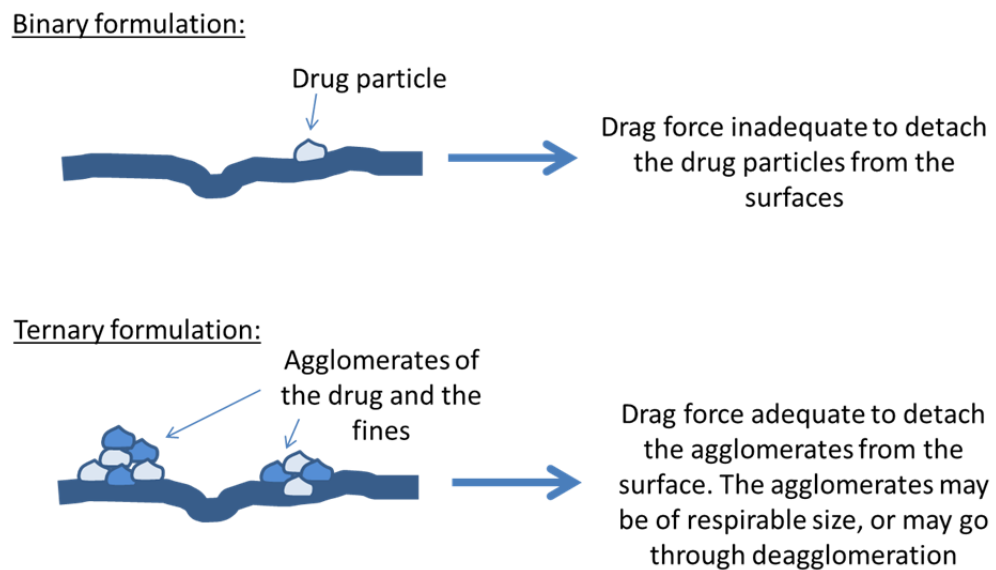
FIGURE 1.10 THE DRUG – FINES AGGLOMERATE FORMATION THEORY ILLUSTRATED

The drug-fines agglomeration theory has also been supported by numerous studies. Podczeck (1999) reported that the fine particle lactose was more efficient in improving the *in vitro* performance of salmeterol xinafoate when formulated with a large lactose carrier with a rough surface than one with a smooth surface. In this study, the finding was attributed to the tendency of the fines and the drug to form agglomerates on a rough surface and monolayers on smooth surface (Podczeck 1999).

The agglomerate formation theory is further supported by a study where wet granulation techniques were used for producing spherical agglomerates of an inhaled steroid. The study showed that the agglomerated systems formulated with a coarse lactose carrier produced higher respirable fractions than formulations prepared with the primary particles of the crystalline drug (Ikegami *et al.* 2000). Even though the study was not aimed at finding support for the agglomerate formation theory, in retrospect, it proves the

significance of the increased size of the drug for the likelihood of detachment from the coarse lactose surfaces.

In the study conducted by Louey *et al.* (2002) that found contra-indicatory evidence for the active sites theory discussed earlier, it was also reported that the addition of drug was seen to increase the amount of detached lactose fines. This finding suggested a synergistic action between the two types of fines. Because of the finding, the authors concluded that formation of agglomerates or multilayers had to be playing a role in determining the performance of the DPI formulations (Louey *et al.* 2002). This theory was further supported by a study by Islam *et al.* (2004) who showed that the *in vitro* performance of salmeterol xinafoate decreased as the theoretical ratio between the number of salmeterol xinafoate and fine lactose particles decreased.

Jones *et al.* (2008) used a cohesive-adhesive balance (CAB) approach to determine the interaction energies between fine excipient particles and micronised drug particles. The study concluded that when the drug-excipient interaction was adhesive, i.e. the drug preferred adhering to the excipient rather than to another drug particle, the formulation performance improvement was due to agglomerate formation between the drug and the fines.

1.4.4.3   Increased cohesion theory

The most recent theory suggested for being responsible for improving the DPI formulation performance upon the addition of fine particle lactose is the increased cohesion theory. During the years, it has been shown that the inclusion of fine particle lactose in DPI formulations increases the cohesive strength of the bulk powder (Thalberg *et al.* 2004). However, Shur *et al.* (2008a) were the first to realise the potential connection between the increased cohesion of the carrier upon the addition of lactose fines and the improved final formulation performance. According to the increased cohesion theory, the drag forces created by the inspiratory effort are not able to initiate the fluidisation until a critical air flow velocity, the minimum fluidisation velocity, has been reached. The minimum fluidisation velocity, on the other hand, is dependent on the extent of interparticulate contact forces within the formulation (Shur *et al.* 2008a).

According to the increased cohesion theory, a carrier with low interparticulate contact forces, such as coarse grades of lactose, will be entrained in the air flow gradually, resulting to an erosion mechanism for fluidisation. A cohesive formulation on the other hand resists the fluidisation for longer, and once the fluidisation takes place, it follows the

fracture mechanism. This results in large agglomerates being formed upon fluidisation (Shur *et al.* 2008a). The kinetic energy of an agglomerate formed upon fluidisation, E_{Kin}, is defined by Equation 1.10, where ρ_{Agg} is the density of the agglomerate, Φ_{Agg} is the diameter of the agglomerate and V is the air velocity (Begat *et al.* 2004a).

$$E_{Kin} = \frac{\pi}{12} \rho_{Agg} \Phi_{Agg}^3 V^2$$

<div align="right">**EQUATION 1.10**</div>

Equation 1.10 shows that the kinetic energy of an agglomerate is related to the cube of the diameter of the agglomerate. Therefore, the larger the agglomerate formed upon fluidisation, the more kinetic energy is stored in the agglomerate. Consequentially, the larger the agglomerate, the more likely that deagglomeration will take place, because the collisions between the device and the formulation will be more energetic (Shur *et al.* 2008a).

Shortly after the study by Shur *et al.*, another research group confirmed that fluidisation could take place via the erosion or fracture mechanisms (Tuley *et al.* 2008). A paper by Watling *et al.* (2010) reported that the severity of the fracture could be qualitatively classified as mild or severe. With mild fracture the powder bed entrained as numerous small plugs and with severe fracture as one large plug. The mechanism of fracture could be anything between these two endpoints and was shown to be related to the powder flowability. It was concluded that the more cohesive the powder, the more severe fracture it exhibited upon fluidisation.

1.4.5 Predicting DPI performance on the basis of lactose properties

It is hoped that increasing the understanding of the mechanisms by which the lactose properties affect the performance of DPIs will permit improvements in formulation design. In particular, models that would enable predicting the DPI performance on the basis of the properties of lactose are currently being established. This is because the United States Food and Drug Administration (FDA) recently published the recommendations for the Process Analytical Technologies (PAT) (FDA 2004) and Quality by Design (QbD) initiatives (FDA 2006). The PAT initiative encourages the industry to follow and apply the most recent scientific discoveries in the product development and manufacturing processes to improve the quality of the pharmaceutical products supplied to the consumer (FDA 2004). The QbD initiative on the other hand encourages the industry to characterise the raw materials that go into the products and to use statistical tools for establishing

relationships between the properties of the raw materials and the product performance (FDA 2006).

With regards to the lactose used as the carrier in DPI formulations, several studies have reported correlations between the properties of the lactose and the resulting formulation performance. Traditionally, the proportion of fines present in the carrier has been a good measure for estimating the formulation performance. Islam *et al.* (2004) suggested that the proportion of fine lactose particles (<5 µm) in the carrier could be used as an indication of the final formulation performance. Guchardi *et al.* (2008) on the other hand suggested, that for every 1% increase in the proportion of lactose particles below 10 µm, an improvement of 3% in the fine particle fraction for formoterol fumarate was achieved. Similarly, Guenette *et al.* (2009) reported a linear relationship between the proportion of particles finer than 10 µm in the carrier and the fine particle dose of salbutamol sulphate.

In addition to the proportion of fines present in the carrier, other techniques and parameters have been reported to be useful in understanding the relationship between the carrier properties and the formulation performance. Louey *et al.* (2001) suggested atomic force microscopy would be a suitable tool for predicting DPI formulation performance on the basis of the adhesion forces between the lactose carrier and the drug particles. The surface energy of the carrier lactose as determined by inverse gas chromatography has been shown to be inversely proportional to the formulation performance of budesonide (Saleem *et al.* 2008) and salbutamol sulphate (Traini *et al.* 2008). A linear relationship between the formulation performance of salbutamol sulphate and the tapped and true densities of the lactose carriers crystallised in different conditions was reported by Kaialy *et al.* (2012b).

In terms of powder flow and fluidisation properties, Le *et al.* (2010) reported a correlation between the air permeability of DPI formulations and the fine particle fraction produced. However, the method required preparation and characterisation of the final formulation. Therefore, the value of the method as a quality by design tool can be questioned. Pitchayajittipong *et al.* (2010) successfully correlated the increasing energy required to fluidise the carrier and the resulting improved formulation performance of budesonide.

1.5 AIMS OF THE STUDY

Despite all the research that has taken place over the years, there is still debate as to the mechanism by which the lactose fines affect the DPI performance. Furthermore, the majority of the correlations between the carrier properties and the DPI formulation

performance reported in the literature are based on relatively small datasets and the window across which most of the models are capable of modelling the relationship is relatively narrow. Therefore, to date, a universal model for predicting DPI performance on the basis of the characteristics of the lactose carrier still remains to be introduced.

Therefore, the aim of this project is two-fold. Firstly, the validity of the active site, agglomerate formation and the increased cohesion theories in governing the DPI performance was to be investigated. Secondly, the project also aimed to establish a universal relationship between the properties of the lactose carrier and the final DPI formulation performance when a wide range of different lactoses were used as the carriers.

In Chapter 3 the impact of loaded drug dose on the formulation performance and fluidisation characteristics was investigated. The aim of this chapter was to study the validity of the active sites theory and the increased cohesion theories in governing the DPI performance.

In Chapter 4 the impact of increasing concentration of lactose fines on the flow and fluidisation characteristics of the lactose carriers and the formulation performance were studied. This chapter aimed to test the validity of the increased cohesion theory and also to screen potential properties of the lactose that could be used for predicting the DPI performance.

In Chapter 5 the importance of different lactose characteristics in governing the DPI performance was investigated by the means of multivariate statistical analysis methods and artificial neural networks. The chapter aimed at building a more holistic picture of the lactose characteristics that govern the DPI performance.

In Chapter 6 the regional deposition of the drug in the impactor was studied in more detail by using complementary techniques in parallel with conventional *in vitro* testing of DPI formulations. This chapter aimed to relate the lactose characteristics to the regional drug deposition within the impactor.

CHAPTER 2   GENERAL MATERIALS AND METHODS

OVERVIEW

The aim of the current chapter is to introduce the theoretical background of the experimental methods central to the PhD project. In addition, the details of the experiments conducted are given in this chapter. In the later chapters, a brief materials and methods section is given, but the current chapter should be referred to for more detailed description of the experimental setup and the theoretical background of the frequently used methods. The theoretical background and the experimental details of the methods specific to each of the results' chapters will be outlined in the chapters themselves.

2.1   RAW MATERIALS

2.1.1   Inhalation grade lactose

2.1.1.1   Coarse grades of lactose

Lactohale® (LH) is the brand of inhalation grade lactose manufactured by DFE Pharma (Borculo, Netherlands). Two different coarse grades of Lactohale supplied by DFE Pharma were used in the study, LH100 (Batch #625484) and LH206 (Batch #632599). The former is a sieved grade of coarse lactose and the latter a coarse but lightly milled lactose grade. Additionally, a sieved grade of coarse lactose SV010 (Batch #10523871) manufactured at a different plant of DFE Pharma was used in the studies.

2.1.1.2   Lactose fines

The fine grades of lactose used in the study were also Lactohale products donated by DFE Pharma (Borculo, Netherlands). LH300 (Batch #632955) is a micronised grade of lactose, LH230 (Batch #632868) a finely milled fine lactose and LH210 (Batch #632309) a coarsely milled fine lactose. In addition, Sorbolac 400 (Batch #0137, Meggle, Germany), which is a milled, fine grade of lactose with a broad particle size distribution, was used during the studies.

2.1.1.3 Preparation of lactose pre-blends

The fine fractions of lactose were added to the coarse carriers in-house using low shear mixing to prepare pre-blends. The fines were added to the coarse carriers at concentrations of 2.5, 5, 10 and 20 wt-%. The total mass of the pre-blends was 100 g. The fine grades of lactose were sandwiched between the coarse carrier in two (2.5% blends) or 3 layers (5, 10 and 20% blends). A stainless steel cylindrical vessel with internal dimensions of 100 mm (inner diameter) by 150 mm (depth) was used for preparing the blends. With 100 g of lactose, the headspace in the vessel was approximately two thirds of the volume of the vessel, depending on the fines content of the pre-blend. Blending on a Turbula mixer (Glen Creston, Middlesex, UK) at 46 rpm was applied for 60 minutes. The pre-blends were stored at 44% RH and 20±2°C for at least a week before any further work was carried out.

2.1.2 Model drugs

Micronised fluticasone propionate (FP, Batch #R362400) (GlaxoSmithKline, Singapore) and micronised budesonide (Batch #364R, AstraZeneca, Lund, Sweden) were used as the model drugs during the project. Both these molecules are corticosteroids used for reducing airway inflammation.

2.1.3 Other chemicals

All the solvents (methanol, acetonitrile, cyclohexane and hexane) used during the study were purchased from Sigma (Gillingham, UK) and were of HPLC grade. Similarly, silicone oil and lecithin granules were purchased from Sigma. The water was reverse osmosis purified (Millipore, France).

2.2 PHYSICAL AND PHYSICOCHEMICAL CHARACTERISATION OF THE LACTOSE CARRIERS

2.2.1 Particle size

2.2.1.1 Theory

Measuring the particle size distributions of raw the materials of inhalation formulations is important for various reasons. Firstly, it was shown in the introduction that for achieving successful drug delivery to the lungs it has to be ensured that the particle size of the drug is within the respirable range (Section 1.1.4) Secondly, it was discussed in the introduction

(Section 1.4.2.5) that the particle size of the coarse carrier itself has an impact on the drug detachment from the carrier surface. Thirdly, the proportion of fine lactose particles present in the carrier is known to correlate with the final formulation performance (Section 1.4.5). For these reasons, particle sizing is one of the most fundamental characterisation techniques in inhalation product manufacturing.

When a monochromatic ray of light with an intensity of I_0 interacts with a particle, the light can be absorbed, refracted or scattered. Laser diffraction is a particle sizing technique based on measuring the angle of the scattered light, θ, as a result of an interaction with a particle. The smaller the particle, the larger the angle of scattered light. Also, the smaller the particle, the smaller the intensity of the scattered light, I_s (Newton 1982). These principles are illustrated in Figure 2.1, where the angle and the size of the arrows scattered from the particles represent the scattering angle and the intensity of the scattered light, respectively.
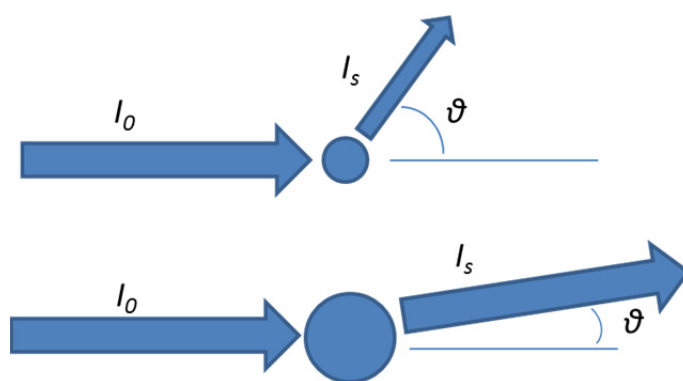
FIGURE 2.1 THE PRINCIPLE OF LASER DIFFRACTION WITH SMALL PARTICLES SCATTERING THE INCIDENT LIGHT I_0 AT A LARGE ANGLE θ AT LOW INTENSITY I_s (TOP) AND LARGE PARTICLES SCATTERING THE LIGHT AT SMALL ANGLE AT HIGH INTENSITY (BOTTOM)

Measuring the scattering data for a sample is based on the first principles described above. However, the scattering pattern for a polydisperse ensemble of particles can be complex (Newton 1982). To convert the measured scattering data into a particle size distribution, calculations with different assumptions have to be made. Two different theories, the Fraunhofer and Mie theories, are predominantly used for obtaining the particle size distributions from the scattering data. The Fraunhofer theory assumes the particles are much larger than the wavelength of the incident light. Additionally, the theory assumes no interactions other than scattering take place upon the interaction between the light and a particle. Mie theory requires more computational power to be solved but provides a more accurate model for analysing the scattering data by taking into account also the refraction and absorption of the light by a particle (Newton 1982).

To obtain laser diffraction data of high quality, the particles have to be dispersed to primary particles. However, simultaneously, the concentration of the particulate matter in the measurement zone has to be maintained low enough. That is because multiple light scattering, which is a phenomenon taking place in concentrated suspensions, results in the measured particle size being smaller than the true particle size. The phenomenon occurs when the light already scattered by one particle hits another particle and as a result is scattered again (Kokhanovsky *et al.* 2001). This phenomenon is illustrated in Figure 2.2.
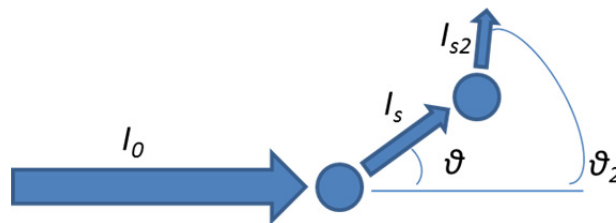
FIGURE 2.2 MULTIPLE LIGHT SCATTERING IS A PHENOMENON WHERE THE SCATTERED LIGHT (I_s) AT AN ANGLE θ IS RE-SCATTERED ON ITS WAY TO THE DETECTOR DUE TO A HIGH CONCENTRATION OF PARTICULATES. THIS RESULTS IN MEASUREMENT OF LOWER LIGHT INTENSITY I_{s2} AND A LARGER SCATTERING ANGLE θ_2 THAN THE TRUE VALUES. CONSEQUENTIALLY, A PARTICLE SIZE SMALLER THAN THE REAL SIZE IS REPORTED

2.2.1.2   *Measurement methodology*

The particle sizing experiments were conducted using a Helos laser diffraction unit in conjunction with Windox 5 software, both from Sympatec GmbH (Clausthal-Zellerfield, Germany). The system uses a 632.8 nm wavelength He-Ne laser as the light source. The optical bench was equipped with R3 and R4 Fourier lenses for focusing the diffraction patterns of equally sized particles to the same position on the array of detector rings. These lenses cover particle size ranges between 0.9 and 175 µm and 1.8 and 350 µm, respectively. The principle of using Fourier lens for focusing the scattering is illustrated in Figure 2.3.
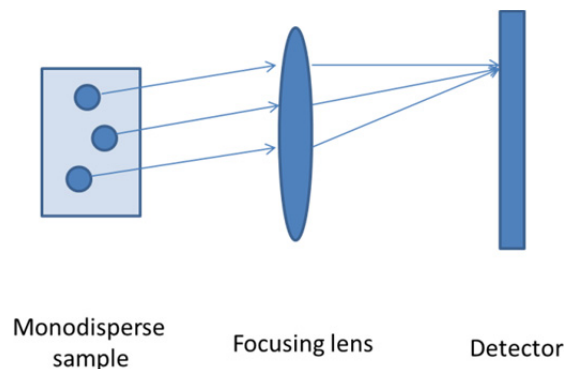
FIGURE 2.3 PRINCIPLE OF OPERATION OF THE FOCUSING LENS AND DETECTING THE SCATTERING FROM PARTICLES OF IDENTICAL SIZES ON THE SYMPATEC LASER DIFFRACTION SYSTEM

The high resolution Fraunhofer model provided by the Windox software (HRLD) was used for calculating the particle size distributions from the raw scattering data. According to the manufacturer, the HRLD calculation mode is able to take the background noise into account more accurately when converting the measurement data to the size distribution than the standard Fraunhofer model provided by the software.

The lactose powders were measured using the R4 lens and dispersed dry using the Rodos dry powder disperser in conjunction with the Vibri dry powder feeder (both from Sympatec). Before the measurements, the vacuum was switched on and the background scattering was recorded for 10 seconds. The sample was then introduced to the measurement zone with a steady flow rate. This was obtained by adjusting the gap between the funnel and the powder feeder tray to 2 mm. The feed rate was adjusted such that an optical concentration of between 0.5% and 5% was achieved. For most of the powders, the feed rate required to achieve this was approximately 30%. To ensure a high signal to noise ratio, no data was recorded until the threshold value of 0.5% for optical concentration was exceeded. A pressure titration was performed to assess the disperser pressure at which the particles were fully dispersed and no attrition took place. On the basis of the results, a disperser pressure of 2 bar was selected for measuring the lactose samples.

The particle size distributions of the drugs were measured using the R3 lens and the Cuvette wet dispersion system. The aliquots of the materials were dispersed in cyclohexane that contained 0.1% lecithin to aid the dispersion. The stir speed using the magnetic flea was set to 1500 rpm. Prior to the measurements, the background scattering caused by the dispersant was recorded for a period of 10 seconds. To achieve the primary particle size, ultrasound at 50% intensity of the maximum with the internal probe of the disperser system was applied for 1 minute for budesonide and for a total of 5 minutes in one minute intervals for fluticasone propionate. After every minute of sonication, a pause of one minute was applied to allow thermal gradients within the dispersant to dissipate. After the sonication, the final optical concentration was between 3 and 10%. 5 repeated measurements of 5 seconds duration were recorded for both the samples.

2.2.2 Scanning electron microscopy

2.2.2.1 Theory

Knowledge of the powder structure is important if an understanding of the different theories regulating the DPI performance in the presence of lactose fines is to be achieved. However, at present, suitable techniques for characterising the powder structure at the bulk level are scarce. Therefore, scanning electron microscopy (SEM) is often used for qualitative assessment of the formulation structure in DPI manufacturing.

When a conductive specimen is irradiated with a finely focused electron beam, secondary electron scattering and backscattering take place upon the interaction between the specimen surface and the electron beam. The backscattered electrons are defined as the electrons that scatter from the sample specimen through the same surface as they entered the specimen. Secondary electrons on the other hand are any low energy electrons scattered from the specimen. SEM is a surface visualisation technique based on detecting the secondary and backscattered electrons (Goldstein *et al.* 1992). The basic components of a scanning electron microscope are an electron source, condenser lenses, a deflection system, an objective lens, secondary electron and backscattering detectors and the sample holder, all held under vacuum. (Goldstein *et al.* 1992). A schematic of the instrumental setup and data collection is presented in Figure 2.4 and will be discussed in detail in the following paragraphs.

The electron source creates an electron beam with up to 40 keV of energy. However, the spatial resolution of SEM is affected by the diameter of the electron beam. The diameter of the beam produced by the electron source, also termed as the spot size, is too large to obtain high resolution images. Therefore, condenser lenses are used for focusing the beam and thus reducing the spot size. A beam with a small diameter has a high energy density. Consequentially, smaller spot sizes result in a high enough intensity for the scattered electrons. This way, good spatial resolution is ensured. For optimal resolution, the electron beam fine tuning on to the specimen surface is done by adjusting the focus with the objective lens (Goldstein *et al.* 1992).

The magnification of the scanning electron micrograph is adjusted by the deflection system. The system consists of two pairs of electromagnetic coils that split the electron beam to create a raster on the sample surface. The magnification of the image is determined by the ratio between the raster size of the display and the raster size on the surface of the specimen. Therefore, to enable the determination of the magnification, the deflection system of a SEM is also connected to the scan generator and the display.

Assuming the size of the display is fixed, higher magnifications result from reducing the raster distance on the specimen surface (Goldstein *et al.* 1992).

The detectors for the secondary and backscattered electrons consist of collector plates, a scintillator and an amplifier. The collector plates are positively charged screens that attract the scattered electrons. The collected electrons are then accelerated and sent to the scintillator. Upon contact between an electron and the scintillator, light is emitted. This light is sent to a photomultiplier tube and converted to an amplified electrical signal that is then displayed on the screen (Goldstein *et al.* 1992).
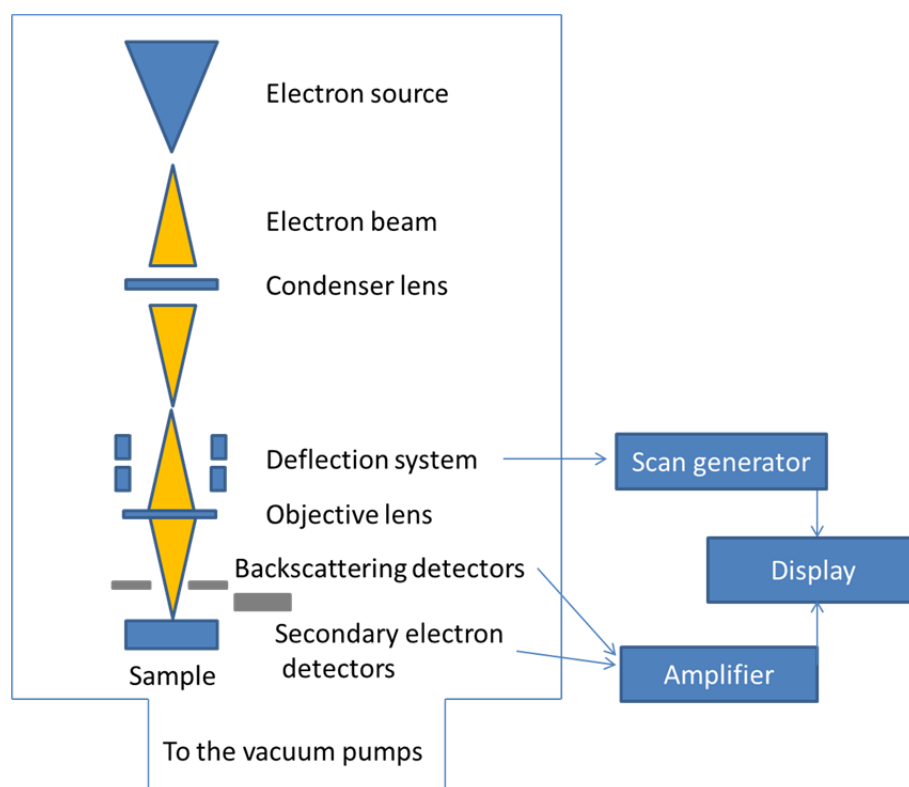
FIGURE 2.4 SCHEMATIC PRESENTATION OF CONFIGURATION OF A SCANNING ELECTRON MICROSCOPE

2.2.2.2   *Measurement methodology*

Pharmaceutical powders are electrical insulators. Therefore, SEM imaging of these materials is impossible unless a conductive coating is applied. The materials under investigation in the current study were mounted on conductive, sticky carbon tabs. The samples were then coated with gold under vacuum using an Edwards Sputter Coater (Edwards, Israel). Sputter coating is a process where atoms are created from a target by means of highly energetic collisions with neutral molecules or atoms under vacuum. These atoms are then deposited on the surface of the specimen to be coated (Goldstein

et al. 1992). A coating time of 5.5 minutes was applied for sample preparation in the current study.

A JEOL-6480LV scanning electron microscope (Jeol, Tokyo, Japan) was used for imaging the samples. The acceleration voltage applied was 10 keV. The spot size was set to 15 and the samples were observed at a magnification of 900x.

2.2.3 Bulk and tapped density, Hausner ratio and the Carr Index

2.2.3.1 Theory

One aim of the project was to assess the impact of increasing cohesion of the carrier on the DPI formulation performance. The Hausner ratio (HR) and Carr index (CI) have traditionally been used as measures of powder flow properties within the pharmaceutical industry. Both these parameters are calculated based on the bulk and tapped densities of the powders.

Bulk density (ρ_B) of a powder describes how closely the particles pack when allowed to settle under gravity. The bulk density is determined by the force balance between the gravitational and interparticulate forces within the bulk powders (Mohammadi *et al.* 1997). It was discussed in the introduction (Section 1.2.3.3) that in free flowing powders, the magnitude of the gravitational forces is significantly higher than the magnitude of the interparticulate forces. Consequentially, gravitational forces prevail in free flowing powders and the particles in the bulk powder pack closely, resulting in a high bulk density. In contrast, in cohesive powders the interparticulate forces dominate over the gravitational forces. This results in a more open packing structure, and consequentially in a low bulk density, for cohesive powders.

When the tapped density (ρ_T) of a powder is measured, the force balance between gravitational and interparticulate forces is altered by the mechanical forces induced by the vibrations (Mohammadi *et al.* 1997). For free flowing powders, the application of mechanical forces does not significantly change the packing characteristics of the bulk powder. This is because gravitational forces were significantly larger than the interparticulate forces in the first place. Therefore, no significant changes in the packing densities of free flowing powders are seen as a result of tapping. In contrast, for cohesive powders, the mechanical forces induced by the tapping combined with the gravitational forces experienced by the particles are often enough to overcome the interparticulate forces. This results in a more compact packing structure, and thus a higher density, upon tapping.

The Hausner ratio is a parameter describing the friction of the particles as they move past each other in a bulk powder (Hausner 1967). The Hausner ratio is defined by the ratio between the tapped and bulk density of the powder as per Equation 2.1.

$$HR = \frac{\rho_T}{\rho_B}$$

Shortly after the Hausner ratio was reported in the literature, it was realised that the parameter correlated with the parameters describing the flow properties of powders. Cohesive powders demonstrate higher values of Hausner ratio than free flowing powders (Grey *et al.* 1969).

The Carr index was introduced at a similar time to the Hausner ratio (Carr 1965). The Carr index is calculated on the basis of the bulk and the tapped densities of the powder according to Equation 2.2. The higher the value of Carr index, the more cohesive the powder is.

$$CI = \frac{\rho_T - \rho_B}{\rho_T} * 100$$

2.2.3.2   Measurement methodology

The bulk and tapped densities were measured using the FT4 powder rheometer (Freeman Technology, Tewkesbury, UK). For the measurement of bulk density, a 25 mm diameter, 20 ml volume split measurement vessel was placed on the measurement table of the instrument and the weight of the vessel was tared. The vessel was then filled with the powder under investigation. A conditioning cycle was then run to remove the influence of the filling procedure on the powder packing. For measuring the bulk density, after the conditioning cycle, the measurement vessel was split and the split mass recorded. For measuring the tapped density, the measurement vessel was placed on a jolting volumeter (J. Engelsmann, Germany)) and 250 taps were applied. The measurement vessel was then transferred back on to the measurement table of the FT4, the vessel was split and the split mass recorded. All the measurements were performed in triplicate for all the powders. The results were calculated by dividing the mass of the powder in the measurement vessel after the cell had been split by 20 ml, which was the volume of the split cell.

2.3 METHODS FOR CHARACTERISING THE POWDER FLOW AND FLUIDISATION PROPERTIES

2.3.1 Importance of characterising powder flow properties

It was discussed in the introduction of the thesis (Section 1.2.1) that powders exhibit properties of gases (compressibility), liquids (fluidised state, pouring), and solids (plastic and elastic deformation). It was also shown that, for example, the fluidisation behaviour of the powders is closely related to the cohesion of the powder bulk. Therefore, to be able to predict the behaviour of powders under different processing conditions, knowledge of the powder flow properties is of paramount importance.

In addition, it was discussed in the introduction that powders have a memory of the past consolidation history (Section 1.2.1) Therefore, the measurement methodology will greatly affect the results obtained. Consequentially, it is important to understand the conditions that prevail in the powder during the characterisation and the process; it is unlikely that the flow properties of a powder measured under high consolidation stresses describe the fluidisation behaviour of the powder very accurately. To simulate different powder handling process conditions, such as flow in hoppers or the fluidisation behaviour, as precisely as possible, different powder flow characterisation techniques are commercially available. These techniques can be divided in to two classes, namely static and dynamic methods (Krantz *et al.* 2009). During static measurements the powders are consolidated. During dynamic testing no consolidation stresses are applied on the powder and the particles are free to move during the measurements (Krantz *et al.* 2009).

For the carriers and the DPI formulations themselves, low to moderate consolidation stresses are encountered during manufacturing and storage. Therefore, characterising the formulations at low consolidation stresses or using dynamic methods should give the results that are the most relevant to the final product performance. However, dynamic methods are often empirical whereas static methods are based on well described principles. Therefore, also static characterisation was performed in the current study.

2.3.2　Static characterisation – Schulze Ring Shear tester

2.3.2.1　Theory

2.3.2.1.1　Mohr circles

When a Newtonian liquid is stored in a bulk container, the pressure applied on the surface of the liquid is evenly distributed against the container walls (Schulze 2010). If the walls are removed, the system will spontaneously return to the equilibrium state where the vertical and horizontal forces are equal, i.e. to a puddle of liquid. In contrary, in powders, the horizontal stress is always a result of applying vertical stress (Schulze 2010). Therefore, for example, in the absence of stress from above, a sand castle will retain its shape. However, if weight is applied on the top of the sand castle, the sand castle will deform in the horizontal direction. Yet a sandcastle may be ruined, but it will rarely be completely flattened by consolidating the top. That is because the force balance found in liquids is inexistent in powders. Therefore, stresses can be found in powders even at rest (Schulze 2010). The magnitude of horizontal stresses σ_h for liquid and powder stored in a container compared to the vertical stress σ_v applied on the surface are illustrated in Figure 2.5.

$$\sigma_v \qquad \sigma_v$$

$$\sigma_h \qquad \sigma_h$$

Newtonian liquid
in a container
$\sigma_v = \sigma_h$

Bulk powder in a
container
$\sigma_v > \sigma_h$
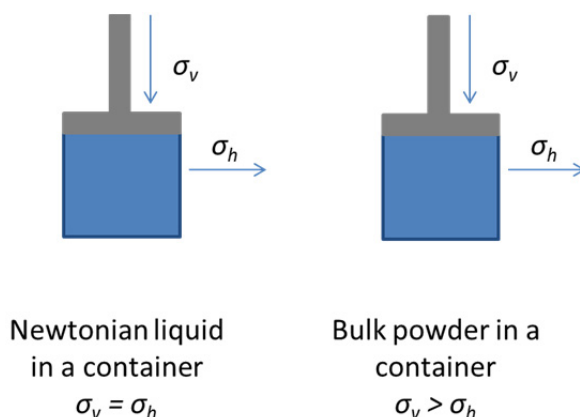
FIGURE 2.5 THE RELATIONSHIP BETWEEN THE VERTICAL STRESS σ_v AND HORIZONTAL STRESS σ_h IN NEWTONIAN LIQUID (LEFT) AND IN BULK POWDER (RIGHT)

The rheological properties of liquids under pressure and shear stress are simply defined by the force balance with the forces distributed evenly throughout the liquid. Due to the lack of the force balance, defining the rheological properties of powders under consolidation and shear stress is more complicated. However, the stresses within the powder bulk can be described using Mohr stress circles (Schulze 2010). The principle of Mohr circles is illustrated in Figure 2.6. The bottom left corner of the schematic shows a powder in a container under vertical consolidation stress σ_v. The powder in the container is sheared at shear stress of τ. As a result of the shear stress, different shear planes appear in the powder bulk. The schematic in the top left corner of Figure 2.6 is a

magnification of one of the sections of the powder created by the shear plane. The shear plane has formed at an angle α in the powder bulk. The Mohr circle for this shear plane is presented on the right hand side of the schematic. The relationship between the powder segment and the Mohr circle will be discussed in the following.

In the diagram for the Mohr circle, the y-axis represents the shear stress τ and the x-axis the consolidation stress σ. In the powder segment, the planes X and Y do not experience any shear stresses τ. Therefore, these two planes are described as points on the x-axis of the Mohr circle diagram, where τ is 0. It was discussed above that the horizontal stresses in powders are always a consequence of the vertical stresses, and therefore of smaller magnitude. Consequentially, σ_h is closer to the origin in the Mohr circle diagram than the σ_v. Both the centre and the radius of the Mohr circle are defined using the average between the horizontal and vertical consolidation stresses (Schulze 2010). This is also illustrated in Figure 2.6.

The plane A in the powder segment that is shown on the top left of Figure 2.6, is a shear plane confining the segment highlighted in light blue in the insert on the bottom left of the schematic. The shear plane A has formed at an angle of α as a consequence of the shear stress τ_α. This plane experiences a consolidation stress of σ_α. The magnitude of the consolidation stress experienced by a shear plane within the bulk powder is always smaller than the vertical consolidation stress σ_v but larger than the horizontal consolidation stress σ_h. When the values of the shear stress τ_α and consolidation stress σ_α for a shear plane within the powder bulk are plotted against each other, a point on the perimeter of the Mohr circle is obtained. If the same procedure is repeated for all the possible shear plane angles, the perimeter of the Mohr circle will be fully defined (Schulze 2010).
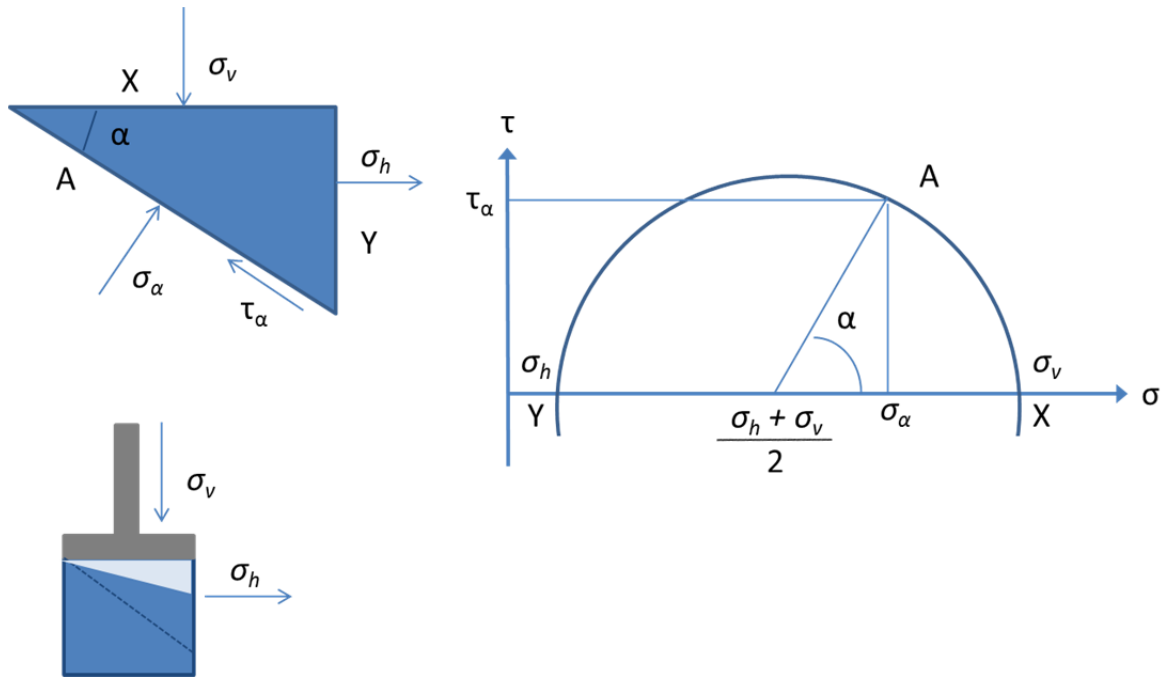
FIGURE 2.6 THE PRINCIPLE OF MOHR CIRCLES AND THE RELATION OF THE PARAMETERS TO THE POWDER UNDER STRESS. **A, X** AND **Y** ARE PLANES DESCRIBING THE POWDER SEGMENT HIGHLIGHTED LIGHT BLUE IN THE SCHEMATIC ON THE BOTTOM LEFT, A CLOSE UP OF WHICH IS PRESENTED ON THE TOP LEFT OF THE SCHEMATIC. α DEFINES THE ANGLE BETWEEN PLANES **X** AND **A**. σ_v, σ_h, AND σ_α ARE CONSOLIDATION STRESSES ENCOUNTERED BY THE POWDER SEGMENT IN VERTICAL, HORIZONTAL AND NORMAL TO PLANE **A** DIRECTIONS CORRESPONDINGLY. τ_α IS THE SHEAR STRESS ACTING ON PLANE **A**. THESE PARAMETERS FULLY DEFINE THE **M**OHR CIRCLE SHOWN ON THE RIGHT OF THE SCHEMATIC.

An important consequence of the Mohr stress circle analysis of powder properties is that the powder properties can only be defined if at least two of the parameters are known (Schulze 2010). Following on from the definition of the Mohr stress circle, the simplest way for constructing the Mohr stress circle for a powder would be using the average of the vertical and horizontal consolidation stresses, σ_v and σ_h, to define the centre and the radius for the circle. However, in practice, defining these values is not straightforward. Therefore, a reverse approach for determining the Mohr stress circle for a powder from a yield locus that can be easily measured is often applied. The yield locus and the relationship between the yield locus and the Mohr circles will be introduced in the following.

2.3.2.1.2   Yield locus

Returning to the example of the sandcastle, another important feature of a sandcastle is that the more consolidated the sand in the container before the bucket is turned over, the

stronger the resulting sand castle. This example illustrates that the magnitude of the consolidation stress applied has a significant impact on the flow properties of the powder, with higher consolidation stresses resulting in a powder more resistant to deformation and flow. Therefore, when characterising powder flow properties, the results will strongly depend on the magnitude of the consolidation stresses experienced by the powder before the testing. Therefore, in static powder testing, the powder properties are characterised by defining a yield locus for a powder. The yield locus describes the properties of the powder after application of a particular consolidation stress (Schulze *et al.* 2003).

The process of constructing the yield locus for a powder is illustrated in Figure 2.7. The powder is first consolidated under a pre-defined pre-shear consolidation stress σ_{Pre}. The sample is then sheared until a steady state flow is obtained. The steady state flow is defined as a state where neither the density nor the shear required for maintaining the movement of the powder change over time. This is illustrated as the flat plateau in the shear vs. time curve during the first phase, as shown on the left hand side diagram in Figure 2.7. The shear and the consolidation stresses are then eased off before a pre-defined consolidation stress σ_{Shear}, lower than the σ_{Pre}, is applied and the powder is sheared until failure to resist the flow. The failure to resist flow is characterised by the sharp decrease in the required shear stress, and is illustrated in the second phase of the diagram on the left hand side in Figure 2.7. The powder is then returned to the initial state by repeating the pre-shear step before another shearing phase at a different, pre-defined consolidation level is applied. The yield locus that is shown on the right in Figure 2.7, is achieved by plotting the pairs of values for the consolidation stresses σ and the corresponding values of shear stresses τ against each other (Schulze *et al.* 2003).
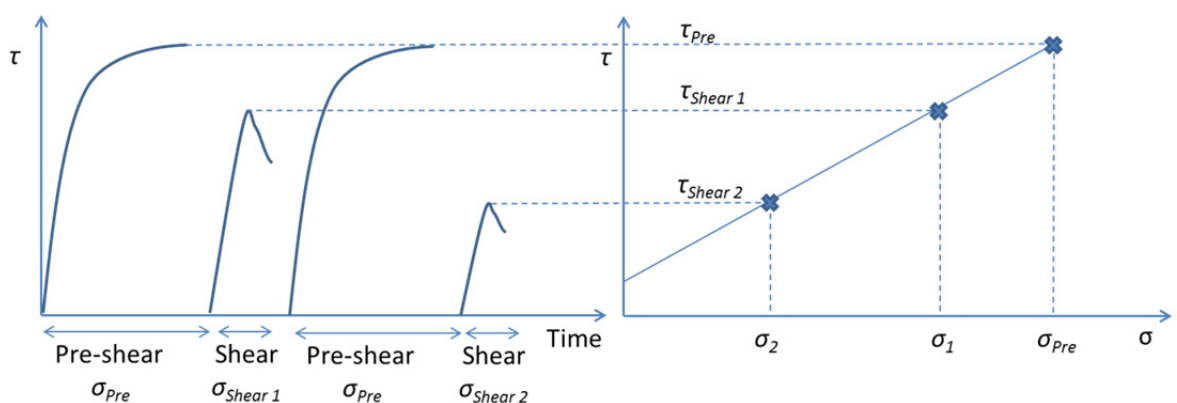
FIGURE 2.7 OBTAINING STEADY STATE FLOW UNDER A PRE-SHEAR STRESS σ_{Pre} AND SUBSEQUENT SHEARING OF THE SAMPLE AT A LOWER, PRE-DEFINED CONSOLIDATION STRESS σ_{Shear} UNTIL FAILURE (LEFT) AND THE CONSTRUCTION OF THE YIELD LOCUS ON THE BASIS OF THE PRE-SHEAR AND SHEAR EXPERIMENTS. ADAPTED FROM SCHULZE *ET AL.* (2003)

2.3.2.1.3   The relationship between the yield locus, the Mohr circle and the powder flow properties

Based on the measured yield locus, two different Mohr stress circles for a powder under a certain stress can be constructed (Schulze *et al.* 2003). These circles are shown in Figure 2.8. The larger of the circles is constructed by using the end point of the yield locus, i.e. the pre-shear point (τ_{Pre}, σ_{Pre}). This point on the yield locus is shown in the right hand side of Figure 2.7. This point is the intersect for the tangent between the yield locus and the larger Mohr circle. The larger Mohr circle defines the vertical consolidation stress of the powder at the pre-sheared state, i.e. at steady flow. This is indicated as the point σ_1 in Figure 2.8. The smaller Mohr stress circle intersects the origin of the graph and is tangential to the yield locus. This stress circle represents the stresses in the powder if stored in a container without walls. Therefore, the principal stress labelled as σ_c in Figure 2.8 is defined as the unconfined yield strength.
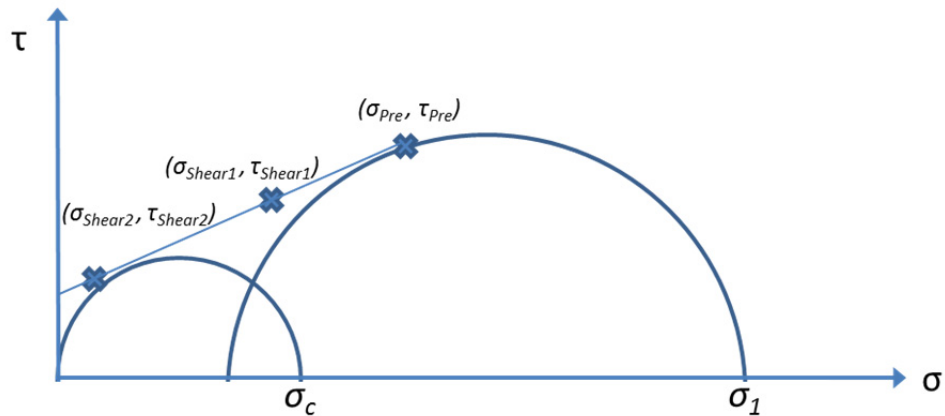
FIGURE 2.8 CONSTRUCTING THE MOHR CIRCLE FOR A POWDER ON THE BASIS OF THE YIELD LOCUS. THE THREE LABELLED POINTS CORRESPOND TO THOSE IN FIGURE 2.7. σ_1 IS THE CONSOLIDATION STRESS AND σ_c THE UNCONFINED YIELD STRENGTH

Because the powder properties are heavily dependent on the consolidation stress, the powder flow properties from static tests are often reported as the flow function, *ffc*. The flow function of a powder is defined as the ratio between the consolidation stress σ_1 and the unconfined yield strength σ_c as per Equation 2.3 (Schulze *et al.* 2003).

$$ff_c = \frac{\sigma_1}{\sigma_c}$$

EQUATION 2. 3

The larger the value of *ffc* for a powder, the better the flow properties it exhibits (Schulze *et al.* 2003). The classification of powder flow properties according to values of *ffc* is summarised in Table 2.1.

ff_c	Powder flowability
<1	Not flowing
1-2	Very cohesive
2-4	Cohesive
4-10	Easy flowing
>10	Free flowing

2.3.2.2   Measurement methodology

The samples were characterised using the RST-XS ring shear tester controlled by RST-Control 95 software (both from Dietmar Schulze, Germany). The 30 ml annular shear cell was filled with the powder under investigation and the surface of the powder was subsequently evened out by a spatula. The filled shear cell was then mounted on the measurement table of the instrument and the lid of the shear cell was carefully placed on top of the sample without compacting the powder. For applying the normal force, the loading rod was then inserted. The tie rods were connected to the shear cell and the loading beams that measure the shear force. The pre-shear consolidation stress (σ_{Pre}) was set to 1 kPa in the software and the sample was then sheared until steady state flow was achieved. The shear stress at this stage was measured and used as τ_{Pre}. The sample was then consolidated at 750, 500 and 250 Pa and the corresponding shear stresses measured for each of the consolidation stresses. Before each of the measurements, the pre-shear step was repeated to return the sample to its initial state. The yield locus and the corresponding Mohr stress circles were then constructed using the instrument software. The results were reported as the flowability number ff_c. The measurements were performed in triplicate for all the samples characterised.

2.3.3   Dynamic characterisation – FT4 powder rheometer

2.3.3.1   Theory

In static powder testing the movement of particles relative to each other is limited due to the consolidation stresses from above. In contrast, in dynamic powder characterisation, the powder is not consolidated during the measurements. This means the particles can move freely relative to each other in the powder bulk during the measurements (Krantz *et al.* 2009). This situation is similar to a dose of DPI formulation in a capsule, where the powder occupies the volume of the capsule, which is often considerably larger than the volume of the powder containing the dose. Therefore, dynamic methods are anticipated to

be suitable for characterising the flow properties that are relevant to fluidisation and deagglomeration behaviour of DPI formulations and excipients.

The approach of the FT4 powder tester for determining the flow properties of powders is empirical and cannot be described theoretically like the static methods. Different measurements can be performed using the FT4 powder rheometer (Freeman 2007). These include, for example, measurements of the powder flow of the bulk or aerated powders or the compressibility of the powders. All the measurements reported in the current thesis are based on determining the torque (τ) and a downward force (F) required to keep a blade moving though a powder bed at a constant speed and helical angle as a function of height (h) of the blade within the powder bed. This principle of the measurements is illustrated in Figure 2.9. The force and torque profiles as a function of the blade height are then integrated to produce total energy for initiating powder flow (Freeman 2007).
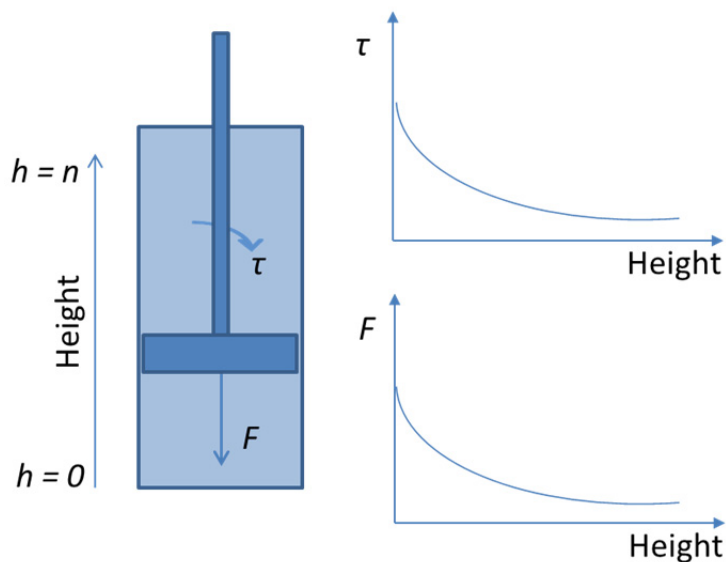
FIGURE 2.9 THE PRINCIPLE OF CHARACTERISING THE RESISTANCE OF A POWDER TO FLOW USING THE FT4 POWDER RHEOMETER WITH THE TORQUE (τ) AND FORCE (F) MEASURED AS A FUNCTION OF THE BLADE HEIGHT (h)

The flow patterns of the powder, and thus the measured energies, during the measurements are influenced by the helical angle of the blade movement, α, and the blade tip speed. These parameters can be altered for the measurements, so that relevant information for the powder properties under process conditions of practical interest can be recorded. The blade tip speed and the helical angle trigonometrically define the rotational and vertical speed for the blade assembly, as illustrated in Figure 2.10.
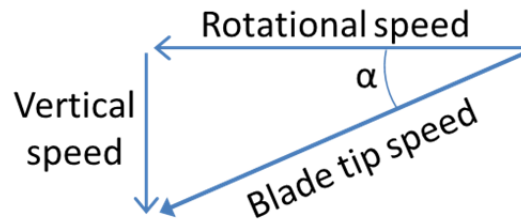
FIGURE 2.10 THE BLADE TIP SPEED AND THE HELICAL ANGLE α DEFINE THE ROTATIONAL AND VERTICAL SPEED OF THE BLADE ASSEMBLY

The blade geometry is designed so that different powder flow patterns can be initiated depending on the direction of the helical movement. An anti-clockwise motion of the blade with a positive helical angle produces a bulldozing action. Clockwise movement of the blade, corresponding to negative helical angles, results in a gentle displacement of the powder (Freeman 2007). The clockwise motion of the blade, illustrated on the right in Figure 2.11, is used for erasing the packing history of the powder by gently displacing the powder before the measurements are performed. This step, termed the conditioning cycle, results in a loosely packed and constant initial state of powder packing before the measurements are performed. Therefore, it removes the operator influence on the results (Freeman 2007).

The bulldozing action of the anti-clockwise movement of the blade, shown on the left in Figure 2.11, results in the forces created by the blade movement being transferred throughout the powder bulk (Freeman 2007). The powder packing structure and its influence on the extent of the force transmission zone ahead of the blade are essential in understanding the results of powder characterisation when using the FT4 powder rheometer. Free flowing powders normally have higher bulk densities than cohesive powders (Thalberg *et al.* 2004). As discussed earlier in the chapter (Section 2.2.3.1), this means that the particles in free flowing powders are more closely packed than in cohesive powders. Therefore, free flowing powders have less air within the powder bulk structure. Only particles will create resistance to the blade movement and any air trapped in between the particles does not resist the blade movement. Therefore, when the blade is moved though a free flowing powder at a constant speed, the force transmission zone ahead of the blade is larger than it would be for a cohesive powder.
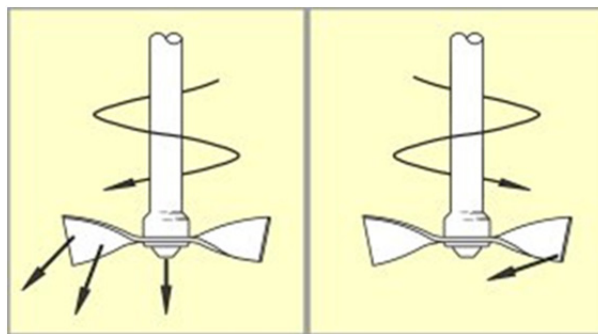
FIGURE 2.11 THE ANTI-CLOCKWISE MOTION OF THE BLADE PRODUCING A BULLDOZING ACTION (LEFT) AND THE CLOCKWISE MOTION OF THE BLADE RESULTING IN A GENTLE DISPLACEMENT OF THE POWDER (RIGHT). THE IMAGES ARE COURTESY OF AND REPRODUCED WITH THE PERMISSION OF FREEMAN TECHNOLOGY

The normalised basic flow energy (BFE_{Norm}) measurement characterises the resistance of one gram of the powder to flow at a constant speed (Freeman 2007). The more cohesive the powder, the lower the basic flow energy. This may appear unintuitive at first. However, as discussed above, this can be explained by the packing structure and resulting extent of the force transmission zone ahead of the blade. Therefore, the force and torque required to maintain a constant speed of the blade in a free flowing powder is higher than in a cohesive powder, resulting in a higher value of BFE_{Norm} (Freeman 2007).

Flow rate index (FRI) is a dimensionless parameter describing how different powders react to changes in the rate at which they are moved around. The more cohesive the powder, the more sensitive it is to the changes in the flow rate (Freeman 2007). Cohesive powders have low packing density and therefore more air entrapped within the powder bulk. When the blade is moved though a cohesive powder slowly, the air within the powder bulk ahead of the blade has enough time to escape from the structure as a result of the forces created by the blade movement. Consequentially, the force transmission zone ahead of the blade is extended at slow tip speeds. Therefore, at slow tip speeds, the force and the torque required to keep the blade moving though the powder bulk at constant speed are higher than at higher tip speeds. In contrast, the force and torque required for maintaining a constant tip speed in free flowing powders is not affected to such a great extent by changes in the tip speed. This is because the powders have less entrapped air in the first place. Therefore, the extent of the force transmission zone is not altered upon changing the flow rate.

The normalised fluidisation energy (FE_{Norm}) defines the energy required to keep the blade moving through one gram of fluidised powder bed at a constant speed. Particulate and aggregative fluidisation were discussed in the introduction of the thesis (Section 1.2.3.5). The results of the fluidisation energy measurements can be explained by the combination

of the force transmission zone ahead of the blade and the extent of particulate fluidisation in the powder. To illustrate this, the following example should be considered. If the aeration test was performed without any powder in the measurement cell but with the fluidising gas flow enabled, no resistance would be encountered by the blade. Therefore, the measured flow energy would be zero. Following this, the closer to full particulate fluidisation the powder is, the lower the measured fluidisation energy will be. This is because the more completely fluidised the powder is, the less likely it is that a fluidised particle will encounter another one as the blade is moved through the bed of fluidised powder. Therefore, the blade encounters very little resistance and the measured fluidisation energy is low. The larger the fluidised agglomerates, the more likely it is that the agglomerates will interact with each other as a result of the impelling action of the blade. Therefore, the force transmission zone will be large and the measured energy high.

Dynamic flow index (DFI) describes the reactivity of the powder to an air flow through the powder bed. The value of DFI is calculated as a ratio between normalised basic flow energy (BFE_{Norm}) and the normalised fluidisation energy (FE_{Norm}) of a powder. The higher the value of DFI, the more the powder structure is affected by the fluidising gas flowing through the powder bulk. Free flowing powders have high bulk densities but are easily aerated upon passing fluidising gas through the powder bed. Cohesive powders on the other hand have a loose packing structure and the gas permeation through the powder bulk is not as complete as for free flowing powders.

2.3.3.2   Measurement methodology

The BFE_{Norm} and FRI were measured during the same test procedure. For the measurement, the powder was loaded in the 25mm bore diameter, 20 ml volume split vessel. At first, a downward conditioning cycle was run at a tip speed of -40 mm/s and a helical angle of 5° to remove the packing history of the powder. This was followed by an upward conditioning cycle at a tip speed of 40 mm/s and a helical angle of 5°. After the full conditioning cycle, the measurement cell was split and the split mass recorded. Consecutive cycles of conditioning and measuring the BFE were then repeated seven times to assess the stability of the powder under agitation. The downward BFE measurement cycle was performed at a tip speed of -100 mm/s and helical angle of -5°. After each of the BFE measurements, the blade was moved upward at a tip speed of 40 mm/s and helical angle of -5°. If the BFE measured during the repeated measurements remained stable, the BFE recorded in the 7th test was divided by the split mass to calculate the BFE_{Norm}. To measure the FRI, four additional measurement cycles at tip speeds -100, -70, -40 and -10 mm/s were run with an unaltered conditioning cycle

between each of them. The FRI is calculated as the ratio of the flow energy measured at a tip speed of -10mm/s over the flow energy measured at -100 mm/s tip speed.

The FE_{Norm} and DFI were measured during the same measurement program. Also for these measurements, the powder was loaded in the 25mm bore diameter, 20ml volume split vessel. At first, a conditioning cycle was repeated 8 times at a tip speed of -60 mm/s downward and 60 mm/s upward and helical angles of 5° and -5°, respectively, to remove the packing history of the powder. The high number of conditioning cycles was seen to improve the reproducibility of the measurements. The improvement was attributed to obtaining a uniform powder structure and thus avoiding the formation of rat holes in the cohesive powders. After the conditioning cycles, the measurement cell was split. The cycle of the conditioning and the measuring of the flow energy was then repeated at different air velocities, controlled by the Aeration Control Unit (ACU) accessory of the FT4. The air velocity was adjusted such that, during the conditioning cycle, the air velocity was equal to the air velocity of the following measurement. The measurement cycles at the different air velocities were performed at a tip speed of -100 mm/s and a helical angle of -5°, followed by an upward motion at a tip speed of 60mm/s and a helical angle of 10°.

2.3.4 Dynamic characterisation - Fluidisation and defluidisation properties by pressure drop measurements

2.3.4.1   Theory

The fluidisation properties of powders can also be dynamically studied by measuring the pressure drop across the powder bed when fluidising gas is passed through a column of powder (Valverde *et al.* 1998). Unlike the powder testing based on measuring the torque and force required to move an impeller blade through powder, characterising the cohesion of powders by pressure drop measurements during fluidisation and defluidisation is an accepted and theoretically well-established technique (Castellanos 2005). The pressure drop generated across the powder bed is caused by interparticle forces and the friction between the particles and the fluidising gas (Holdich 2002). Figure 2.12 presents a typical pressure drop curve for a cohesive powder as the velocity of the fluidising gas is increased and decreased in a stepwise fashion. During the fluidisation branch (solid line), the pressure drop initially increases linearly as the velocity of the fluidising gas is increased. The slope upon increasing the velocity of the fluidising gas is defined by the Carman-Kozeny law (Carman 1956). The law describes the relationship between the pressure drop and the void fraction within the powder bed with larger void fractions

resulting in a smaller slope. Therefore, the slope describes the packing structure of the bulk powder.

For a free-flowing powder with very weak interparticulate forces the pressure drop continues to increase up to the fluidising gas velocity labelled (a) in Figure 2.12. At this point, for a free-flowing powder, the weight of the powder is fully supported by the drag force exerted by the fluidising gas and the powder becomes fully fluidised. The pressure drop measured across the powder bed equals the weight of the powder bed per cross-sectional area of the fluidising vessel. However, for cohesive powders, interparticulate forces have to be overcome before fluidisation can occur. Therefore, the pressure drop for a cohesive powder would continue to increase above the weight of the powder to the gas velocity labelled as (b) in Figure 2.12. At this point, the pressure drop is equal to the weight of the powder and the strength of the cohesive forces within the powder bed (Valverde *et al.* 2000). With increasing air flow velocities, the pressure drop returns to a level equal to that of the weight of the powder bed. Thus, this overshoot in the pressure drop, indicated by the arrow labelled as σ, provides an indication of the strength of the cohesive forces within the powder bed (Valverde *et al.* 1998). Some studies, however, have shown that the pressure drop hysteresis is also related to the wall friction created between the particles and the walls of the fluidising vessel and that the friction must therefore be taken into account (Loezos *et al.* 2002).

The dashed line in Figure 2.12 illustrates the pressure drop of the powder bed when the fluidising gas velocity is decreased stepwise. The pressure drop hysteresis is absent on this defluidisation branch. This is because all the cohesive forces within the powder bed have been overcome during the fluidisation of the powder. The particles are re-forming a packing structure as they settle under gravity when the drag forces exerted by the fluidising gas become inadequate to maintain the particles suspended.

The gas velocity at which the powder becomes fully fluidised is the minimum fluidisation velocity (U_{mf}). In some previous studies, the minimum fluidisation velocity has been used as a measure of powder cohesion both experimentally (Wright *et al.* 1998) and theoretically (Weber *et al.* 2006). These studies concluded that the higher the minimum fluidisation velocity, the more cohesive the powder. Depending on the powder properties, the minimum fluidisation velocity can be defined as three different points, indicated by a (Castellanos 2005), b (Shur *et al.* 2008a) and c (Delebarre *et al.* 2004) in Figure 2.12. Typical DPI formulations exhibit a certain degree of cohesion. Therefore, during the current study, point b was used as the minimum fluidisation velocity.
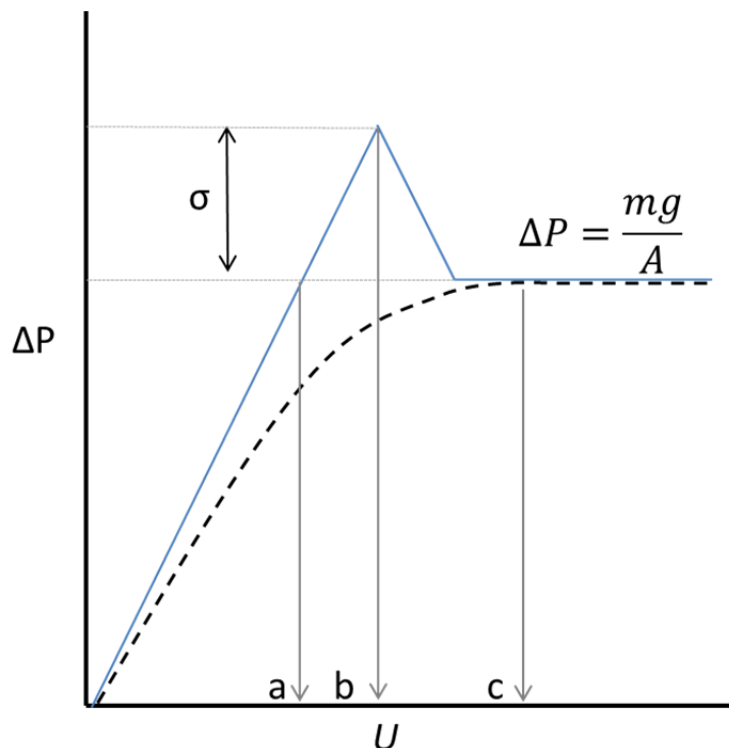
FIGURE 2.12 SCHEMATIC OF A PRESSURE DROP CURVE DURING FLUIDISATION (SOLID LINE) AND DEFLUIDISATION (DASHED LINE) EXPERIMENTS OF A COHESIVE POWDER AS A FUNCTION OF THE FLUIDISING GAS VELOCITY. POINTS a, b AND c HIGHLIGHT THE DIFFERENT DEFINITIONS FOR THE MINIMUM FLUIDISATION VELOCITY AND σ REPRESENTS THE COHESIVE STRENGTH OF THE POWDER. THE EQUATION DESCRIBES THE THEORETICAL PRESSURE DROP FOR A POWDER BED WITH A MASS OF m AND CROSS-SECTIONAL AREA OF A

To the author's knowledge, the FT4 rheometer has not been previously used for measuring the pressure drop of powders. Therefore, the steps followed during method development will be described in detail with supporting results in Chapter 3, section 3.5.

2.4 DRUG CONTENT ASSAY BY HPLC

2.4.1 Theory

To assess the performance of the DPI formulations, an analytical method is required for quantifying the amount of drug in various samples. High performance liquid chromatography (HPLC) was used for assaying the drug contents in the current study.

HPLC is a widely used analytical technique where analytes in a solution are separated and quantified. As in any chromatographic technique, the separation of analytes in HPLC is based on the distribution coefficient of the analyte (D), which is defined as the ratio between the affinity of the analyte to the stationary phase (A_s) and to the mobile phase (A_m). In HPLC, the stationary phase is packed in a column, through which the mobile

phase is pumped. Once eluted, the concentration of the analytes can be quantified by using, for example, spectrophotometric, fluorescence or mass spectrometric methods (Lough *et al.* 1995).

The stationary phase material, such as octadecyl silane (ODS), for HPLC is often immobilised on the surface of material consisting of small silica particles. These particles are packed in the column in such a way that the column has a low permeability. Therefore, pumps are required to maintain a constant flow of the mobile phase through the column. However, because of the low permeability, pumping the mobile phase creates a pressure differential between the inlet and the outlet of the column. In HPLC, the pressure differential is the driving force for the mobile phase movement through the column. Despite the high packing density of the column, a descent flow rate of the mobile phase is achieved due to the pressure differential. Consequentially, more efficient separation can be achieved with HPLC in equivalent time when compared with traditional, gravity driven open column liquid chromatography (Lough *et al.* 1995). The higher the pressure the pump can create, the smaller the particle size of the stationary phase can be. This improves the separation efficiency due to the increased surface area of the stationary phase. For the same reason, increasing the column length in HPLC improves the separation of analytes (Lough *et al.* 1995)

Retention time is the time that it takes for an analyte to be eluted. In a mixture of analytes, a large enough difference between the retention times for the different analytes is needed if a baseline resolution is to be achieved. The retention time is dependent on the analyte interactions with the stationary and mobile phases. Therefore, the resolution of the method can be influenced by altering the composition of one of the phases. The choice of stationary phase materials is often limited and some of the less common columns are very expensive. Therefore, the easiest and the most economical way of modifying the retention times of analytes to achieve a complete separation is changing the composition of the mobile phase. For example, if the stationary phase is non-polar, non-polar analytes will have longer retention times than polar analytes. The retention times of non-polar molecules can be increased by adding water to the mobile phase. This causes the analyte molecules to favour the hydrophobic stationary phase over the hydrophilic mobile phase. Similarly, the addition of water in the mobile phase has an opposite effect on the retention times of polar analytes, decreasing the retention time (Lough *et al.* 1995).

Once separated within the column, the analytes can be quantified by using, for example, UV spectrophotometry or mass spectrometry for detection. The area under the curve or the peak height, depending on the method of detection, is proportional to the amount of the analyte in the sample. If standards with known amounts of the analyte are run with the

samples, the amount in the samples can be quantified based on the calibration (Lough *et al.* 1995).

2.4.2 Measurement methodology

In the current study, HPLC was used for quantifying the concentration of drug in binary mixtures with lactose. Due to the chemical similarity of the drug molecules used, principally the same method could be used for both budesonide and fluticasone propionate. The samples were dissolved in a mobile phase that consisted of 20% water, 35% acetonitrile and 45% methanol. The mobile phase was pumped through the system at a flow rate of 1.5 ml/min using a Jasco PU-980 pump (Jasco, Tokyo, Japan). 100 µl of the samples were injected into the system using a Jasco AS-950 autosampler (Jasco, Tokyo, Japan). The 250 mm long Hypersil-ODS column with an inner diameter of 4.6mm and packing material particle size of 5 µm (Thermo Scientific, Loughborough, UK) was held at 40°C using a Jasco CO-965 column oven (Jasco, Tokyo, Japan). The eluted drug was detected using a Jasco UV-975 detector (Jasco, Tokyo, Japan) at a wavelength of 244 nm for budesonide and 235 nm for fluticasone propionate. The retention time for budesonide was 3.75 min and 3.25 min for fluticasone propionate.

The amount of drug in the unknown samples was determined based on calibration for the area under the curve versus the concentration of standard samples that were run in every sample rack.

2.5 PREPARATION OF DRY POWDER INHALER FORMULATIONS

2.5.1 Background

To study the impact of the carrier properties on the final formulation performance, model formulations were prepared. The following section of the chapter describes the processes involved in manufacturing the blends and assuring the quality of the blending.

Powder mixing is a fundamental process in DPI formulation, where the aim is to prepare a uniform formulation from two or more components. When mixing two powders that consist of equally sized, free flowing particles of equal density and that exhibit no significant interparticulate forces, mixing takes place by randomisation via diffusion or convection (Hersey 1975). However, in binary DPI formulations, the size difference between the drug particles and the large lactose carrier particles is often two orders of magnitude.

Therefore, the principles of random mixing are not applicable for the system. In a ternary DPI formulation, the situation is further complicated by the presence of the third component that can be polydisperse in size. For describing these kind of mixtures, Hersey (1975) was the first to introduce the concept of ordered mixing. In these mixtures, the blending takes place as a result of particle-particle interactions, also known as adhesive forces. The fine particle component is distributed on the surface of the large particles due to adhesive forces, such as electrostatic, capillary or van der Waals forces, taking place between the components. Therefore these mixtures have been later more appropriately termed as adhesive mixtures (Dickhoff *et al.* 2002).

For mixing to take place, movement of particles is required so that relocation of the particles within the mixture can take place. The particles can be moved around in a mixer for example by tumbling, shearing, fluidising or scooping (Harnby 2000). The energy input of the process can also be altered. Particles in free flowing powders can be moved around easily. Therefore, preparing uniform blends of free flowing powders is relatively simple. However, ensuring the stability of the final mixture is difficult, because the particles can easily segregate due to the lack of interparticulate forces. In cohesive powder mixing, the challenge is to break the network of the interparticulate contact forces within the original powder, so that the particles within the agglomerates can be relocated. However, due to the existence of the interparticulate forces, mixtures prepared with cohesive powders are often less prone to segregation. Having said that, if segregation takes place in an adhesive mixture, the mixing quality can be severely affected because the size of the segregated agglomerates can be large (Harnby 2000).

The quality of the blending can be assessed by taking random samples and measuring the content of one of the components in these samples. The variation in the content in terms of how close the assessed amount is to the theoretical amount and the standard deviation in the content of a component between the samples describes the quality of the blending (Williams 1968).

2.5.2 Preparation of the formulations

2.5.2.1 Blending

The formulations investigated during the current study were prepared using low shear convective mixing. A Turbula mixer was used for preparing the blends at a speed of 46 rpm. Before formulating, the lactose blends were passed through a 850 µm aperture sieve to break any large agglomerates formed upon the storage of the pre-blends. The required

amounts of drug and lactose were weighed. One quarter of the lactose was transferred to the blending vessel described earlier (Section 2.1.3). The drug was added to the top of the lactose and one quarter of the lactose was added on top of the drug. This was blended for 10 minutes. The remaining half of the coarse lactose was then added before blending the formulation for 45 minutes. After the blending, the formulations were passed through a 250 μm sieve and stored at 20 ± 2°C and 44% RH for at least a week before the content uniformity of the blends was assayed.

2.5.2.2   Content uniformity

The quality of the blending was ensured by taking 10 aliquots of each of the formulations and assessing the drug content in the aliquots. Aliquots equal to the capsule fill weight (12.5 or 25 mg) were taken in volumetric flasks (50 or 100 ml) and dissolved in the mobile phase by placing the volumetric flasks in an ultrasonic bath for 60 minutes to dissolve the lactose. After the sonication, the solutions were allowed to cool to the room temperature before the volumetric flasks were topped up to the mark with the mobile phase. Aliquots were then taken in HPLC vials and the drug content assayed using HPLC. The mean dose of drug in each of the aliquots was calculated based on the linear response from the standard samples of known concentrations that were analysed in the same measurement sequence as the samples. The quality of the blending was deemed to be satisfactory if the variation coefficient of the drug dose was less than 6% in the 10 samples assayed. The nominal dose was ensured to be between 90 and 110% of the loaded dose.

2.5.2.3   Capsule filling

After the satisfactory dose content uniformity and nominal dose had been assured, the formulations were loaded in capsules. Size 3 Quali-V hydroxypropylmethylcellulose (HPMC) capsules (Qualicaps, Spain) were filled by hand. A fill weight of 12.5 or 25 mg was applied for different studies. The amount used in each particular study will be specified in the results chapters.

2.6   *IN VITRO* TESTING OF THE FORMULATIONS

2.6.1   Theory

In the industry, the *in vitro* formulation testing is used for assessing the formulation performance for formulation development and quality control purposes. In the current

study, the *in vitro* assessment of performance of the model formulations prepared was performed to relate the impact of the addition of lactose fines to the formulation performance. In addition, the properties of the lactose were to be related to the final formulation performance of the model formulations.

2.6.1.1   Devices

It has been reported in the literature that the resistance of the device is an important factor in determining the extent of deagglomeration for DPI formulations (Olsson *et al.* 1994). Therefore, three different devices were used during the studies. The Rotahaler (GlaxoSmithKline), Cyclohaler (Teva) and Handihaler (Boehringer Ingelheim) are all capsule based, single dose, breath actuated devices with low, medium and high resistance to air flow, respectively (Srichana *et al.* 1998a).

2.6.1.2   Next generation impactor testing

2.6.1.2.1   General introduction

The aerodynamic particle size distribution of the drug aerosolised from an inhaled product is crucial in determining the lung deposition characteristics of the drug. The deposition of the drug could be investigated *in vivo* using a combination of radiolabelled drug and medical imaging (Carvalho *et al.* 2011). However, this method is impractical for testing every released formulation. Instead, as specified by the pharmacopoeias (European Medicines Agency 2007), aerodynamic particle size classification systems are used for testing the extent of drug delivery from DPI products.

In the early days of inhalation testing, methods that were widely used for characterising the size distributions and the lung deposition of environmental pollutant particles were adopted for inhalation product development and release testing (Broadhead *et al.* 1995). However, these impactors are often limited in their capability of being used at different air flow rates, are most suitable for sampling of dilute aerosols and are labour intensive (Marple *et al.* 1995). To try and address these issues, the first impactor that was specifically designed for inhalation testing was the Marple-Miller impactor (Marple *et al.* 1995). However, although an improvement in usability in pharmaceutical applications and a wider selection of flow rates compared to the predecessors was achieved with the Marple-Miller impactor, there still was room for improvement. Consequentially, a consortium of pharmaceutical companies involved in inhalation product manufacturing

listed the "must have" and "would like to have" features of a pharmaceutical impactor. The ultimate aim of the consortium was to develop a universal impactor capable of operating over a range of flow rates and less labour intensive to operate, with the possibility of automating the testing procedure (Marple *et al.* 2003a). As a result, the Next Generation Impactor (NGI) was developed.

2.6.1.2.2 The general layout and the principle of operation

A photograph of the NGI equipped for DPI testing is shown in Figure 2.13. The NGI set-up for DPI testing consists of an induction port that mimics the oropharyngeal region of the respiratory tract, the pre-separator that mimics the upper airways and the impactor body that contains the collection cups for the fine particles. The principle of operation for the system aims to mimic the inhalation manoeuvre and consequential regional particle deposition within the lungs of the patient. This is achieved by connecting the impactor to a vacuum pump at the distal end of the impactor body, as highlighted in Figure 2.13. The primed device with the dose of drug loaded is connected to the induction port using a mouthpiece. Air is then drawn through the system. As a consequence, the dose of the drug is fluidised, deagglomerated and entrained in the airflow. The entrained particles are separated in the impactor according to their aerodynamic properties, mainly their inertia. The design principles of the NGI by which the separation of the particles is achieved will be introduced in detail in the following.
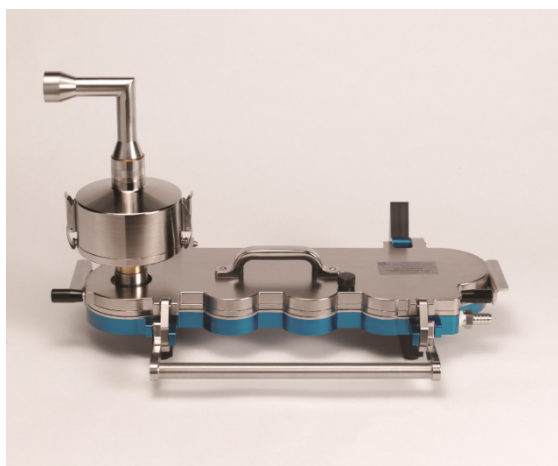
FIGURE 2.13 THE NEXT GENERATION IMPACTOR LAYOUT FOR DPI TESTING WITH THE USP INDUCTION PORT AND A PRE-SEPARATOR. THE IMAGE IS COURTESY OF AND REPRODUCED WITH THE PERMISSION OF COPLEY SCIENTIFIC

2.6.1.2.3   The induction port

The United States Pharmacopoeia (USP) induction port is a very crude model of the oropharyngeal region. It is generally believed that particle deposition in the USP throat is governed by the inertial moment of the particles (Longest *et al.* 2008). Particles that are large have a high inertia and therefore are impacted in the 90° bend, mimicking the back of a human throat. Finer particles, in contrast, have lower inertia. These particles are therefore able to negotiate the sudden change in the direction of the air flow. However, the most recent developments in the *in vitro* testing of inhalation products include the introduction of an anatomically realistic induction port. The induction port is based on medical imaging of human mouth and throat region (Ilie *et al.* 2008).

2.6.1.2.4   The pre-separator

The pre-separator aims to mimic the upper airways of the respiratory tract. The pre-separator is only used as an add-on part of the impactor for testing DPI formulations with the purpose of collecting the large carrier lactose particles and any drug adhering to the surfaces of these particles. The particle deposition in the pre-separator is believed to be governed by gravitational forces rather than impaction (Marple *et al.* 2003b). This is because the carrier lactose particles are generally large enough to be affected by gravitational forces.

2.6.1.2.5   The impactor body

The impactor body where the collection cups are housed acts as an air classifier. The air classifier separates the particles by impaction according to their aerodynamic diameters. Large particles have large inertia and are therefore unable to react to sudden changes in the direction of the airflow. Consequentially these particles get deposited on the impaction surface. In contrast, small particles with lower inertia remain suspended in the airflow (Marple *et al.* 2003a). This basic principle of an impactor stage is illustrated in Figure 2.14. By placing a series of impactor stages and changing the aerodynamic design parameters of the different stages, particles with different aerodynamic diameters can be separated. The design principles according to which this is achieved with the Next Generation Impactor will be discussed in the following.

FIGURE 2.14 THE PRINCIPLE OF PARTICLE IMPACTION WITH LARGE PARTICLES UNABLE TO NEGOTIATE THE SUDDEN CHANGE IN THE DIRECTION OF AIRFLOW WHILST SMALL PARTICLES ARE CARRIED IN THE AIRFLOW

The first design principle in achieving reliable particle classification by impaction is to ensure the air flow throughout the impactor is laminar. This is because particle deposition by impaction in turbulent air flow, characterised by constant, random changes in the direction of the airflow, may occur earlier than would be predicted on the basis of the aerodynamic properties of a particle. Reynold's number (R_e) is a parameter describing the extent of turbulence within the air flow. In a straight tube, laminar flow is characterised by a Reynolds number between 500 and 3000. The Reynolds number is defined by Equation 2.4, where ρ is the density, u is the velocity, μ is the viscosity of the fluid and d'' the diameter of the tube through which the fluid is flowing (Marple *et al.* 2003a)

$$R_e = \frac{\rho u d''}{\mu}$$

EQUATION 2.4

A schematic of the design and the principle of operation for an impactor stage is shown in Figure 2.15. The particles are carried in the air flow that has a flow rate of Q through n nozzles of diameter W. The distance between the nozzle orifice and the impaction plate is S. The average velocity of the air though each of the nozzles (V_0) is defined by Equation 2.5 (Marple *et al.* 2003a).

$$V_0 = \frac{4Q}{\pi n W^2}$$

EQUATION 2.5

By replacing the air velocity u and the diameter of the pipe d in Equation 2.4 by the air velocity through the nozzles V_0 as determined by Equation 2.5 and the diameter of a nozzle W, respectively, the Reynolds number for the air flow through the nozzles can be written as per Equation 2.6 (Marple *et al.* 2003a)

$$R_e = \frac{4\rho Q}{n\pi\mu W}$$

EQUATION 2.6

Assuming no changes in the air flow velocity, the denominator in Equation 2.6 is constant. Therefore, it follows from Equation 2.6 that the air flow through the impactor can be kept laminar by increasing the number of nozzles n in the nozzle orifice upon decreasing the nozzle diameter W. This is the reason the NGI stages have an increasing number of smaller holes the lower the stage. This is illustrated in Table 2.2, where the number and diameter of the nozzles on the different stages of the NGI are summarised.
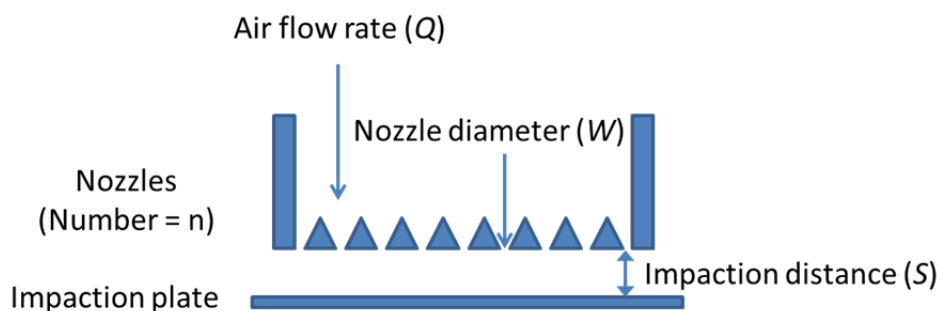
FIGURE 2.15 A SCHEMATIC OF THE SETUP OF A NOZZLE OF THE NEXT GENERATION IMPACTOR WITH THE PARAMETERS THAT GOVERN THE PARTICLE IMPACTION

The second design principle for the NGI ensures good particle collection efficiency. To achieve high particle collection efficiency, the impaction distance S for a stage should be between 1 and 10 times the nozzle diameter W. Therefore, in impactor design, in addition to the Reynolds number, which is affected by the number n and the size W of the nozzles, attention has to be paid to the W/S ratio (Marple *et al.* 2003a). The values of S for the different NGI stages are also listed in Table 2.2.

TABLE 2.2 THE AERODYNAMIC DESIGN OF THE NEXT GENERATION IMPACTOR STAGES IN TERMS OF NUMBER OF NOZZLES (n), THE DIAMETER OF EACH OF THE HOLES (W) AND THE DISTANCE BETWEEN THE NOZZLE ORIFICE AND THE IMPACTION SURFACE (S). ADAPTED FROM MARPLE *et al.* (2003a)

Stage	N	W (mm)	S (mm)
1	1	14.300	15.000
2	6	4.880	9.764
3	24	2.185	6.555
4	52	1.207	3.621
5	152	0.608	1.824
6	396	0.323	1.001
7	630	0.206	1.000
MOC	4032	0.070	0.500

The theoretical mean particle size (d_{50}) of the material collected on the different impactor stages is defined by Equation 2.7, where ρ_p is the particle density and $\sqrt{St_{50}}$ is the square root of Stokes' number calculated for a stage based on the mean cut off diameter of the stage. For particles depositing by inertial impaction, the square root of Stokes' number

97

$\sqrt{Stk_{50}}$ should have a value of close to 0.495 when the Reynolds number is between 500 and 3000 and the W/S ratio between 1 and 10 (Marple *et al.* 2003b). It follows from Equation 2.7 that the d_{50} decreases when the nozzle diameter W is decreased.

$$d_{50} = \sqrt{\frac{9\pi\mu n W^3}{4\rho_p Q}} \sqrt{Stk_{50}} \qquad \text{EQUATION 2.7}$$

The d_{50} can be calculated using Equation 2.7. However, for routinely defining the d_{50} of the different stages at different flow rates, a calibration of the system was performed upon the release of the system design (Marple *et al.* 2003b). As a result of the calibration, Equation 2.8, where A and B are constants that are listed for the different stages in Table 2.3, was introduced for calculating the cut off values for the different stages at different flow rates.

$$d_{50} = A \left(\frac{60}{Q}\right)^B \qquad \text{EQUATION 2.8}$$

In addition to the constants A and B, the calculated d_{50} values based on Equation 2.8 for the different stages at 30, 60 and 90 litres per minute air flow rates are listed in Table 2.3.

TABLE 2.3 THE CONSTANTS A AND B USED FOR CALCULATING THE CUT-OFF DIAMETERS OF THE NEXT GENERATION IMPACTOR STAGES AT DIFFERENT FLOW RATES AND THE CALCULATED VALUES OF d50 AT FLOW RATES OF 30, 60 AND 90 LITRES PER MINUTE

Stage	A	B	d_{50} (µm)		
			30 l/min	60 l/min	90 l/min
1	8.06	0.54	11.72	8.06	6.48
2	4.46	0.52	6.40	4.46	3.61
3	2.82	0.50	3.99	2.82	2.30
4	1.66	0.47	2.30	1.66	1.37
5	0.94	0.53	1.36	0.94	0.76
6	0.55	0.60	0.83	0.55	0.43
7	0.34	0.67	0.54	0.34	0.26

2.6.1.2.5   Mean mass aerodynamic diameter, geometric standard deviation and fine particle mass

The mean mass aerodynamic diameter (MMAD) determines the average particle size of the material collected from the impactor stages and the geometric standard deviation (GSD) the width of the distribution. Both these parameters are calculated from the cumulative impactor stage-by-stage deposition data (European Medicines Agency 2007). The cumulative mass of the drug recovered from the stages, starting from the Stage 8, is

plotted against the logarithm of the d_{50} for the stage. This plot is shown in Figure 2.16. The MMAD is the size of the 50th percentile of the cumulative distribution. The GSD is defined on the basis of the 16th (y) and the 84th (x) percentiles of the distribution as per Equation 2.9.

$$GSD = \sqrt{\frac{x}{y}}$$

The fine particle mass (FPM) describes the amount of respirable particles aerosolised from a formulation. This is often defined as the mass of particles finer than 5 µm. The mass of particles <5 µm can be obtained from the cumulative drug mass versus stage cut-off size plot shown in Figure 2.16 either by extrapolation or regression. However, according to the pharmacopoeial specifications (European Medicines Agency 2007), only the data points falling between 16th and 84th percentiles should be used for both obtaining the fine particle mass and defining the MMAD. This is because the points outside these limits may skew the distribution in case of abnormal particle deposition pattern on the highest or the lowest stages.
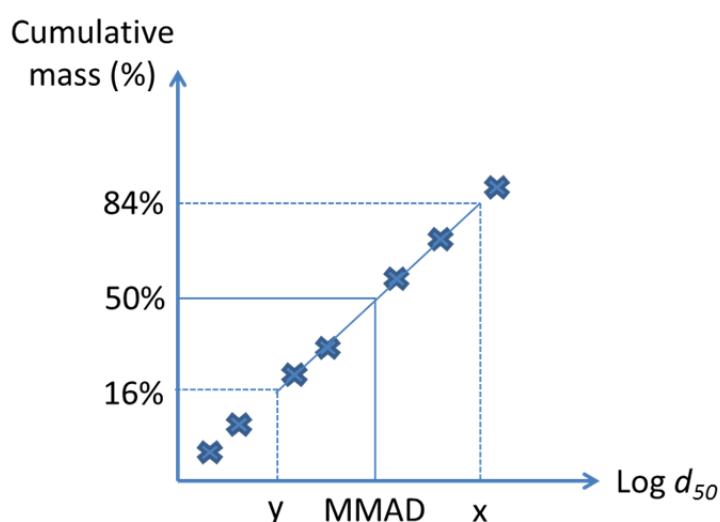
FIGURE 2.16 THE DEFINITION OF THE MEAN MASS AERODYNAMIC DIAMETER (MMAD) AND THE 16TH AND THE 84TH PERCENTILES (Y AND X, RESPECTIVELY) OF THE CUMULATIVE STAGE-BY-STAGE DRUG DEPOSITION PLOT AS A FUNCTION OF THE STAGE CUT-OFF SIZE USED FOR CALCULATING THE GEOMETRIC STANDARD DEVIATION (GSD)

2.6.2   Methodology

2.6.2.1   *Determination of air flow rates on different devices*

The flow rates required to produce a 4 kPa pressure drop across the mouthpiece without the capsules placed in the devices were measured using the TPK critical flow controller (Copley Scientific, Nottingham, UK). The device was connected to the dose content uniformity sampling apparatus (DUSA, Copley Scientific, Nottingham, UK) via a mouthpiece. The flow rate was adjusted such that the P1 on the TPK was 4 kPa. The equivalent flow rate was then read from a DFM2000 flow meter (Copley Scientific, Nottingham, UK). The measured flow rates producing the 4 kPa pressure drop were 160 l/min for Rotahaler, 100 l/min for Cyclohaler and 54 l/min for Handihaler. The NGI is calibrated between flow rates of 30 and 100 l/min. Therefore, to obtain reliable *in vitro* performance data for the model formulations, a flow rate of 90l/min was used for Rotahaler and Cyclohaler.

2.6.2.2   *Next Generation Impactor testing*

To prevent re-bounce of particles to the air flow after impaction, the NGI collection cups and the base plate of the pre-separator were coated with silicone oil before each run. This was done by covering the surfaces with 1 v/v-% silicone oil in hexane solution. The hexane was then allowed to evaporate leaving behind a thin coat of oil.

The impactor was then assembled and 15 ml of the mobile phase was added in the insert cup of the pre-separator. The flow rate was then adjusted to the correct value, determined by the device used, by the Copley TPK critical flow controller. Once the flow rate had been adjusted, the ratio between the P2 and P3 measured by the TPK was inspected. To ensure sonic flow through the impactor, and consequentially no sudden changes in the air flow pattern within the impactor altering the particle deposition, was maintained, the value of P2 has to be at least twice as high as for P3.

Once the flow rate had been adjusted, the flow meter was replaced by a mouthpiece. The device was primed and attached to the mouthpiece. The valve of TPK was then opened for either 2.7 s (90l/min flow rate) or for 4.4 s (54 l/min flow rate) so that 4 litres of air was drawn through the impactor during the test. The actuation was repeated between 2 and 10 times. The number of actuations in each of the studies will be specified in the results chapters.

After all the doses had been actuated, the capsules, device, mouthpiece and throat, pre-separator and the stages were washed in the mobile phase. Aliquots of the wash solutions were taken for assessing the drug content in the different parts of the impactor by HPLC. For each of the formulations, the test was performed in triplicate.

Fine particle mass (<5 µm), MMAD and GSD were determined as described in section 2.6.1.2.5. The fine particle fraction of emitted dose (FPF_{ED}) is defined as the ratio between the fine particle mass and the dose of the drug recovered after the capsule and device. Fine particle fraction of recovered dose (FPF_{RD}) is the ratio between the fine particle mass and the total dose of the drug recovered from the analysis.

CHAPTER 3   THE EFFECT OF LOADED DOSE ON *IN VITRO* PERFORMANCE AND THE FLUIDISATION PROPERTIES OF DRY POWDER INHALER FORMULATIONS

3.1 INTRODUCTION

Previous studies have highlighted the dependency of dry powder inhaler performance on the loaded drug dose (El-Sabawi *et al.* 2006; Young *et al.* 2005). It was found that initially, as the salbutamol sulphate loading increased from 0.02 to 0.27 wt-%, the *in vitro* performance decreased to a minimum value. However, at higher drug loadings (>0.27 wt-%), a linear increase in *in vitro* deposition performance was obtained (Young *et al.* 2005). Furthermore, the drug loading with the minimum in DPI performance was observed to be dependent on the degree of surface roughness of the large lactose carrier, with the smoother lactose carrier reaching a minimum in *in vitro* performance at a lower drug concentration of 0.13 wt-%. The findings of these studies were explained by the active site theory (Staniforth 2000) based on Hershey's (1975) concept of ordered mixtures. The smoother lactose would have fewer high energy binding sites on the surface, and consequentially require a lower drug loading to occupy all the active sites before the drug was bound to low energy binding sites, where it could be more easily detached upon fluidisation (El-Sabawi *et al.* 2006).

Based on the results of Young *et al.* (2005) and El-Sabawi *et al*. (2006), Muresan and Hebbink (2009) developed a theoretical model for *in vitro* performance governed by the active site theory. In their model they were able to predict the number of active sites on a lactose carrier surface and the probability of drug detachment from the normal surface. It was found that for the surface etched lactose used by El-Sabawi et al. (2006) the number of active sites was significantly lower and the probability of drug detachment higher than for the 'as-received' lactose used by Young and co-workers (2005).

Recently, Le *et al.* (2012c) investigated the impact of loaded dose on DPI performance with formoterol fumarate. In their study, the formoterol fumarate concentrations were varied between 0.09 and 0.17 wt-%. A linear increase in the fine particle fraction was reported upon increasing the drug concentration. The increased performance upon increasing formoterol fumarate content was speculated to be caused either by the saturation of active sites or agglomerate formation between the drug particles and intrinsic lactose fines of the carrier (Le *et al.* 2012c).

This chapter aims to investigate the validity of the active site hypothesis in improving dry powder inhaler performance. To do that, model DPI formulations of fluticasone propionate with two different coarse lactose carriers were prepared and the *in vitro* performance of the formulations assessed.

It is also known that there are two different fluidisation mechanisms for dry powders, namely erosion and fracture (Shur *et al.* 2008a; Tuley *et al.* 2008). Free flowing, Geldart group A powders (Geldart 1973) fluidise following the erosion mechanism whereas cohesive, Geldart group C powders fluidise via a fracture mechanism. It was anticipated that the trends in the formulation performance observed by Young and co-workers (Young *et al.* 2005) and El-Sabawi *et al.* (El-Sabawi *et al.* 2006) may also be explained by possible change in the fluidisation mechanism from erosion to fracture, which may lead to a consequential change in drug de-agglomeration efficiency. Therefore, in the current study, the fluidisation mechanisms of selected model formulations were assessed using high speed imaging.

Increased cohesion of DPI carriers has also been reported to correspond to improved DPI performance (Shur *et al.* 2008a). To investigate the role of this hypothesis in governing the DPI performance, a method to characterise the fluidisation and defluidisation properties of the formulations was developed according to the theory described in Chapter 2, section 3.4, and the formulations were characterised.

3.2 MATERIALS AND METHODS

3.2.1 Materials

The coarse lactose carriers used in the study were LH100 and SV010, both supplied by DFE Pharma, Netherlands. The drug was micronised fluticasone propionate (FP), manufactured by GlaxoSmithKline (Jurong, Singapore). The solvents were obtained from Fisher (Loughborough, UK) and Sigma Aldrich (Gillingham, UK) and were of HPLC quality. Water was reverse osmosis purified (Millipore, France).

3.2.2 Particle sizing

A Sympatec Helos laser diffraction system (Sympatec, Germany) was used for particle sizing experiments in conjunction with Windox 5 software. The coarse lactose materials and the DPI formulations were dispersed dry at 2 bar disperser pressure using the Rodos T4 dry dispersion unit with a Vibri powder feeder. The gap width was adjusted to 2 mm

and the feed rate such that an optical concentration of between 0.5 and 5% was achieved. Five replicate measurements were recorded. The Geldart group C powder, FP, was dispersed wet using the Cuvette dispersion system and 0.1% lecithin in cyclohexane as the dispersant. A small aliquot of FP was suspended in the dispersant. The suspension was ultrasonicated for 5 minutes in one minute intervals before five consecutive measurements were recorded at an optical concentration of between 5 and 10%. The results reported are based on the average of five repeated measurements.

3.2.3 Scanning electron microscopy

Scanning electron micrographs of the powder samples were obtained with a Jeol JSM-6480LV SEM (Jeol, Tokyo, Japan) system using an acceleration voltage of 10 kV and a spot size of 15. Samples were mounted on sticky carbon tabs and excess powder was removed by a gentle tap. This approach was used to avoid any fines being dusted off from the surfaces of the large carrier particles. Prior to SEM analysis, samples were coated with gold for 5.5 minutes by an Edwards SB150 sputter coater (BOC Edwards, UK).

3.2.4 Preparation of carrier based DPI formulations

Carrier based DPI formulations were prepared in quantities of 40 g in a 500 cm^3 stainless steel vessel. The desired amount of drug and lactose were weighed and the drug was sandwiched between half of the lactose and blended for 10 minutes in a Turbula blender (Glen Creston Ltd, Middlesex, UK) at 46 rpm. The remaining lactose was then added and the formulation blended for a further 45 minutes. Once the blending was complete, the formulation was passed through a 250 µm aperture sieve to break any large agglomerates remaining within the blend.

The quality of the blending was assured by examining the drug content uniformity of the formulations. This was done by sampling 10 random aliquots of 25 mg and quantifying the drug content in the aliquots according to the HPLC assay described in the general materials and methods of the thesis (Chapter 2.4.2).

3.2.5 *In vitro* testing of the formulations

Size 3 hydroxypropylmethylcelluloce (HPMC) capsules (Qualicaps, Spain) were manually filled with 25 mg of the formulations. A Cyclohaler DPI device was used for aerosolising

the formulations into a Next Generation Impactor (Copley Scientific, Nottingham, UK) equipped with a pre-separator. Air was drawn through the impactor at 90 l/min for 2.7 seconds as controlled by a TPK critical flow controller (also from Copley Scientific). A total of 10 capsules were aerosolised for the low concentration formulations (≤ 0.4 wt%) and 5 capsules for the high concentration (> 0.4 wt%) formulations. Due to the low amount of drug in the low drug loading formulations, stages 6, 7, and 8 were grouped and washed together in 10 ml of the mobile phase. This was done to ensure the drug content of the low dose formulations could be reliably determined with the HPLC assay described in Chapter 2.4.2. The limit of detection for FP for the HPLC assay was determined to be 0.01 μg/ml and the response was linear between concentrations of 0.01 and 50 μg/ml.

3.2.6 High speed imaging of the fluidisation event

High speed imaging of the fluidisation events of low, medium and high drug concentration formulations were recorded by using an Oxford Lasers Firefly high speed imaging system (Oxford Lasers, Oxford, UK). The formulations were fluidised using the Sympatec Rodos T4 dry dispersion system at 0.1 bar disperser pressure and the Aspiros sample feeder. The test tube was filled with approximately 25 mg of the powder under investigation and the powder was dispersed from the test tubes. High speed imaging footage of the powder fluidisation event was recorded at 8000 frames per second.

3.2.7 Powder fluidisation and defluidisation properties

The powder fluidisation and defluidisation properties of the formulations were measured using the FT4 powder rheometer. A powder bed of between 12 and 13 g in a 25 mm bore diameter, 30 ml measurement vessel with a standard aeration base was first conditioned by fully fluidising the powder. The air supply was then switched off and the powder bed was allowed to settle under gravity. This was done to erase the consolidation history of the powder caused by the storage and loading of the powder into the vessel. This allowed a reproducible state of powder packing to be achieved prior to subsequent measurements. The air velocity of the fluidising gas (dry pressurised air supply) was linearly increased in small increments. The pressure differential required to maintain the requested air velocity was measured by the Aeration Control Unit (ACU) of the system. Once an air velocity of 15 mm/s was achieved, the air velocity was decreased gradually and the pressure differential at each air velocity recorded for the defluidisation curve.

3.2.8 Flow rate index

The flow rate index (FRI) is a flow descriptor that can be measured on the FT4 powder rheometer. This parameter was also measured, but a different measurement program based on measuring the torque and force required to keep the impeller blade moving through the powder bed at a constant tip speed was applied. A detailed description of the measurement for determining the FRI can be found in the general materials and methods section of the thesis (Chapter 2.3.3.2). Briefly, a 25 mm inner diameter, 20 ml split cell was filled with powder before a conditioning cycle was run to remove the packing history of the powder. The cell was then split to gain a constant volume of powder between repeated experiments. The FRI was obtained by measuring the torque and force required to move the blade through the powder bed at a tip speed of 100 and 10 mm/s. Flow rate index is the ratio between the flow energies at the two different tip speeds as defined by Equation 3.1:

$$FRI = \frac{Flow\ energy\ at\ 10\ mm/s}{Flow\ energy\ at\ 100\ mm/s}$$

EQUATION 3.1

3.3 RESULTS AND DISCUSSION

3.3.1 Characteristics of the raw materials

The particle size measurements for the Geldart Group A classified coarse carriers, in terms of the 10th, 50th and 90th percentiles of the probability density function distribution and proportion of particles finer than 4.5 µm, are summarised in Table 3.1. In addition, theoretical surface area measurements of the carriers based on the particle sizing data are shown in Table 3.1. Comparing the d10, d50 and d90 of LH100 and SV010, it was seen that SV010 has slightly larger particle size than LH100. This can also be seen in Figure 3.1 where the particle size distributions of the raw materials are presented. However, Table 3.1 indicates that LH100 and SV010 are very similar in terms of their proportion of fine particles and the surface area of the powders. The similarity of the fines content in the carriers is a significant feature because it is known from previous studies that the proportion of fines is more important in determining the DPI performance than the particle size distribution as a whole (Guenette *et al.* 2009).

The particle size of the Geldart Group C fluticasone propionate is also shown in Figure 3.1. The particle size of the material was within the respirable range with values of d10, d50 and d90 of 0.89, 2.13 and 4.07 µm, respectively.

Carrier	d10 ± S.D. (μm)	d50 ± S.D. (μm)	d90 ± S.D. (μm)	<4.5 μm (%)
LH100	37.74 ± 1.06	99.79 ± 0.71	157.01 ± 1.81	1.4
SV010	51.33 ± 2.04	111.24 ± 1.39	176.83 ± 5.95	1.5

FIGURE 3.1 PARTICLE SIZE DISTRIBUTIONS OF THE COARSE CARRIERS LH100 AND SV010 AND FLUTICASONE PROPIONATE (FP) USED IN THE STUDY

Representative scanning electron micrographs of the raw materials are presented in Figure 3.2. Comparing the morphology of LH100 (A) and SV010 (B), it appears that LH100 exhibits the smoother surfaces of the two carriers. Despite the same proportion of intrinsic fines (% of particles <4.5 μm), LH100 appears to have less of the fines attached to the surface than SV010. The explanation for this could be that the fines are tightly adhered to the surface of SV010 and therefore cannot be removed upon dry dispersion. In addition, the volume of the fines is very low compared to the volume of the bulk powder. Thus, subtle differences in the amount of fines in the two carriers may not be accurately reflected by volume based particle size distributions. It is known that LH100 and SV010 are produced at different DFE Pharma plants (DFEPharma 2011). The differences in the morphology of the LH100 and SV010 materials are most likely caused by different manufacturing processes used at the two sites. A scanning electron micrograph of FP is shown in Figure 3.2C. The micrograph indicates that FP is very fine and agglomerated.
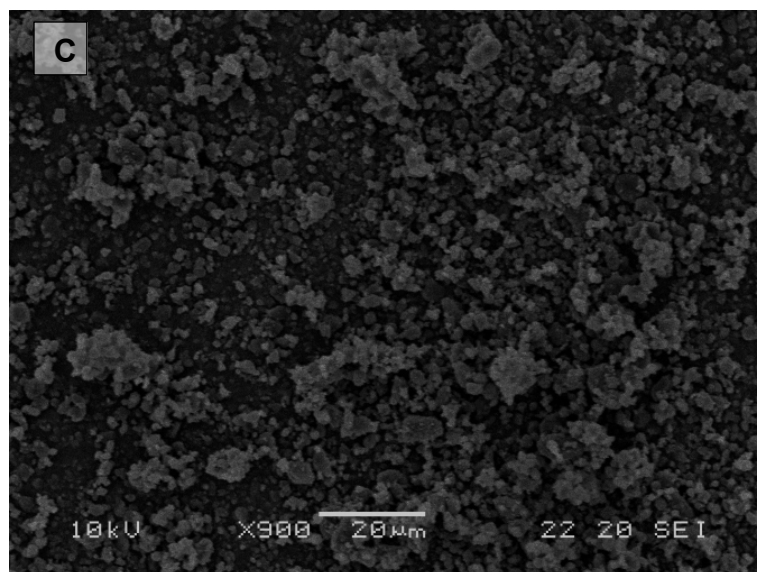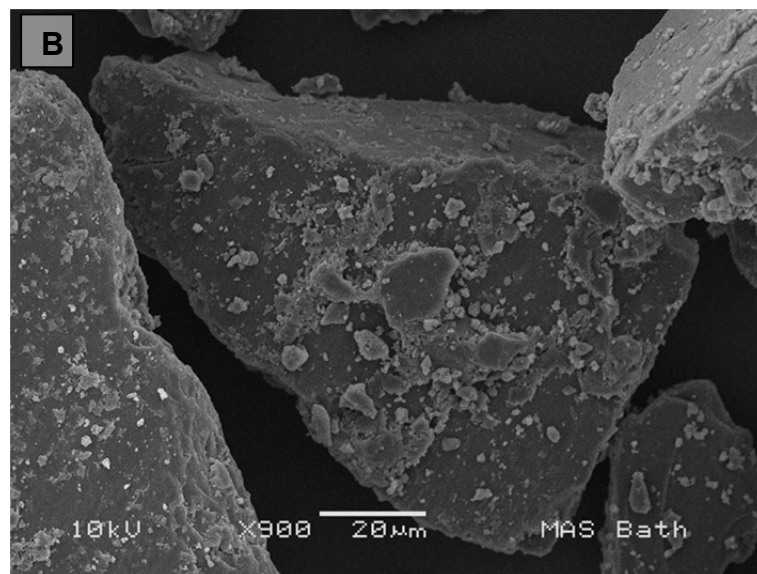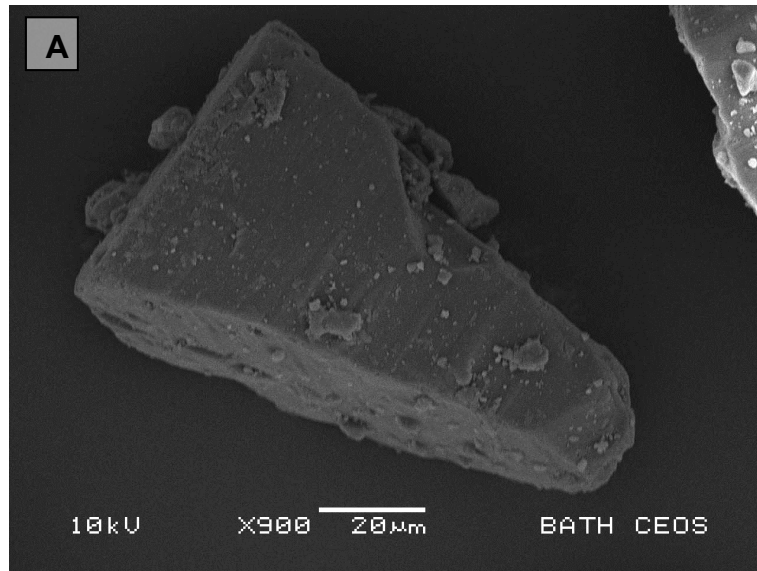
FIGURE 3.2 900X MAGNIFICATION SCANNING ELECTRON MICROGRAPHS OF A) LH100 B) SV010 AND C) FLUTICASONE PROPIONATE

3.3.2 Physical properties of the carrier based DPI formulations

The particle size measurements together with the proportion of particles finer than 4.5 μm and the surface area of the series of carrier based DPI formulations with an increasing amount of FP, dispersed dry, are presented in Table 3.2. It can be seen that the d90 of the formulations remain somewhat unaltered across the entire concentration range for both carriers, as does d50. A decrease in the value of d10 can be observed for both formulation series. For the LH100 series the d10 dramatically decreases for the 2 wt-% FP formulation, while for the SV010 series this decrease occurs at 1 wt-% FP concentration.

However, the most remarkable observation of these data, shown in Table 3.2, is the amount of fine particles detaching from the surface of the carriers upon dry dispersion as the drug concentration is increased. This is graphically presented in Figure 3.3, where the percentage of particles < 4.5 μm measured for the formulations is plotted as a function of the loaded drug dose. It can be seen that a larger proportion of fines are detached from the SV010 formulations across the entire concentration range with respect to the LH100 formulations. As expected, this trend is reflected in the surface area of the powders as calculated from the particle sizing data. This is an interesting finding because, by using pressure titration, the disperser pressure was set such that the primary particle size should have been achieved during the measurements

De Boer *et al.* (2005) and Dickhoff *et al.* (2005) used an air classifier technology for studying the drug detachment from DPI formulations prepared at different drug concentrations with lactose carriers having different surface characteristics. The major findings from their studies suggested that the surface discontinuities on the lactose carrier surface, in the form of rugosities or adhering intrinsic lactose fines, provided shelter from the press-on forces induced during formulation blending. This resulted in improved drug detachment from lactose carriers with a rougher surface. They also saw an improved detachment at higher drug loadings and attributed this to the press-on forces being more efficient at low drug concentrations (de Boer *et al.* 2005; Dickhoff *et al.* 2005). The findings of the current study with more fines detaching from the surface of SV010, which exhibited the rougher surface of the two coarse carriers used, could possibly also be explained by the lower magnitude of press-on forces acting on SV010 during formulation blending.

TABLE 3.2 THE 10TH, 50TH AND 90TH PERCENTILES OF THE DENSITY PARTICLE SIZE DISTRIBUTIONS (d10, d50 AND d90 CORRESPONDINGLY) AND THE PROPORTION OF PARTICLES FINER THAN 4.5 μm FOR THE FLUTICASONE PROPIONATE (FP) FORMULATIONS INVESTIGATED IN THE STUDY. THE DATA FOR d10, d50 AND d90 REPRESENTS MEAN ± STANDARD DEVIATION, N=5. THE DATA FOR <4.5 μm REPRESENTS MEAN, N=5.

Formulation (+ wt-% FP)	d10 ± S.D. (μm)	d50 ± S.D. (μm)	d90 ± S.D. (μm)	<4.5 μm (%)
LH100	37.74 ± 1.06	99.79 ± 0.71	157.01 ± 1.81	1.40
+0.02	45.43 ± 2.15	103.13 ± 0.62	158.26 ± 1.28	1.29
+0.05	43.41 ± 0.22	100.96 ± 0.80	152.89 ± 4.43	1.23
+0.08	44.99 ± 1.23	101.71 ± 1.23	151.00 ± 4.90	1.34
+0.1	45.49 ± 0.45	101.36 ± 0.45	148.49 ± 0.65	1.27
+0.15	44.25 ± 0.77	101.83 ± 0.93	154.65 ± 4.35	1.56
+0.2	48.99 ± 2.98	102.79 ± 1.50	148.22 ± 2.16	1.38
+0.4	45.79 ± 1.06	102.95 ± 0.99	156.17 ± 4.21	1.54
+1	41.69 ± 0.85	102.43 ± 0.76	157.14 ± 0.57	2.28
+2	31.51 ± 4.55	101.03 ± 1.15	160.68 ± 1.75	4.47
SV010	51.33 ± 2.04	111.24 ± 1.39	176.83 ± 5.95	1.50
+0.02	52.86 ± 0.27	110.34 ± 0.32	167.31 ± 0.39	1.68
+0.05	54.50 ± 0.54	111.45 ± 1.31	173.97 ± 7.50	1.49
+0.08	57.05 ± 2.55	113.07 ± 0.26	178.60 ± 3.00	1.31
+0.1	56.15 ± 2.17	112.97 ± 1.02	178.97 ± 4.17	1.43
+0.2	51.76 ± 0.83	110.24 ± 1.59	172.00 ± 7.39	1.87
+0.3	51.53 ± 1.61	111.52 ± 0.40	180.03 ± 1.50	1.69
+0.4	50.89 ± 1.20	111.77 ± 0.80	181.01 ± 0.88	2.14
+1	44.80 ± 2.15	107.99 ± 1.29	169.07 ± 6.66	3.39
+2	30.80 ± 2.75	109.89 ± 0.54	183.72 ± 1.24	5.73
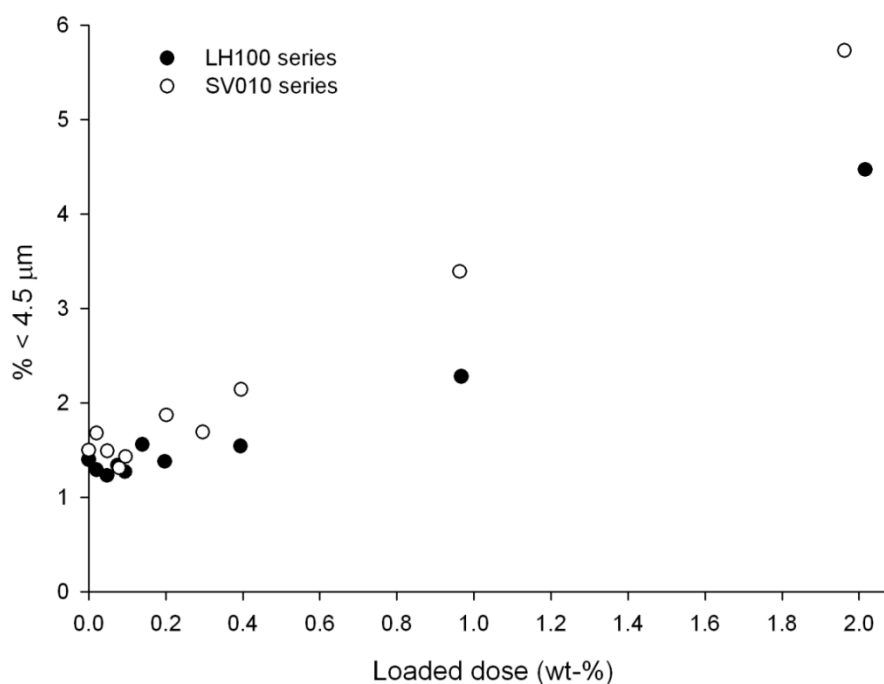
FIGURE 3.3 THE PROPORTION OF PARTICLES FINER THAN 4.5 μm (%<4.5 μm) MEASURED WHEN THE FORMULATIONS WERE DISPERSED DRY AT 2 BAR DISPERSER PRESSURE AS A FUNCTION OF FLUTICASONE PROPIONATE CONTENT OF THE FORMULATIONS (LOADED DOSE)

The distribution of the drug particles on the surface of the coarse lactose particles can be observed by SEM. Representative scanning electron micrographs of the LH100 formulations are shown in Figure 3.4. Very few fines are attached to the surface of LH100 up to 0.2 wt-% concentration (Figure 3.4A to Figure 3.4F). At 0.4 wt-% concentration (Figure 3.4G) more fines are seen on the surface. As the drug concentration is increased further to 1 and 2 wt-% (Figure 3.4H and Figure 3.4I), not only more particles but also agglomerated fine particles are seen adhering to the surface of the coarse lactose.

Scanning electron micrographs of the SV010 formulations are presented in Figure 3.5. In the SV010 formulations, the drug particles start forming agglomerates on the surface of the SV010 at lower concentrations (0.4 wt-%, Figure 3.5G), than on the surface of the LH100 (1 wt-%, Figure 3.4H). The drug coating on the surface of SV010 formulations at 1 and 2 wt-% concentrations (Figure 3.5H and, Figure 3.5I) is also more uniform than the equivalent LH100 formulations (Figure 3.4H and Figure 3.4). The micrographs indicate that all the formulations exhibit characteristics of ordered mixtures (Hersey 1975) with fines adhering to the surfaces of the larger particles with hardly any free fines present in the blends.

The presence of fine particle agglomerates at lower concentrations of the SV010 formulations may be an explanation for the increased amount of fine particles <4.5 μm detaching from the surface, as shown in Figure 3.3. The agglomerates will experience greater drag forces during dispersion and are therefore more likely to be detached from the surface of the large lactose particles than individual particles (Begat *et al.* 2004a).
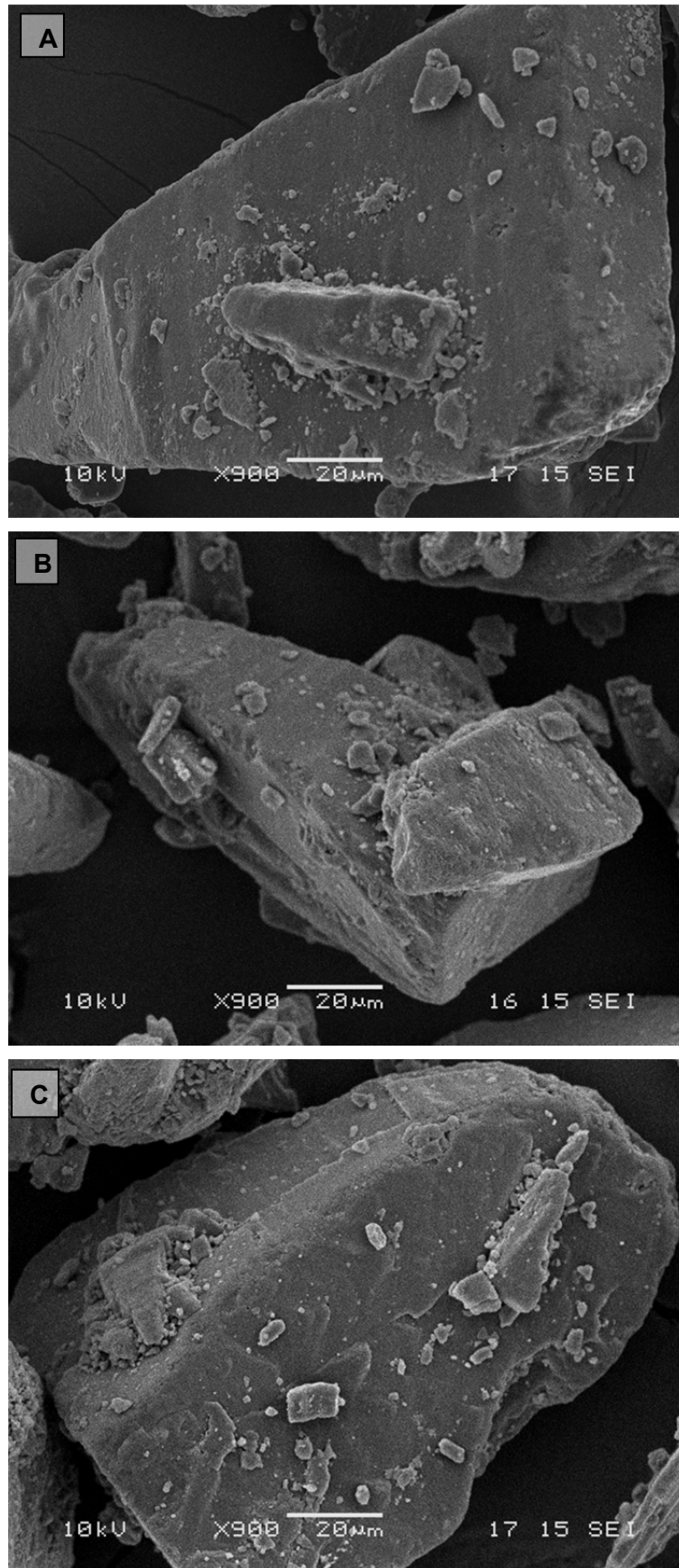
FIGURE 3.4 900X MAGNIFICATION SCANNING ELECTRON MICROGRAPHS OF A) 0.02% B) 0.05% C) 0.08% D) 0.1% E) 0.15% F) 0.2% G) 0.4% H) 1% AND I) 2% FLUTICASONE PROPIONATE FORMULATIONS WITH LH100 AS THE CARRIER

FIGURE 3.4(CONTINUED)

113
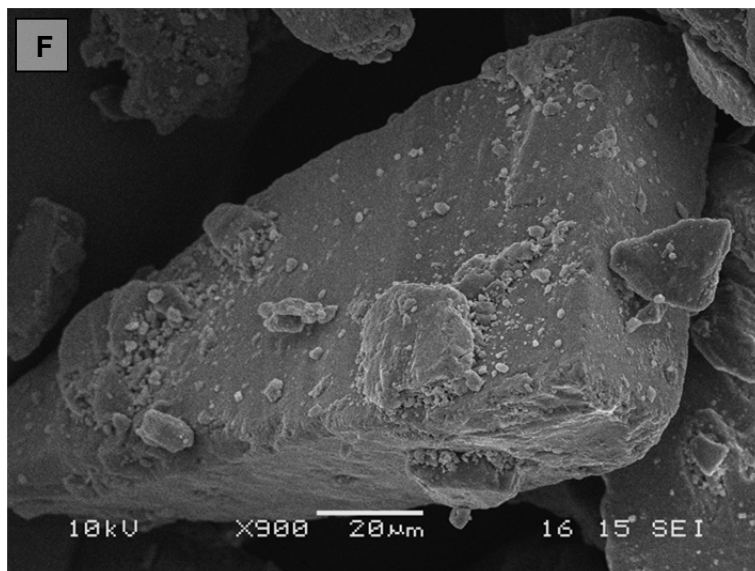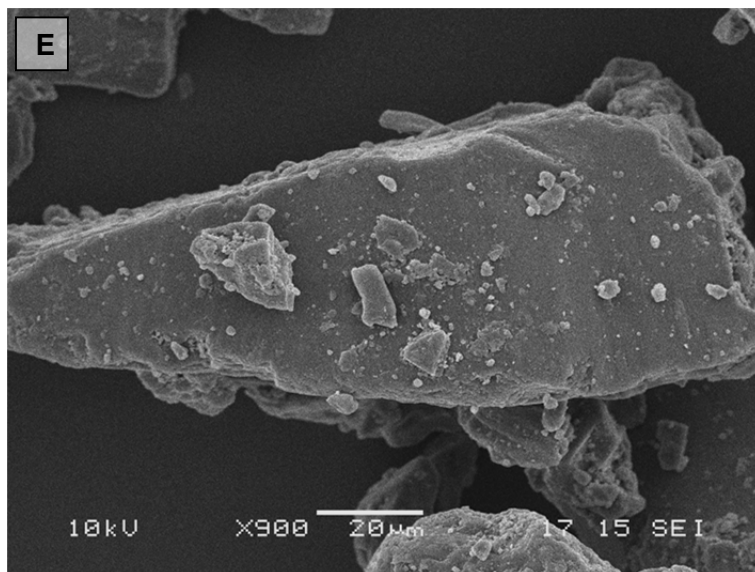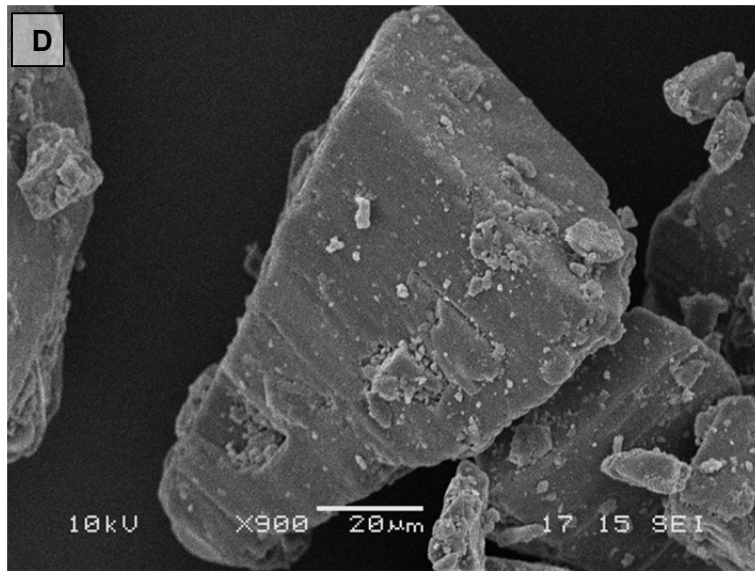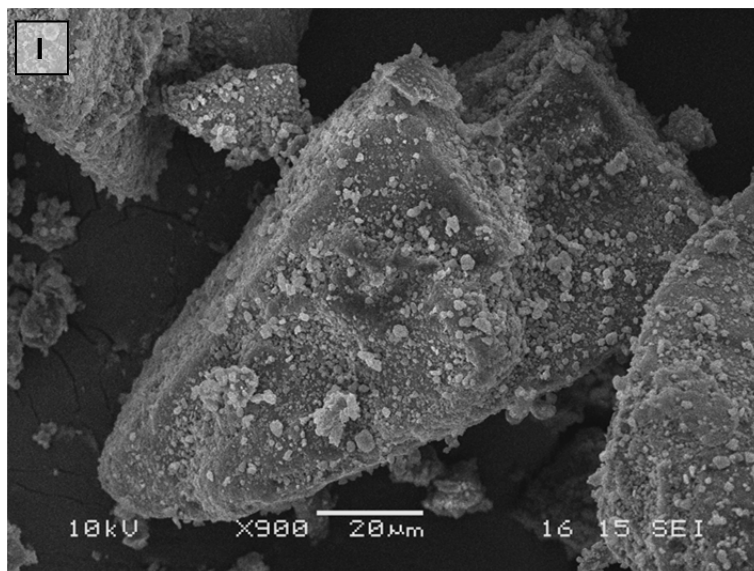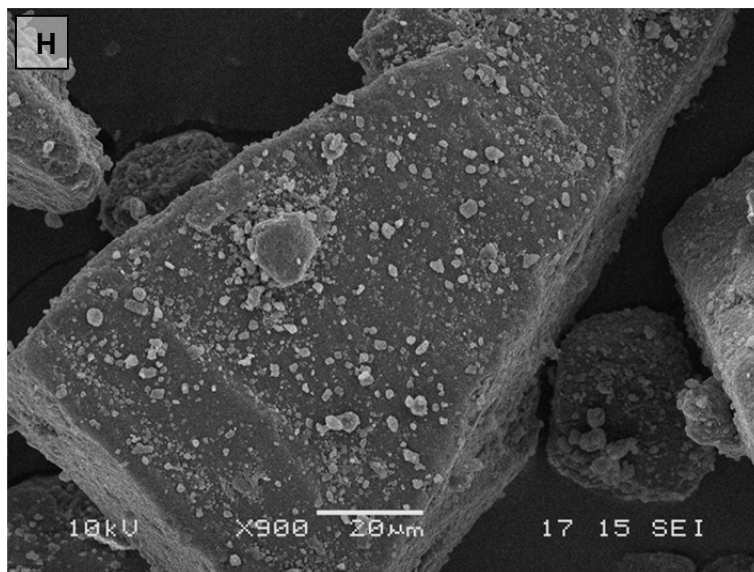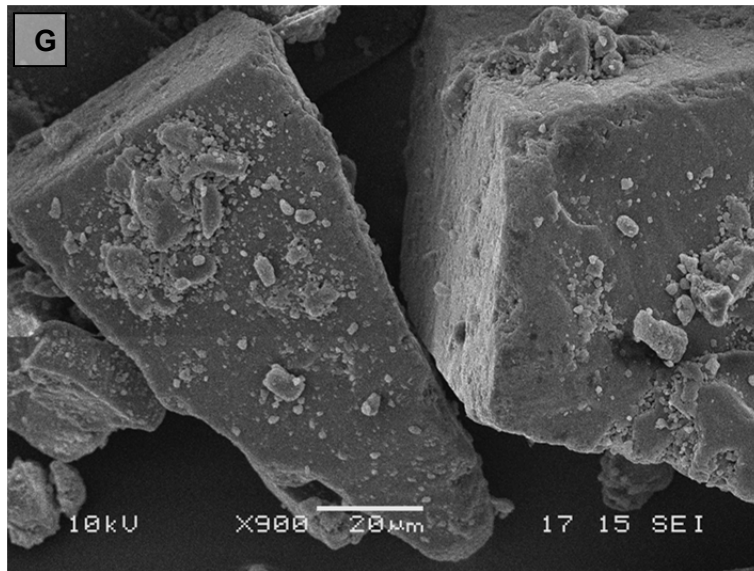
FIGURE 3.4(CONTINUED)
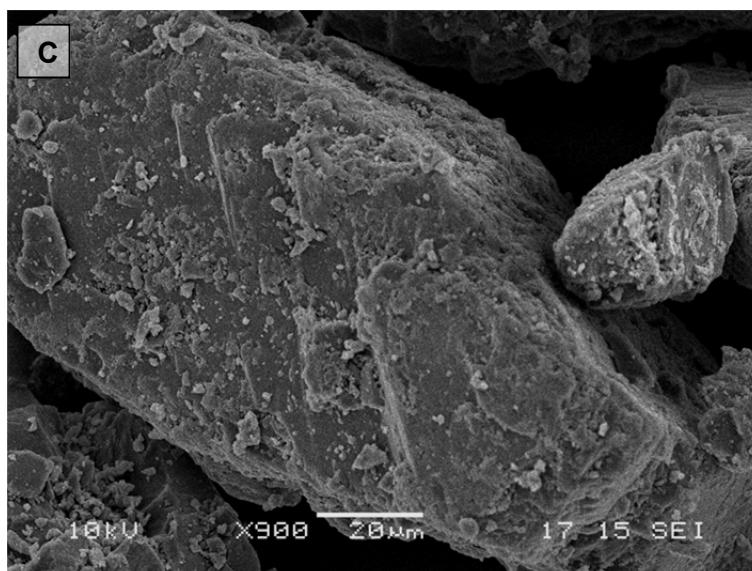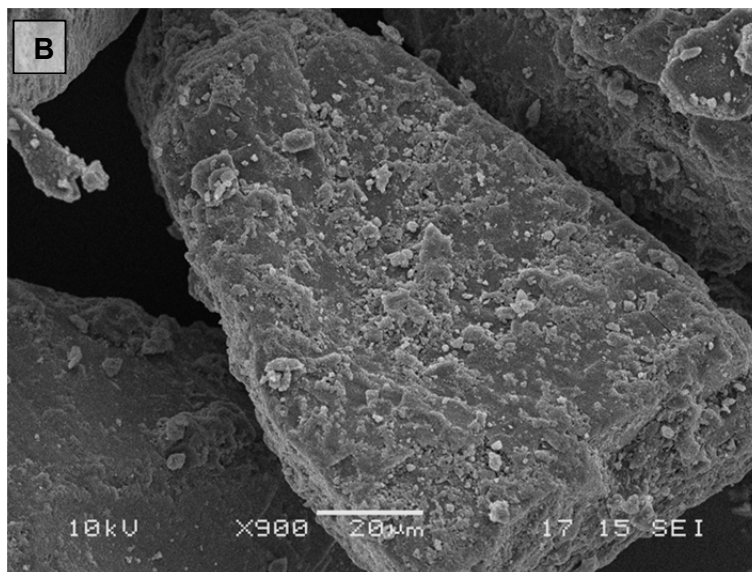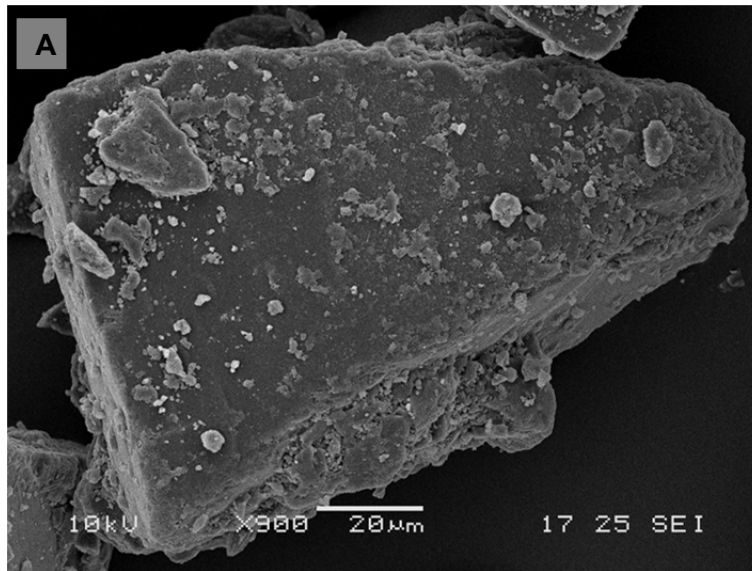
FIGURE 3.5 900X MAGNIFICATION SCANNING ELECTRON MICROGRAPHS OF A) 0.02% B) 0.05% C) 0.08% D) 0.1% E) 0.2% F) 0.3% G) 0.4% H) 1% AND I) 2% FLUTICASONE PROPIONATE FORMULATIONS WITH SV010 AS THE CARRIER
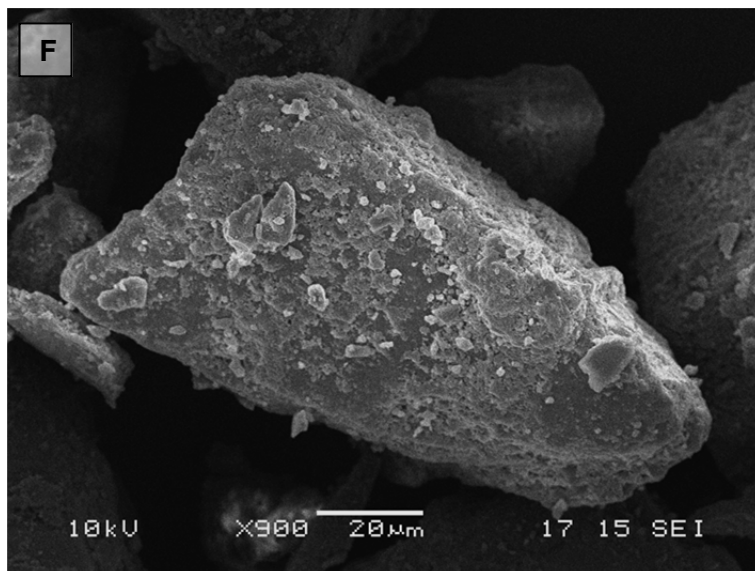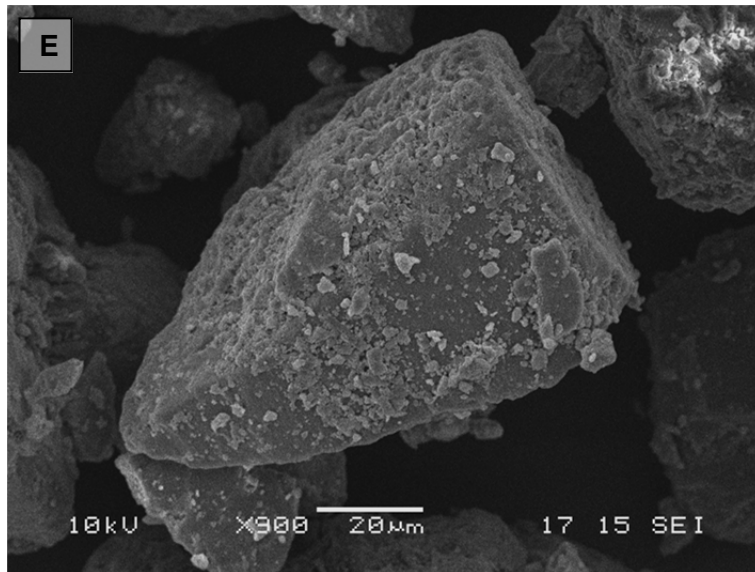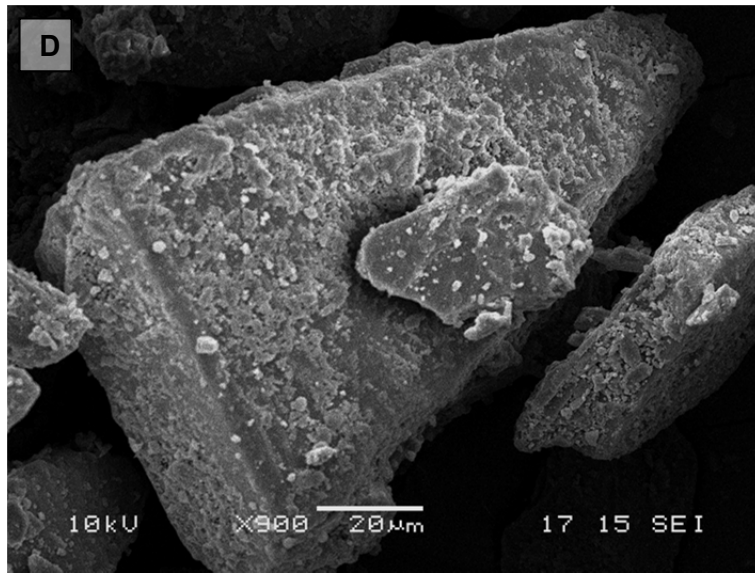
FIGURE 3.5(CONTINUED)
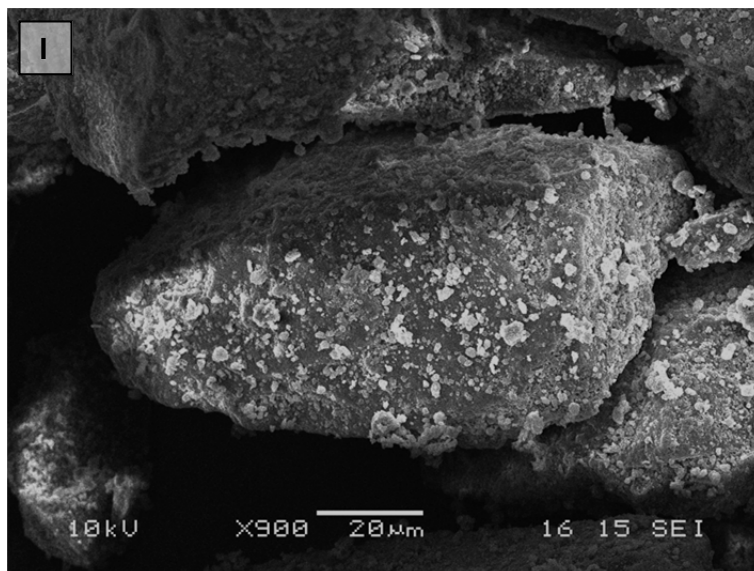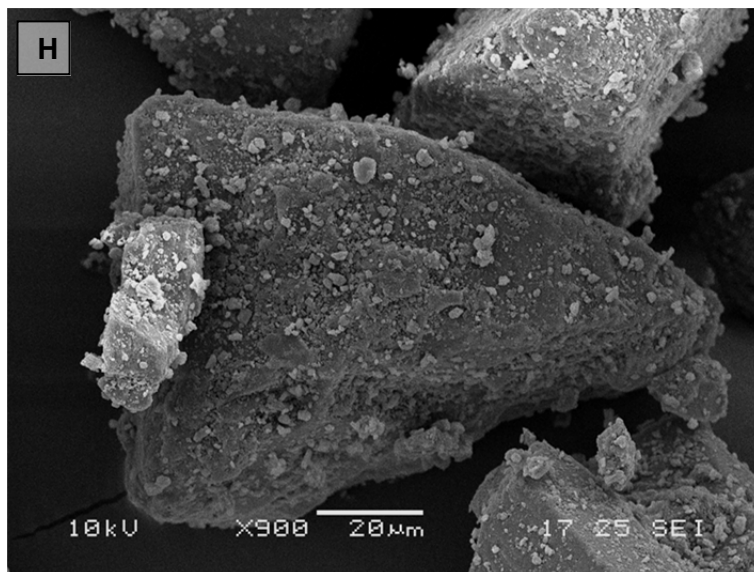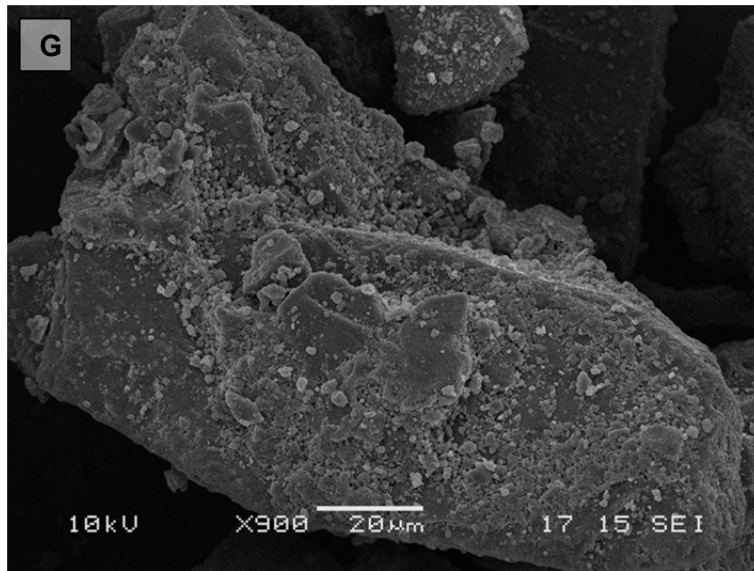
FIGURE 3.5(CONTINUED)

3.3.3 In vitro performance of the formulations

The results from dose content uniformity determination for the different formulations are summarised in Table 3.3. The actual dose in the formulations is close to the formulated dose. These data indicate that no significant amount of either the drug or the carrier was lost during the blending procedure due to adhesion to the blending vessel walls. The variation in the dose in ten random samples was generally seen to be at an acceptable level with the variation coefficient being less than or close to 6%. The variation coefficient is plotted as a function of the loaded drug dose in Figure 3.6. The figure highlights that at lower drug concentrations a high variation and fluctuations in the dose content uniformity were apparent for both the carriers. However, at higher drug concentrations, a plateau level in the dose variation was reached. Remarkably, the plateau level was lower for the formulations prepared with SV010 than for LH100 formulations. This indicates the FP particles were more evenly distributed in the formulations prepared with SV010 than in the formulations prepared with LH100. As discussed above, based on the SEM images, the SV010 formulations were seen to form agglomerated systems at lower drug concentrations. These findings suggest that agglomerate formation promotes even drug distribution within the formulations.

TABLE 3.3 THE ACTUAL DOSE OF FLUTICASONE PROPIONATE IN THE DIFFERENT FORMULATIONS IN TERMS OF WEIGHT PERCENTAGE (WT-%) AND DOSE IN MICROGRAMS. THE DATA REPRESENTS MEAN ± STANDARD DEVIATION, n=10). THE COEFFICIENT OF VARIATION (%CV) FOR THE DOSE WITHIN THE TEN SAMPLES FOR THE DIFFERENT FORMULATIONS IS ALSO TABULATED.

Carrier	Blend (wt-%)	Dose ± S.D. (wt-%)	Dose ± S.D. (µg)	%CV
LH100	0.02	0.02 ± 0.00	5.16 ± 0.20	4.39
	0.05	0.05 ± 0.00	12.06 ± 0.41	2.90
	0.08	0.07 ± 0.00	18.71 ± 0.56	2.37
	0.1	0.09 ± 0.00	23.63 ± 0.38	1.03
	0.15	0.14 ± 0.01	35.12 ± 2.35	6.28
	0.2	0.20 ± 0.01	50.15 ± 1.23	2.55
	0.4	0.39 ± 0.01	99.04 ± 1.74	1.61
	1	0.97 ± 0.02	242.80 ± 4.57	1.81
	2	2.02 ± 0.07	507.46 ± 19.93	3.67
SV010	0.02	0.02 ± 0.00	5.14 ± 0.19	3.49
	0.05	0.05 ± 0.00	12.29 ± 0.28	1.71
	0.08	0.08 ± 0.00	19.86 ± 0.78	3.84
	0.1	0.10 ± 0.00	23.98 ± 0.31	1.18
	0.2	0.20 ± 0.00	50.75 ± 0.82	1.35
	0.3	0.30 ± 0.02	74.09 ± 4.30	5.33
	0.4	0.40 ± 0.01	99.77 ± 2.19	3.16
	1	0.96 ± 0.01	241.52 ± 2.33	0.76
	2	1.96 ± 0.03	494.71± 10.07	1.33
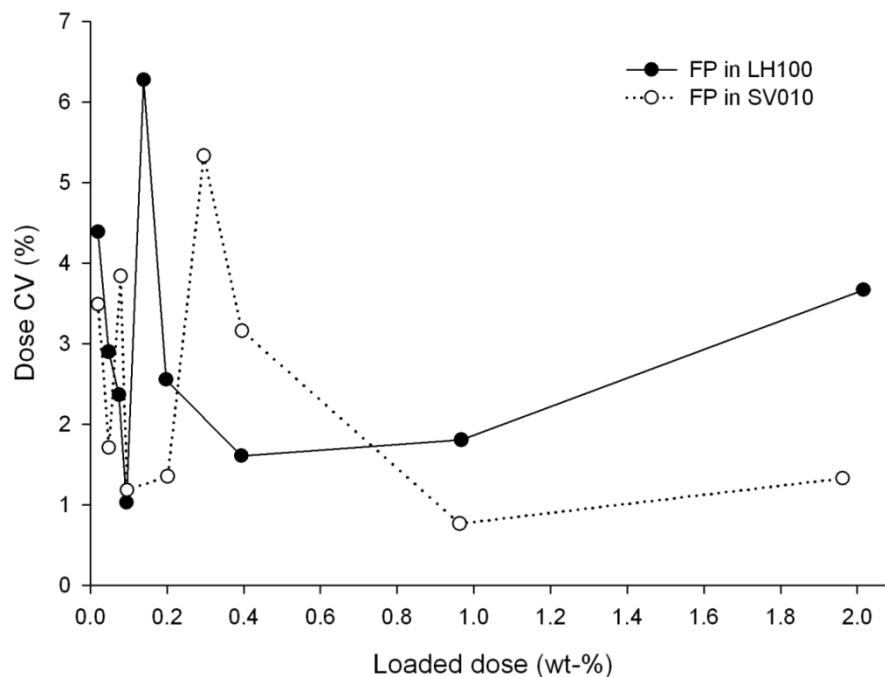
FIGURE 3.6 THE VARIATION IN THE DRUG CONTENT (DOSE CV) FOR THE FORMULATIONS PREPARED WITH LH100 AND SV010 AS THE CARRIERS AS A FUNCTION OF THE FLUTICASONE PROPIONATE CONCENTRATION (LOADED DOSE)

The emitted dose of drug from the different formulations is shown in Table 3.4. These data are plotted against the loaded drug dose in Figure 3.7. In the case of both formulation series, a linear response was observed. The R^2 values were 0.9926 and 0.9952 for the LH100 and SV010 formulation series, respectively. These data are in an agreement with the earlier studies investigating the impact of loaded drug dose on DPI performance, where it was found that the drug loading did not have an impact on the proportion of salbutamol sulphate being left behind in the device and capsule (El-Sabawi *et al.* 2006; Young *et al.* 2005).

TABLE 3.4 THE MEAN EMITTED DOSE ± STANDARD DEVIATION FOR THE DIFFERENT FORMULATIONS DURING *IN VITRO* TESTING (n=3)

Carrier	Blend (wt-%)	ED ± S.D. (µg)	Carrier	Blend (wt-%)	ED ± S.D. (µg)
	0.02	5.20 ± 0.22		0.02	4.84 ± 0.21
	0.05	11.76 ± 0.11		0.05	10.89 ± 0.37
	0.08	17.47 ± 0.21		0.08	17.75 ± 0.06
	0.10	20.60 ± 0.97		0.10	21.89 ± 0.15
LH100	0.15	32.45 ± 0.15	SV010	0.20	47.09 ± 0.66
	0.20	42.97 ± 0.17		0.30	64.35 ± 0.44
	0.40	85.74 ± 0.94		0.40	84.30 ± 0.82
	1	201.11 ± 2.80		1	192.28 ± 2.17
	2	363.86 ± 1.13		2	359.66 ± 5.04
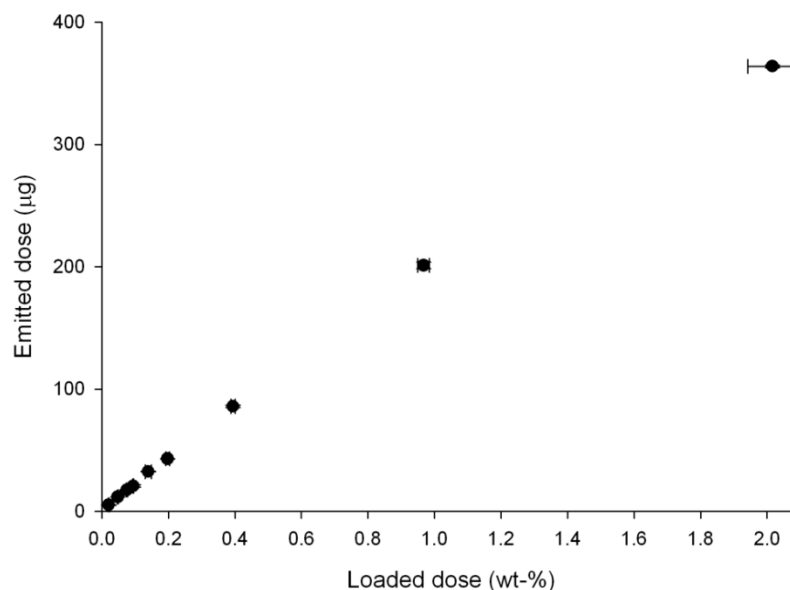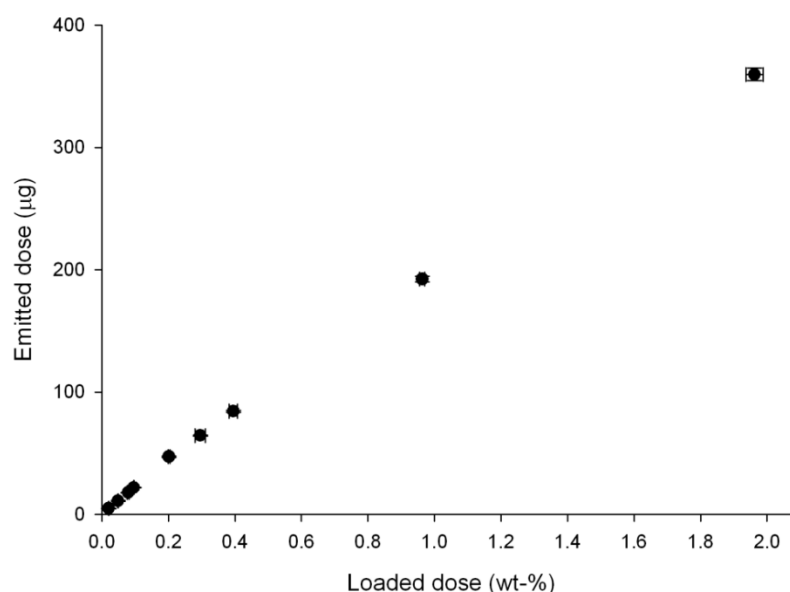
119

LH100 formulations

SV010 formulations

The total mass of fluticasone propionate recovered from the impactor during NGI testing and the mass of drug recovered from the impactor stages, impactor stage mass (ISM, mass of particles smaller than 6.48 µm at 90 l/min) (Marple *et al.* 2003b) together with the performance of the formulations in terms of fine particle fraction of the emitted and recovered dose are summarised in Table 3.5. A measurement of the drug

deagglomeration efficiency from the formulations as characterised by mean mass aerodynamic diameter is also presented in Table 3.5.

In the previous studies investigating the impact of the loaded drug dose on DPI performance, it was reported that the fine particle mass exhibited an initial increase upon an increase in the drug dose after which a plateau level was achieved (El-Sabawi *et al.* 2006; Young *et al.* 2005). However, after a critical concentration, an asymptotic increase in the fine particle mass was achieved at higher drug loadings. These studies claimed that the concentration where the change from the plateau level to the asymptotic increase took place was indicative of the filling of the active sites on the coarse carrier. In these studies, the drug concentrations where this transition took place were different for carriers exhibiting different surface roughness.

The mass of the drug delivered to the impactor stages in the current study is plotted as a function of the drug concentration in Figure 3.8. For SV010, there was no evidence of a plateau level in the impactor stage mass. In the case of LH100, the formulations exhibited similar impactor stage mass at 0.08 and 0.1 wt-% concentrations and 0.15 and 0.20 wt-% concentrations.

The results of Young *et al.* (2005) and El-Sabawi *et al.* (2006) also demonstrated an initial decrease in the fine particle fraction of the drug as the drug concentration was increased until a minima was reached. After the minimum, the performance increased. Different carriers exhibited a minimum fine particle fraction at different concentrations with a smoother carrier lactose exhibiting the minimum at a lower concentration of active pharmaceutical ingredient (API). This finding was attributed to a lower critical concentration requirement to occupy and saturate the active sites. The fine particle fractions of emitted and recovered doses in the current study are plotted as a function of the drug concentration for LH100 and SV010 formulations in Figure 3.9 and in Figure 3.10, respectively. For both carriers, there was no initial dip in the fine particle fraction of the FP formulations. At lower drug concentrations, the fine particle fraction remained somewhat unaltered for both carriers. However, the experimental errors were relatively large. In terms of fine particle fraction performance of emitted and recovered dose, an increasing trend for LH100 formulations was seen from 0.4 wt-% drug loading onwards. For SV010, the increase started earlier with an increasing trend in the fine particle fractions from 0.2 wt-% drug concentration upwards.

As discussed, the surface roughness of SV010 is greater than that of LH100. Thus, one would expect that the critical concentration for active site filling for SV010 would be higher than for LH100. However, the data from the current study indicate the opposite. Also, the performance of SV010, as measured by the impactor stage mass and fine particle

fractions of both the emitted and recovered dose, was superior to LH100. Furthermore, the proportion of fine particles detaching from SV010 during the particle sizing experiments as illustrated in Figure 3.3 was much higher than for LH100. Unlike the previous reported studies, this study questions the validity of the active site theory with the increasing addition of FP to the SV010 and LH100.

TABLE 3.5 SUMMARY OF NGI TESTING OF THE FORMULATIONS IN TERMS OF TOTAL RECOVERED DOSE (RD) OF FLUTICASONE PROPIONATE, MASS OF DRUG DELIVERED TO THE IMPACTOR STAGES (ISM), THE FINE PARTICLE FRACTIONS OF EMITTED (FPF$_{ED}$) AND RECOVERED DOSE (FPF$_{RD}$) AND THE MEAN MASS AERODYNAMIC DIAMETER (MMAD) OF THE DRUG FOR THE DIFFERENT FORMULATIONS. THE DATA REPRESENTS AVERAGE FROM 3 DETERMINATIONS ± STANDARD DEVIATION.

	Blend (wt-%)	RD ± S.D. (µg)	ISM ± S.D. (µg)	FPF$_{ED}$ ± S.D. (%)	FPF$_{RD}$ ± S.D. (%)	MMAD±S.D. (µm)
LH100	0.02	5.45 ± 0.20	0.32 ± 0.06	6.21 ± 1.40	5.92 ± 1.30	4.26 ± 0.49
	0.05	12.50 ± 0.15	0.92 ± 0.06	7.82 ± 0.52	7.36 ± 0.49	3.73 ± 0.06
	0.08	18.72 ± 0.20	1.56 ± 0.22	8.92 ± 1.18	8.33 ± 1.11	3.47 ± 0.22
	0.10	22.95 ± 0.97	1.58 ± 0.00	7.66 ± 0.37	6.87 ± 0.30	3.71 ± 0.01
	0.15	36.54 ± 0.21	3.00 ± 0.12	9.24 ± 0.35	8.21 ± 0.33	3.17 ± 0.05
	0.20	48.02 ± 0.35	3.24 ± 0.14	7.54 ± 0.34	6.75 ± 0.33	2.94 ± 0.05
	0.40	96.76 ± 0.98	6.20 ± 0.12	7.23 ± 0.07	6.41 ± 0.09	3.04 ± 0.01
	1	238.13 ± 2.44	19.13 ± 0.75	9.52 ± 0.46	8.04 ± 0.36	2.70 ± 0.07
	2	467.38 ± 9.87	43.88 ± 1.41	12.06 ± 0.21	9.39 ± 0.11	2.94 ± 0.03
SV010	0.02	5.83 ± 0.48	0.42 ± 0.05	8.59 ± 0.70	7.12 ± 0.25	3.21 ± 0.22
	0.05	12.39 ± 0.13	0.97 ± 0.04	8.88 ± 0.24	7.80 ± 0.24	3.13 ± 0.04
	0.08	19.72 ± 0.07	1.65 ± 0.09	9.28 ± 0.48	8.36 ± 0.41	3.03 ± 0.07
	0.10	24.25 ± 0.13	2.08 ± 0.08	9.50 ± 0.32	8.58 ± 0.27	2.92 ± 0.04
	0.20	52.75 ± 0.53	4.08 ± 0.49	8.67 ± 0.81	7.74 ± 0.76	2.74 ± 0.12
	0.30	72.13 ± 1.71	5.83 ± 0.12	9.06 ± 0.15	8.09 ± 0.28	2.80 ± 0.03
	0.40	98.13 ± 0.49	8.07 ± 0.51	9.57 ± 0.50	8.22 ± 0.51	2.62 ± 0.02
	1	233.42 ± 2.97	25.39 ± 0.32	13.21 ± 0.20	10.88 ± 0.15	2.44 ± 0.01
	2	454.7 ± 11.33	58.15 ± 1.60	16.17 ± 0.38	12.79 ± 0.40	2.45 ± 0.02
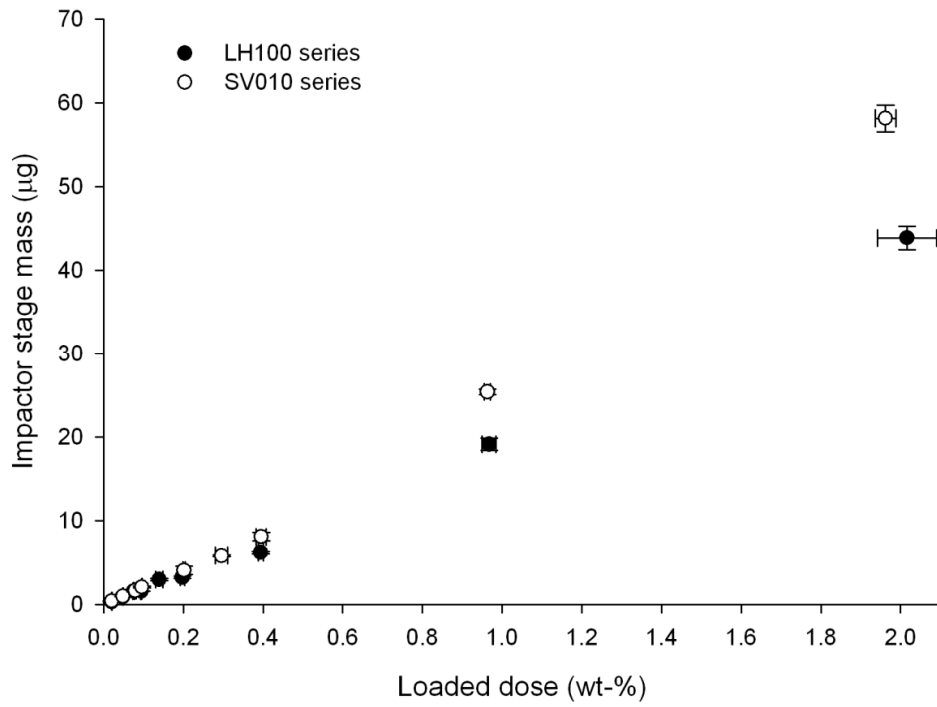
FIGURE 3.8 THE MASS OF DRUG DELIVERED TO THE IMPACTOR STAGES AS A FUNCTION OF THE FLUTICASONE PROPIONATE CONTENT (LOADED DOSE) OF THE FORMULATIONS. THE DATA REPRESENTS MEAN ± STANDARD DEVIATION, N=10 FOR THE FLUTICASONE PROPIONATE CONTENT AND N=3 FOR IMPACTOR STAGE MASS.
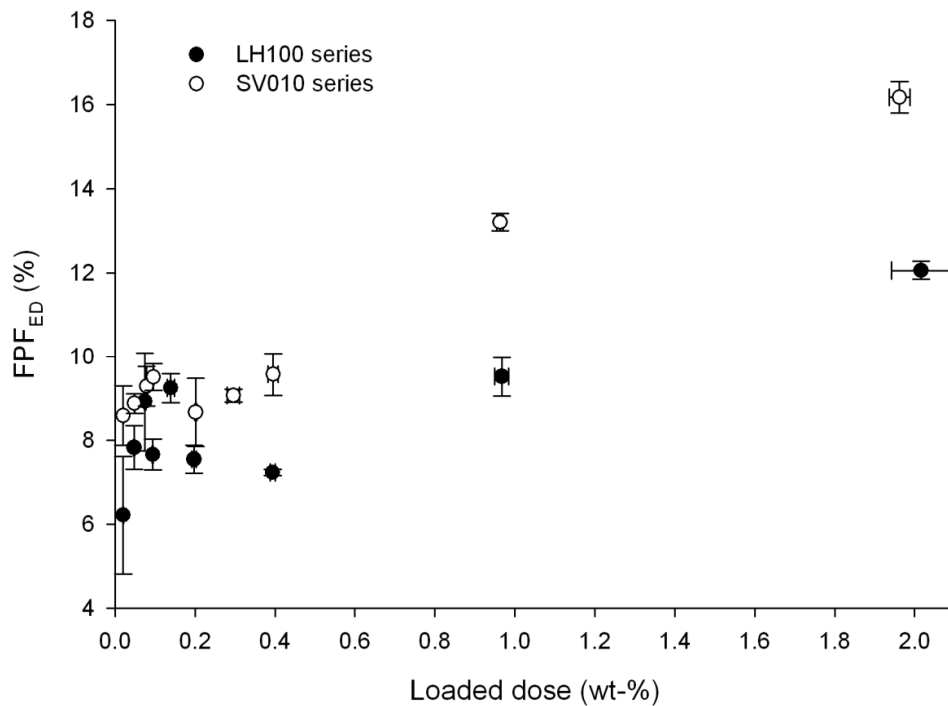
FIGURE 3.9 THE FINE PARTICLE FRACTION OF EMITTED DOSE (FPF$_{ED}$) AS A FUNCTION OF THE FLUTICASONE PROPIONATE CONTENT (LOADED DOSE) FOR THE FORMULATIONS INVESTIGATED. THE DATA REPRESENTS MEAN ± STANDARD DEVIATION, N=10 FOR THE FLUTICASONE PROPIONATE CONTENT OF THE FORMULATIONS AND N=3 FOR FINE PARTICLE FRACTION OF EMITTED DOSE.
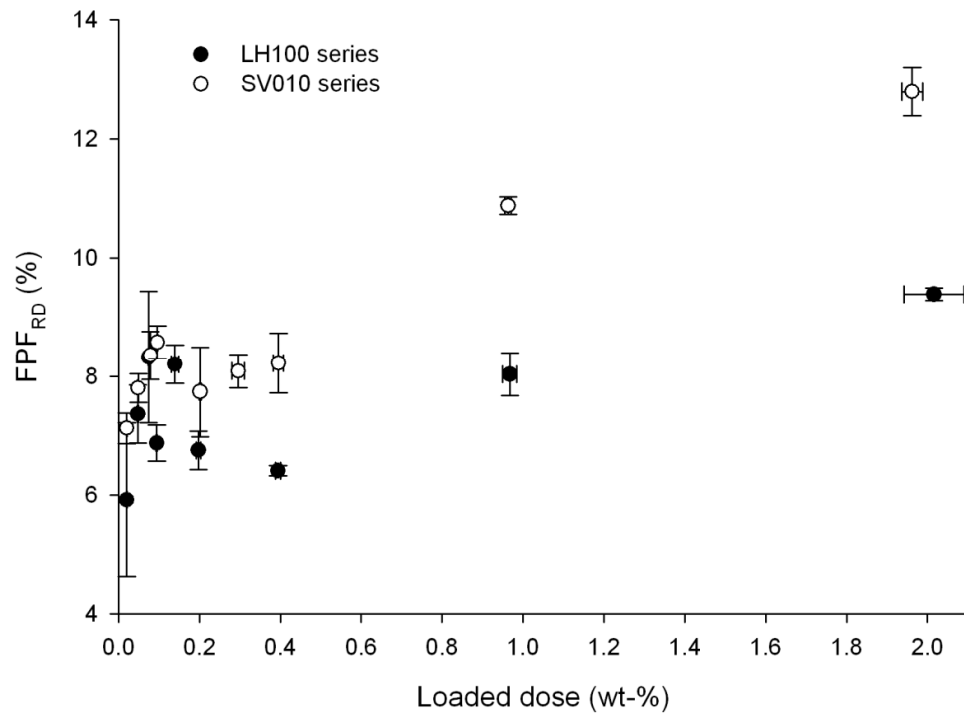
FIGURE 3.10 THE FINE PARTICLE FRACTION OF RECOVERED DOSE (FPF$_{RD}$) AS A FUNCTION OF THE FLUTICASONE PROPIONATE CONTENT (LOADED DOSE) OF THE FORMULATIONS INVESTIGATED. THE DATA REPRESENTS MEAN ± STANDARD DEVIATION, N=10 FOR FLUTICASONE PROPIONATE CONTENT OF THE FORMULATIONS AND N=3 FOR FINE PARTICLE FRACTION OF RECOVERED DOSE.

Calculations of the mean mass aerodynamic diameter (MMAD) of the drug delivered on the impactor stages of the respective formulations, raises further questions regarding the validity of the active sites theory. The values of MMAD are listed in Table 3.5 and are plotted as a function of the loaded drug dose in Figure 3.11. Across the entire concentration range investigated, the MMAD of the LH100 formulations was greater than for the SV010 formulations. These data indicate different drug deagglomeration behaviour for the formulations prepared with different carriers, with SV010 producing a higher degree of drug deagglomeration.

A previous study has reported a similar decrease in the MMAD as drug concentration was increased (Dickhoff *et al.* 2005). The authors attributed the higher MMAD at low drug loading to the lower magnitude of press on forces at low drug concentration. Consequentially, due to the weak press on forces at low drug loadings, the mixing was less efficient and thus the drug was distributed on the surface of the large lactose carriers as large agglomerates. These agglomerates were not efficiently dispersed upon inhalation thus resulting in a high MMAD at low drug concentrations. The same study also suggested that the larger the carrier particles, the larger the press on forces, and the more efficient the drug re-distribution during blending (Dickhoff *et al.* 2005). As in the current study, the SV010 was seen to have slightly larger overall particle size than LH100 (See

124

Figure 3.1 and Table 3.1), this could explain why the MMAD for SV010 formulations was smaller than for LH100 formulations over the entire concentration range.

However, the suggestion by Dickhoff *et al.* (2005), according to which the formation of agglomerated systems at low drug loadings resulted to an increased MMAD, can be questioned. This is because the drag force experienced by a particle or an agglomerate upon fluidisation is proportional to the square of its diameter (Begat *et al.* 2004a). Furthermore, the kinetic energy of a particle or an agglomerate is proportional to its diameter cubed (Begat *et al.* 2004a). Therefore, firstly, the detachment of a particle or an agglomerate from a surface of a coarse carrier becomes more likely as its size is increased. Secondly, the likelihood of deagglomeration increases upon increasing the kinetic energy of the entities detached from surfaces upon fluidisation. Therefore, agglomerated systems should produce better drug deagglomeration efficiency, and consequentially, smaller MMAD. In the current study the formulations prepared with SV010 were seen to produce both a higher delivered dose and smaller MMAD. These data indicate the detachment of the drug from the surface of SV010 was more complete and that the formulations prepared with SV010 also went through a more complete deagglomeration than the formulations prepared with LH100. Therefore, the current data indicate agglomerate formation may be able to explain the differences seen in the formulation performance of LH100 and SV010 formulations.
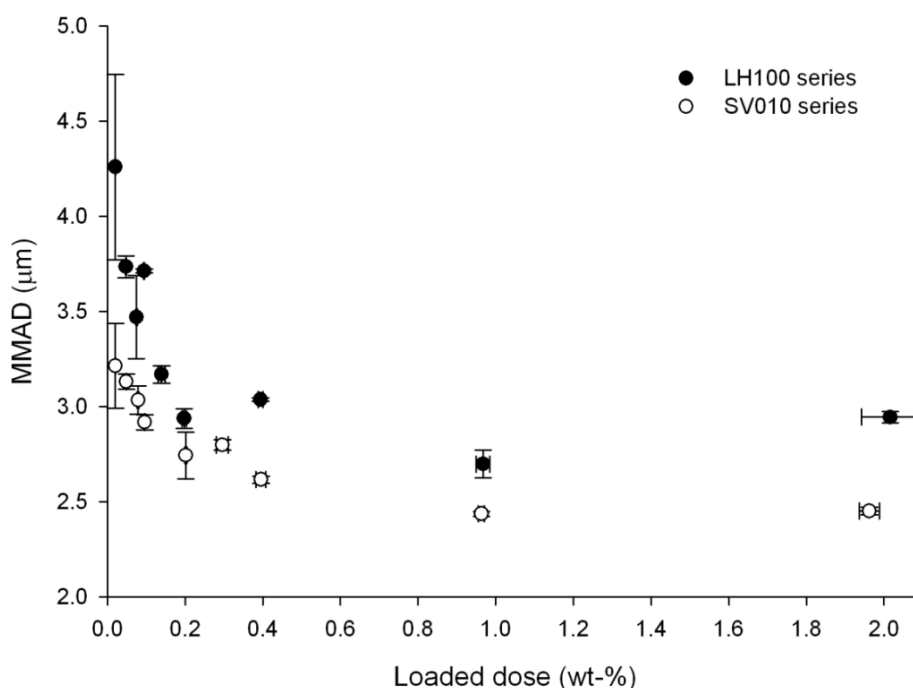
FIGURE 3.11 MEAN MASS AERODYNAMIC DIAMETER (MMAD) OF FLUTICASONE PROPIONATE DELIVERED TO THE IMPACTOR STAGES AS A FUNCTION OF FLUTICASONE PROPIONATE CONTENT (LOADED DOSE) OF THE FORMULATIONS. THE DATA REPRESENTS MEAN ± STANDARD DEVIATION, N=10 FOR FLUTICASONE PROPIONATE CONTENT OF THE FORMULATIONS AND N=3 FOR MEAN MASS AERODYNAMIC DIAMETER

Pre-separator deposition is of particular interest if evidence for the active site theory is being sought. This is because the majority of the large lactose particles will deposit in the pre-separator, with any drug adhered to the surface of the large carriers also depositing in the pre-separator. Figure 3.12 illustrates the pre-separator deposition patterns in a hypothetical case where the DPI performance is determined by the active sites theory. At low drug loading, well below the critical concentration, a high proportion of drug should be deposited in the pre-separator with very little drug being delivered to the impactor stages. As the drug concentration increases, but remains below the critical concentration, an increased proportion of the drug should be recovered from the pre-separator. This is because the added drug is preferentially binding to the active sites and therefore does not detach upon inhalation. At the critical concentration, pre-separator deposition should exhibit a peak value, as all the active sites are filled. If the drug concentration is then further increased, there should be an increase in the proportion of detached drug and a decrease in the pre-separator deposition with increasing drug concentration. This is because all the active sites have been saturated. Consequentially, the excess drug should bind to the low energy binding sites and thus detach easily upon the dose delivery.
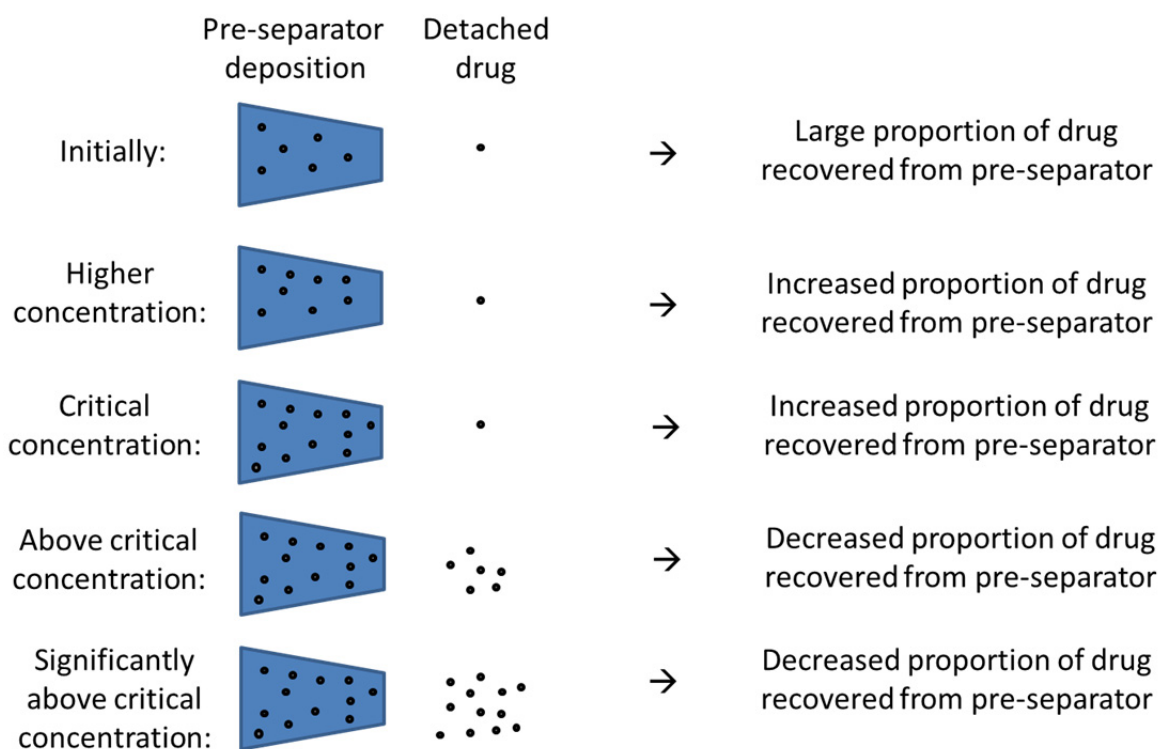
FIGURE 3.12 SCHEMATIC PREDICTION OF THE PROPORTION OF DRUG DEPOSITED IN THE PRE-SEPARATOR IF THE ACTIVE SITES THEORY HOLDS TRUE

The stage-by-stage deposition profiles of the delivery of FP from the prepared formulations as a proportion of total recovered drug dose are shown in Figure 3.13. As

shown by the pre-separator deposition profiles of the formulations in Figure 3.13, it appears that the active sites theory could govern the drug detachment and carrier retention for SV010 formulations. However, the pre-separator deposition pattern seen for the series of SV010 formulations may also be explained by the additional amount of drug retained in the capsule and device at low drug concentrations. If the drug retained within the capsule and the device would have been emitted, the pre-separator deposition profile may have been similar to that exhibited for the LH100 formulations. In general, these data suggest limited evidence for active sites theory.

The proportion of drug retained in the capsule exhibited a generally increasing trend upon increasing the drug loading with both the carriers. The increase in capsule deposition was seen to be statistically significant for the 0.15 wt-%, 1 wt-% ($p<0.05$) and for the 2 wt-% formulations ($p<0.01$) prepared with LH100 compared to the 0.02 wt-% formulation prepared with the same carrier. The device deposition patterns showed that at low drug loading, a higher proportion of drug was deposited in the device from the SV010 formulations than from the equivalent LH100 formulations. However, at higher drug loadings the formulation series were similar in terms of device deposition. The device deposition of the drug from all the LH100 formulations was significantly higher than from the 0.02% formulation ($p<0.05$). For SV010 formulations, a significant increase in the device deposition was seen at 0.4 wt% and higher drug concentrations.

The proportion of drug deposited in the mouthpiece and throat was not significantly affected by loaded drug dose ($p>0.05$). A slightly lower proportion of drug was retained in the throat from SV010 formulations than for the LH100 formulations.

When the proportion of drug delivered to the impactor stages in Figure 3.13 was inspected, it was show that the proportion of drug recovered from Stage 1 of the impactor significantly decreased as the concentration of FP was increased. This trend was observed for both the carriers. As discussed above, the drug may either become more efficiently redistributed on the surface of the large carrier at higher drug concentrations or form agglomerates which reside on the lactose. Some of the agglomerates that should on the basis of their size be deposited in the pre-separator are sometimes carried through and deposited on Stage 1 of the impactor. Therefore, the decrease in the amount of drug recovered from Stage 1 is likely to be a consequence of either better drug re-distribution during formulation blending or greater drug deagglomeration upon fluidisation as a result of agglomerate formation.

For the LH100 formulations, the proportion of drug deposited on Stage 2 did not indicate a clear trend with increasing drug concentrations. A significantly higher proportion of drug

was collected on Stage 3 at drug concentrations above 0.08 wt%. Drug deposition on Stages 4 to 8 did not exhibit clear trends. For the SV010 formulations, increasing proportion of drug was recovered from Stage 2 to Stage 5 as the loaded drug dose was increased. The stage deposition patterns for the formulations reflected the overall performance of the formulations, with SV010 formulations outperforming the formulations prepared with LH100.

The *in vitro* performance data obtained for the formulation series prepared with the two different carriers provided very limited evidence for the active sites theory. To investigate whether changes in the fluidisation mechanism from erosion to fracture could explain the trends seen in the *in vitro* performance of the formulations, high speed imaging of fluidisation of selected formulations was performed. The findings will be described in the following section.

LH100 series
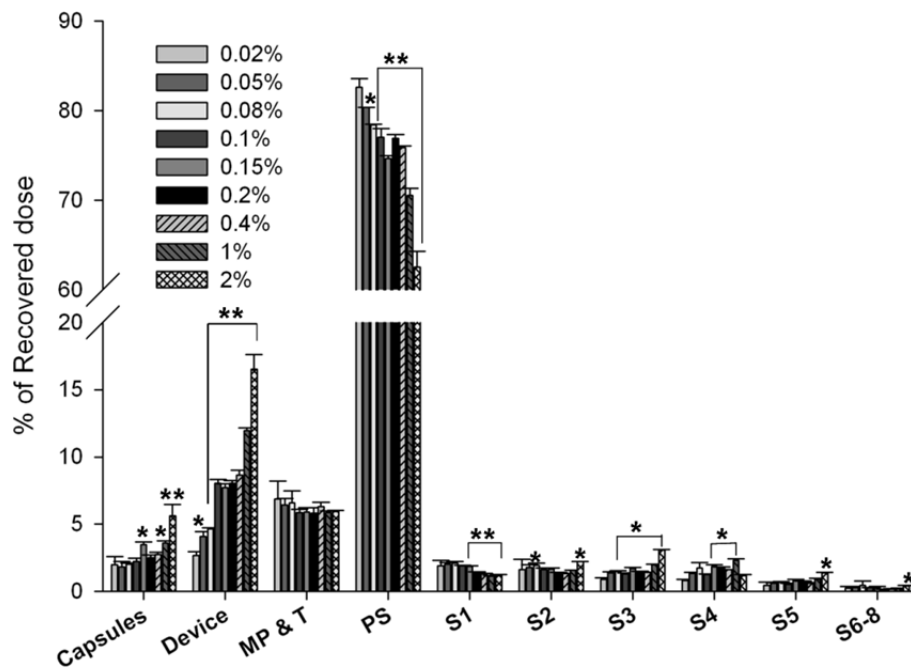
SV010 series
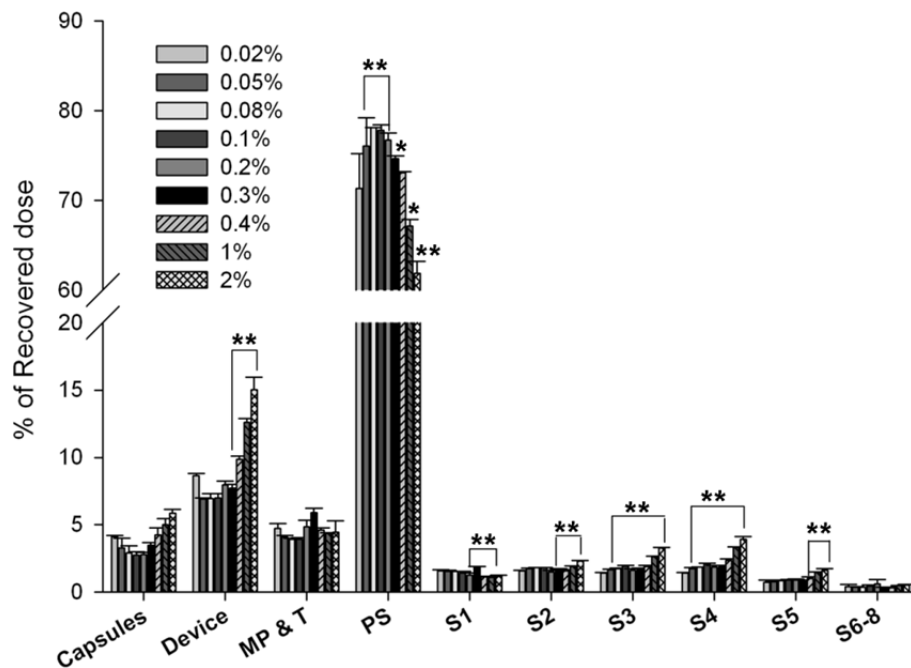
FIGURE 3.13 STAGE-BY-STAGE DEPOSITION PROFILES OF FLUTICASONE PROPIONATE FROM THE FORMULATIONS PREPARED WITH LH100 (TOP) AND SV010 (BOTTOM) AS THE IN TERMS OF PROPORTION OF THE DOSE RECOVERED FROM DIFFERENT PARTS OF THE IMPACTOR. THE DATA REPRESENTS MEAN ± STANDARD DEVIATION, N=3. ASTERISKS DENOTE STATISTICALLY SIGNIFICANT DIFFERENCE * $p<0.05$, ** $p<0.01$ (1 WAY ANOVA, FISHER PAIRWISE COMPARISON WITH 95% CONFIDENCE LIMIT). MP & T = MOUTHPIECE AND THROAT, PS=PRE-SEPARATOR, S=STAGE.

3.3.4 Characterisation of the fluidisation mechanisms of the formulations

It has been shown that there are two different mechanisms for fluidisation of DPI formulations, namely erosion and fracture (Shur *et al.* 2008a; Tuley *et al.* 2008). These studies demonstrated that free flowing powders exhibit an erosion mechanism and more cohesive powders fluidise via the fracture mechanism. (Tuley *et al.* 2008). It has also been shown that powders exhibiting the fracture mechanism upon fluidisation produce a better DPI performance (Shur *et al.* 2008a). In the aforementioned study, the improved performance for formulations fluidising following the fracture mechanism was attributed to the higher amount of particle-particle and particle-device collisions taking place when the powder fractures due to the high density of particles entrained upon a fracture of the powder bed. One of the objectives of the current study was to investigate whether these two different mechanisms of fluidisation may have influenced the improved fine particle fraction behaviour observed by Young *et al.* (2005) and El-Sabawi *et al.* (2006) for increased drug concentration.

To study the fluidisation mechanism of the formulations, high speed imaging of the fluidisation event was recorded for low, intermediate and high drug loadings with both the carriers. Snapshots of the fluidisation events for 0.02, 0.4 and 2 wt-% FP formulations with LH100 and SV010 as the carriers are presented in Figure 3.14. No evidence of a change in the fluidisation mechanism was seen. All the formulations fluidised following the erosion mechanism.
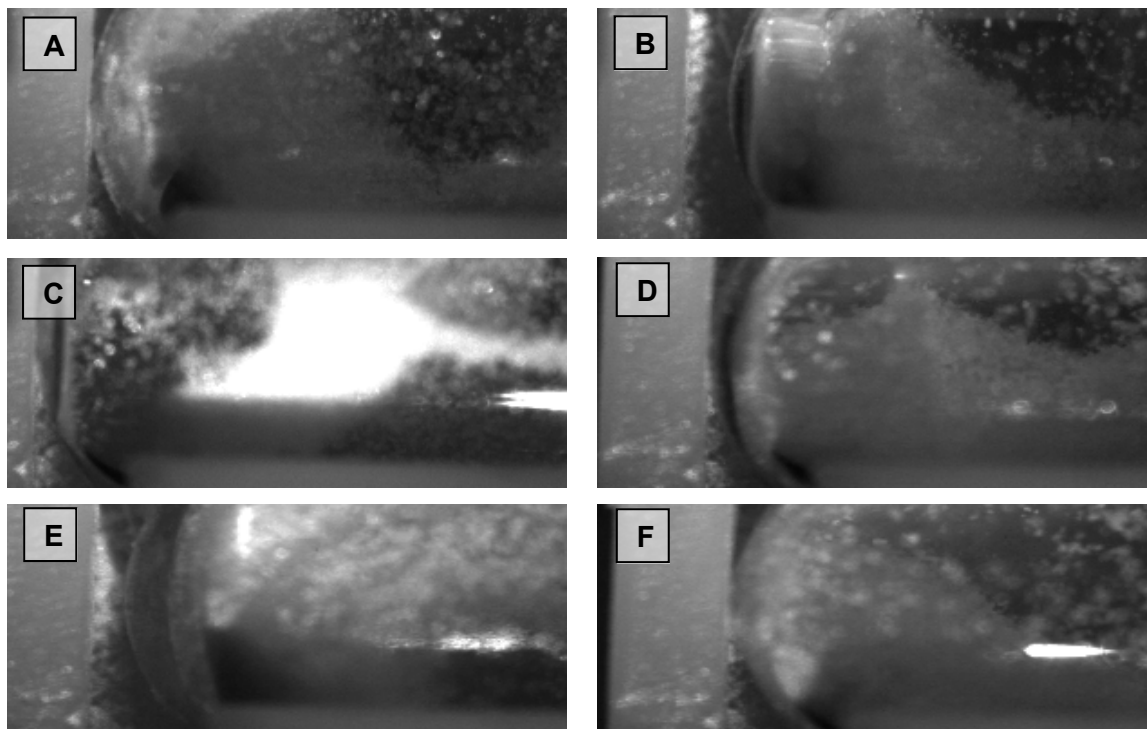
FIGURE 3.14 REPRESENTATIVE SNAPSHOTS OF HIGH SPEED IMAGING FOOTAGE OF THE FLUIDISATION EVENT OF 0.02% FLUTICASONE PROPIONATE IN A) LH100 AND B) SV010, 0.4% FLUTICASONE PROPIONATE IN C) LH100 AND D) SV010 AND 2% FLUTICASONE PROPIONATE IN E) LH100 AND F) SV010

3.3.5 Characterising the fluidisation and defluidisation properties of the formulations

3.3.5.1   Method development

The theoretical foundations of characterising the powder cohesion by means of measuring the pressure drop across the powder bed as a function of the fluidising gas velocity was described in Chapter 2, section 3.4. To the author's knowledge, this technique has not been previously applied as a tool for understanding DPI formulation structure and performance. Therefore, the following section describes the method development for measuring the pressure drop across the powder bed using the FT4 powder rheometer.

It has been shown that the pressure drop of the air distributor may play a significant role in the quality of fluidisation and recommendations for the resistance of the air distributor plate are available in the literature (Geldart *et al.* 1985). The consensus is that the pressure drop of the gas distributor plate should be high enough so that the fluidising gas is evenly distributed throughout the powder bed. If the resistance is too low the fluidising gas will find the path through the powder with the lowest resistance. As a consequence, the gas flow will not be evenly distributed throughout the powder bed. This ultimately

131

affects the quality of fluidisation. The pressure drop curve for the air distributor plate of the FT4 as a function of the fluidising gas velocity is presented in Figure 3.15. The figure shows that the pressure drop of the air distributor plate is negligible. The distributor's low resistance to air flow was expected to affect the quality of fluidisation because, as discussed above, the fluidising gas was unlikely to be distributed uniformly throughout the powder bed.

The pressure drop profile of the gas distributor plate was re-engineered to a higher pressure drop by placing a filter paper underneath the frit. However, this resulted in too high a pressure drop across the distributor indicating that the air could not permeate through the distributor. As a result, the gas distributor without modifications was used for the fluidisation experiments.

Another critical parameter to the quality of the fluidisation is the height to diameter (H/D) ratio of the powder bed (Alavi *et al.* 2005; Valverde *et al.* 1998). The recommendation regarding the optimum H/D ratio varies and ranges from a ratio of 4 to 1 (Alavi *et al.* 2005; Valverde *et al.* 1998). The H/D ratio of 4 was recommended because the quality of fluidisation was seen to improve upon increasing the H/D ratio of the fluidised bed. This was attributed to proportionally higher inertia at low H/D ratios that had to be overcome to initiate the fluidisation (Alavi *et al.* 2005). Meanwhile, the H/D ratio of 1 was recommended to avoid wall friction effects (Valverde *et al.* 1998). It is important to note that the former study concentrated on Geldart group A powders with added Geldart C powders, while the latter concentrated on Geldart group C powders with added flow enhancers. The recommendations from the study by Alavi *et al.* (2005) were likely to be more applicable for the purposes of the current study because of the similarity of the powder system under investigation in the current study.

To study the effect of the H/D ratio on the fluidisation properties of the current system, fluidisation experiments with different amounts of powder were conducted. Pressure drop profiles from fluidisation experiments for different amounts of SV010 are shown in Figure 3.15. It can be seen that the mass of powder has an impact on the U_{mf} with the onset of fluidisation shifting towards lower air velocities at higher powder loading. This is also illustrated in Figure 3.16 where the U_{mf} is plotted against the mass of the powder bed. It can be concluded that a constant and high powder loading is required for reliable measurements of U_{mf}.
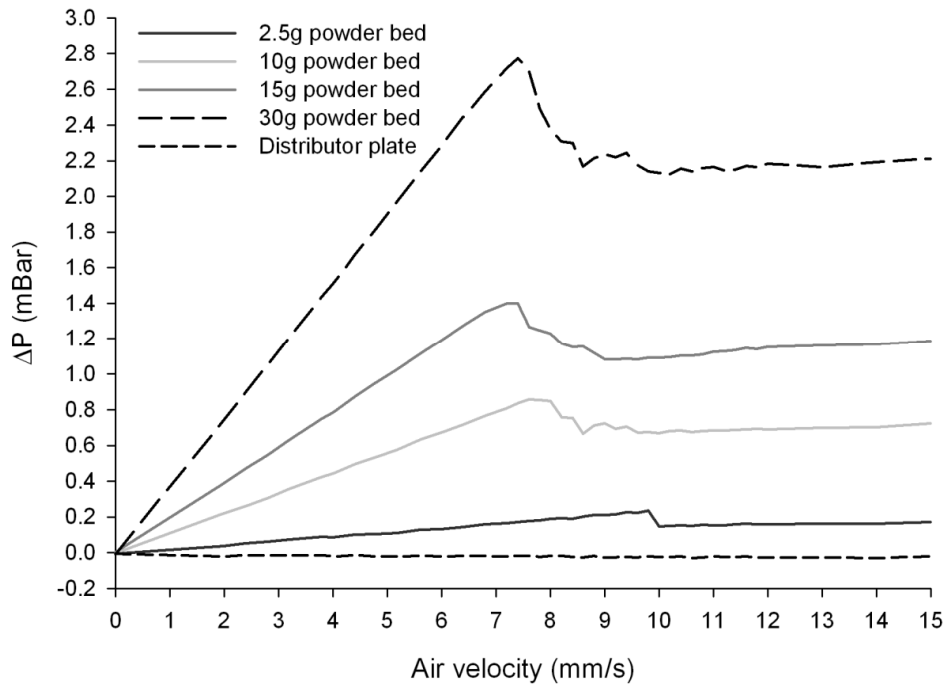
FIGURE 3.15 PRESSURE DROP CURVES FOR THE AIR DISTRIBUTOR PLATE AND POWDER BEDS OF DIFFERENT MASSES DURING FLUIDISATION EXPERIMENTS OF SV010 LACTOSE
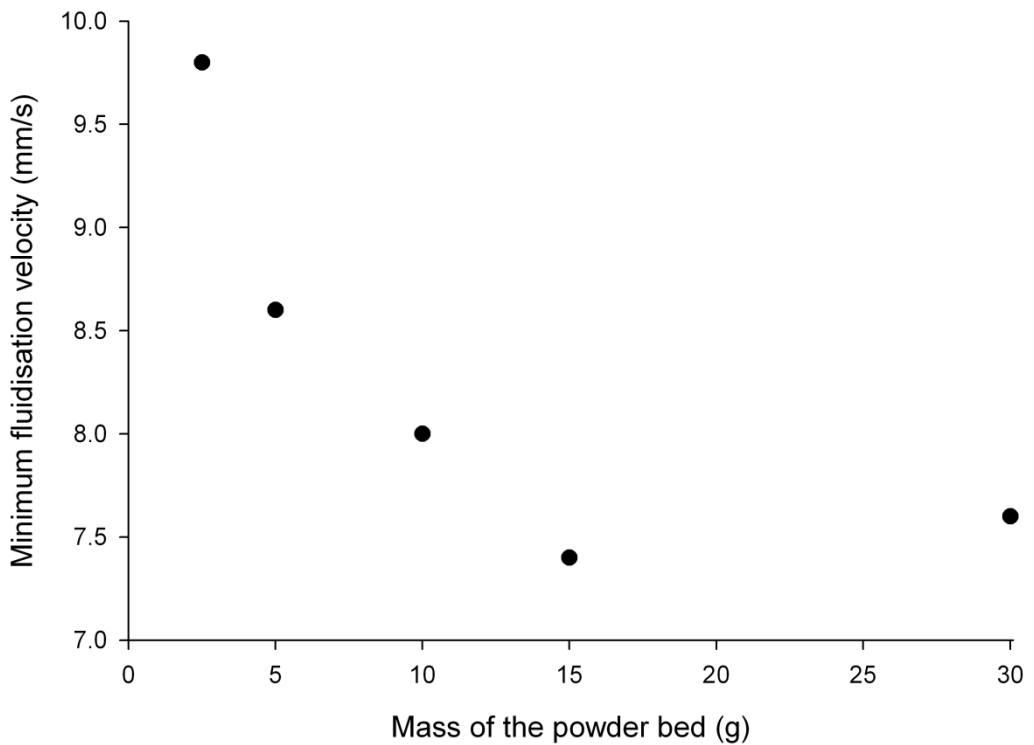
FIGURE 3.16 MINIMUM FLUIDISATION VELOCITY AS A FUNCTION OF THE MASS OF SV010 LACTOSE MEASURED (N=1)

To examine whether the H/D ratio of the powder bed was affecting the extent of fluidisation, the measured pressure drop at 15 mm/s fluidising gas velocity, at which the powders under examination had reached a steady pressure drop, was normalised against

133

the theoretical pressure drop (ΔP_{Theor}), that is defined by Equation 3.2, where m is the mass of the powder bed (kg), g is the acceleration due to gravity (9.81 ms^{-2}) and A is the cross sectional area of the powder bed (m^2).

$$\Delta P_{Theor} = \frac{mg}{A}$$

<div align="right">**EQUATION 3.2**</div>

The normalised pressure drop curves that describe the fraction of powder that has been fluidised for different amounts of SV010 are shown in Figure 3.17. It can be seen that with the lowest mass of powder (2.5 g), the lowest extent of fluidisation was achieved. Increasing the mass of powder above this resulted in a marginally higher fluidised fraction, a finding in an agreement with the study by Alavi *et al.* (2005). Figure 3.17 also shows that the slope of the pressure drop measured across the powder bed below U_{mf} as the fluidising gas velocity was increased became steeper when the mass of the powder was increased. These data indicate that as the powder loading was increased, the void fraction within the powder bed became smaller, as defined by the Carman-Kozeny law (Carman 1956). It is likely therefore that the walls of the fluidising vessel were supporting the weight of the powder when the H/D ratio was too low. These findings indicate that the recommendations of the H/D ratio by Alavi *et al.* (2005) are indeed more suitable for the current system than the recommendations by Valverde *et al.* (1998).
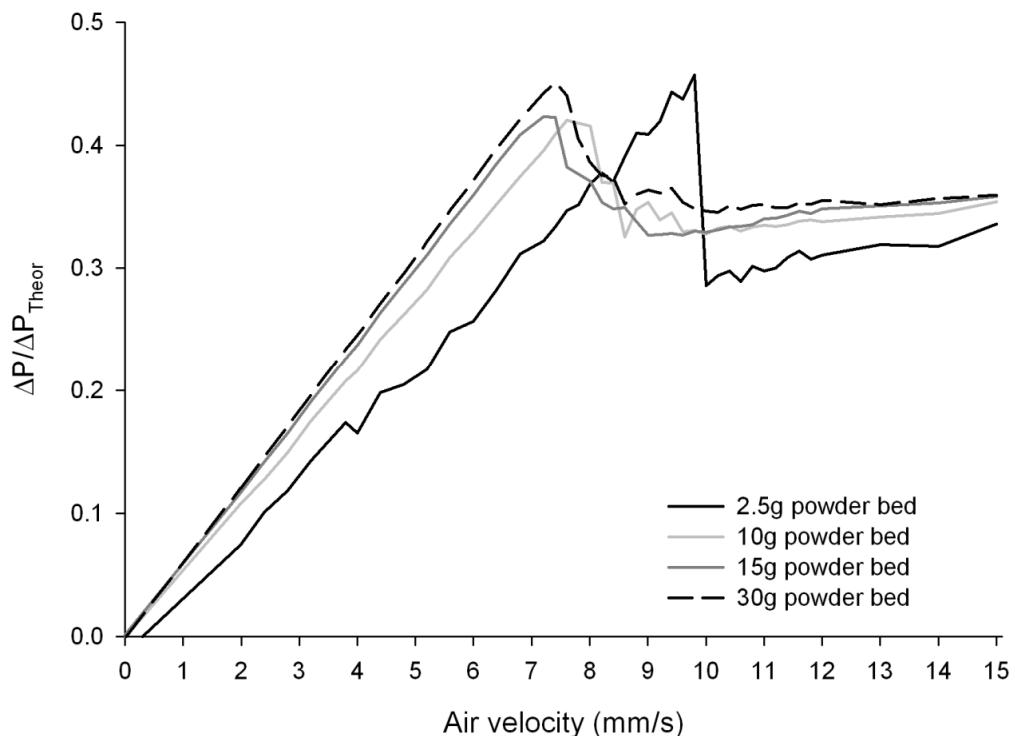
FIGURE 3.17 NORMALISED PRESSURE DROP CURVES FOR DIFFERENT AMOUNTS OF SV010 LACTOSE DURING THE FLUIDISATION EXPERIMENTS (N=1)

On the basis of the method development experiments discussed so far, all fluidisation measurements were performed with between 12 and 13 g of powder. This loading was shown to produce stable U_{mf} and a high fluidised fraction. Moreover, this amount of powder provided a high enough H/D ratio to avoid wall friction effects.

Another factor that may contribute towards the more compact powder packing for increasing H/D ratios observed in the current study is the consolidation stresses induced by the increasing gravitational force acting on the powder bed. It has been shown by Valverde *et al.* (1998) that these stresses may increase the cohesion of a powder over a period of few hours. In their study, this was attributed to the increasing number of particle-particle contacts taking place as a result of consolidation as a function of time. However, the investigators addressed this issue by showing that consolidation history of a powder could be erased by fully fluidising the powder less than five minutes before the measurements and allowing the powder to settle under gravity before pressure drop measurements commenced. In the current study, to erase the memory of the powder, the powder under investigation was fully fluidised for one minute. The air supply was then switched off for one minute to allow the powder to settle under gravity. The fluidisation experiment was started immediately after this settling period. It is therefore unlikely that the impact of increasing H/D ratio on the packing and fluidisation properties of the powder in the current study was due to increasing consolidation.

In addition to the fluidisation cycle, a defluidisation cycle was undertaken to investigate the defluidisation properties of the formulations. A typical fluidisation/defluidisation profile for SV010 is presented in Figure 3.18. The pressure drop hysteresis has been used for defining the powder cohesion (Valverde *et al.* 2000; Valverde *et al.* 1998). On the other hand, during the defluidisation cycle the interparticulate forces are non-existent because the particles have been suspended by the fluidising gas and settle under gravity as the fluidising gas velocity is decreased (Wang *et al.* 2004). Therefore, in the current study, the area enclosed by the fluidisation/defluidisation curve was used as one of the measures for the interparticulate contacts in the powders, in essence powder cohesion.
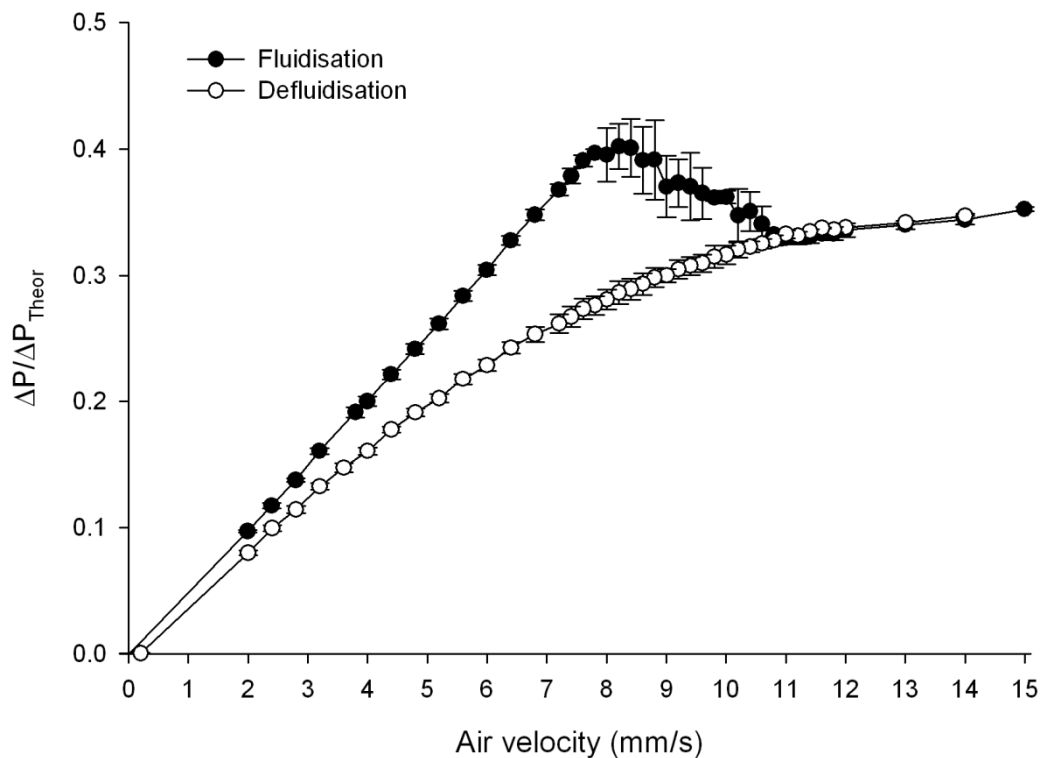
FIGURE 3.18 FLUIDISATION-DEFLUIDISATION CURVES FOR SV010 (m=12.9 g). THE DATA REPRESENTS MEAN ± STANDARD DEVIATION, N=3.

3.3.5.2   Cohesive properties of the formulations

The fluidisation curves for the series of LH100 and SV010 formulations are plotted in Figure 3.19 and Figure 3.20, respectively. In both figures it can be seen that the addition of drug fines clearly alters the fluidisation behaviour of the formulations compared to the coarse carriers. These changes are characterised by the changes in U_{mf}, area enclosed by the fluidisation/defluidisation curve and the fluidised fraction, values of which are listed in Table 3.6. These data will be discussed in more detail in the following paragraphs. For the individual fluidisation/defluidisation curves for each of the formulations the reader is referred to Appendix I.

As shown in Figures 3.19 and 3.20, the initial gradient of the fluidisation curve for both the coarse carriers are different to those of the respective formulations. According to the Carman-Kozeny law (Carman 1956), this indicates that the void fraction in the coarse carriers is larger than in the formulations. Therefore, the addition of the drug fines to the coarse carrier produces a more compact powder packing structure under no consolidation. This is as expected because the drug particles will fill the voids within the randomly packed large lactose carrier particles.

TABLE 3.6 THE FLUIDISATION AND FLOW PROPERTIES OF THE COARSE CARRIERS AND THE FORMULATIONS IN TERMS OF MINIMUM FLUIDISATION VELOCITY (U_{mf}), AREA ENCLOSED BY THE FLUIDISATION-DEFLUIDISATION CURVE (AUC, DIMENSIONLESS PARAMETER), FLUIDISED FRACTION AT AN AIR VELOCITY OF 15 mm/s ($\Delta P/\Delta P_{Theor}$) AND THE FLOW RATE INDEX (FRI). THE DATA REPRESENTS MEAN ± STANDARD DEVIATION, N=3.

	$U_{mf} \pm$ S.D. (mm/s)	AUC ± S.D. (-)	$\Delta P/\Delta P_{Theor} \pm$ S.D.	FRI ± S.D.
LH100	8.47 ± 0.23	2.39 ± 0.18	0.32 ± 0.00	1.02 ± 0.01
+0.02% FP	5.53 ± 0.12	1.22 ± 0.09	0.36 ± 0.00	1.02 ± 0.01
+0.05% FP	6.13 ± 0.23	1.32 ± 0.06	0.36 ± 0.00	1.05 ± 0.01
+0.08% FP	5.20 ± 0.00	0.82 ± 0.05	0.38 ± 0.01	1.10 ± 0.01
+0.1% FP	5.60 ± 0.00	0.77 ± 0.07	0.37 ± 0.00	1.12 ± 0.01
+0.15% FP	5.07 ± 0.23	0.72 ± 0.33	0.37 ± 0.01	1.13 ± 0.01
+0.2% FP	5.47 ± 0.23	0.67 ± 0.08	0.39 ± 0.01	1.13 ± 0.01
+0.4% FP	4.80 ± 0.00	0.58 ± 0.14	0.37 ± 0.00	1.15 ± 0.01
+1% FP	4.80 ± 0.00	0.75 ± 0.05	0.37 ± 0.00	1.12 ± 0.02
+2% FP	4.80 ± 0.00	0.93 ± 0.15	0.34 ± 0.00	1.09 ± 0.02
SV010	8.33 ± 0.50	2.03 ± 0.07	0.35 ± 0.00	1.11 ± 0.00
+0.02% FP	5.60 ± 0.00	0.86 ± 0.05	0.37 ± 0.00	1.13 ± 0.01
+0.05% FP	5.60 ± 0.00	0.91 ± 0.07	0.37 ± 0.00	1.14 ± 0.01
+0.08% FP	5.60 ± 0.00	0.87 ± 0.06	0.37 ± 0.00	1.14 ± 0.02
+0.1% FP	5.73 ± 0.23	0.94 ± 0.02	0.36 ± 0.00	1.14 ± 0.03
+0.2% FP	5.60 ± 0.00	0.86 ± 0.06	0.37 ± 0.00	1.12 ± 0.01
+0.3% FP	5.47 ± 0.23	0.90 ± 0.04	0.38 ± 0.00	1.16 ± 0.02
+0.4% FP	5.60 ± 0.00	0.80 ± 0.13	0.38 ± 0.00	1.16 ± 0.02
+1% FP	6.27 ± 0.23	1.00 ± 0.12	0.35 ± 0.00	1.15 ± 0.02
+2% FP	6.00 ± 0.40	1.42 ± 0.20	0.34 ± 0.00	1.12 ± 0.02

The U_{mf} for the formulations are plotted as a function of the loaded drug dose in Figure 3.21. The U_{mf} for the carriers is higher than for the formulations. It can be seen that SV010 and LH100 have a very similar U_{mf} (~8.5 mm/s) indicating similar powder cohesion behaviour. However, when the drug is added to the carriers, a gradual decrease in the U_{mf} is seen for LH100 formulations up to 0.4 wt-% drug concentration (U_{mf} =4.8 mm/s), after which no change in the U_{mf} of the formulations takes place. For SV010, a sudden drop to ~5.6 mm/s in the U_{mf} is observed as a consequence of adding drug between concentrations of 0.02 and 0.4 wt-%, suggesting a decrease in powder cohesion as a result of the addition of low amounts of the API. However, the U_{mf} for the formulations with 1 and 2 wt-% drug concentrations increases up to ~6 mm/s indicating the formulations with higher drug concentration become more cohesive. Because of the smaller change between the U_{mf} of the coarse carrier and the formulations, these data indicate that SV010 is less sensitive to the addition of drug fines than LH100. In addition, SV010 formulations at higher drug loading (0.2 wt-% and above) are more cohesive than equivalent LH100 formulations.
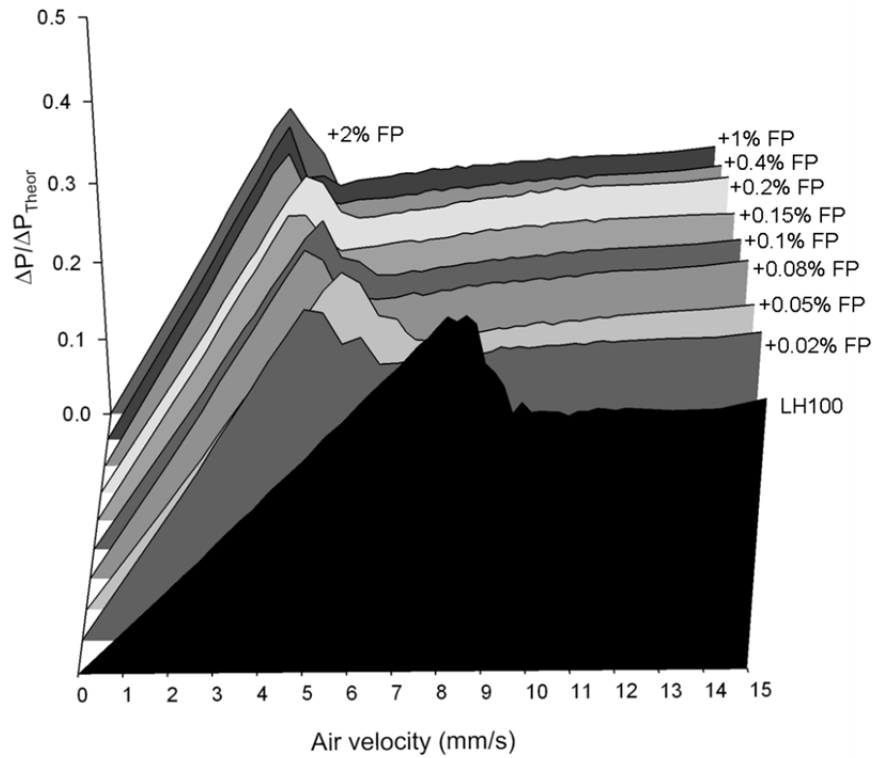
FIGURE 3.19 THE FLUIDISATION CURVES OF FLUTICASONE PROPIONATE (FP) FORMULATIONS PREPARED WITH LH100 AS THE CARRIER IN AN ORDER OF INCREASING DRUG CONCENTRATION WITH LH100 IN THE FRONT AND 2% FORMULATION AT THE BACK. THE CURVES REPRESENT AVERAGE FROM 3 DETERMINATIONS.
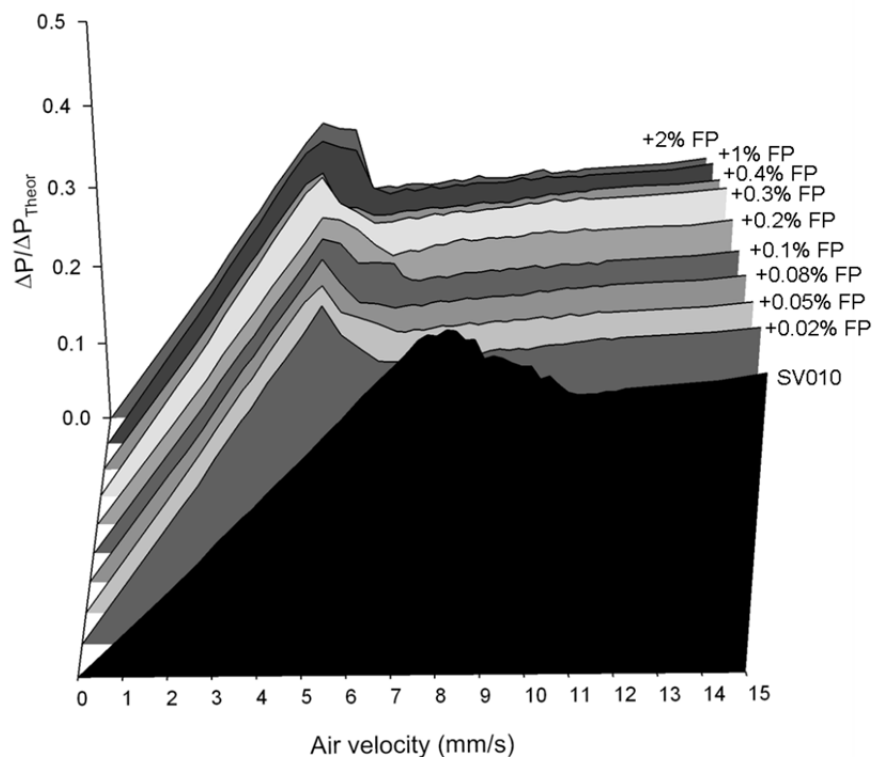
FIGURE 3.20 THE FLUIDISATION CURVES OF FLUTICASONE PROPIONATE (FP) FORMULATIONS PREPARED WITH SV010 AS THE CARRIER IN AN ORDER OF INCREASING DRUG CONCENTRATION WITH SV010 IN THE FRONT AND 2% FORMULATION AT THE BACK. THE CURVES REPRESENT AVERAGE FROM 3 DETERMINATIONS.

138

Similar trends were also seen by quantification of the area enclosed by the fluidisation/defluidisation curves. Since the air velocity measurement interval for the fluidisation/defluidisation curves was the same for all the samples, the areas were calculated as dimensionless areas, with the air velocity normalised by the air velocity measurement interval. The values of AUC for the formulations are summarised in Table 3.6 and presented in Figure 3.22. These data suggest that LH100 is marginally more cohesive than SV010. The addition of drug decreased the cohesion of LH100 formulations gradually from 2.4 for LH100 to minimum of 0.6 which was achieved with a 0.4 wt-% drug concentration. At higher drug concentrations, an increase in the area enclosed by the fluidisation/defluidisation curve is observed for LH100 formulations. For the SV010 formulations, an instant drop from 2 to 0.8 is achieved upon the addition of drug fines at 0.02 wt-%. The values remain constant up to 1 wt-% concentration, when an increase in the cohesion as quantified by the area enclosed by the fluidisation/defluidisation curves is seen. Again, the range of values for SV010 is smaller than for LH100 formulations. As with the U_{mf} data, these data indicate that the fluidisation properties of SV010 are less sensitive to the addition of the fines than LH100, and the SV010 formulations are more cohesive than the LH100 formulations at higher drug loadings.

The fluidised fraction of the formulations, as quantified by the ratio between the measured and theoretical pressure drop for the powder bed, are plotted against the loaded drug dose in Figure 3.23. The numerical values are presented in Table 3.6. These data show that LH100 is fluidised to a lesser (0.32) extent than SV010 (0.35). However, as soon as the drug is added to LH100, the fluidised fraction increases up to 0.36 and continues increasing until a peak of ~0.39 is reached at 0.2 wt-% drug concentration. For SV010, a similar increase is seen with the peak value of ~0.38 at 0.3 wt-% concentration. After the peak concentration, a decrease in the fluidised fraction is observed with both carriers. Once again, the range of values for SV010 (0.35 to 0.38) is smaller than for LH100 (0.32 to 0.38).

The flow rate index (FRI), which is a dimensionless descriptor of general flow properties of powders, is an independent measurement from the fluidisation experiments. As discussed in the general materials and methods chapter of the thesis (Chapter 2.3.3) powders that are insensitive to changes in the flow rate have an FRI value of 1. These powders are generally free-flowing. Cohesive powders react to a decrease in the flow rate and thus have an FRI higher than 1. The values of FRI for the formulations presented in Table 3.6 are plotted against the loaded drug dose in Figure 3.24. According to these data, LH100 flows more freely than SV010 as it exhibits the lower FRI of the two carriers. When drug fines are added to the carriers, LH100 gradually gets more cohesive, until a peak value of 1.15 is reached at 0.4 wt-% concentration, after which the FRI gradually decreases. For

SV010, hardly any change is observed in the value of FRI up to the concentration of 0.2 wt-%. After this, an increase in FRI is seen with a peak value of 1.16 at 0.4 wt-% drug concentration and decay at higher concentrations. Yet again, LH100 demonstrates higher sensitivity to the addition of drug fines because of the wider range of values between the LH100 and the formulations.

LH100 formulations
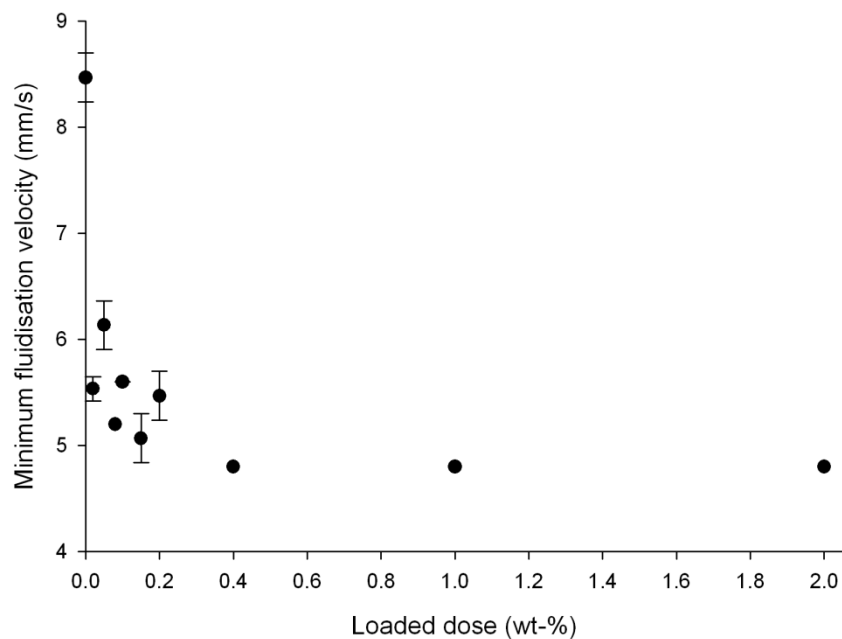
SV010 formulations
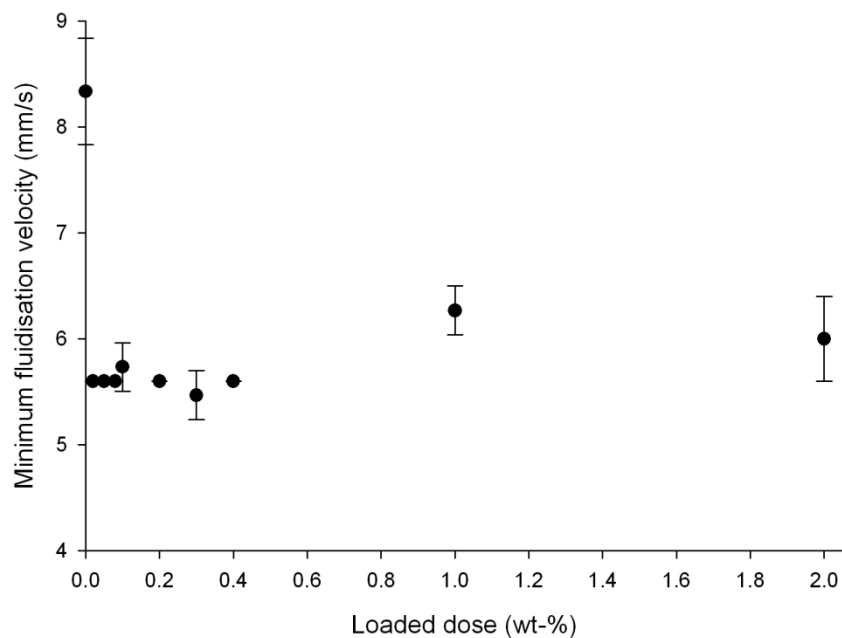
FIGURE 3.21 THE MINIMUM FLUIDISATION VELOCITY (U_{mf}) OF THE LH100 (TOP) AND SV010 FORMULATIONS (BOTTOM) AS A FUNCTION OF FLUTICASONE PROPIONATE CONCENTRATION (LOADED DOSE) . THE DATA REPRESENTS MEAN ± STANDARD DEVIATION, N=3.

LH100 formulations
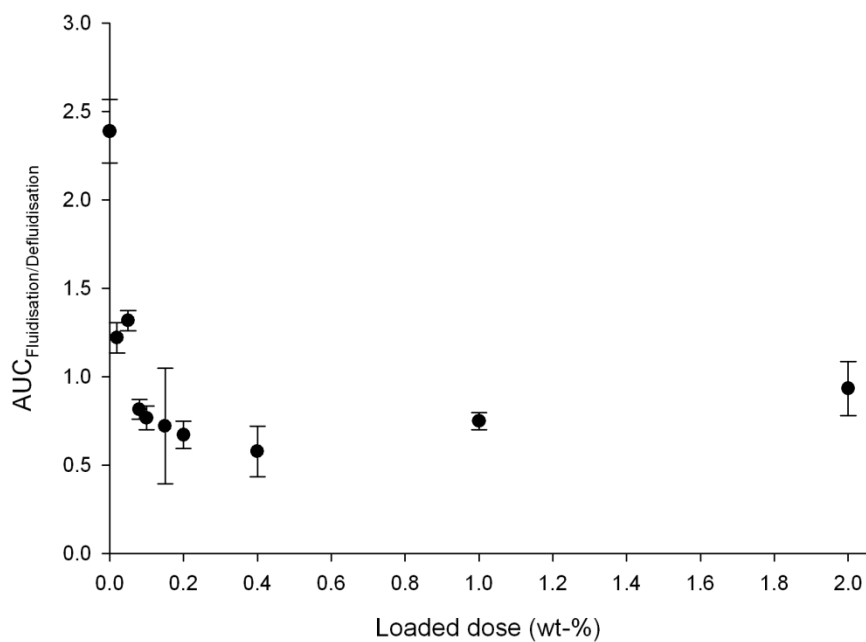
SV010 formulations
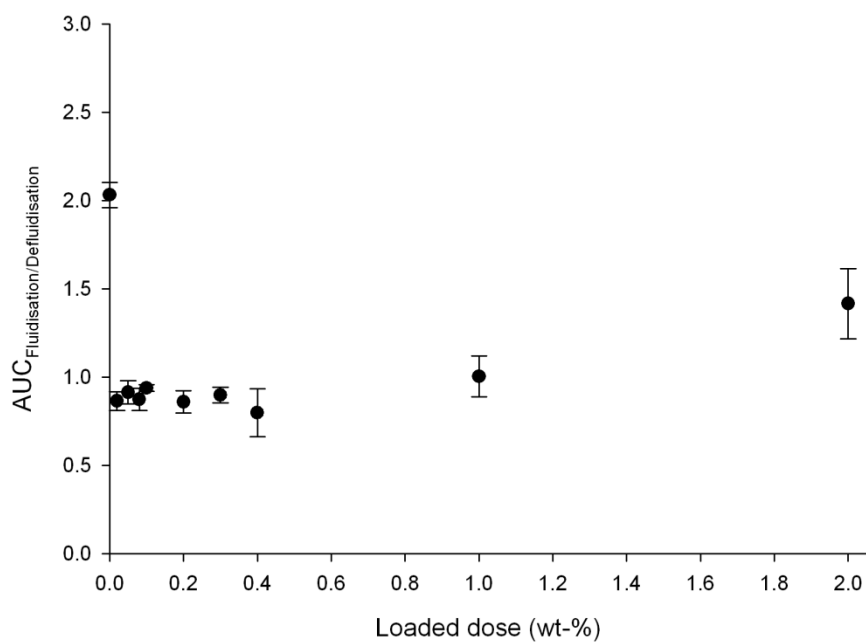
FIGURE 3.22 COHESION OF THE FORMULATIONS AS QUANTIFIED BY THE AREA ENCLOSED BY THE FLUIDISATION AND DEFLUIDISATION CURVES AS A FUNCTION OF FLUTICASONE PROPIONATE CONCENTRATION (LOADED DOSE) FOR LH100 (TOP) AND SV010 FORMULATIONS (BOTTOM). THE DATA REPRESENT MEAN ± STANDARD DEVIATION, N=3.

LH100 formulations
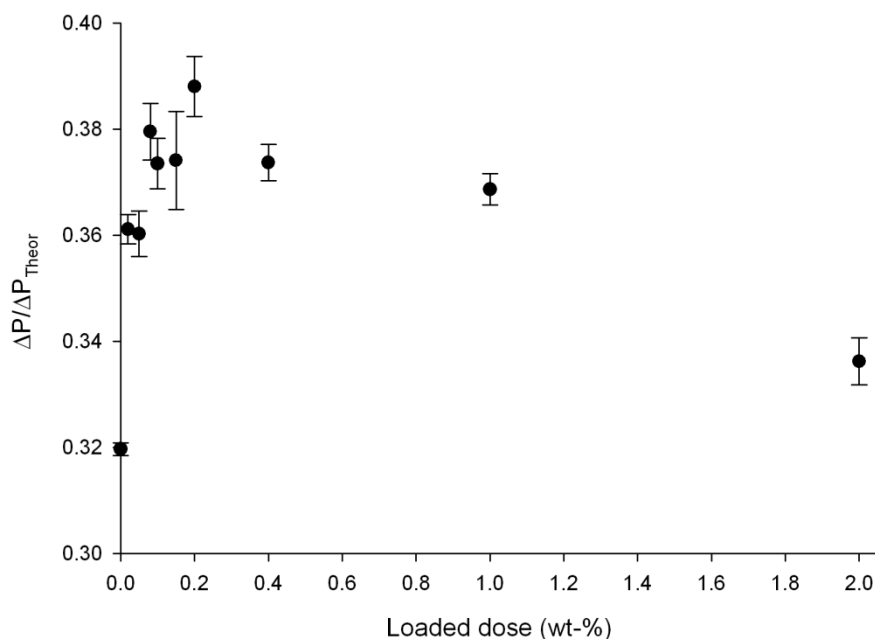
SV010 formulations
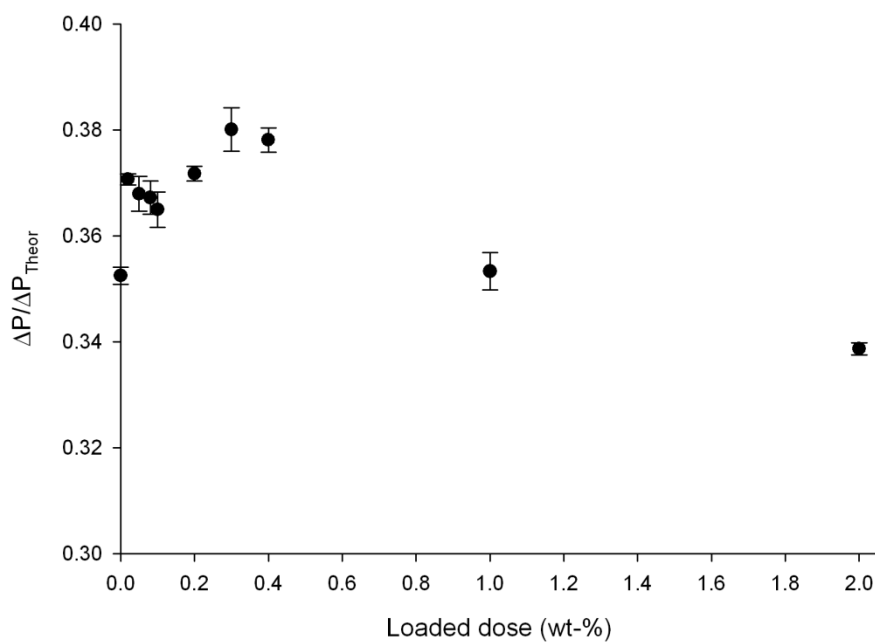
FIGURE 3.23 THE FLUIDISED FRACTION ($\Delta P / \Delta P_{Theor}$) OF THE MODEL FORMULATIONS AS A FUNCTION OF FLUTICASONE PROPIONATE CONTENT (LOADED DOSE) WITH LH100 (TOP) AND SV010 (BOTTOM) AS THE CARRIERS. THE DATA REPRESENT MEAN ± STANDARD DEVIATION, N=3.

LH100 formulations
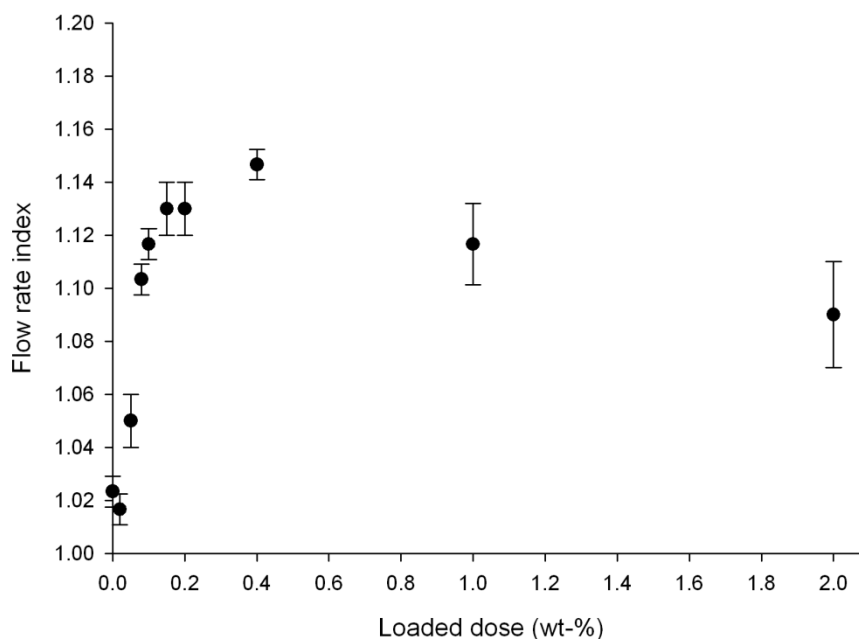
SV010 formulations
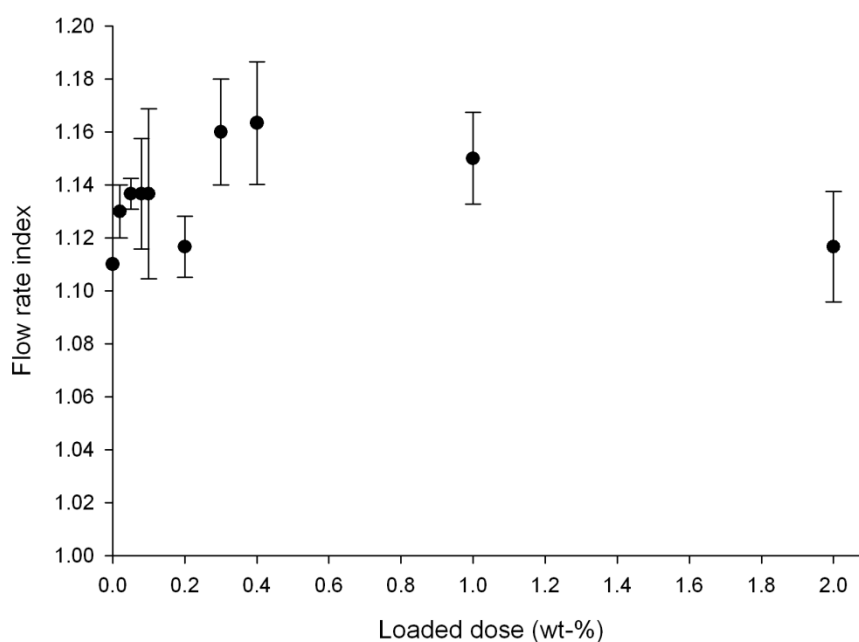
FIGURE 3.24 THE MEASURED VALUES OF FLOW RATE INDEX (FRI) AS A FUNCTION OF FLUTICASONE PROPIONATE CONTENT (LOADED DOSE) OF THE FORMULATIONS PREPARED WITH LH100 (TOP) AND SV010 (BOTTOM) AS THE CARRIERS. THE DATA REPRESENT MEAN ± STANDARD DEVIATION, N=3.

These results indicate that the fluidisation and flow properties of SV010 are affected by the addition of drug fines to a lesser extent than LH100. This may be due in part to the rougher surface of the SV010 accommodating some of the drug fines. The rheometric analysis of the two lactose batches suggested that SV010 formulations at high drug concentrations were more cohesive than the LH100 formulations at equivalent drug loadings. At these concentrations, SV010 formulations produced a significantly higher fine

particle mass and fraction than the LH100 formulations (p<0.05). Therefore, the increased cohesion of the formulations might be able to explain some of the trends seen in the formulation performance. These data agree with previous studies, where an increase in the cohesive properties of the bulk powder significantly increased the performance of carrier based DPI formulations (Shur *et al.* 2008a; Shur *et al.* 2008b). However, the fluidisation properties do not reflect all the changes in DPI performance over the full range of drug loadings studied here.

3.4. CONCLUSIONS

This study focussed on investigating the validity of active sites theory in governing DPI performance. The results of the study provided contradictory evidence for the active sites theory, particularly as the lactose carrier with the rougher surface outperformed the smoother carrier in terms of various *in vitro* performance measures and demonstrated a lower concentration where an improvement in the DPI formulation performance became obvious.

No changes in the fluidisation mechanism of the formulations over the concentration range studied here were observed and all the formulations fluidised following the erosion mechanism. Therefore, changes in the fluidisation mechanism are not capable of explaining the trends seen in the *in vitro* performance of the formulations either. The role of increased cohesion in improving the DPI performance was also investigated, and a novel pressure drop measurement method for characterising DPI formulations was developed. The results indicated that at higher drug concentrations, increased cohesion might play a part in determining the DPI performance. However, the increased cohesion was not capable of explaining the trends in *in vitro* performance over the whole range of drug loadings studied here.

The results of the current study indicated that the redistribution of the drug agglomerates during blending of the formulations and their detachment from the carrier surface and deagglomeration upon inhalation may play a crucial role in determining the DPI performance. This will be further investigated in Chapter 4 of the thesis.

CHAPTER 4   THE IMPACT OF ADDED LACTOSE FINES TO THE CARRIER FLOW AND FLUIDISATION PROPERTIES AND DRY POWDER INHALER PERFORMANCE

4.1   INTRODUCTION

The particle size distribution of the added fine lactose is an important factor in determining whether the DPI formulation performance increases as more lactose fines are added. Finer sub-cuts of the lactose fines have been shown to be more effective in improving DPI performance (Adi *et al.* 2006; Adi *et al.* 2009; Guenette *et al.* 2009; Zeng *et al.* 1999). In the study reported here, the impact of adding lactose fines with different process histories, and thus particle size distributions, to the performance of DPI formulations was investigated.

One aim of the study reported in the current chapter was to assess the suitability of different parameters describing the properties of the lactose carriers for predicting the formulation performance. Traditionally, characterisation of the amount of fines associated with the lactose carrier has been the holy grail of DPI formulators' toolbox in estimating the performance of the final product. However, during the last years, an increasing amount of research effort has been concentrated in further understanding the relationship between the powder bulk properties and DPI performance. Understanding the relationship between raw material properties and DPI performance would enable a quality-by-design approach for manufacturing DPI products. Some studies have been successful in relating the fluidisation characteristic of the carrier to the final performance of the formulation (Pitchayajittipong *et al.* 2010; Shur *et al.* 2008a). Recent research also include a study where the permeability of the DPI formulation was related to the performance of the final product (Le *et al.* 2010), although the methodology suggested in the study did not prove the applicability of the method for quality-by-design purposes as only the permeability of the final formulations were related to performance. However, due to these promising reports, it was anticipated that powder flow and fluidisation characteristics of the lactose carriers may be suitable to be used as a quality-by-design tools.

The role of the active sites theory and increased cohesion in governing the dry powder inhaler performance was investigated in Chapter 3. It was shown that the active sites theory is an unlikely explanation behind the improved DPI performance upon the addition of lactose fines, and that increased cohesion may play only a minor part in explaining the improvement. Instead, preliminary evidence for the role of agglomerate formation in

improving the formulation performance was seen. Therefore, the study reported here aimed also to examine whether drug-fines agglomerate formation could play a role in governing DPI performance.

4.2 MATERIALS AND METHODS

4.2.1 Materials

The different inhalation grades of lactose used in the study were Lactohale (LH) products obtained from DFE Pharma (Borculo, Netherlands) and were as follows: a sieved grade coarse carrier LH100, micronised lactose fines LH300 and two different grades of milled lactose fines, LH230 and LH210. Micronised budesonide (Astra Zeneca) was used as received. The cohesive-adhesive balance (CAB) value (Begat *et al.* 2004b) for the budesonide was 0.75 meaning the drug preferred to adhere to the lactose rather than to itself and the particle size was within the respirable range with the value of d_{90} at 4.40 µm. Methanol and acetonitrile were of HPLC grade (Fisher Scientific, Loughborough, UK) and water was reverse osmosis purified. (Millipore, France).

4.2.2 Preparation of lactose pre-blends

Three different series of lactose pre-blends were prepared at fines concentrations of 2.5, 5, 10 and 20 wt-% in quantities of 100 g by sandwiching each of the fines between LH100 in three layers in an earthed 500 ml stainless steel vessel described in Section 2.1.1.3 and blended using a Turbula T2F mixer (Glen Creston Ltd., Middlesex, UK) at 46 rpm for 60 minutes. The pre-blends were stored at 20 ± 2 °C and 44% relative humidity (RH) for at least 24 hours before any further work or characterisation was performed.

4.2.3 Particle sizing of the raw materials and the pre-blends

The particle size distributions of the lactose raw materials and the pre-blends were measured dispersed dry at a pressure of 2 bar using a Sympatec Helos laser diffraction system with an R4 lens in conjunction with a Rodos T4 disperser and a Vibri feeder controlled by WINDOX software (all from Sympatec Gmbh, Germany). The feed rate was adjusted such that an optical concentration between 0.5 and 5% was obtained. Five repeat measurements were taken for each of the samples and the high resolution Fraunhofer model was applied for calculating the particle size distribution from the scattering data. An aliquot of budesonide was dispersed in 0.1% lecithin in cyclohexane

and ultrasonicated for one minute in an ultrasonic bath. The resulting suspension was added to the Cuvette dispersing system (Sympatec Gmbh, Germany) until an optical concentration of between 5 and 10% was obtained. Five repeated measurements of 5 seconds duration using an R3 lens configuration were then taken.

4.2.4 Scanning electron microscopy

The scanning electron microscopy (SEM) for the raw materials and the pre-blends was performed on a JEOL JSM-6480LV (JEOL, Tokyo, Japan). The samples were mounted on stainless steel sample holders using sticky carbon tabs and coated with an Edwards sputter coater S150B (BOC Edwards, UK) for 5.5 minutes prior to the analysis. An acceleration voltage of 10 kV was applied for imaging.

4.2.5 Powder flow properties on the Schulze RST-XS

The following procedure was followed for characterizing the samples on the RST-XS annular ring shear tester controlled by RST-Control 95 software (both from Dietmar Schulze, Germany). For each test, a 30 ml annular shear cell was filled with the material under investigation without applying force to the upper surface of the powder bed. The powder was pre-sheared with a normal stress of 1000 Pa (τ_{pre}) until steady-state flow was achieved. A yield locus was then constructed by measuring the shear stress required to cause the powder to fail under three normal stresses lower than τ_{pre} (250 Pa, 500 Pa and 750 Pa) and the flowability calculated using the instrument software. Each powder was tested three times and the mean flowability ratio (ff_c) at 1000 Pa pre-shear stress was calculated. The ff_c is the ratio between the consolidation stress and the unconfined yield strength of the powder, both of which are parameters that can be determined from the yield locus, and is a dimensionless parameter, which increases as powder flowability improves. Hence, the more cohesive the powder system, the lower the value of ff_c for the system. A detailed description of the theory of measuring powder flow properties based on the yield locus, and the measurement methodology, see Chapter 2, section 2.3.2.

4.2.6 Powder flow and fluidisation properties on the FT4

The flow and fluidization behaviour of the lactose pre-blends were also characterised using the FT4 Powder Rheometer (Freeman Technology, Tewkesbury, UK). Detailed

background information and measurement methodologies can be found in Chapter 2, Section 3.3.

Briefly, a 25mm bore diameter, 20 ml glass split vessel is filled with the powder under investigation before a conditioning cycle is run using a 23.5mm blade that is moved downwards in a clockwise helical path with an angle of 5 degrees at 60 mm/s. The split vessel is then opened to achieve a constant powder mass in the vessel before a specific measurement program is run. During a measurement the blade is moved through the powder in an anti-clockwise motion at a tip speed of 100 mm/s and a helical angle of 5 degrees unless otherwise stated. Normalised basic flow energy (BFE_{Norm}), flow rate index (FRI), normalised fluidisation energy (FE_{Norm}), dynamic flow index (DFI), bulk and tapped densities were characterised for the lactose pre-blends. All the measurements were performed in triplicate:

The Hausner ratio and Carr's index for the lactose pre-blends were calculated from the bulk and tapped densities as per Equations 2.1 and 2.2, respectively.

4.2.7   Preparation of model formulations with budesonide

The lactose pre-blends were formulated with budesonide at 0.8 wt-% concentration to produce an array of model DPI formulations for *in vitro* testing. The formulations were prepared in quantities of 40 g by using the same stainless steel vessel as for blending the lactose pre-blends. The lactose pre-blends were sieved at 850 μm before the formulations were prepared in order to break any large agglomerates present in the pre-blends. 0.32 g of the drug was weighed and sandwiched between half of the lactose, which was blended for 10 minutes with a Turbula at 46 rpm, after which the remaining the lactose was added and blending was continued for a further 45 minutes. The formulations were sieved at 250 μm in order to break any large agglomerates and stored at 20 ± 2 °C and 44% RH for at least 24 hours before any further work. The drug content uniformity of the blends was measured by taking ten random samples of 12.5 mg and determining the amount of drug in the samples by high performance liquid chromatography (HPLC). Dose variation of less than 6% was achieved for all blends.

4.2.8   Drug content assay by HPLC

The drug content was determined by high performance liquid chromatography (HPLC) following the method described in Chapter 2, Section 4.2.

4.2.9 *In vitro* testing of the formulations

The *in vitro* performance of the formulations was tested using a Next Generation Impactor (NGI) equipped with a pre-separator (Copley Scientific, Nottingham, UK). Two hydroxypropylmethylcellulose (HPMC) capsules, containing 12.5 mg of the formulation each, were aerosolised through the system with Rotahaler (GlaxoSmithKline, UK) and Handihaler (Boehringer Ingelheim, Germany). The flow rates were adjusted using the TPK critical flow control unit (Copley Scientific, Nottingham, UK) such that 90L/min was used for Rotahaler and 52 L/min for Handihaler. A 4kPa pressure drop for Rotahaler was measured at a flow rate of 160 L/min. However, the NGI is only calibrated to flow rates up to 100 L/min, and therefore 90 L/min was used for the Rotahaler. For Handihaler, 52 L/min was measured as the flow rate producing a pressure drop of 4kPa without a capsule. The duration of aerosolisation was adjusted so that 4L of air was withdrawn through the system. Each determination was performed in triplicate. The NGI stages have different cut-off values at different airflow rates (See section 2.6.1.2.6). To compare the performance of the formulations on different devices, results were normalised by calculating the mean mass aerodynamic diameters (MMAD) and the fine particle fraction of particles less than 5 μm calculated by extrapolation. The fine particle fraction was normalised to the emitted dose (FPF_{ED}).

4.2.10 Analysis of statistical significance

Statistical analysis of the results was performed using Minitab v15 software (Minitab Inc., Pennsylvania, USA). Comparisons were performed using one-way analysis of variance (ANOVA) with Fisher comparison confidence level set to 95% or 99% depending on the outputs evaluated.

4.3 RESULTS AND DISCUSSION

4.3.1 Physical properties of the raw materials

Representative SEM photomicrographs of the coarse lactose carrier and lactose fines used in the study are shown in Figure 4.1. The coarse lactose carrier LH100 (Figure 4.1A) exhibited a typical tomahawk morphology of alpha lactose monohydrate (Graham *et al.* 1997), with a few intrinsic fine lactose particles adhering to the surfaces. Micronised lactose LH300 (Figure 4.1B) had a uniform, fine particle size. All the micronised particles imaged were smaller than 20 μm. The milled fines LH230 and LH210 (Figure 4.1C and Figure 4.1D respectively) were composed of particles with wider particle size distributions.

149

In both these milled materials, only a small proportion of the particles were less than 5 µm. The coarser particles made up the bulk of the milled lactose materials and it is worth noting that the very fine lactose particles were adhering to the surfaces of these larger particles.

The particle size distributions of the lactose fines, as measured by laser diffraction, are summarised in Table 4.1 and shown in Figure 4.2 together with the particle size distribution of LH100, whose data is summarised in Table 4.2. These results support the general observations of the SEM images. For the coarse carrier lactose (LH100), the mode of the particle size distribution was approximately 100 µm with a tail of finer material and a very small proportion (1.3%) of fine lactose particles present below 4.5 µm. For the micronised lactose (LH300), the median particle size was 2.41 µm, with 90% of the particles finer than 7.76 µm. Of the two milled fines used in the study, LH230 particles exhibited the smaller particle size distribution, with a d50 of 8.05 µm compared to a d50 of 14.30 µm for LH210 particles.
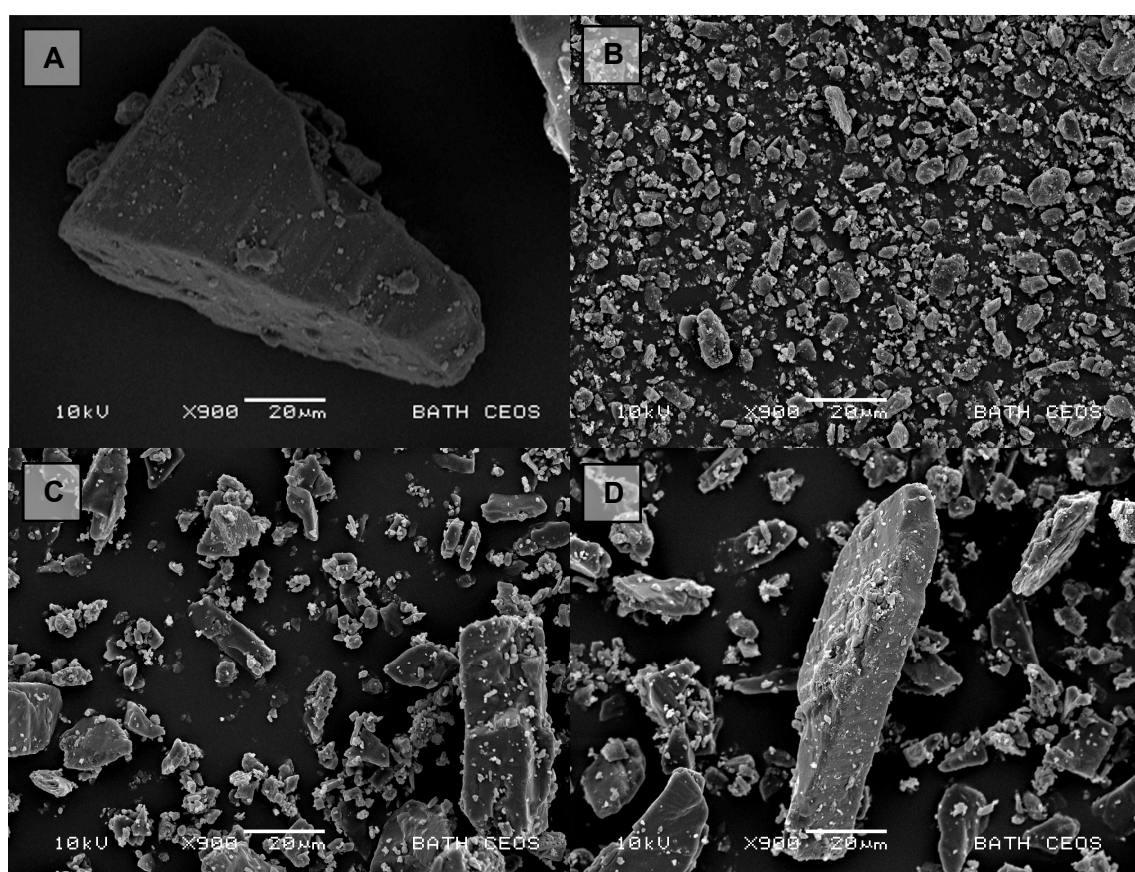
FIGURE 4.1 900X MAGNIFICATION SCANNING ELECTRON MICROGRAPHS OF A) LH100 B) LH300 C) LH230 AND D) LH210

TABLE 4.1 PARTICLE SIZE DISTRIBUTIONS OF THE LACTOSE FINES USED IN THE STUDY IN TERMS OF d10, d50 AND d90. THE DATA REPRESENTS MEAN ± STANDARD DEVIATION (S.D.), n=5.

	d10 ± S.D. (µm)	d50 ± S.D. (µm)	d90 ± S.D. (µm)
LH300	0.84 ± 0.01	2.41 ± 0.07	7.76 ± 0.27
LH230	1.31 ± 0.01	8.05 ± 0.06	21.97 ± 0.09
LH210	1.64 ± 0.01	14.3 ± 0.22	39.45 ± 0.54
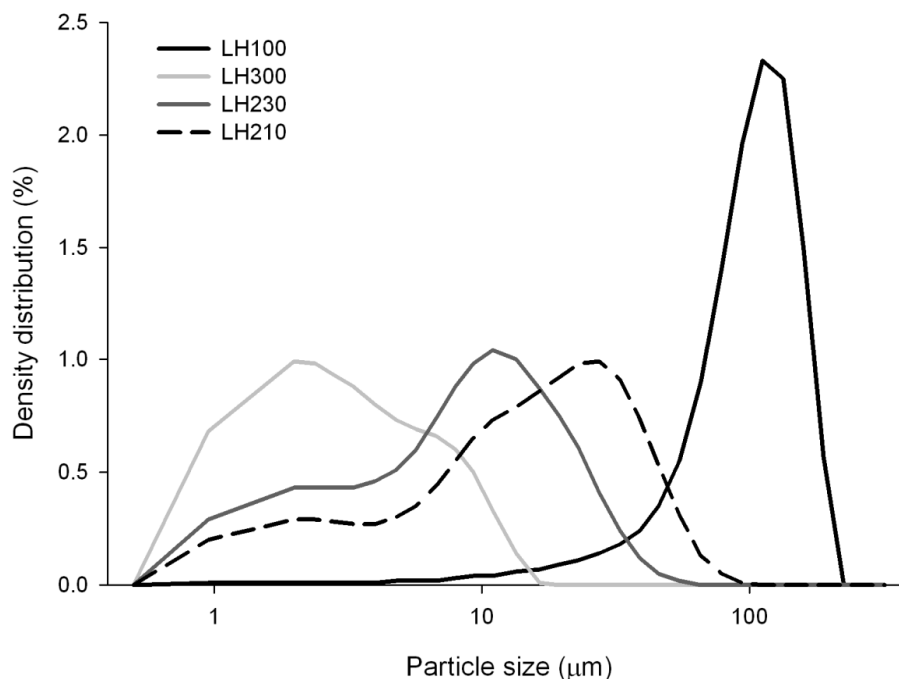
FIGURE 4.2 PARTICLE SIZE DISTRIBUTIONS OF THE RAW MATERIALS USED IN THE STUDY. THE DISTRIBUTIONS SHOWN ARE AVERAGES OF FIVE REPEATED MEASUREMENTS.

4.3.2   Physical properties of the lactose pre-blends

The proportion of fine lactose particles in the carrier has been reported to be a key attribute in increasing the performance of DPI products in several studies (Adi *et al.* 2009; Guenette *et al.* 2009; Louey *et al.* 2003). The particle size distributions of the lactose pre-blends prepared with micronised (LH300) and milled lactose fines (LH230 and LH210) with LH100 as the coarse carrier are summarised in Table 4.2. The particle size distributions of the series of LH300 pre-blends at 2.5, 5, 10 and 20 wt-% concentrations are shown in Figure 4.3 (top). The proportion of intrinsic lactose fines less than 4.5 µm associated with the batch of LH100 was 1.3%. Upon the initial addition of 2.5 wt-% of micronised (LH300) fines to the coarse carrier (LH100), the proportion of particles <4.5 µm increased to 4.9%. Upon increasing the concentration of the micronised component (LH300) to 5, 10 and 20 wt-%, the cumulative percentage of fines below 4.5 µm present in the carrier blends increased to approximately 9, 17 and 23%, respectively (Table 4.2).

The particle size distributions of the pre-blends prepared with the finer of the two milled lactose fines (LH230) are also shown in Figure 4.3 (middle). These data indicate that the addition of fines up to a concentration of 10 wt-% altered the particle size distribution of the lactose pre-blends mainly in the size range between 5 and 50 µm. Meanwhile, Table 4.2 shows that the addition of the LH230 fines at 2.5, 5 and 10 wt-% concentrations resulted in 2.8, 4.3 and 7.2% proportion of particles below 4.5 µm, respectively. A concentration of 20 wt-% was required to initiate a more pronounced contribution towards the fine end of the particle size distribution, whereby the percentage of particles <4.5 µm increased to approximately 12.5%. The particle size distributions of the pre-blends prepared with the coarser grade of the milled lactose fines (LH210) are also shown in Figure 4.3 (bottom). The addition of the LH210 fines contributed mainly to the particle size distribution between 10 and 50 µm. Table 4.2 shows that even at a concentration of 20 wt-%, the proportion of fine lactose particles <4.5 µm was only 6%.

Representative scanning electron micrographs of the LH300 pre-blends are shown in Figure 4.4. Up to 10 wt-% concentration, the lactose fines were distributed on the surfaces of the large carrier particles mainly as agglomerates. At 20 wt-% concentration, the fines appeared to form a more uniform surface coverage rather than distributing themselves on the surface of the large carrier particles as smaller agglomerates.

Scanning electron micrographs of the LH230 pre-blends are presented in Figure 4.5. The larger fines have been distributed between the large carrier particles. Up to 10 wt-% concentration (Figure 4.5A to C), mainly single fine particles (<10 µm) were seen adhered on the surfaces of the large carrier crystals. At 20 wt-% concentration (Figure 4.5D), agglomerates of fines were also observed on the surfaces of the large carrier particles.

Representative scanning electron micrographs of the LH210 pre-blends are shown in Figure 4.6. The micrographs indicate that at all fines concentrations of LH210, some primary fine particles (<10 µm) and also some larger fine particles (~20 µm) were adhering to the surfaces of the large carrier particles. The surfaces of the large carrier particles remained relatively free of agglomerated fine particle lactose across the range of concentrations.

Recently, it was suggested that there are five different regimens governing DPI performance (Young *et al.* 2011). According to the suggestions, the initial regimen was the filling of active sites followed by the filling of low energy binding sites. After this, the third regimen is where monolayer coverage of the carriers was approached. The fourth regimen was agglomerate formation just before a monolayer coverage is reached. The final regimen suggested was formulation segregation due to too high a fines content. However, SEM images from the current study showed no evidence of monolayer

formation. The size range of lactose fines (<10 µm) that have been previously demonstrated to be efficient in improving DPI performance (Guenette *et al.* 2009), appeared, on the basis of the SEM, to form agglomerated systems on the surface of the larger carrier particles when present at concentrations favourable for agglomerate formation. For the LH300 based formulations, the concentration where agglomerate formation began to appear was 5 wt-% (Figure 4.4B). For the LH230 formulation the critical concentration was 20 wt-% (Figure 4.5D). With the LH210 formulations, a high enough fines content was not reached to achieve agglomerate formation (Figure 4.6.).

TABLE 4.2 PARTICLE SIZE DISTRIBUTIONS OF THE LACTOSE CARRIERS USED IN THE STUDY IN TERMS OF d10, d50 AND d90. THE DATA REPRESENTS MEAN ± STANDARD DEVIATION (S.D.), n=5. IN ADDITION, THE MEAN VALUES (n=5) OF PROPORTION OF PARTICLES FINER THAN 4.5 AND 30 µm PRESENT IN THE CARRIERS ARE TABULATED.

	d10 ± S.D. (µm)	d50 ± S.D. (µm)	d90 ± S.D. (µm)	<4.5 µm (%)	<30 µm (%)
LH100	44.30 ± 1.58	103.37 ± 1.01	159.62 ± 0.56	1.29	6.24
+2.5% LH300	23.44 ± 1.01	99.66 ± 0.35	161.02 ± 2.15	4.88	11.48
+5% LH300	5.22 ± 0.32	95.19 ± 0.79	157.27 ± 3.31	9.34	17.03
+10% LH300	2.08 ± 0.02	87.30 ± 0.85	154.55 ± 3.77	17.43	26.97
+20% LH300	1.73 ± 0.06	60.76 ± 2.11	139.93 ± 3.40	23.04	42.75
+2.5% LH230	26.41 ± 0.84	99.78 ± 0.37	160.88 ± 0.31	2.76	10.95
+5% LH230	14.70 ± 0.29	96.58 ± 0.64	159.82 ± 3.02	4.32	15.13
+10% LH230	7.33 ± 0.14	89.55 ± 0.38	156.65 ± 1.02	7.23	23.23
+20% LH230	3.26 ± 0.21	67.18 ± 1.55	134.32 ± 2.77	12.47	38.15
+2.5% LH210	31.53 ± 1.05	100.23 ± 0.64	158.57 ± 2.12	1.98	9.56
+5% LH210	23.63 ± 0.61	97.72 ± 0.62	159.85 ± 1.74	2.62	12.27
+10% LH210	14.25 ± 0.27	91.51 ± 0.70	156.18 ± 3.04	4.08	17.89
+20% LH210	8.72 ± 0.12	79.30 ± 1.53	151.45 ± 6.27	6.02	26.79

LH300 pre-blends
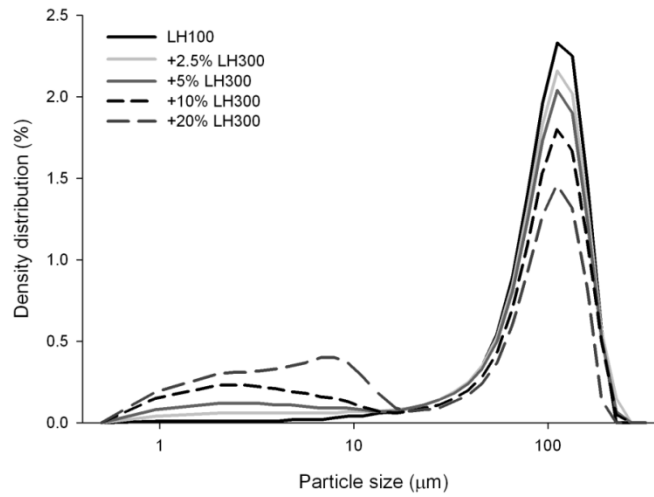
LH230 pre-blends
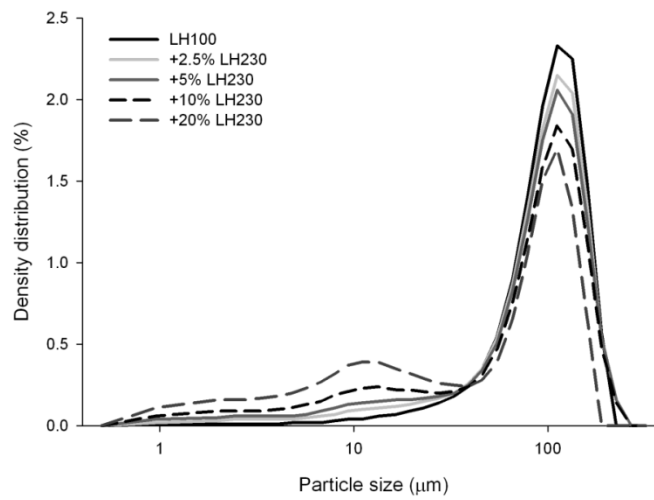
LH210 pre-blends
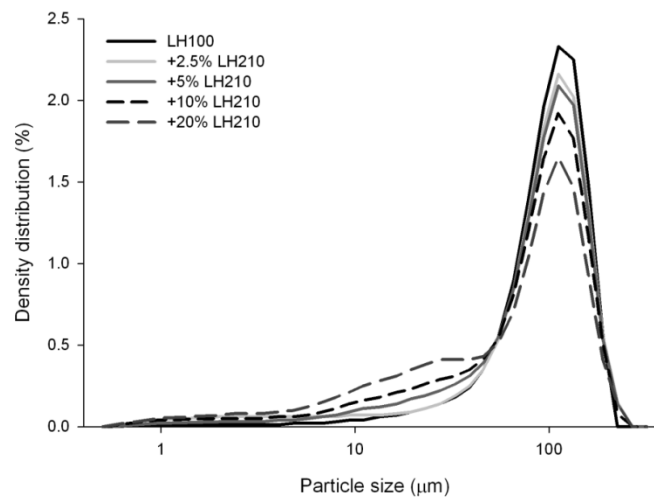
FIGURE 4.3 PARTICLE SIZE DISTRIBUTIONS OF THE LACTOSE PRE-BLENDS PREPARED WITH LH300 (TOP), LH230 (MIDDLE) AND LH210 (BOTTOM). THE DISTRIBUTIONS ARE AVERAGES FROM FIVE REPEATED MEASUREMENTS.
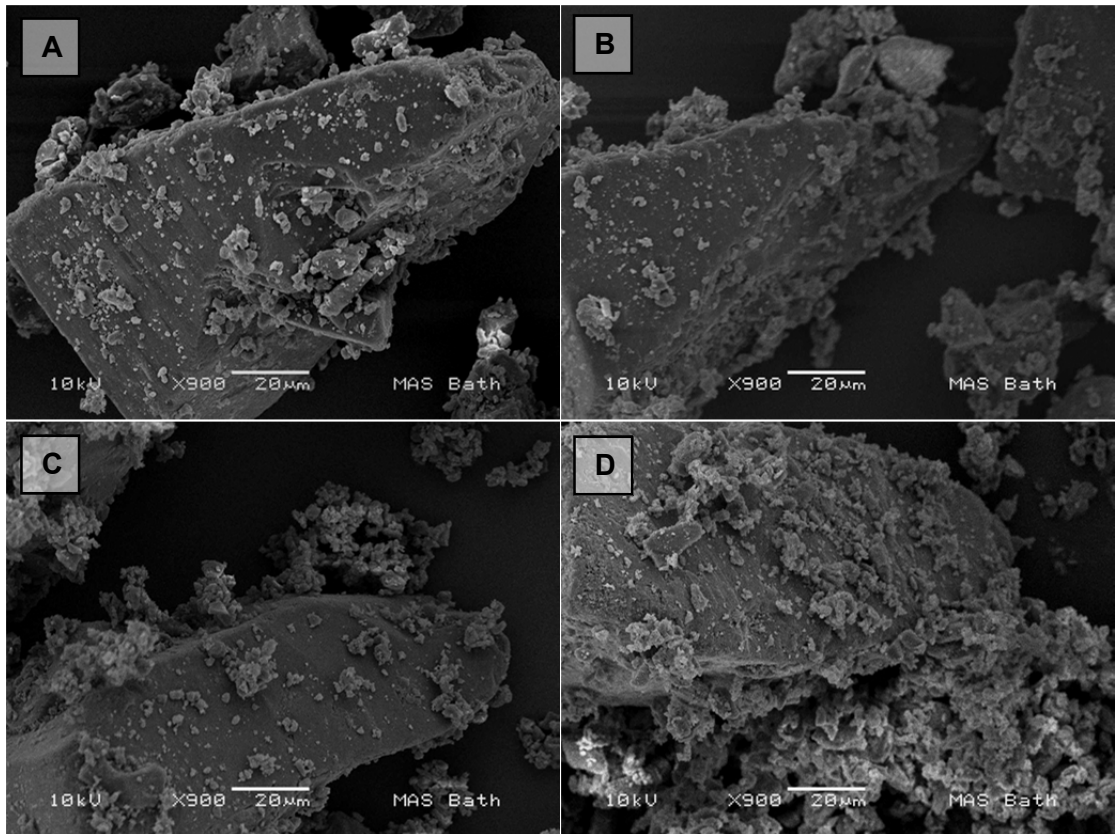
FIGURE 4.4 SCANNING ELECTRON MICROGRAPHS OF **A)** 2.5 **B)** 5 **C)** 10 AND **D)** 20 WT-% LH300 PRE-BLENDS AT **900X** MAGNIFICATION. THE LENGTH OF THE SCALE BAR IN ALL THE IMAGES IS **20 μm**
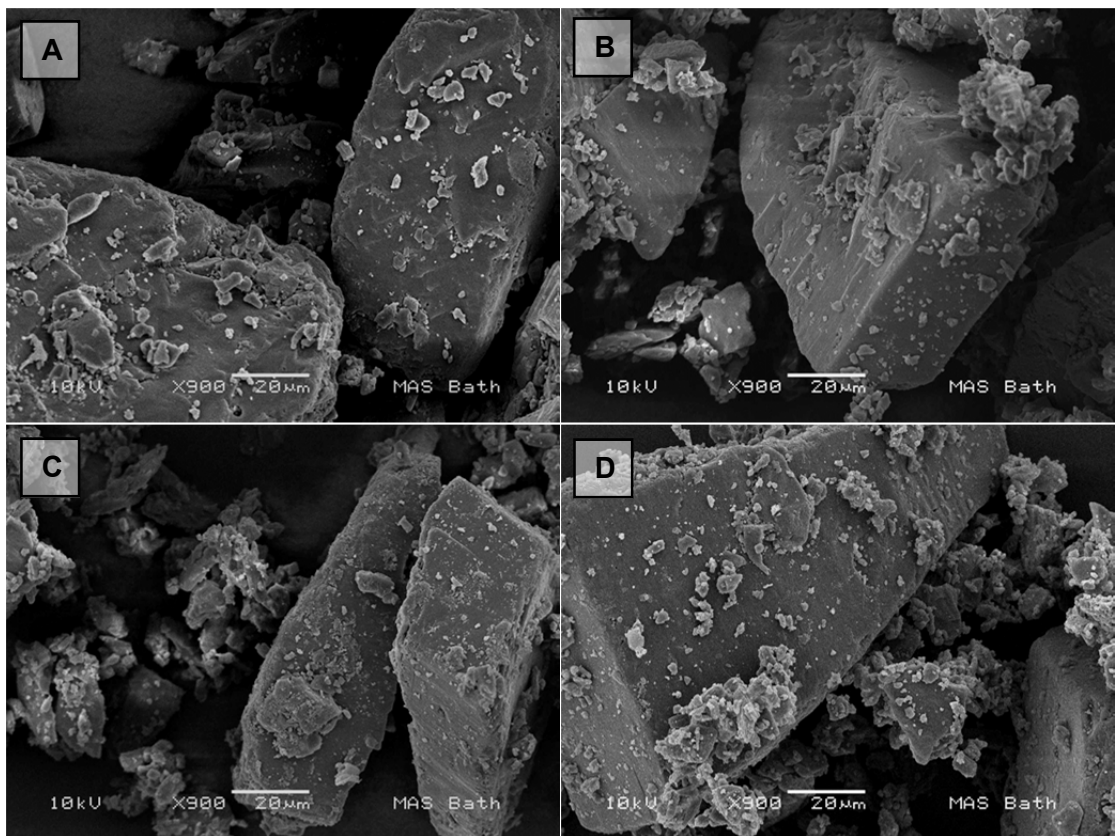
FIGURE 4.5 SCANNING ELECTRON MICROGRAPHS OF **A)** 2.5 **B)** 5 **C)** 10 AND **D)** 20 WT-% LH230 PRE-BLENDS AT **900X** MAGNIFICATION. THE LENGTH OF THE SCALE BAR IN ALL THE IMAGES IS **20 μm**
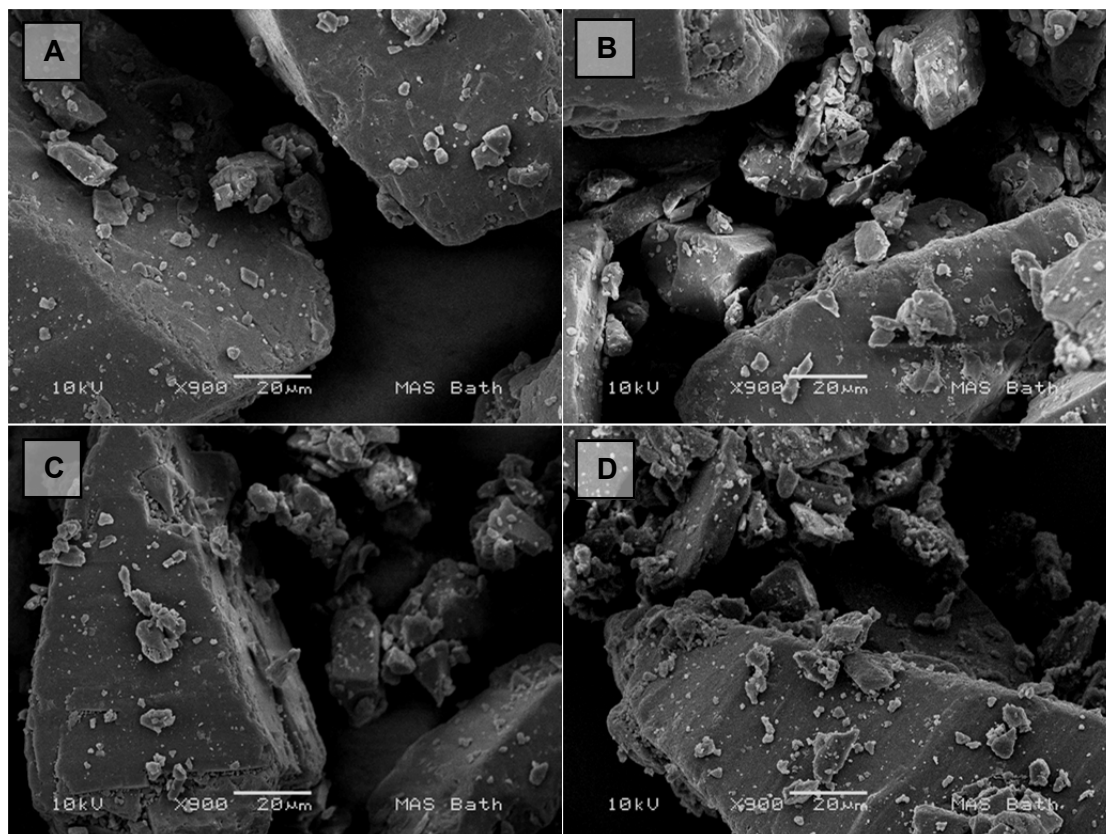
FIGURE 4.6 SCANNING ELECTRON MICROGRAPHS OF A) 2.5 B) 5 C) 10 AND D) 20 WT-% LH210 PRE-BLENDS AT 900X MAGNIFICATION. THE LENGTH OF THE SCALE BAR IN ALL THE IMAGES IS 20 μm

4.3.3 Powder flow and fluidisation properties of the lactose pre-blends

Measuring the powder flow properties using a shear cell tester is an established and widely accepted technique (Schwedes *et al.* 1990). The dynamic approach used for example by the Freeman Technology FT4 powder rheometer is more empirical and based on characterising differences amongst a group of powders based on their resistance to flow under a bulldozing action of an impeller blade and relating the measurement results to the observed powder bulk behaviour during processing (Freeman 2007). However, recent theoretical work has been carried out to gain greater understanding of the powder properties affecting the results obtained on the dynamic FT4 system (Bharadwaj *et al.* 2010). A factor that has possibly limited the popularity of the FT4 for characterising powder flow properties is that the results obtained with the system are sometimes not intuitive. For example, during a basic flow energy test, non-cohesive powders exhibit high flow energies and the more cohesive the powder, the lower is the basic flow energy. However, it has been described in the literature (Freeman 2007) that the results obtained on the FT4 can be explained by the powder transmission zone ahead of the blade. The extent of the zone is dependent on the particle-particle interactions taking place as the impeller blade moves through the powder bed. In the case of free flowing material, the

powder transmission zone in front of the blade is larger because less air is entrapped between the particles. Due to the close packing of the particles, the bulldozing action of the blade is transmitted further ahead of the blade within the powder. Consequentially, more energy is required to keep the blade moving at a constant speed through a bed of free flowing powder than a bed of cohesive powder.

To validate the rheometry results obtained on the FT4 in this study, measurements of the lactose pre-blends were performed alongside Schulze RST-XS ring shear testing. The results of the powder flow and fluidisation properties as characterised on the two different instruments are summarised in Table 4.3. Additionally, traditional indicators of powder flowability used in the pharmaceutical industry, the Hausner ratio and Carr's Index, of the lactose carriers were measured.

The normalised basic flow energies (BFE_{Norm}) of the lactose pre-blends are plotted against the powder flowability number (ff_c) measured on the Schulze ring shear tester in Figure 4.7. The figure shows a linear relationship ($R^2 = 0.9403$) existed between the ff_c and the BFE_{Norm} of the powder for the series of lactose pre-blends used in this study. These data suggest that the normalised basic flow energy of the lactose samples in this study can be used as a descriptor for the general powder flow properties. However, it has to be noted that the correlation between results obtained using static and dynamic measurements, as observed here for the series of lactose pre-blends, does not necessarily exist if a series of chemically different materials are characterised with static and dynamic measurement methods (Freeman 2007; Krantz *et al.* 2009).

TABLE 4.3 SUMMARY OF THE POWDER FLOW AND FLUIDISATION PROPERTIES OF THE CARRIERS AS CHARACTERISED BY FLOWABILITY NUMBER (ff_c), NORMALISED BASIC FLOW ENERGY (BFE_{Norm}), FLOW RATE INDEX (FRI), NORMALISED FLUIDISATION ENERGY (FE_{Norm}), DYNAMIC FLOW INDEX (DFI), CARR'S INDEX AND HAUSNER RATIO. THE DATA REPRESENTS MEAN ± STANDARD DEVIATION (S.D.), n=3.

	ff_c ± S.D.	BFE_{Norm} ± S.D. (mJg^{-1})	FRI ± S.D.	FE_{Norm} ± S.D. (mJg^{-1})	DFI ± S.D.	Carr's Index ± S.D.	Hausner Ratio ± S.D.
LH100	5.55±0.23	25.12±0.40	1.02±0.01	0.70±0.08	37.37±4.01	13.8±0.2	1.16±0.00
+2.5% LH300	4.35±0.25	22.06±0.31	1.10±0.01	0.84±0.09	27.90±3.14	18.3±0.5	1.22±0.01
+5% LH300	3.43±0.10	20.34±0.49	1.19±0.02	1.23±0.07	16.61±1.33	20.0±1.0	1.25±0.01
+10% LH300	2.25±0.06	15.68±0.54	1.52±0.02	1.44±0.07	10.87±0.57	27.5±0.5	1.38±0.01
+20% LH300	1.63±0.02	9.93±0.14	2.41±0.15	1.75±0.01	5.69±0.35	31.7±2.0	1.46±0.04
+2.5% LH230	4.28±0.26	21.65±0.11	1.06±0.00	0.95±0.10	24.07±0.35	17.7±0.3	1.22±0.00
+5% LH230	3.45±0.37	19.37±0.17	1.09±0.00	1.12±0.13	18.49±2.63	20.1±0.7	1.25±0.01
+10% LH230	2.59±0.04	16.07±0.15	1.29±0.01	1.54±0.10	10.74±1.46	26.4±0.6	1.36±0.01
+20% LH230	1.74±0.03	10.52±0.33	1.81±0.06	1.93±0.17	6.15±0.44	32.1±1.5	1.47±0.03
+2.5% LH210	4.97±0.13	23.48±0.42	1.03±0.01	0.78±0.02	31.39±0.73	15.5±0.7	1.18±0.01
+5% LH210	4.14±0.19	21.11±0.59	1.06±0.05	1.00±0.14	21.14±0.44	18.1±0.1	1.22±0.00
+10% LH210	3.51±0.14	19.54±0.31	1.14±0.01	1.04±0.09	19.56±0.56	20.9±0.3	1.26±0.01
+20% LH210	2.28±0.02	13.24±0.10	1.41±0.02	1.60±0.03	9.21±0.67	27.0±0.2	1.37±0.00
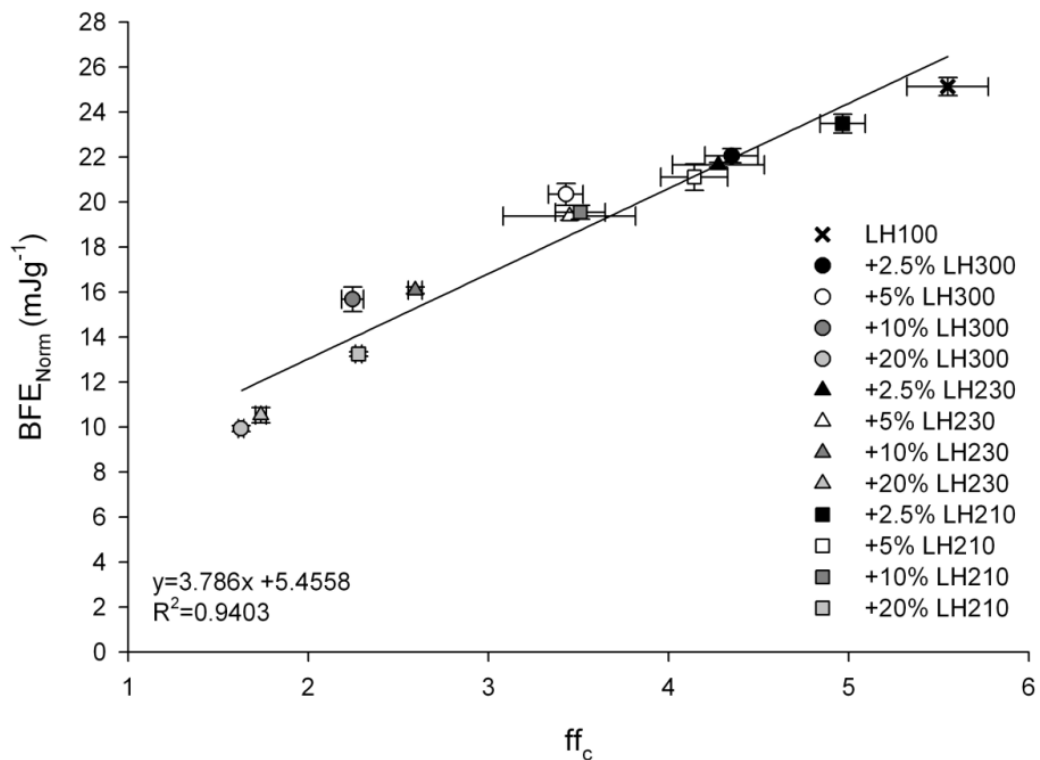
FIGURE 4.7 THE RELATIONSHIP BETWEEN THE ff_c NUMBER MEASURED ON THE SCHULZE RST-XS RING SHEAR TESTER AND THE NORMALISED BASIC FLOW ENERGY (BFE$_{Norm}$) MEASURED ON THE FT4 POWDER RHEOMETER FOR THE LACTOSE PRE-BLENDS INVESTIGATED IN THE STUDY. THE DATA REPRESENTS MEAN ± STANDARD DEVIATION, n=3.

Powder cohesion can be classified according to the ff_c number measured on the Schulze RST-XS system, as shown in Table 4.4. Powders with ff_c values between 2 and 4 are classified as cohesive and powders with values from 4 to 10 as free flowing (Schulze 2010). Figure 4.7 indicates that, for the lactose pre-blends used in this study, a BFE$_{Norm}$ < 20 mJg^{-1} was associated with cohesive powders. 5, 10 and 20 wt-% blends of LH300 and LH230 were classified as cohesive according to their ff_c numbers. In the case of LH210, an addition of at least 10 wt-% of the fines was required for the pre-blends to be classified as cohesive.

The Hausner ratio and Carr's index are widely used as descriptors of powder flow for pharmaceutical applications (Emery *et al.* 2009; Shah *et al.* 2008; Thalberg *et al.* 2004) and can also be used for classifying powder cohesion (Shah *et al.* 2008). The values of Carr's Index and the Hausner ratio for the pre-blends are summarised together with the other flow descriptors in Table 4.3. The classification of the powder flow properties of the pre-blends according to ff_c, Hausner ratio and Carr's Index is presented in Table 4.4. The classification of the flowability of the pre-blends by the Hausner ratio and Carr's index are in good agreement with the classification by ff_c. These data show that the parameters are

158

well suited for qualitatively describing the flow properties of lactose and the influence of the addition of fine lactose to the carriers.

Flow rate index (FRI) measures the sensitivity of a powder to a change in the tip speed of a blade (Freeman 2007). The parameter is a descriptor of powder cohesion. In general, free-flowing powders are not sensitive to changes in the flow rate due to the consistency of the powder transmission zone ahead of the blade at different flow rates. Therefore, free-flowing powders often have values of FRI close to one (Freeman 2007). The flow rate index of the lactose carriers investigated in the current study are plotted against the flowability number ff_c in Figure 4.8. The plot demonstrates that for free-flowing lactose carriers, the flow rate index was insensitive in distinguishing between powders with different cohesive properties. However, once the powder blends were classified as cohesive, the flow rate index became sensitive to the changes in the powder flow properties. Therefore, flow rate index measurements could be used as a parameter for differentiating between cohesive powders when the ff_c is below 3.

The universal FT4 powder tester also enables the study of powder properties under aeration, which may allow characterization of the rheological properties of aeratable powders over a range of fluidization conditions (Shur *et al.* 2008a; Shur *et al.* 2008b) The dynamic flow index (DFI) and normalised fluidization energy (FE_{Norm}) measurements of the lactose pre-blends under aeration are summarised in Table 4.3. These parameters, which are descriptors of change in flow and cohesive properties of the powders under fluidisation, are plotted in Figure 4.9. The DFI describes the reactivity of the powder to aeration. A high value of DFI indicates the air permeates easily through the powder bed and the material will flow readily. On the other hand, a low value of FE_{Norm} indicates that the powder can be easily and homogeneously suspended in air as single particles or small agglomerates. This is because the torque and the force required to keep the blade moving through a fully fluidised powder bed at a constant speed are low due to the lack of particle-particle contacts. Thus, the extent of the powder transmission zone in front of the blade is small. In contrast, if the powder is cohesive, more work is required to move the blade through the agglomerated, poorly aerated powder leading to a higher torque and consequentially higher values of FE_{Norm}. The relationship between the change in the aeratability of a powder (DFI) and its fluidization behaviour (FE_{Norm}) are illustrated by the polynomial relationship in Figure 4.9. These data indicate that powders that are more reactive to an airflow are also more readily suspended in the air when fluidising gas is permeated through the powder bed.

TABLE 4.4 CLASSIFICATION OF POWDER FLOW PROPERTIES OF THE LACTOSE PRE-BLENDS ACCORDING TO FLOWABILITY NUMBER (ff_c), CARR'S INDEX AND HAUSNER RATIO THAT ARE PARAMETERS DESCRIBING POWDER FLOW

	ff_c	Carr's Index	Hausner Ratio
LH100	Easy flowing	Good	Free flowing
+2.5% LH300	Easy flowing	Intermediate	Free flowing
+5% LH300	Cohesive	Intermediate	Poor
+10% LH300	Cohesive	Poor	Poor
+20% LH300	Cohesive	Poor	Poor
+2.5% LH230	Easy flowing	Intermediate	Free flowing
+5% LH230	Cohesive	Intermediate	Poor
+10% LH230	Cohesive	Poor	Poor
+20% LH230	Cohesive	Poor	Poor
+2.5% LH210	Easy flowing	Intermediate	Free flowing
+5% LH210	Easy flowing	Intermediate	Free flowing
+10% LH210	Cohesive	Intermediate	Poor
+20% LH210	Cohesive	Poor	Poor
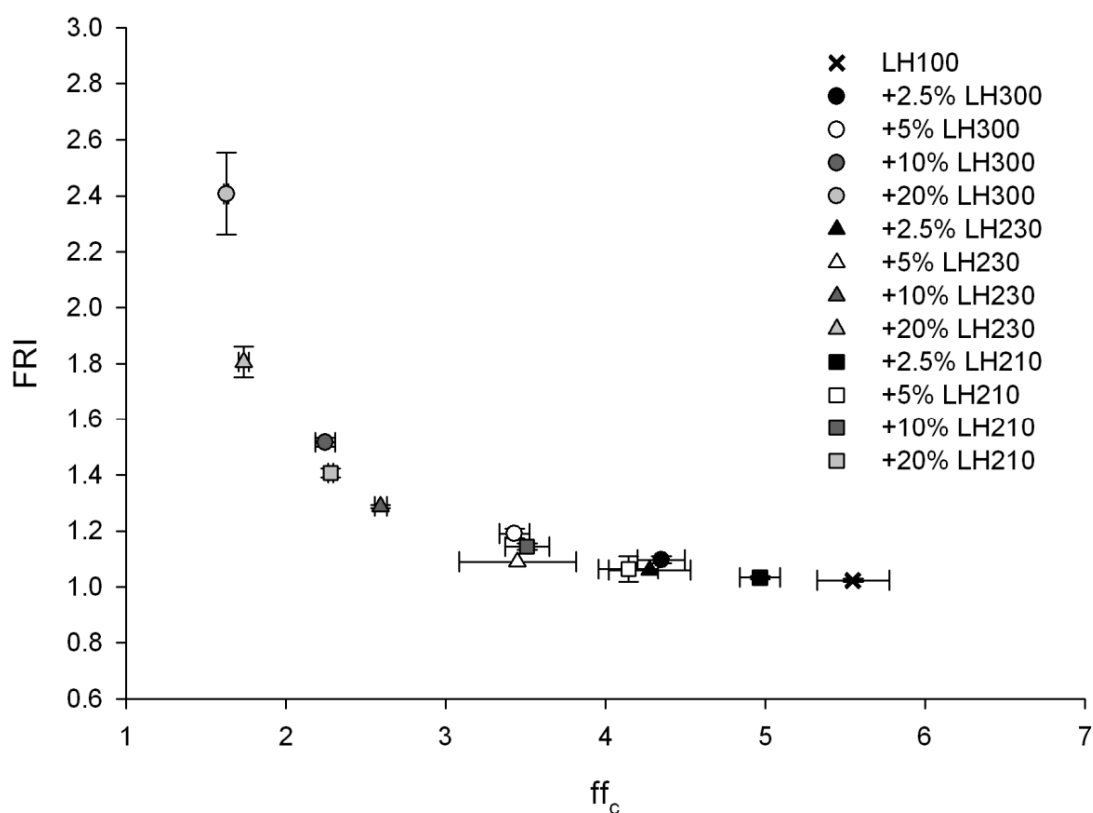
FIGURE 4.8 THE RELATIONSHIP BETWEEN FLOW RATE INDEX (FRI) AND FLOWABILITY NUMBER ff_c FOR THE LACTOSE CARRIERS INVESTIGATED IN THE STUDY. THE DATA REPRESENTS MEAN ± STANDARD DEVIATION, n=3.
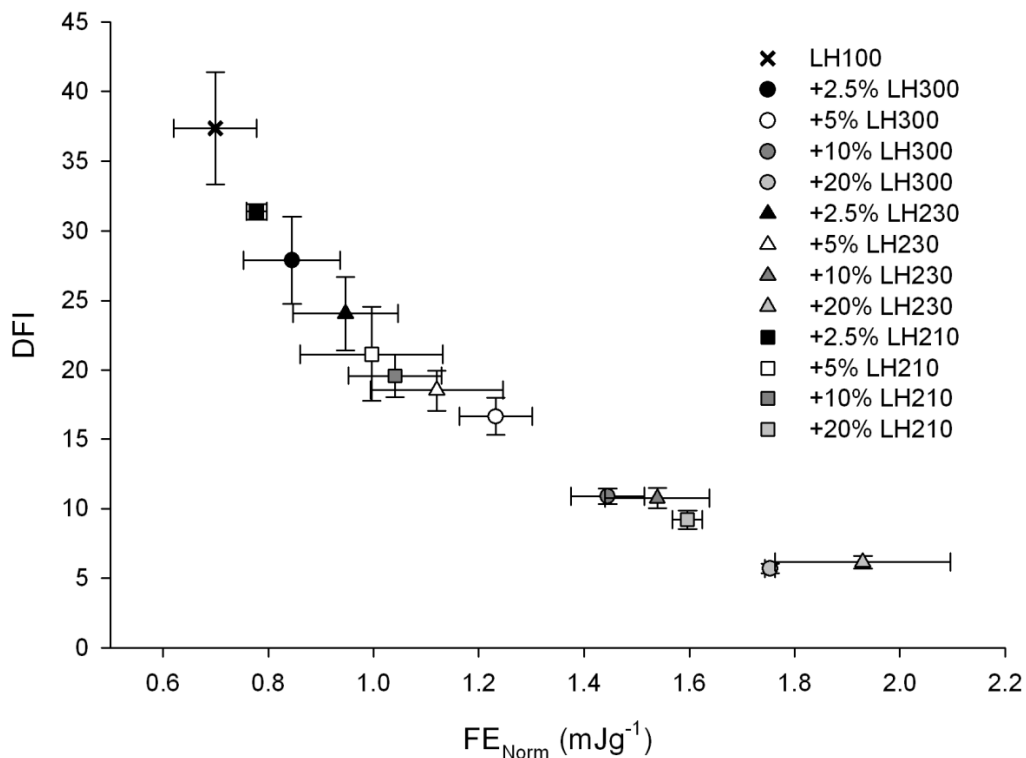
FIGURE 4.9 THE RELATIONSHIP BETWEEN THE NORMALISED FLUIDISATION ENERGY (FE$_{Norm}$) AND THE DYNAMIC FLOW INDEX (DFI) FOR THE LACTOSE CARRIER BLENDS INVESTIGATED IN THE CURRENT STUDY. THE DATA REPRESENTS MEAN ± STANDARD DEVIATION, n=3.

4.3.4   The relationship between the fines content and the flow properties of the lactose pre-blends

According to the recent hypothesis of Shur et al., the addition of lactose fines may improve DPI performance by increasing the cohesive strength of the formulations (Shur *et al.* 2008a). This section of the chapter aims to investigate whether a relationship between the types of fines, increasing fines concentration and the cohesive strength of the pre-blends can be established.

When ff$_c$ values of the lactose carriers are plotted against the proportion of particles finer than 4.5 µm present in the pre-blends, the micronised fines (LH300) data follow a very different trend to both the milled fines grades (LH230 and LH210), as shown in Figure 4.10. However, if the ff$_c$ is plotted against the proportion of particles below 30 µm as per Figure 4.11, all data points follow a single gradient, independent of the type of fines added. These data may be explained by the fact that if only the proportion of fines below 4.5 µm is taken into account, the impact of only a small proportion of the added fines to the powder flow properties is inspected. However, if fines below 30 µm are inspected, a more complete description of the situation with the added fines is achieved. These data

161

are in an agreement with a study by Guenette *et al.* (2009), where it was shown that the fines below 10 µm had the largest negative effect on the flow properties of lactose carriers for inhalation, but that also the fines fraction between 10 and 40 µm decreased the powder flowability. In their study, it was shown that particles larger than 40 µm had no impact on the powder flow properties.

A plot of the FE_{Norm} of the lactose pre-blends as a function of the percentage of particles <4.5 µm is shown in Figure 4.12. This figure demonstrates that the presence of micronised (LH300) fines also had a different impact on the fluidisation properties of the pre-blends than the milled fines (LH230 and LH210). For example, 10 wt-% addition of micronised fines (LH300) finer than 4.5 µm resulted in an FE_{Norm} of approximately 1.2 mJ/g, whereas a similar proportion of milled fines (LH230 and LH210) produced FE_{Norm} of approximately 1.6 mJ/g. The relationship between FE_{Norm} and the proportion of fines below 30 µm present in the carriers is illustrated in Figure 4.13. The data points in this graph are scattered to a greater extent than those shown in Figure 4.11, where the ff_c was plotted against the proportion of fines below 30 µm. These data indicate that flow and fluidisation characteristics of the lactose pre-blends are governed by different mechanisms. Therefore, measuring the fluidisation properties of the pre-blends in addition to the flow properties may add value to the characterisation of lactose carriers for DPI formulations.
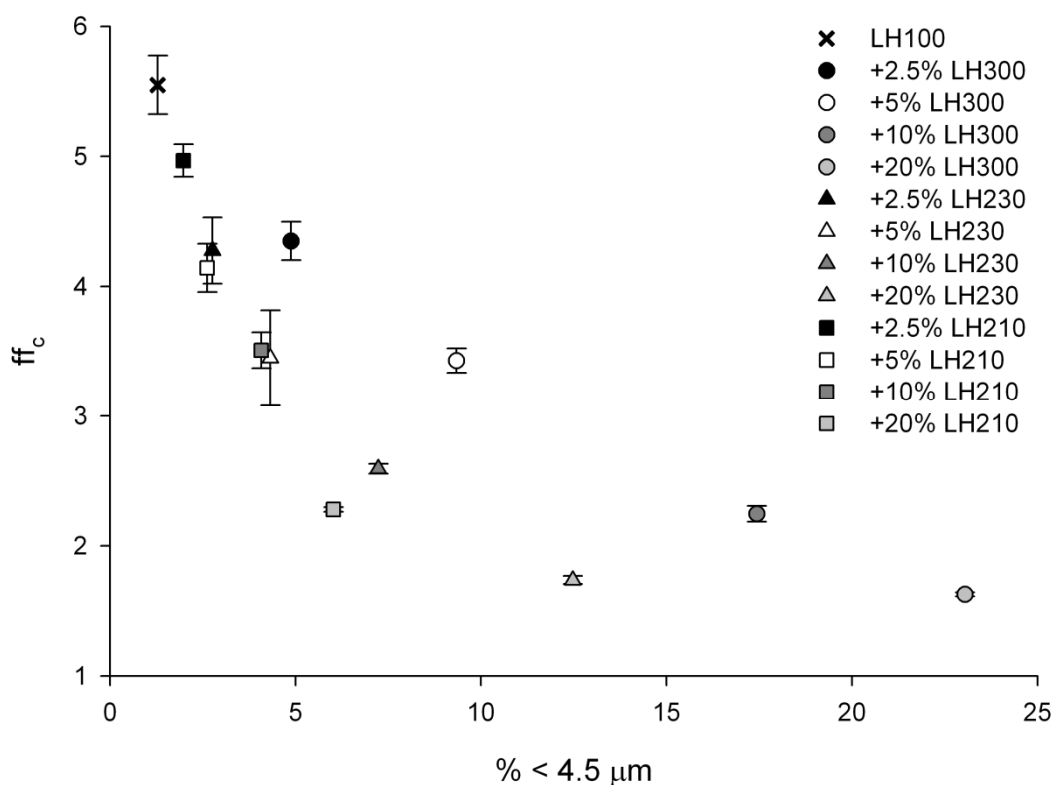
FIGURE 4.10 THE RELATIONSHIP BETWEEN ff_c AND THE PROPORTION OF FINES <4.5µm IN THE LACTOSE PRE-BLENDS. THE DATA FOR ff_c REPRESENTS MEAN ± STANDARD DEVIATION, n=3. THE DATA FOR PROPORTION OF PARTICLES FINER THAN 4.5 µm REPRESENTS MEAN OF 5 DETERMINATIONS.
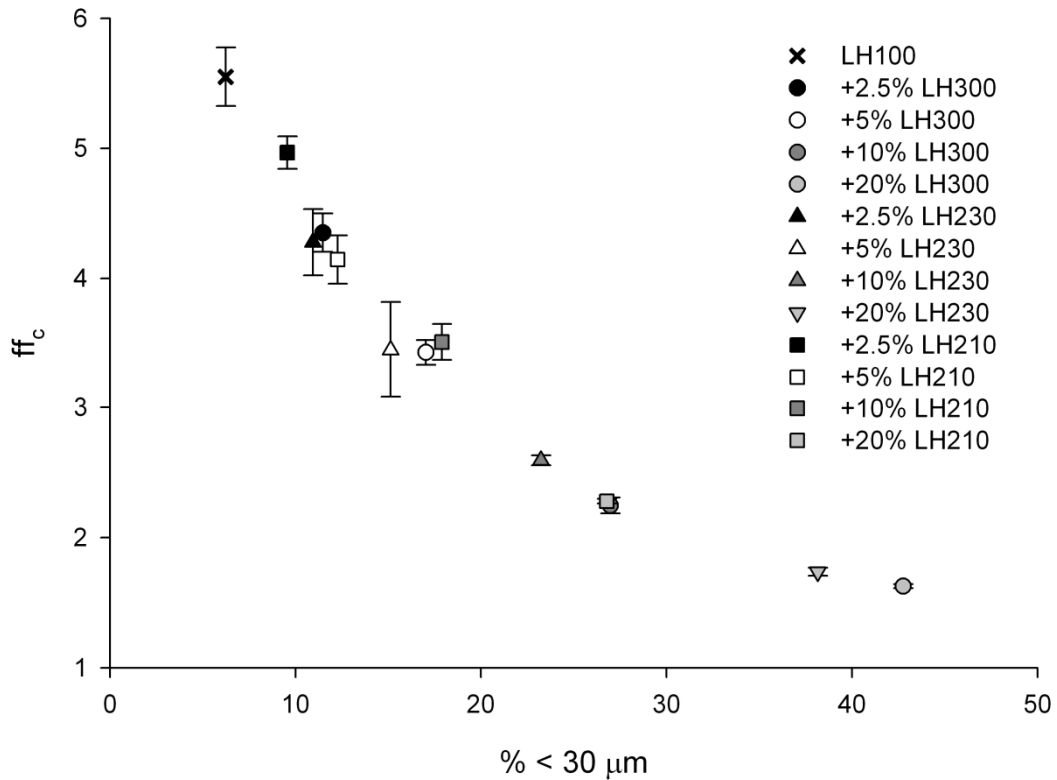
FIGURE 4.11 THE RELATIONSHIP BETWEEN ff_c AND THE PROPORTION OF FINES <30µm IN THE LACTOSE PRE-BLENDS. THE DATA FOR ff_c REPRESENTS MEAN ± STANDARD DEVIATION, n=3. THE DATA FOR PROPORTION OF PARTICLES FINER THAN 30 µm REPRESENTS MEAN OF 5 DETERMINATIONS.
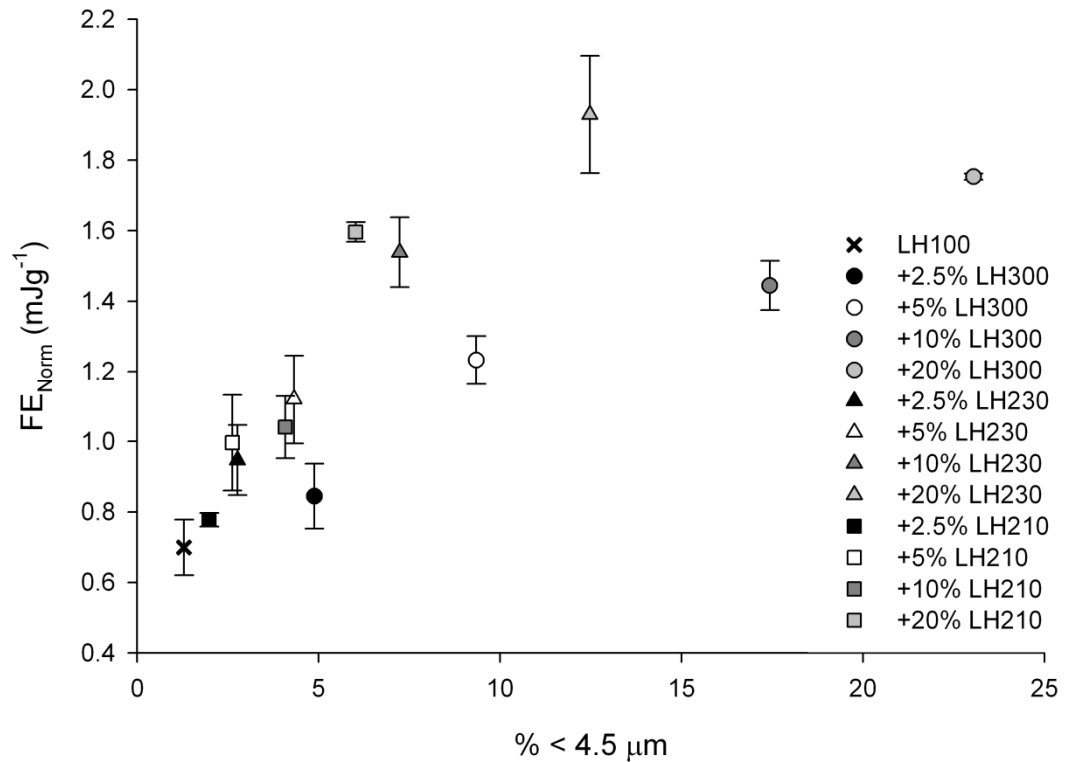
FIGURE 4.12 THE RELATIONSHIP BETWEEN THE PROPORTION OF FINES BELOW 4.5 µm PRESENT IN THE CARRIER AND THE NORMALISED FLUIDISATION ENERGY (FE_{Norm}) OF THE LACTOSE PRE-BLENDS. THE DATA FOR FE_{Norm} REPRESENTS MEAN ± STANDARD DEVIATION, n=3. THE DATA FOR PROPORTION OF PARTICLES FINER THAN 4.5 µm REPRESENTS MEAN OF 5 DETERMINATIONS.
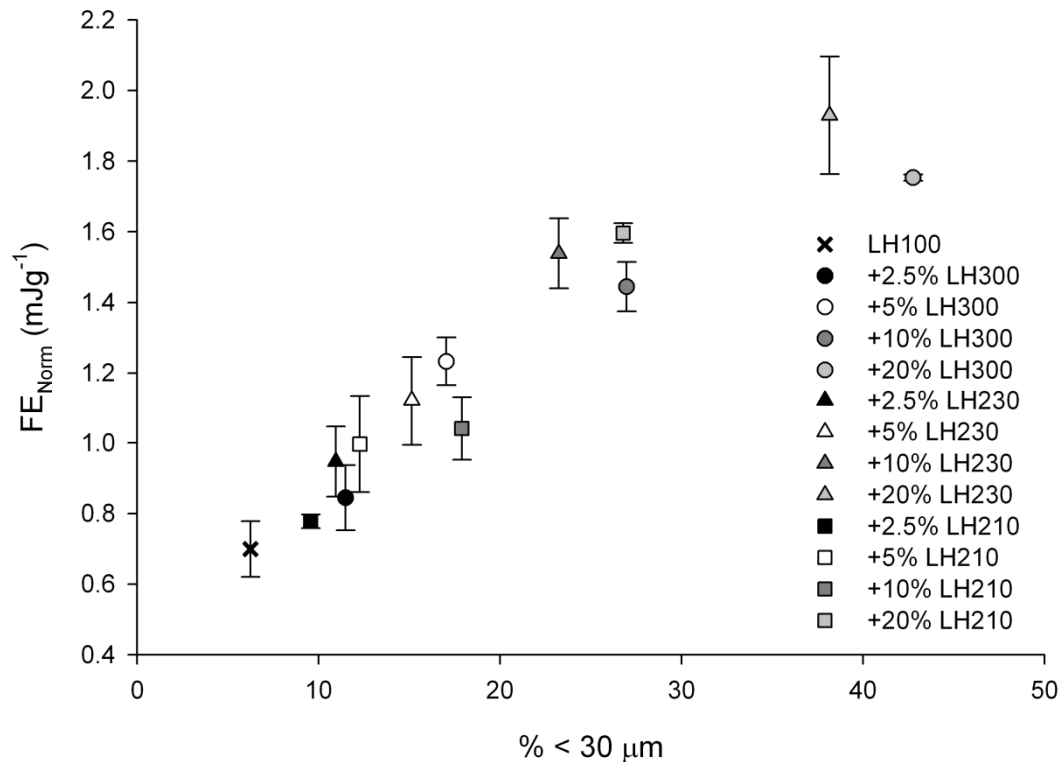
FIGURE 4.13 THE RELATIONSHIP BETWEEN THE PROPORTION OF FINES BELOW **30 μm** PRESENT IN THE CARRIER AND THE NORMALISED FLUIDISATION ENERGY (**FE**$_{Norm}$) OF THE LACTOSE PRE-BLENDS. THE DATA FOR **FE**$_{Norm}$ REPRESENTS MEAN ± STANDARD DEVIATION, **n=3**. THE DATA FOR PROPORTION OF PARTICLES FINER THAN **30 μm** REPRESENTS MEAN OF **5** DETERMINATIONS.

To summarise, this section of the chapter has addressed that the addition of lactose fines to the carrier pre-blends increases the cohesion of the powder bulk both in terms of flow and fluidisation properties. The increase in the cohesive strength is defined by the presence of lactose fines below approximately 30 μm, as suggested by the Geldart powder classification system (Geldart 1973).

4.3.5   *In vitro* performance of DPI formulations prepared with the lactose pre-blends as carriers

The *in vitro* performance of budesonide formulations prepared using the lactose blends were tested with the Rotahaler™ and the Handihaler™ DPI devices, and are summarised in Table 4.5 in terms of their fine particle fraction (FPF$_{ED}$) and mean mass aerodynamic diameter (MMAD) values.

Rotahaler is a low resistance device (0.040 cmH$_2$0$^{0.5}$/(l/min)(Clark *et al.* 1993), while Handihaler is a high resistance device (0.158 cmH$_2$O$^{0.5}$/(l/min)(Al-Showair *et al.* 2007). Thus, aerolisation performance of the formulations from these two devices could be

164

expected to be different. However, as shown in Table 4.5 and illustrated in Figure 4.14, the FPF_{ED} for all of the formulations were nearly identical when aerosolised from the two different devices. These data indicate that the de-agglomeration process of the formulations may be governed by the powder properties rather than the device properties.

Figure 4.14 highlights that an addition of 5 wt-% or more of LH300 was required to significantly ($p<0.01$) increase the DPI performance compared to the formulation prepared with LH100. For LH230, a 20 wt-% addition was required to significantly improve aerolisation performance compared to LH100. Across the range of concentrations investigated, the addition of LH210 did not significantly increase performance compared to LH100 ($p>0.05$). These data show that the addition of milled lactose fines to a carrier-based lactose formulation which is aerosolised from a capsule-based device does not necessarily improve the dry powder inhaler formulation performance.

Figure 4.14 indicates that only a low wt-% concentration of micronised LH300 fines is required to significantly improve DPI performance. These data suggest that the addition of micronised fines can significantly alter the fine particle delivery performance of micronised budesonide in capsule based DPI devices. These findings are in agreement with previous studies by Zeng *et al.* (1999) and Adi *et al.* (2006; 2009) who observed that micronised lactose fines were more efficient in improving DPI performance than coarser sized lactose fines. The former study attributed the observation to the active site theory with larger lactose fines being less effective in occupying the high energy binding sites on the surface of the large lactose. The latter two studies concluded that the larger lactose fines were acting as secondary carriers, therefore being less efficient in improving the performance of DPI products.

The mean mass aerodynamic diameter of the drug aerosolised from the different formulations on the two different devices are summarised in Table 4.5 and illustrated in Figure 4.15. Although the devices appeared to be identical in delivering the drug from the formulations as characterised by FPF_{ED}, the values of MMAD indicate that Handihaler was capable of de-agglomerating the formulations to a greater extent than Rotahaler resulting in smaller MMAD values

In a previous study, changes in the values of MMAD were reported as lactose fines were added to DPI formulations and these changes were attributed the formation of drug-fines agglomerates that were distributed within the impactor (Podczeck 1999). When the trends in the MMAD for the different formulations are inspected (Figure 4.15), it is shown that the MMAD for the formulations containing LH300 remain somewhat unchanged over the range of fines concentrations for both devices. These data indicate that the extent of de-agglomeration did not significantly change for the formulations containing micronised fines

despite the increasing fines content. For the formulations prepared with the milled fines, LH230 and LH210, an increasing trend in the MMAD was seen as the fines content of the formulations was increased. For the Rotahaler, the MMAD was significantly higher for 5 and 10 wt-% LH230 formulations and the 10 and 20 wt-% LH210 formulations than for the LH100 formulation. For the Handihaler, all additions of LH230 or LH210 increased the MMAD of the drug significantly compared to the formulation prepared with LH100 only.

However, Figure 4.15 demonstrates that the addition of 20 wt-% LH230 formulation was an outlier from the increasing trend in the MMAD with increasing concentration of milled fines for both devices. The MMAD for this formulation decreased compared to the 10 wt-% LH230 formulation. It was also shown earlier that when 20 wt-% of LH230 fines were added to the formulation, a significant improvement in the DPI performance in terms of FPF_{ED} was achieved. The increase in the FPF_{ED} and the simultaneous decrease in MMAD suggest that the powder properties of the lactose pre-blends prepared with LH230 changed drastically at high enough wt-% concentrations so that deagglomeration of the formulation became a more favourable process.

TABLE 4.5 *IN VITRO* PERFORMANCE OF THE FORMULATIONS PREPARED WITH THE LACTOSE PRE-BLENDS AS THE CARRIERS IN TERMS OF FINE PARTICLE FRACTION OF EMITTED DOSE (FPF_{ED}) AND MEAN MASS AERODYNAMIC DIAMETER (MMAD). THE DATA FOR FPF_{ED} REPRESENTS MEAN ± STANDARD DEVIATION, n=3. THE DATA FOR MMAD REPRESENTS MEAN ± GEOMETRIC STANDARD DEVIATION (GSD), n=3.

	Rotahaler		Handihaler	
	FPF_{ED} ± S.D. (%)	MMAD ± GSD (µm)	FPF_{ED} ± S.D. (%)	MMAD ± GSD (µm)
LH100	15.68 ± 0.42	3.28 ± 1.92	15.21 ± 1.55	3.00 ± 1.81
+2.5% LH300	20.18 ± 1.56	3.73 ± 1.79	22.72 ± 2.42	3.16 ± 1.74
+5% LH300	28.37 ± 2.26	3.71 ± 1.77	33.94 ± 1.78	3.01 ± 1.73
+10% LH300	40.02 ± 4.03	3.41 ± 1.82	43.07 ± 0.62	2.95 ± 1.77
+20% LH300	37.80 ± 3.43	3.48 ± 1.96	37.00 ± 4.39	3.22 ± 1.87
+2.5% LH230	17.31 ± 3.02	3.50 ± 2.02	17.63 ± 1.11	3.26 ± 1.90
+5% LH230	16.13 ± 1.95	4.31 ± 1.86	20.84 ± 3.39	3.31 ± 1.97
+10% LH230	20.92 ± 2.55	4.40 ± 1.87	22.50 ± 2.10	3.62 ± 1.98
+20% LH230	32.07 ± 2.85	3.74 ± 2.12	31.51 ± 0.31	3.45 ± 2.08
+2.5% LH210	14.52 ± 1.34	3.60 ± 1.88	16.18 ± 0.70	3.26 ± 1.80
+5% LH210	15.39 ± 2.57	3.66 ± 1.89	18.27 ± 0.21	3.34 ± 1.87
+10% LH210	18.11 ± 3.33	4.13 ± 1.83	19.36 ± 3.67	3.41 ± 1.85
+20% LH210	17.95 ± 0.94	4.04 ± 2.05	18.82 ± 1.08	3.56 ± 2.04

Rotahaler
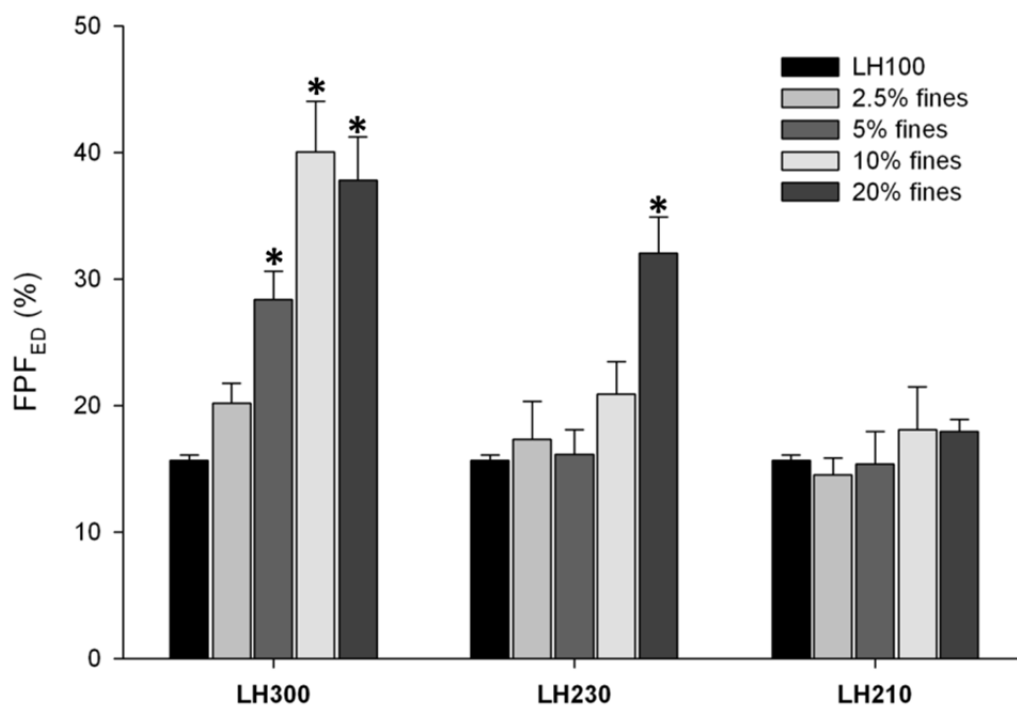
Handihaler
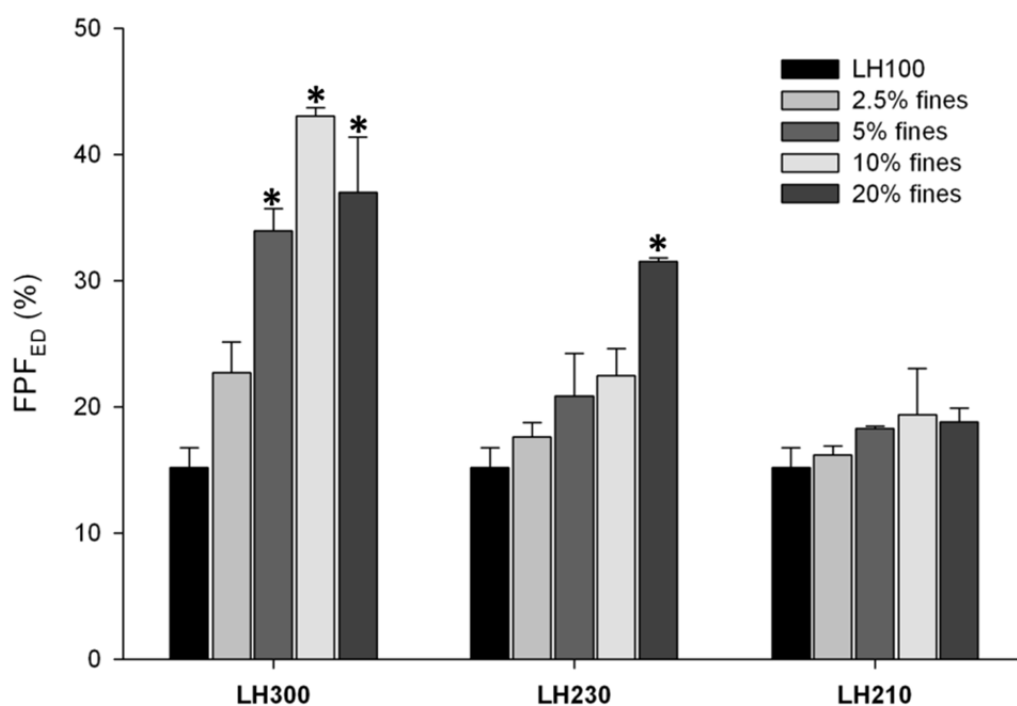
FIGURE 4.14 THE FINE PARTICLE FRACTION OF EMITTED DOSE FROM THE DIFFERENT FORMULATIONS WITH ROTAHALER (TOP) AND HANDIHALER (BOTTOM). THE DATA REPRESENTS MEAN ± STANDARD DEVIATION, n=3. AN ASTERISK DENOTES STATISTICALLY SIGNIFICANT DIFFERENCE (p<0.01) COMPARED TO THE FORMULATION PREPARED WITH LH100 ONLY.

Rotahaler
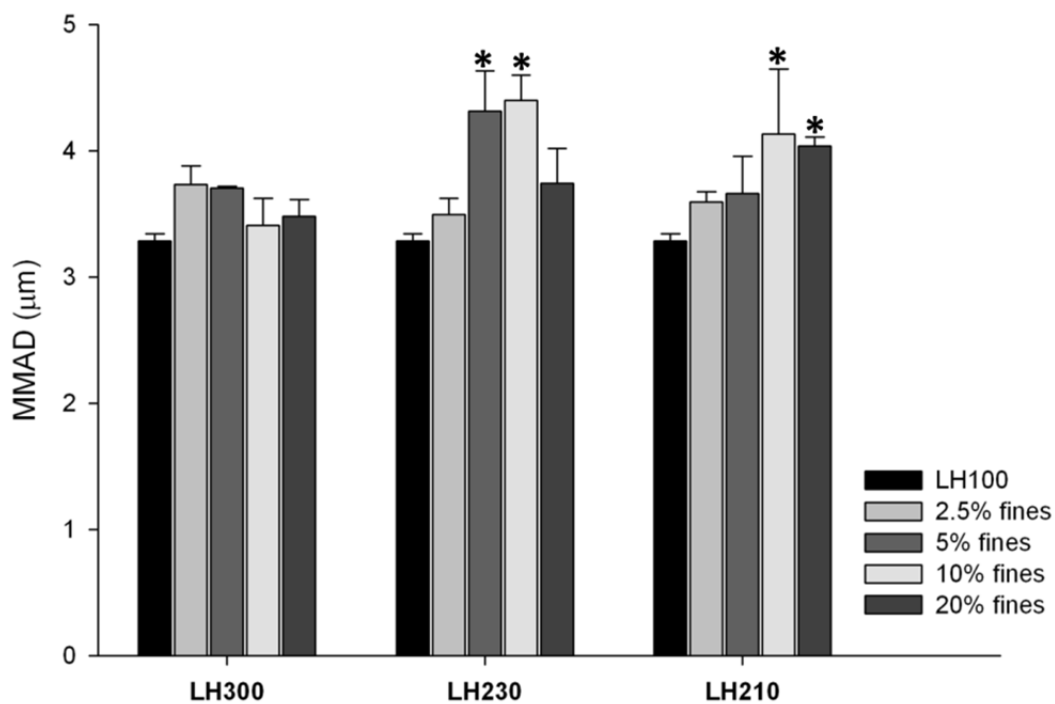
Handihaler
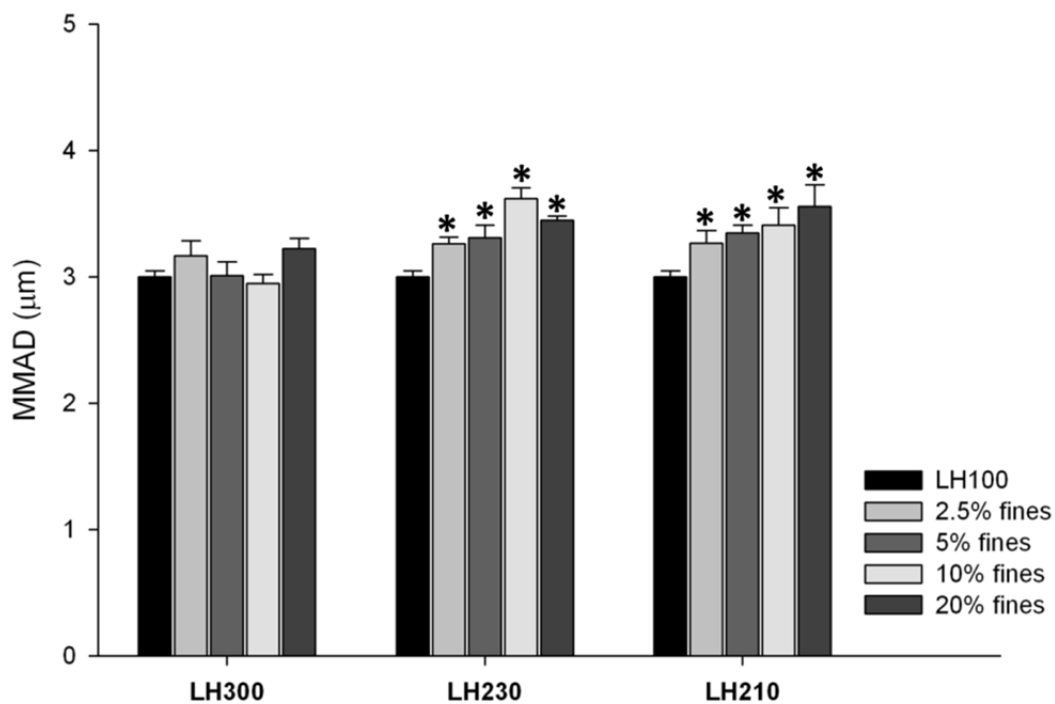
FIGURE 4.15 THE MEAN MASS AERODYNAMIC DIAMETER OF THE DRUG AEROSOLISED FROM THE DIFFERENT FORMULATIONS WITH ROTAHALER (TOP) AND HANDIHALER (BOTTOM). THE DATA REPRESENTS MEAN ± STANDARD DEVIATION, n=3. AN ASTERISK DENOTES A STATISTICALLY SIGNIFICANT DIFFERENCE (p<0.01) IN MMAD COMPARED TO THE FORMULATIONS PREPARED WITH LH100 ONLY

Figure 4.16A, B and C show the stage-by-stage deposition of budesonide from a Rotahaler device for a series of formulations prepared with LH300, LH230 and LH210, respectively. Figure 4.17A, B and C show the equivalent data for the Handihaler device. It can be seen that when the concentration of the fines is increased, the capsule deposition from Rotahaler remained constant over all the fines concentrations with all the fines. With the Handihaler, the addition of all the fines at 2.5 wt-% concentration decreased the capsule deposition very slightly compared to the LH100 formulation. However, increasing the concentration of fines did not further decrease dose retention within the capsule.

Figure 4.16 suggests that for all fines, the proportion of drug recovered from the Rotahaler increased with the addition of lactose fines. The increase in the device deposition was more pronounced for the micronised fines (LH300) with the amount of drug recovered from the device doubling as the fines concentration was increased from 0 to 20 wt-%. The increase in the proportion of drug deposited in the Rotahaler was statistically significantly greater ($p<0.01$) for LH300 formulations at 5 wt-% or higher fines content than for the LH100 only formulation. For the LH230 milled fines, an addition of 20 wt-% of fines was required to cause a significant increase in the proportion of drug recovered from the Rotahaler device. The increasing addition of LH210 fines only affected device deposition very little with no statistically significant increase in the proportion of drug recovered from the device over the range of fines concentrations added.

Increased device deposition upon an increasing fines concentration has been previously reported by Podczeck (1998; 1999), who used a Monohaler device in their study. In contrast, Figure 4.17 shows that device retention for the Handihaler device was very low, with approximately 5% retained, and remained unchanged with all the different fines and at all the fines concentrations. The difference in the proportion of the drug retained in the different devices is likely to be due to the larger volume of the chamber of 11.58 ml of Rotahaler (Behara *et al.* 2011a) compared to a volume of 0.76 ml of Handihaler (Behara *et al.* 2011a). Because of the larger volume chamber of the Rotahaler, a larger surface area is available for the drug to adhere on. Also, in Handihaler the powder is retained in the capsule until it is fluidised. Therefore, the movement of the capsule and the emptying of the powder from the device appear to be highly efficient and insensitive to the cohesive properties of the formulations.

Figure 4.16A, B and C show that an increase in the proportion of the drug deposited in the mouthpiece and throat compared to the formulation prepared with LH100 only was observed for all the different fines with the Rotahaler device. Compared with the LH100, the increase in mouthpiece and throat deposition was statistically significant for 5, 10 and 20% LH230 formulations and 20% LH210 formulation ($p<0.05$). However, the proportion

of drug aerosolised on Rotahaler recovered from the mouthpiece and throat was relatively low, approximately 10% of the recovered dose.

Figures 17A, B and C show that, for all fines, the proportion of drug deposited in the mouthpiece and throat from the Handihaler device increased when the fines concentration was increased. For the LH100 formulation, approximately 18% of budesonide was recovered from the mouthpiece and throat. With 20 wt-% LH300, the proportion of drug deposited in the mouthpiece and throat was roughly 30%, with 20 wt-% LH230 approximately 32% and with 20 wt-% LH210 approximately 35%. It has been shown that the throat deposition from DPI formulations is governed both by particle impaction due to the high velocity jet exiting the device and the kinetic energy of the particles following turbulence created by the device (DeHaan *et al.* 2004). The same study addressed that the kinetic energy is dependent on the diameter of the device outlet with smaller outlets producing higher turbulence, and thus higher kinetic energies. Handihaler has a smaller outlet diameter than Rotahaler. Therefore, the conclusions by DeHaan *et al.* (2004) may explain the results of the current study with more drug depositing in the throat from Handihaler than from Rotahaler.

Figure 4.16 demonstrates that the proportion of drug depositing in the pre-separator when aerosolised on Rotahaler was greatly affected by the addition of lactose fines. The addition of micronised fines LH300 was shown to have the largest impact with the pre-separator deposition reducing from 50% to less than 40% for 2.5 wt-% fines blend, to less than 30% for the 5 wt-% blend and, furthermore, to less than 20% for the 10 wt-% blend. Interestingly, a plateau was then reached and further addition of the micronised fines did not further decrease the proportion of drug deposited in the pre-separator. In the case of the finer of the two milled fines, LH230, a decrease in the pre-separator deposition was also observed, with fines concentrations up to 10 wt-% showing a significant decrease from 50% deposition down to 30%. The addition of 20 wt-% LH230 decreased the amount of drug recovered from the pre-separator to a similar level of less than 20% as the 10 and 20 wt-% LH300 blends. As discussed, the 20 wt-% LH230 formulation performed significantly better than any other formulations prepared with milled fines investigated during the current study. These data indicate that once a critical concentration of LH230 milled fines in the formulation was achieved, the drug detachment from the particles depositing in the pre-separator, i.e. the large carrier crystals and the larger fraction of the fine particle lactose itself, became favourable. With the addition of 20 wt-% LH210, pre-separator deposition decreased, from 50% in the absence of added fines, to 35%. The trends observed in the pre-separator deposition with Handihaler (Figure 4.17) were very similar to those observed for the Rotahaler.

These data showing a decrease in the amount of drug recovered from the pre-separator as more lactose fines were added to the formulations are in an agreement with studies carried out by Podczeck (1998; 1999), Srichana *et al.* (1998b), Guchardi *et al.*(2008) and Shur *et al.* (2008a). Podczeck (1998; 1999) attributed the observation to the smaller proportion of large lactose carrier particles present in the formulations as the fines concentration was increased. Therefore, less surface area of the large lactose carrier crystals was available for the drug particles to adhere on, and simultaneously, the drug was possibly carried to the impactor stages as agglomerates with the lactose fines. This theory is significant for the current study especially in terms of the pre-separator deposition saturation for 10 and 20 wt-% LH300 formulations. In number terms, the 20 wt-% LH300 pre-blend contains a much lower number of large carrier crystals than the 10 wt-% blend. Therefore, less drug should be expected to be recovered from the pre-separator from the 20 wt-% formulation. However, this was not the case. Therefore, it is likely that the drug was deposited in the pre-separator as large agglomerates with the lactose fines from this formulation.

Figure 4.16 shows that the stage-by-stage deposition of budesonide was significantly improved on all stages by adding LH300 at 10 or 20 wt-% concentrations or LH230 at 20 wt-% concentration compared to LH100. Figure 4.17 shows that for the Handihaler device, the stage deposition of budesonide significantly increased for 5, 10 and 20 wt-% blends of LH300 on stage 2 and below ($p < 0.05$). In the case of LH230, the stage deposition significantly increased for 10 and 20 wt-% formulations on stage 2 and below ($p < 0.05$). For the LH210 series of formulations, a significant increase in the amount deposited on the stages were only seen up to stage 3 with 5, 10 and 20 wt-% fines added.
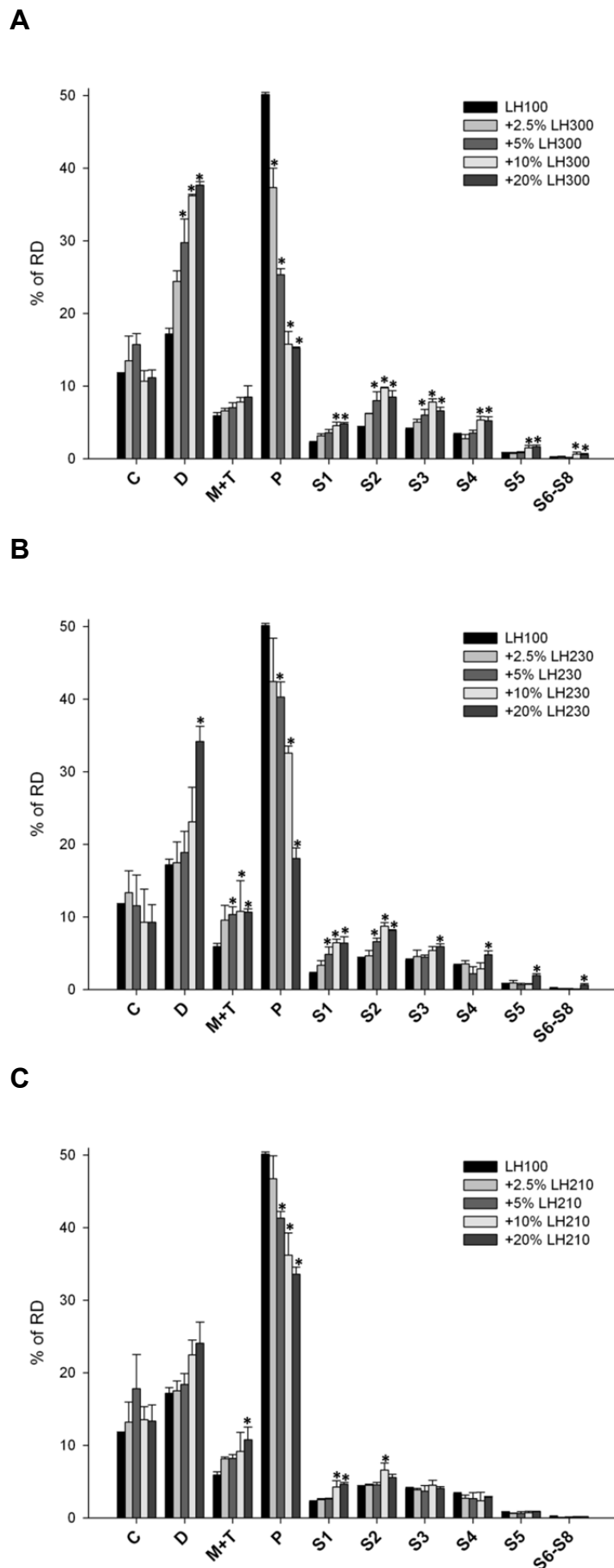
FIGURE 4.16 THE STAGE-BY-STAGE DEPOSITION PROFILES OF BUDESONIDE FROM THE MODEL FORMULATIONS AEROSOLISED ON ROTAHALER WITH A) LH300 B) LH230 AND C) LH210 AS THE FINES IN THE CARRIER. THE DATA REPRESENTS MEAN ± STANDARD DEVIATION, n=3.
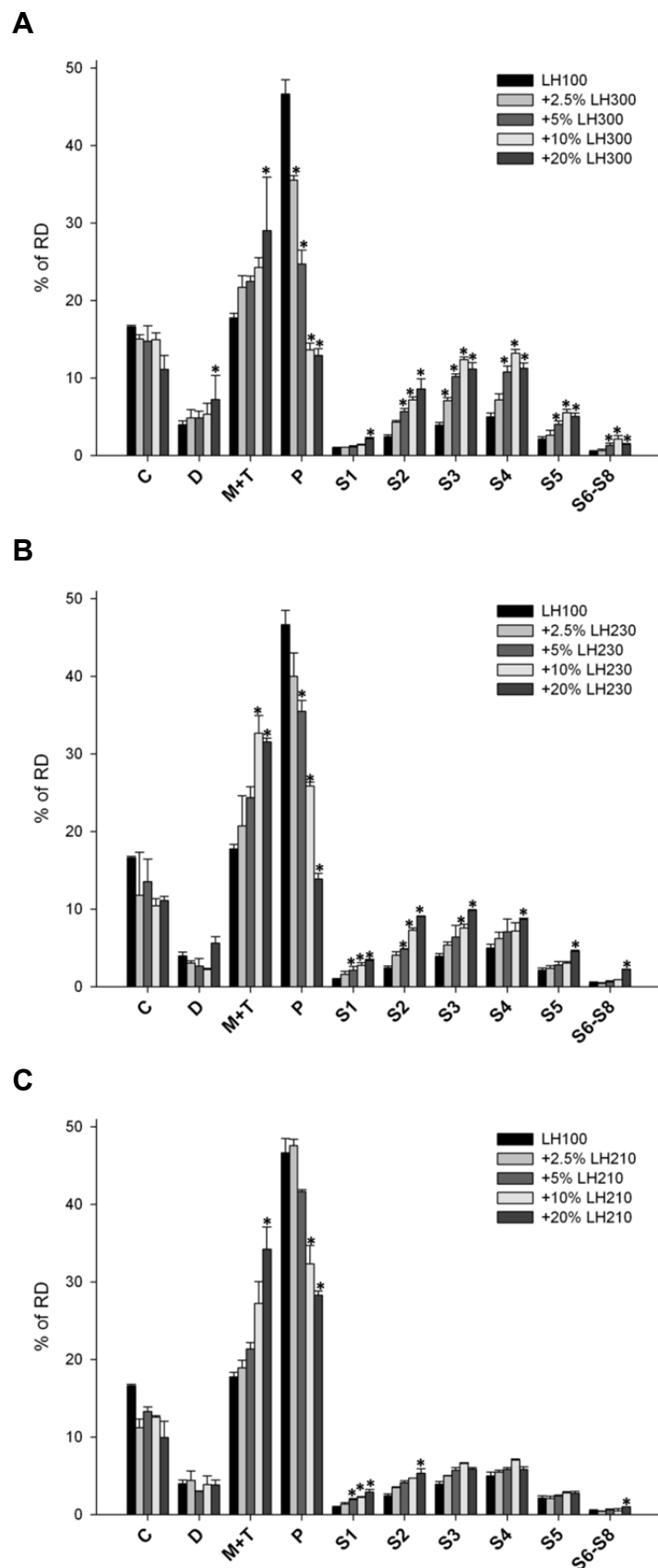
FIGURE 4.17 THE STAGE-BY-STAGE DEPOSITION PROFILES OF BUDESONIDE FROM THE MODEL FORMULATIONS AEROSOLISED ON HANDIHALER WITH A) LH300 B) LH230 AND C) LH210 AS THE FINES IN THE CARRIER. THE DATA REPRESENTS MEAN ± STANDARD DEVIATION, n=3.

4.3.6 The relationship between the physical properties of the carrier pre-blends and the *in vitro* performance of the formulations

The fine particle fraction of emitted dose of the formulations investigated in the current study on Rotahaler and Handihaler are plotted against the percentage of particles finer than 4.5 µm present in the carrier in Figure 4.18. It can be observed that with both the devices a weak correlation between the proportion of fines and the FPF_{ED} existed when the proportion of the fines was below ~17%. The data at lower fines concentrations were more scattered for Handihaler than for Rotahaler. Various previous studies have reported a correlation between the proportion of fines present in the carrier and the DPI performance. Some of these studies were conducted using Rotahaler (Adi *et al.* 2009; Louey *et al.* 2003). However, linear correlations between the FPF and fines content of the carriers have also been observed with other devices, such as Monohaler (Guenette *et al.* 2009).

Figure 4.18 shows that, with both devices, the fine particle delivery performance of budesonide from the formulations reached a maximum with the addition of 10 wt-% LH300 fines, with 17.4% of the particles in the carrier less than 4.5 µm. Using the 20 wt-% LH300 pre-blend containing 23% of particles finer than 4.5 µm led to a decrease in the FPF_{ED} with both devices. These data are in agreement with a previous study, where the addition of 10 wt-% was reported as the optimum concentration of micronised fines, and where higher lactose fines concentrations decreased performance (Louey *et al.* 2003). In their study, the observed behaviour was attributed to the dilution of the drug in the agglomerates formed between the lactose fines and the drug when the lactose fines concentrations were higher. Similar observations were also made by Young *et al.*(2011), who attributed the decrease to the segregation of the formulation in the presence of excess fines.

It is also important to note from Figure 4.18 that the relationship between the proportion of fine particles present in the carrier and DPI performance was not affected by the process history (micronised vs. milled) of the added fine component.

Rotahaler
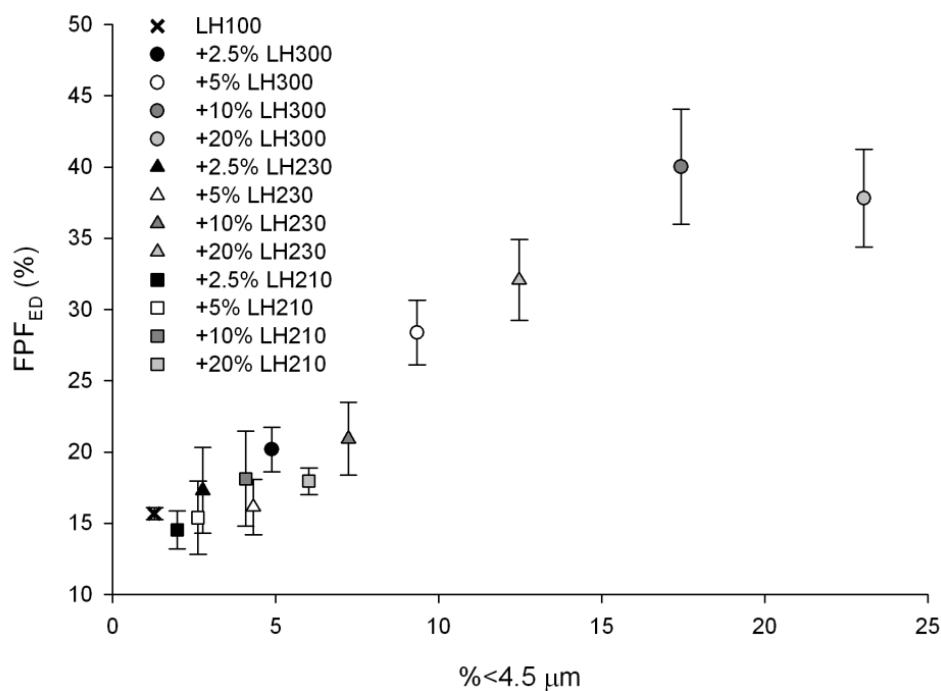
Handihaler
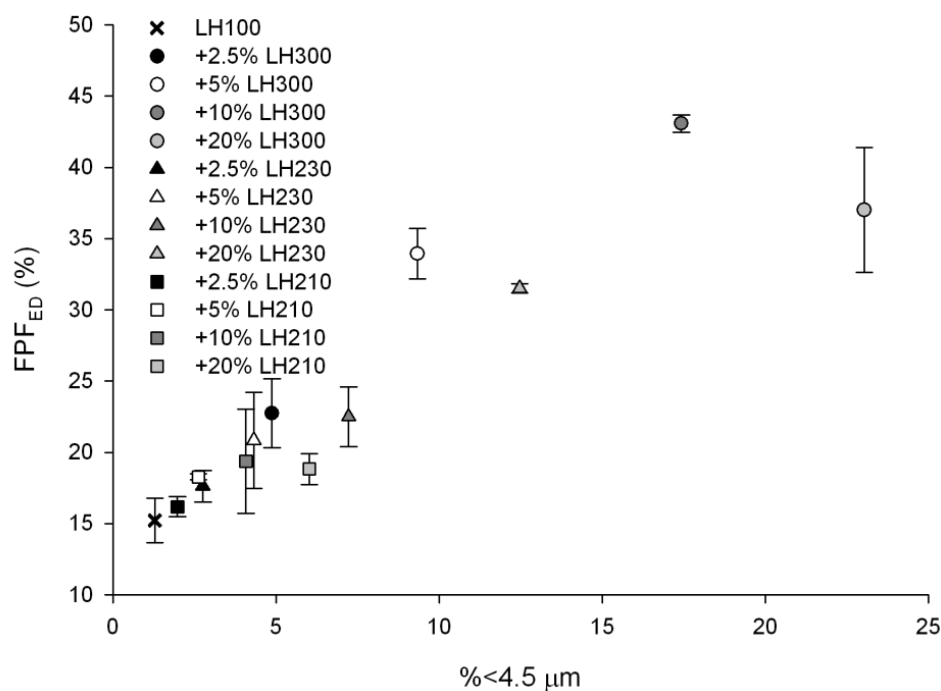
FIGURE 4.18 THE RELATIONSHIP BETWEEN THE PROPORTION OF FINE PARTICLE LACTOSE (<4.5 μm) AND THE DPI PERFORMANCE IN TERMS OF FINE PARTICLE FRACTION OF EMITTED DOSE (FPF$_{ED}$) FOR ROTAHALER (TOP) AND HANDIHALER (BOTTOM). THE DATA FOR FPF$_{ED}$ REPRESENTS MEAN ± STANDARD DEVIATION (N=3) AND THE DATA FOR PROPORTION OF PARTICLES FINER THAN 4.5 μm THE MEAN FROM FIVE REPEATED MEASUREMENTS.

Fluidisation of the DPI formulation is a key step in delivering the API to the patient's lungs. Therefore, the fluidisation properties of the carrier pre-blend, which forms the bulk of the DPI formulations, are anticipated to give information on the aerosolisation efficiency of the DPI formulations. It has already been shown by Shur *et al.* (2008a) and Pitchayajittipong *et al.* (2010) that in some cases the fluidisation energy of the carrier lactose correlates with the performance of DPI model formulations.

The FPF_{ED} of the formulations used in the current study were plotted against the fluidization energy of the carrier blend for each of the formulations and shown in Figure 4.19. In the case of the addition of micronised fines (LH300), there was a linear relationship between the energy required to fluidise the formulation and the fine particle fraction delivered up to 10 wt-% fines concentration with both the Rotahaler and the Handihaler. However, at 20 wt-% concentration, despite the increase in the fluidisation energy, the fine particle fraction decreased. Figure 4.19 also shows that with the milled fines (LH230 and LH210) the response between the FPF_{ED} and the fluidisation energy was linear with both the Rotahaler and the Handihaler. Figure 4.19 shows that for the milled fines an increase in the fluidisation energy only corresponded to a very slight improvement in the performance.

The process of delivering the medication to the patient's lungs from a DPI formulation involves fluidisation, entrainment and deagglomeration of the formulation. Gac *et al.* (2008) showed that the energy required to achieve de-agglomeration of the DPI formulation is higher than the energy required to fluidise the formulation. Therefore, it is not surprising that the fluidisation energy fails to predict the DPI performance of the formulations over a wide range of different fines concentrations and types of fines. However, the current study has shown that although a universal correlation between the fluidisation energy and DPI performance is not possible correlations do exist over certain ranges. Therefore, fluidisation properties may be suitable for predicting the DPI performance for a less variable set of carriers, such as for investigation of batch to batch variability of processed lactose.

Rotahaler – LH300
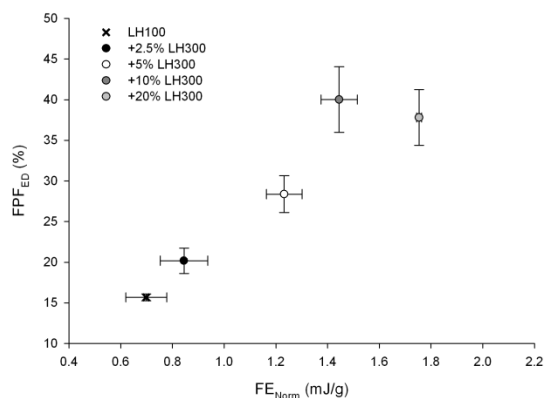
Rotahaler – LH230 and LH210
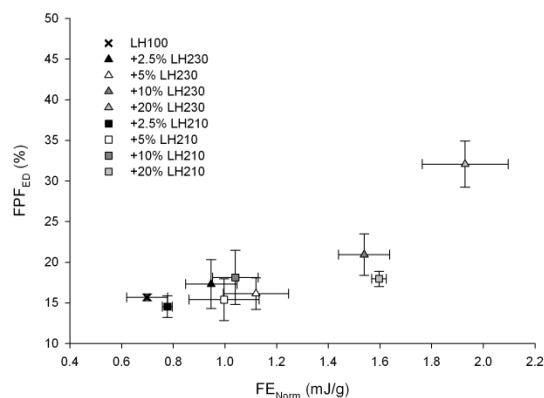
Handihaler – LH300
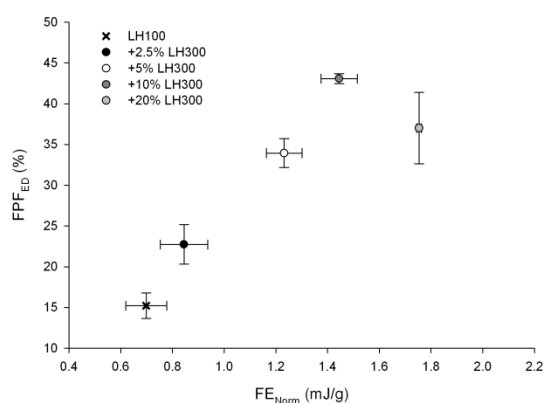
Handihaler- LH230 and LH210
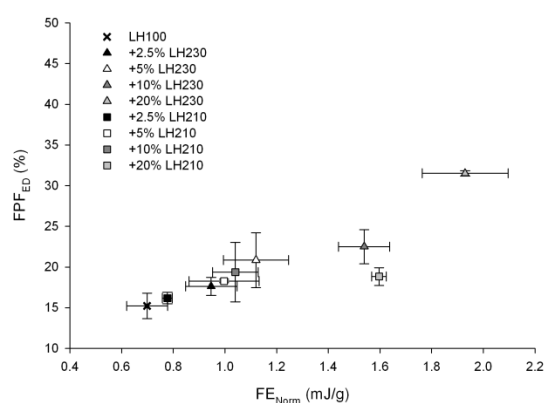
FIGURE 4.19 THE RELATIONSHIP BETWEEN THE NORMALISED FLUIDISATION ENERGY (FE$_{NORM}$) OF THE CARRIER PRE-BLENDS AND THE DPI PERFORMANCE IN TERMS OF FINE PARTICLE FRACTION OF EMITTED DOSE (FPF$_{ED}$) FROM FORMULATIONS PREPARED WITH DIFFERENT FINES AND AEROSOLISED WITH DIFFERENT DEVICES. THE DATA REPRESENTS MEAN ± STANDARD DEVIATION, n=3.

4.3.7   Microstructure of the formulations prepared with the different fines

Due to the different components of dry powder inhaler formulations (drug + fines + coarse carrier), the resulting powders are complex. An added complication is the device used for delivering the dose. Therefore, achieving a complete understanding of the detachment and deagglomeration of the drug from DPI products has proved to be difficult. Recent research has concentrated on understanding the powder microstructure and the resulting deagglomeration mechanisms (Behara *et al.* 2011b). This study showed that blending different concentrations of micronised lactose with micronised drug altered the structure and the deagglomeration mechanism of the resulting blends. However, the model formulations in this study did not contain the coarse lactose carrier component. Thus, the applicability of these findings to the current research problem is questionable, because

177

both the fluidisation properties and the microstructure of the formulations will be significantly different due to the presence of the large carrier component.

A schematic of the microstructure of the formulations in the current study is presented in Figure 4.20. The *in vitro* data suggests that improved performance can be easily obtained by the addition of micronised fines. However, improved performance was also achieved when the finer of the milled fines was present in a large concentration, so that the proportion of the fine particle lactose was sufficient to achieve agglomerate formation. SEM images (Figures 4.4, 4.5 and 4.6) of these formulation blends with budesonide support the theory of agglomerate formation.

From findings presented in this chapter, the following hypothesis on the action of the different fines is presented. With micronised fines, agglomerates between the drug and the lactose fines are formed readily due to the large number of lactose fines present already at low concentrations. With milled fines at low concentrations, not a high enough proportion of the fine particle lactose is present in the formulation. Therefore, agglomerate formation cannot take place. Instead, the drug particles are distributed on the surfaces of the medium sized fines (>15um) and the coarse carrier particles. The deagglomeration efficiency of the drug from these particles is thought to be low. Therefore, low DPI performance is obtained from these formulations, with a large proportion of the drug deposited in the pre-separator. However, if the concentration of the milled component is increased, the proportion of the finest lactose in the carrier may become sufficient to achieve agglomerate formation with the finer sized particles which are co-delivered as an agglomerate within the *in vitro* apparatus. Consequentially, increased DPI performance can be achieved from formulations prepared with milled fines.
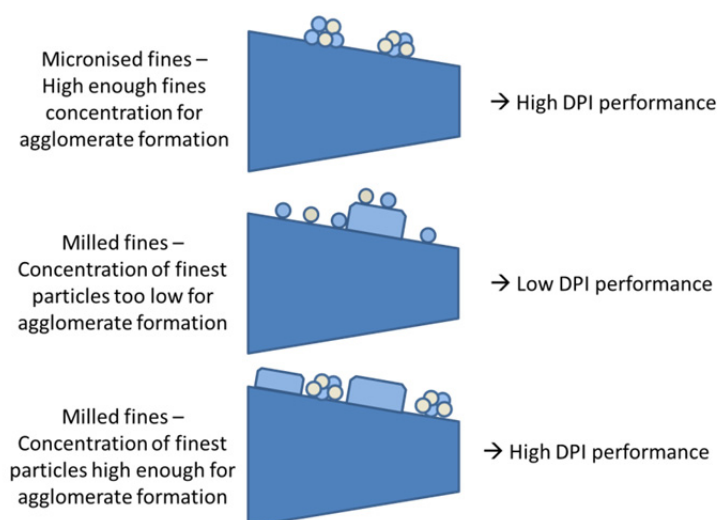
FIGURE 4.20 SCHEMATIC OF THE MICROSTRUCTURE OF THE FORMULATIONS CONTAINING MICRONISED FINES (TOP) AND MILLED FINES AT LOW (MIDDLE) AND HIGH (BOTTOM) CONCENTRATIONS, AND THE IMPACT OF THE MICROSTRUCTURE ON THE DPI PERFORMANCE. BLUE SHADES REPRESENT DIFFERENT SIZE LACTOSE (LARGE, INTERMEDIATE AND FINES) AND PINK REPRESENTS DRUG PARTICLES

4.4 CONCLUSIONS

This chapter investigated the role of drug-fines agglomerate formation and increased cohesion in improving the DPI performance. The data showed that the addition of lactose fines increased the cohesion of the bulk powder. The increase in cohesion was determined by the presence of lactose fines <30 µm. However, despite previous studies showing promising preliminary results for using the flow properties of the carrier for predicting the performance of DPI formulations for simple series of lactose carriers (Pitchayajittipong *et al.* 2010; Shur *et al.* 2008a), no direct correlation between any of the parameters describing powder flow and fluidisation properties and the final DPI performance could be established in this study for a more diverse set of carriers. Therefore, increasing powder cohesion upon the addition fines in improving the DPI performance is unlikely to explain the phenomenon. However, that said, various linear sub-correlations were seen within the current dataset between the fluidisation properties and the formulation performance. Therefore, the flow and fluidisation properties are still likely to be able to differentiate between carriers that are similar in terms of particle size but would produce a slightly different performance. Thus, the characterisation of fluidisation and flow properties of the lactose carriers used in routine DPI manufacturing is recommended.

The results of this chapter indicated that drug-fines agglomerate formation is likely to play a major role in determining DPI performance. The SEM images of the carrier blends indicated that agglomerate formation took place once a high enough fines concentration was available. Unfortunately the bulk powder characterisation techniques available are not able to investigate the micro-structure of agglomerate formation. However, significant improvements in the DPI performance for the different formulation series coincided with the concentration where agglomerate formation was visible in the SEM images. The agglomerate formation theory is further supported by the fact that for LH210, for which no agglomerate formation was seen in the SEM images, the DPI performance did not significantly improve over a range of concentrations of the milled fines.

One of the objectives of the current study was to find parameters that would enable quality-by-design approach for DPI manufacturing. Various different parameters describing properties of the lactose pre-blends were characterised with the aim of finding a parameter that could be used as a tool for accepting or rejecting excipient batches for DPI product manufacturing. However, none of the parameters characterised during the current study were able to predict the performance of DPI formulations uniformly, when such a large and variable set of carriers was used. In the next chapter, multivariate

statistical analysis tools and artificial neural networks are used for establishing a more complete understanding of the lactose characteristics that govern the DPI performance.

CHAPTER 5   STATISTICAL METHODS AND ARTIFICIAL NEURAL NETWORKS AS TOOLS FOR UNDERSTANDING THE MECHANISMS GOVERNING DRY POWDER INHALER PERFORMANCE

5.1   INTRODUCTION

Establishing a structure-function relationship that would allow predicting the formulation performance for DPI formulations on the basis of the properties of the formulation components has proved to be a challenging task. This is most likely due to the batch process nature of the manufacturing operations of the drug, the excipients and the formulations themselves (de Boer *et al.* 2012). A small change in one of the raw materials or the process parameters during the manufacturing process of the materials or the formulation can dramatically change the performance attributes of the final product (de Boer *et al.* 2012). However, despite the incomplete understanding of the mechanisms governing the DPI performance, the physical and physicochemical properties of the drug and the excipient are extensively characterised prior to the formulation process to pinpoint raw materials that may possibly lead to a rejected final product.

There are a number of different lactose characteristics that have been shown to correspond to the final DPI product performance. These properties include, for example, surface energy of the lactose measured by inverse gas chromatography (Tong *et al.* 2006), the specific surface area of the carrier (Kawashima *et al.* 1998), the fine particle content of the carrier (Islam *et al.* 2004; Louey *et al.* 2003) and the energy required to fluidise the carrier (Pitchayajittipong *et al.* 2010). These studies proposed, based on relatively small datasets, that there exists a relationship between a single parameter describing the lactose properties and the DPI performance. However, the data presented in Chapter 4 of the current thesis indicated that the relationships between the lactose properties and the DPI performance do not necessarily follow simple linear correlations when a diverse range of lactose carriers and fines are used in the formulations.

Another potential reason for the lack of a structure-function relationship describing the DPI performance is the limited understanding of the mechanisms governing the drug detachment, deagglomeration and fine particle delivery from these formulations. The current study aims to address the gap in this knowledge from the point of view of the lactose carrier. To illustrate the fundamental problem formulators are facing when trying to link the lactose carrier properties to the formulation performance, the manufacturing process of the lactose carrier blends should be considered. When the lactose grades for

181

DPI formulations are manufactured by the means of air classification, blending, milling or sieving (Guenette *et al.* 2009), the control over the physical and physicochemical properties of the resulting carrier blend is very limited. Other physical and physicochemical properties of the lactose blends also change upon the increasing lactose fines concentration (Guenette *et al.* 2009). Due to the covariant nature of the different parameters, finding a single parameter describing the lactose carrier that could be used for predicting the DPI performance by using linear correlations is very unlikely. Instead, efforts need to be concentrated on understanding more complex relationships relating to the lactose carrier that govern the DPI performance.

Podczeck (1998) was an early researcher who recognised the need for more complex statistical analysis methods for understanding the structure-function relationship in DPI formulations. This was followed by the studies of Zeng *et al.* (2000a), who established a two parameter model for the fine particle delivery from DPI formulations based on parameters describing shape of the carrier particles. In both these studies, multiple linear regression (MLR) was used for establishing the relationship between the lactose properties and the DPI formulation performance. MLR is an extension of linear correlation, where the relationship between the response and various factors is determined simultaneously (Rajalahti *et al.* 2011). The method is based on the assumptions that the underlying relationships are linear and that the input parameters are not co-linear. However, as pointed out by Rajalahti *et al.* (2011), controlling the input variables so that co-linearity would be avoided is difficult unless experimental design is applied. Therefore, due to the lack of control in the resulting physical properties upon the preparation of the carriers for inhalation as discussed above, the method is unlikely to be suitable for analysing structure-function relationships in DPI formulations.

Partial least squares (PLS) regression analysis was developed for analysing biased data and therefore the method is applicable for cases where the factors are highly correlated (Rajalahti *et al.* 2011). As discussed above, this is the case for the parameters describing the carriers used in DPI formulations. The PLS method is based on reducing the input parameters to a set of uncorrelated components. These components describe the underlying structure of the dataset (Rajalahti *et al.* 2011). PLS analysis reports the importance of the different parameters within the components in the form of standardised coefficients (Rantanen *et al.* 2004). These coefficients give information on the relative importance of the different variables within the model, and have been used, for example, to gain an understanding of the mechanisms governing granulation processes (Rantanen *et al.* 2004).

Computers are superior to the human brain in numerical computation and symbol manipulation. However, the human brains' capability of learning, adapting and tolerating faulty or noisy data is not incorporated in a modern computer (Jain *et al.* 1996). Artificial neural networks (ANNs) are computational tools that aim to combine the superior properties of both computers and the human brain (Jain *et al.* 1996). The concept of artificial neural networks is loosely based on what is known of the operation of biological nerve cells and how they connect to form the nervous system (Basheer *et al.* 2000). A schematic presentation of a biological neuron is shown in Figure 5.1. According to Basheer *et al.* (2000), the information is mediated in a nerve cell by electrical impulses that are brought to the cell body by the dendrites. The nucleus located in the cell body determines whether the signal received from the dendrites is strong enough to be forwarded along the axon. When the signal reaches the synapse in the end of an all axon, neurotransmitters are emitted. These substances diffuse across the synaptic gap and are received by the dendrites in the adjacent neurons, causing a synaptic response. The response is not linear as a function of the neurotransmitter concentration, but all or nothing response based on exceeding a threshold concentration of neurotransmitters. The response can also either be inhibitory or exhibitory (Basheer *et al.* 2000). The simplest neural network, called the perceptron, is analogous to a biological neuron (Jain *et al.* 1996). The structure of a perceptron is illustrated in the schematic shown in Figure 5.2. In a perceptron, the nodes represent the dendrites and axons. The connection weights (w) are the synapses. The activation function (Σ) corresponds to the cell body by adding up the connection weights. The threshold function f(Σ) mimics the nucleus by determining whether the intensity of the signal received is strong enough to initiate output (Agatonovic-Kustrin *et al.* 2000; Basheer *et al.* 2000; Jain *et al.* 1996). These basic units of artificial intelligence can be combined to form extensive networks. Feed forward networks are the most commonly used ANNs (Svozil *et al.* 1997). A schematic of a three layer feed forward network is shown in Figure 5.3. Any feed forward ANN consists of an input layer, at least one hidden layer and an output layer. In a feed forward network, each neuron in a certain layer is connected with all the neurons in the adjacent layers. No connections between neurons within a layer are allowed (Svozil *et al.* 1997).
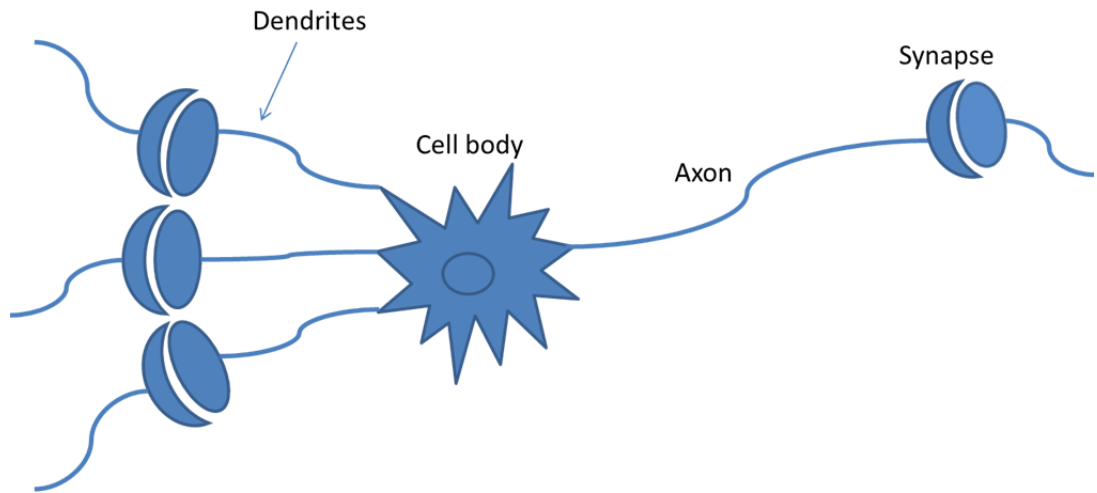
FIGURE 5.1 SCHEMATIC PRESENTATION OF A BIOLOGICAL NEURON
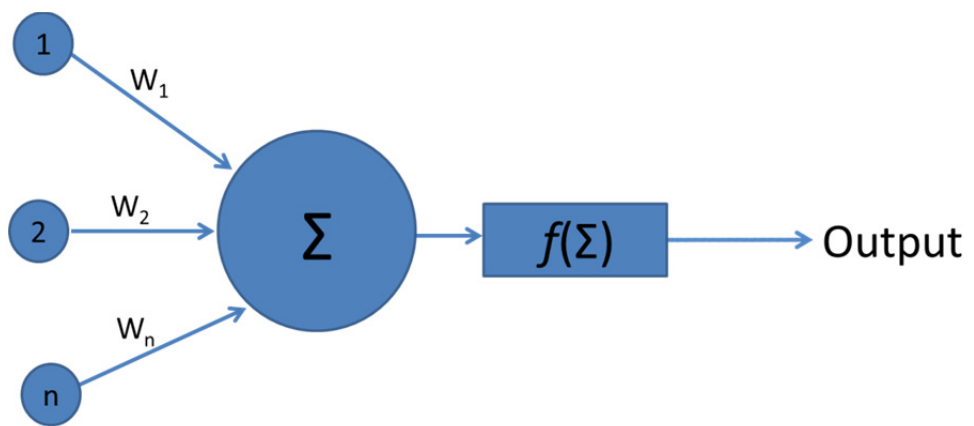
FIGURE 5.2 SCHEMATIC PRESENTATION OF A PERCEPTRON WITH INPUTS (1, 2, ..n) AND THE CONNECTIONS (W$_1$, W$_2$, W$_n$) FROM THE INPUTS TO THE NEURON IN THE HIDDEN LAYER WHERE THE SUM OF THE CONNECTION WEIGHTS (Σ) IS CALCULATED AND PASSED TO THE THRESHOLD FUNCTION f(Σ) TO DETERMINE WHETHER OUTPUT IS CALCULATED
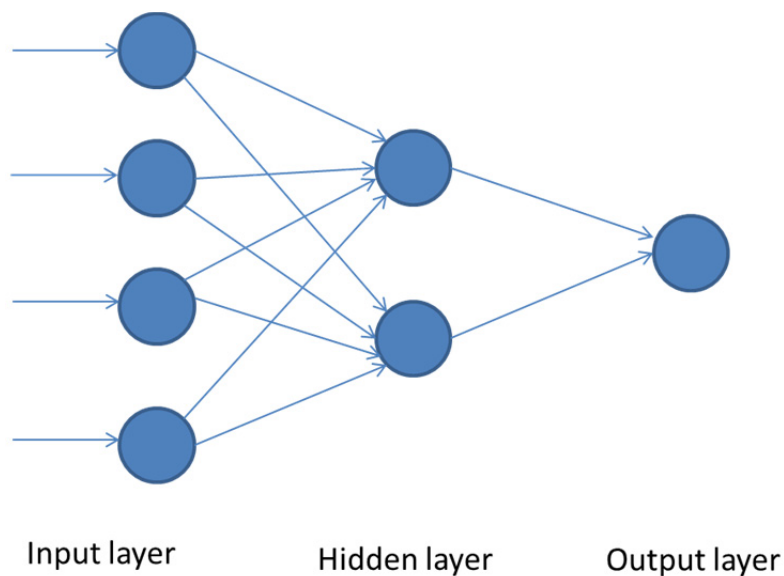
FIGURE 5.3 SCHEMATIC PRESENTATION OF A FEED FORWARD NETWORK CONSISTING OF INPUT, HIDDEN AND OUTPUT LAYERS

Modelling data using ANNs is based on presenting the data to the network and training the network to recognise the underlying trends in the dataset (Jain *et al.* 1996). The training can either be supervised or unsupervised (Jain *et al.* 1996; Svozil *et al.* 1997). In unsupervised learning, data patterns, instead of the output data, are presented to the network. The network is expected to learn data based on data patterns presented to it (Svozil *et al.* 1997). In supervised learning, output data is presented to the network and the weights between the connections are adjusted so that the desired output is reached (Svozil *et al.* 1997). Various network training algorithms are available for learning the underlying data (Jain *et al.* 1996). A brief introduction to supervised learning using feed forward networks and backpropagation learning algorithms is discussed below.

Before data is presented to the network, input and output values are normalised so that all the inputs have equal ranges. This is done to avoid any parameters with larger values from dominating the input and output values and consequentially saturating the hidden nodes (Basheer *et al.* 2000). To train the network, the dataset is divided into training, validation and test subsets (Basheer *et al.* 2000). In backpropagation training, the connection weights are adjusted and the signal is sent towards the output layer of the network. The errors between the actual and predicted output are then computed and the connection weights are adjusted based on the backward feedback on the network error (Basheer *et al.* 2000). The process of network training using the backpropagation training algorithm is illustrated in detail in the schematic shown in Figure 5.4. At first, the connection weights are randomly initialised and the sum of the connection weights (Σ) then computed. If the sum of the connection weights does not exceed the transfer function f(Σ), the weights are re-adjusted and the cycle is restarted (Agatonovic-Kustrin *et al.* 2000). However, if the sum of the connection weights is larger than the transfer function, the data is passed onward to compute the error between the target and the computed output (Agatonovic-Kustrin *et al.* 2000). Computing the network error is often done by the sum of squares method (Basheer *et al.* 2000). The decrease in the network error for training and test sets during the training cycles is monitored as illustrated in Figure 5.5. The network error initially decreases rapidly for both the sets as training cycles are performed. This is because the network is learning the underlying patterns in the dataset. However, the decrease in the error slows down for the training set as the number of training cycles is increased. This is because the network may start memorising or over-fitting the data when the number of training cycles is high enough (Basheer *et al.* 2000). The optimum network is achieved when the error for the test set reaches a minimum (Basheer *et al.* 2000), as illustrated in Figure 5.5. The connection weights are adjusted by an amount defined by the learning rate (η) until the optimum network is identified and then retrieved (Basheer *et al.* 2000). Another critical parameter for network training is the

momentum (μ), which prevents the network error from getting stuck in a local minimum during the training cycles (Basheer *et al.* 2000).

Once the network has been trained, the generalisation capacity of the network can be verified by inspecting the measured output against the output predicted by the network as illustrated in Figure 5.6. A network that is capable of generalising data does not exhibit fluctuations over the range of measured output values in a way that an over trained network would (Basheer *et al.* 2000). The likelihood of network overtraining can be reduced by reducing the number of hidden nodes in the network (Basheer *et al.* 2000). As the number of hidden nodes in a neural network is often based on trial and error, these data are useful in determining whether the optimum number of hidden nodes is applied in the network design (Basheer *et al.* 2000).
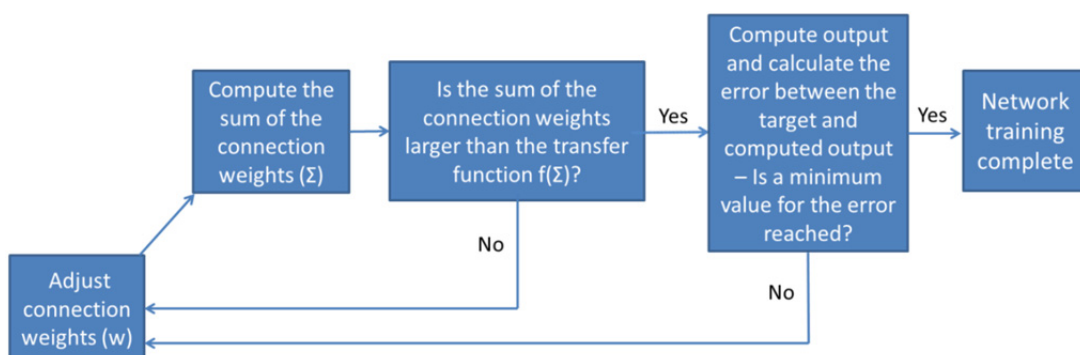
FIGURE 5.4 THE PROCESS OF TRAINING A FEED FORWARD BACKPROPAGATION NEURAL NETWORK
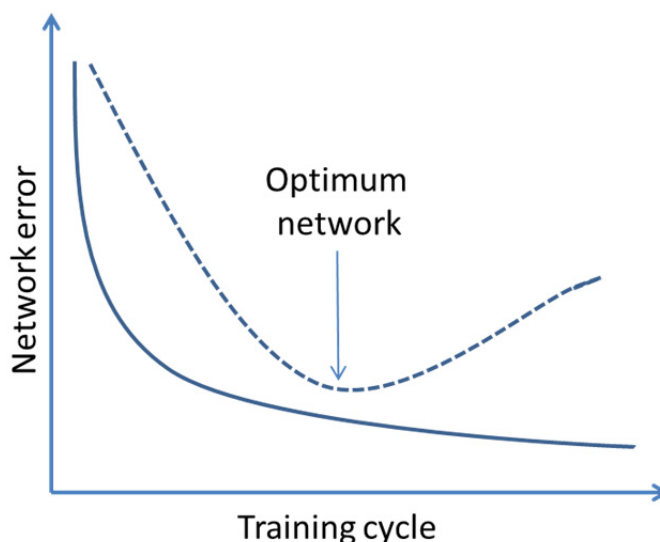
FIGURE 5.5 THE REDUCTION OF ERROR DURING NETWORK TRAINING FOR THE TRAINING SET (SOLID CURVE) AND FOR THE TEST SET (DOTTED CURVE). THE OPTIMUM NETWORK HAS BEEN REACHED WHEN THE ERROR FOR THE TEST SET STARTS INCREASING
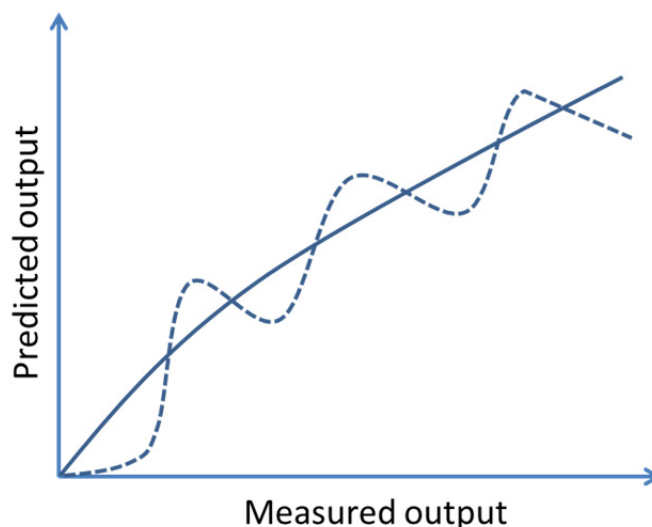
ANNs are a popular data analysis tool in pharmaceutical applications. Studies where ANNs have been used include, for example, relating the flow properties of excipients to the micromeritic properties of the materials (Kachrimanis *et al.* 2003), modelling drug dissolution (Mendyk *et al.* 2005), optimising formulations for controlled release tablets (Barmpalexis *et al.* 2011) and transdermal drug delivery products (Takayama *et al.* 1999) However, to date, the application of neural network analysis in inhalation-related research problems has been limited. To the author's best knowledge, the only investigators who have applied ANNs for inhalation research is De Matas *et al.*, who used ANNs for modelling *in vivo - in vitro* correlations for inhalation formulations (2008), and the clinical effect of inhaled bronchodilators (2010).

The aim of the current study was to establish functional relationships between different lactose properties and DPI performance. This was done by using different statistical methods and artificial neural network analysis in parallel for determining the most important lactose characteristics in governing the DPI performance. The functional relationships were not only established between the lactose properties and the performance in terms of fine particle delivery, but also in terms of drug de-agglomeration and detachment from the large carrier crystals. In addition to establishing a universal correlation between lactose properties and the formulation performance, the results of the current study were used for building an understanding of the mechanisms for how lactose fines govern the DPI performance.

5.2 MATERIALS AND METHODS

Three different coarse lactose carriers and four different fine particle lactose products were used in the study. Two of the coarse carriers were Lactohale (LH) products, namely LH100 (Sieved coarse grade) and LH206 (Lightly milled coarse grade). The third coarse carrier was SV010 (Sieved coarse grade). Three of the fine particle lactose fractions were also Lactohale grades, namely LH300 (micronised fines), LH230 (finer milled fines) and LH210 (coarser milled fines). All the Lactohale products were donated by DFE Pharma (Borculo, Netherlands). The fourth fine particle lactose grade used was Sorbolac 400 from Meggle (Germany).

Carrier lactose pre-blends were prepared by blending the different fine fractions of lactose with the coarse carriers at 2.5, 5, 10 and 20 wt-% concentrations according to Table 5.1. The mixing procedure was as described in Chapter 4 of the thesis. Similarly, the particle size distributions and flow and fluidisation properties of the prepared lactose pre-blends were characterised as described in Chapter 4. The only parameter describing powder flow that was not introduced in Chapter 4 and is used in the current study is the specific energy (SE). This parameter is based on the force and torque measured on the Freeman Technology FT4 powder rheometer during upward blade motion. The specific energy (SE) value describes the flow properties of the powders in a stress free state at near zero consolidation due to the lack of the downward pressing force of the blade (Freeman 2007).

The preparation of the budesonide DPI formulations and assessment of *in vitro* performance were performed as described in Chapter 4. However, the DPI device used for aerosolising the formulations was Cyclohaler (Teva Pharmaceuticals, Netherlands). The flow rate used for aerosolising the formulation was 90 l/min with a duration of 2.7 seconds.

Linear correlations between the physical properties of the lactose carriers and the DPI performance of the formulations were established using the Minitab version 15 statistical analysis package (Minitab Ltd, Coventry, UK). Partial least squares (PLS) analysis was also performed using the Minitab version 15 statistical analysis package (Minitab Ltd, Coventry, UK). No cross validation was used and the number of components was specified at 10.

The artificial neural network analysis of the data was performed using Alyuda Neurointelligence software (Alyuda Neurointelligence, California, USA). The input data

were pre-processed using the pre-processing function of the software so that the range of input values were within the range of [-1…1] and output values within the range of [0…1]. The dataset was partitioned into training, test and validation sets so that 27 records (70%) were in the training set and 6 in the validation and test sets each (15% each). A batch back-propagation training algorithm was used for the network training. The network architecture was selected manually as 12-4-1 for fine particle fraction of emitted dose and 12-5-1 for mean mass aerodynamic diameter and pre-separator deposition. The selection of the network architecture was made based on achieving a network with the optimum generalisation capacity (see Figure 5.6). The logistic transfer function (Benitez *et al.* 1997) and sum of squares error function (Aitkin *et al.* 2003) were used for determining the firing intensity of a neuron and the error between the actual and predicted output, respectively. For all the networks, a momentum of 0.9 was used. The learning rate was set to 0.1 for the ANN modelling of the fine particle fraction of the emitted dose and pre-separator deposition, and 0.25 for the ANN modelling of the mean mass aerodynamic diameter. In all cases, network training was stopped by error change when the mean square error of the network or the dataset error over 10 training cycles changed by less than 0.0000001.

TABLE 5.1 SUMMARY OF THE COARSE AND FINE LACTOSE COMPONENTS USED FOR PREPARING THE CARRIER PRE-BLENDS USED IN THE CURRENT STUDY AND THE PROCESS HISTORY AND THE CONCENTRATIONS OF THE FINES PRESENT IN THE DIFFERENT PRE-BLENDS

Carrier ID	Coarse fraction	Type of Fines	Fines	Wt-% fines
1	LH100	-	-	0
2	LH100	Micronised	LH300	2.5
3	LH100	Micronised	LH300	5
4	LH100	Micronised	LH300	10
5	LH100	Micronised	LH300	20
6	LH100	Milled	LH230	2.5
7	LH100	Milled	LH230	5
8	LH100	Milled	LH230	10
9	LH100	Milled	LH230	20
10	LH100	Milled	LH210	2.5
11	LH100	Milled	LH210	5
12	LH100	Milled	LH210	10
13	LH100	Milled	LH210	20
14	LH100	Milled	Sorbolac 400	2.5
15	LH100	Milled	Sorbolac 400	5
16	LH100	Milled	Sorbolac 400	10
17	LH100	Milled	Sorbolac 400	20
18	LH206	-	-	0
19	LH206	Micronised	LH300	2.5
20	LH206	Micronised	LH300	5
21	LH206	Micronised	LH300	10
22	LH206	Micronised	LH300	20
23	LH206	Milled	LH230	2.5
24	LH206	Milled	LH230	5
25	LH206	Milled	LH230	10
26	LH206	Milled	LH230	20
27	LH206	Milled	LH210	2.5
28	LH206	Milled	LH210	5
29	LH206	Milled	LH210	10
30	LH206	Milled	LH210	20
31	SV010	-	-	0
32	SV010	Micronised	LH300	2.5
33	SV010	Micronised	LH300	5
34	SV010	Micronised	LH300	10
35	SV010	Micronised	LH300	20
36	SV010	Milled	LH210	2.5
37	SV010	Milled	LH210	5
38	SV010	Milled	LH210	10
39	SV010	Milled	LH210	20

5.3 RESULTS AND DISCUSSION

5.3.1 Characterisation of the physical properties of the carriers

The particle size distributions of the pre-blends are summarised in Table 5.2. The table demonstrates that the proportion of fines below 4.5 µm ranged from 1.3% for blend #1 to approximately 23% for blend #5. The three blends with the highest proportion of fines below 4.5 µm were the blends #5, #22 and #35. The proportion of fines below 4.5 µm for these carriers was between 22 and 23%. All these carriers were prepared with 20 wt-% of the micronised fines LH300. Table 5.2 also shows that the range of values measured for the proportion of particles finer than 15 µm ranged approximately from 2.5 to 40% and approximately from 3.8 to 43% for the proportion of particles finer than 30 µm. The similarity of the ranges for these two parameters indicated that the majority of the particles added to the carriers upon the addition of fines were finer than 15 µm. The values of d10 of the carrier blends varied between 1.7 and 50 µm.

The bulk, flow and fluidisation properties of the carrier blends are summarised in Table 5.3. The bulk densities of the pre-blends spanned from 0.560 (Blend #9) to 0.747 g/ml (Blend #1) and tapped densities from 0.845 (Blend #31) to 0.893 g/ml (Blend #17). The values of Hausner ratio for the pre-blends varied between 1.135 (Blend #18) and 1.537 (Blend #26). The factor linking these observations was that the carriers with the highest bulk density and lowest tapped density and Hausner ratio did not contain any added fines. On the other hand, the blends with the lowest bulk density and highest tapped density and Hausner ratio were prepared with 20 wt-% LH230 or Sorbolac 400.

Table 5.3 shows that the values of BFE_{Norm} for the carrier blends varied between 9.55 (Blend #34) and 26.03 mJ/g (Blend #31). The DFI for blend #31 was the largest at 51 whereas the lowest DFI of 4.96 was recorded for blend #22. The values of FRI ranged between 1.02 for blend #1 and 2.41 for blend #35. Blend #1 also had the lowest FE_{Norm} of 0.7 mJ/g. Blends #9 and #21 had the highest FE_{Norm} of 1.93. Blends #1 and 31, which were the least cohesive according to the parameters discussed above, contained no added fines. Blends #34, #22, #35, #9 and #21 on the other hand were characterised as the most cohesive according to these parameters. All of these blends contained at least 10 wt-% of added fines. Specific energy (SE) was included in the study due to a clear increasing trend upon the addition of fines when SV010 was used as the coarse fraction (Blends #31 to #39). The values of SE for the carriers in the current study ranged from 5.58 mJ/g for Blend #18 to 6.59 mJ/g for Blend #24.

TABLE 5.2 SUMMARY OF PARTICLE SIZE OF THE CARRIER PRE-BLENDS IN TERMS PROPORTION OF FINES BELOW 4.5, 15 AND 30 μM AND THE 10TH PERCENTILE OF DENSITY DISTRIBUTION (d10). THE VALUES SHOWN ARE AVERAGES FROM FIVE REPEATED MEASUREMENTS.

Carrier ID	<4.5 μm (%)	<15 μm (%)	<30 μm (%)	d10 (μm)
1	1.29	3.02	6.24	44.30
2	4.88	8.25	11.48	23.44
3	9.34	13.94	17.03	5.22
4	17.43	24.52	26.97	2.08
5	23.04	40.24	42.75	1.73
6	2.76	6.70	10.95	26.41
7	4.32	10.15	15.13	14.70
8	7.23	16.78	23.23	7.33
9	12.47	28.93	38.15	3.26
10	1.98	5.14	9.56	31.53
11	2.62	6.78	12.27	23.63
12	4.08	10.44	17.89	14.25
13	6.02	15.91	26.79	8.72
14	2.37	6.23	10.05	29.77
15	3.32	9.20	13.81	17.01
16	5.88	15.60	21.72	8.68
17	10.20	27.62	36.70	4.39
18	2.44	2.54	3.81	49.78
19	6.13	8.11	9.27	34.3
20	10.42	13.76	14.80	4.11
21	18.16	24.42	25.24	1.95
22	22.43	39.53	40.60	1.8
23	3.69	6.49	8.69	36.76
24	5.29	9.99	13.01	15.08
25	8.04	16.30	20.79	6.74
26	12.40	27.77	35.18	3.28
27	3.45	5.50	7.91	38.48
28	3.66	6.74	10.21	29.09
29	5.05	10.51	16.23	13.97
30	7.01	16.79	26.57	7.67
31	1.55	3.03	5.19	49.61
32	3.17	6.23	8.07	40.48
33	6.51	11.75	13.57	9.18
34	12.08	21.08	22.61	3.49
35	22.47	38.05	39.33	1.74
36	2.01	4.41	7.46	40.97
37	2.57	6.03	10.16	29.42
38	3.63	9.29	15.53	16.54
39	6.53	16.38	26.27	8.13

Carrier ID	Bulk density (g/ml)	Tapped density (g/ml)	Hausner ratio	BFE$_{Norm}$ (mJ/g)	DFI	FRI	FE$_{Norm}$ (mJ/g)	SE (mJ/g)
1	0.747	0.855	1.159	25.12	37.37	1.02	0.70	6.02
2	0.727	0.854	1.224	22.06	27.90	1.10	0.84	5.84
3	0.699	0.847	1.250	20.34	16.61	1.19	1.23	6.06
4	0.667	0.860	1.380	15.68	10.87	1.52	1.44	6.25
5	0.681	0.869	1.464	9.93	5.69	2.41	1.75	6.27
6	0.709	0.865	1.216	21.65	24.07	1.06	0.95	6.14
7	0.676	0.866	1.252	19.37	18.49	1.09	1.12	6.12
8	0.645	0.880	1.358	16.07	10.74	1.29	1.54	6.10
9	0.560	0.867	1.474	10.52	6.15	1.81	1.93	5.66
10	0.731	0.863	1.183	23.48	31.39	1.03	0.78	5.96
11	0.711	0.872	1.221	21.11	21.14	1.06	1.00	6.00
12	0.699	0.881	1.264	19.54	19.56	1.14	1.04	6.08
13	0.621	0.882	1.369	13.24	9.21	1.41	1.60	5.85
14	0.703	0.859	1.223	21.26	24.92	1.08	1.01	5.87
15	0.695	0.871	1.254	20.23	18.91	1.13	1.17	6.13
16	0.669	0.883	1.319	16.95	13.68	1.25	1.33	6.26
17	0.625	0.893	1.428	11.81	8.52	1.88	1.44	6.26
18	0.744	0.861	1.135	22.67	30.23	1.08	0.82	5.58
19	0.708	0.854	1.206	19.85	17.55	1.10	1.14	5.94
20	0.668	0.857	1.284	17.60	11.74	1.16	1.53	6.09
21	0.613	0.856	1.396	15.65	8.02	1.42	1.93	6.29
22	0.604	0.875	1.449	9.96	4.96	2.27	1.88	6.21
23	0.725	0.881	1.214	21.00	23.78	1.08	0.93	6.20
24	0.692	0.874	1.264	19.71	15.90	1.09	1.41	6.59
25	0.663	0.877	1.324	15.75	10.55	1.27	1.56	6.29
26	0.575	0.883	1.537	11.48	6.06	1.66	1.89	5.96
27	0.733	0.869	1.186	21.47	28.66	1.05	0.81	5.68
28	0.720	0.873	1.212	19.68	21.50	1.09	1.00	5.70
29	0.683	0.879	1.288	17.36	15.27	1.15	1.22	5.99
30	0.635	0.885	1.395	13.34	9.70	1.39	1.49	6.01
31	0.729	0.845	1.158	26.03	51.02	1.11	0.57	5.74
32	0.729	0.858	1.177	23.60	41.61	1.10	0.57	5.72
33	0.703	0.849	1.209	20.74	17.52	1.15	1.14	5.99
34	0.636	0.855	1.344	9.55	9.55	1.32	1.91	6.17
35	0.599	0.861	1.438	10.18	6.39	2.45	1.57	6.19
36	0.741	0.858	1.158	25.79	34.31	1.09	0.80	5.80
37	0.725	0.865	1.193	22.83	31.65	1.10	0.78	5.76
38	0.687	0.862	1.255	18.95	24.34	1.15	1.03	5.90
39	0.645	0.887	1.375	15.35	10.63	1.43	1.52	6.21

5.3.2 *In vitro* testing of the formulations

The *in vitro* performance of the formulations is summarised in Table 5.4 in terms of fine particle fraction of emitted dose (FPF$_{ED}$), mean mass aerodynamic diameter (MMAD) and the proportion of drug recovered from the pre-separator (PS of RD). The formulation performance ranged between an FPF$_{ED}$ of 20.8% (Blend #31) and 46.9% (Blend #4). The MMAD of the drug collected from the stages was between 2.58 (Blend #1) and 3.51 µm (Blend #17). The proportion of drug recovered from the pre-separator varied between 12.7% for Blend#5 and 42.9% for Blend #14. Blends #1and #31 contained no added fines. Blend #14 contained 2.5% of Sorbolac 400 resulting in a low proportion of fines (%<4.5 µm = 2.37) within the carrier blend as indicated by Table 5.2. These blends produced the lowest FPF$_{ED}$, smallest MMAD and the highest proportion of drug deposited in the pre-separator. Blends #4, #5 and #17 were at the other end of the spectrum. Blends #4 and #5 had high fine particle content with the proportion of particles finer than 4.5 µm 17.4 and 23%, respectively.

TABLE 5.4 SUMMARY OF *IN VITRO* PERFORMANCE OF THE FORMULATIONS PREPARED WITH THE LACTOSE PRE-BLENDS AS THE CARRIER IN TERMS OF FINE PARTICLE FRACTION OF EMITTED DOSE (FPF$_{ED}$), MEAN MASS AERODYNAMIC DIAMETER (MMAD) AND THE PROPORTION OF TOTAL RECOVERED BUDESONIDE THAT WAS DEPOSITED IN THE PRE-SEPARATOR (PS OF RD). THE RESULTS SHOWN ARE AVERAGES FROM THREE REPEATED IN VITRO ASSESSMENTS.

Carrier ID	FPF$_{ED}$ (%)	MMAD (μm)	PS of RD (%)
1	24.10	2.58	38.23
2	26.56	2.94	31.00
3	35.78	3.04	21.17
4	46.94	3.09	13.37
5	39.74	3.36	12.74
6	23.85	2.78	35.15
7	25.32	3.00	31.68
8	28.21	3.26	21.63
9	35.95	3.25	15.42
10	23.13	2.75	37.09
11	24.14	2.85	33.94
12	27.38	3.00	25.87
13	26.63	3.14	23.97
14	21.03	2.86	42.90
15	22.08	2.92	37.80
16	27.19	3.04	28.27
17	26.90	3.51	20.47
18	24.56	2.62	39.31
19	32.49	2.81	27.04
20	36.09	2.92	21.73
21	44.71	3.19	13.63
22	36.73	3.48	14.53
23	25.50	2.78	32.30
24	26.75	2.89	28.46
25	28.69	3.15	23.31
26	32.89	3.34	18.56
27	23.28	2.70	38.94
28	25.11	2.79	34.34
29	24.33	2.88	30.23
30	30.41	3.01	22.93
31	20.82	2.65	44.25
32	23.28	2.96	34.95
33	30.63	3.04	27.09
34	39.65	3.12	17.12
35	35.15	3.40	13.84
36	22.26	2.77	41.25
37	23.05	2.91	40.17
38	24.42	3.02	36.12
39	25.52	3.01	23.49

5.3.3 Statistical analysis of the dataset

5.3.3.1 *Linear correlations between the physical properties of the carrier and the in vitro performance of the formulations*

Linear correlations have been previously observed between different parameters describing the lactose properties and the DPI performance with smaller datasets (Islam *et al.* 2004; Louey *et al.* 2003; Tong *et al.* 2006). Therefore, the first step in the pursuit of developing a universal model for predicting DPI performance based on the carrier properties and for understanding the mechanisms governing the DPI performance was to conduct statistical analysis for linear correlations. If a good linear correlation could be obtained between the fine particle delivery, deagglomeration and detachment characteristics of the formulations and the properties of the carriers, the prediction and understanding of the DPI formulation performance would be straightforward. In addition, having a single parameter describing the structure-function relationship between the carrier properties and the formulation performance would provide a simple quality-by-design tool for excipient suppliers and pharmaceutical companies manufacturing inhalation products.

The results of the analysis are summarised in Table 5.5. These data indicate that for predicting the fine particle fraction of emitted dose, the percentage of fine particle lactose <4.5 μm in the carrier produced the best linear correlation with a value 0.861. These data are in good agreement with studies published by various investigators where the proportion of lactose fines within the carrier was shown to correlate with the DPI performance (Guenette *et al.* 2009; Islam *et al.* 2004; Louey *et al.* 2003). It is also notable that in the current study the R^2 value for the correlation between the particle size parameters decreased from 0.861 to 0.740 and 0.638 when the fine fractions were defined as %<4.5, %<15 and %<30 μm, respectively. These data are in agreement with a previous study where the finer fractions of lactose were seen to produce better correlations with the DPI performance than the larger size fractions (Adi *et al.* 2009).

One of the theories explaining the improved DPI performance upon the addition of lactose fines is based on the increased cohesive strength of the bulk powder (Shur *et al.* 2008a). In Chapter 4 of the thesis, the increased cohesion of the carrier blend or the formulation itself was shown to correspond to an increased DPI performance in some cases. Increasing FE_{Norm} and FRI and decreasing BFE_{Norm} are measured for powders as they become more cohesive (Freeman 2007). The Hausner ratio on the other hand increases upon increasing cohesive strength of the powder (Shah *et al.* 2008). Table 5.5 shows that the FPF_{ED} had positive correlations of 0.748, 0.649 and 0.578 against FE_{Norm}, Hausner

ratio and FRI, in that order. The relationship between the BFE_{Norm} and FPF_{ED} was characterised by a negative correlation of -0.664. These results for the linear relationship between the different powder flow parameters and FPF_{ED} demonstrate that the more cohesive the carrier blend, the higher the performance. However, because the R^2 values are relatively low, the linear models based on the flow and fluidisation properties are not capable of explaining the variation in the FPF_{ED} as well as the particle size parameters. Therefore, the correlation results between the FPF_{ED} and the different parameters describing the lactose carriers demonstrated that the presence of fine particle lactose was more essential for determining the DPI performance than the increase in the powder bulk cohesion induced by the addition of the fines.

Table 5.5 demonstrates that the linear correlation between the MMAD and the proportion of fines below 30 µm was the highest with an R^2 value of 0.924. A high R^2 value of 0.907 was also produced with the correlation between MMAD and the proportion of particles finer than 15 µm. These data indicate that the interaction of the drug with the larger fines is also an important factor to be taken into account in addition to the proportion of the finest particles when designing a powder formulation for inhalation. In fact, it has been previously suggested that the larger fines may act as secondary carriers (Adi *et al.* 2009). The results of the current data analysis support the hypothesis of the larger lactose fines acting as secondary carriers.

The strongest correlation between the physical properties of the lactose blends and the pre-separator deposition was achieved for FE_{Norm} with a R^2 value of -0.891. The parameters correlating the next best were %<15 µm and %<4.5 µm with values of -0.885 and -0.882, correspondingly. These data may indicate that the drug detachment from the surface of the larger carrier crystals is possibly regulated by the fluidisation properties of the carrier. However, also the proportion of fine particles within the carrier is an important parameter in determining the drug detachment from the surface of the large carrier. However, as shown in Chapter 4 of the thesis, the fluidisation energy of a carrier was somewhat related to the fine particle content below 30 µm. Therefore, it is impossible to conclude by means of linear regression whether the proportion of fines or the fluidisation properties is the most important factor in governing the pre-separator deposition.

TABLE 5.5 COEFFICIENT OF CORRELATION FOR LINEAR RELATIONSHIPS BETWEEN THE DIFFERENT DPI PERFORMANCE MEASURES AND THE PROPERTIES OF THE LACTOSE PRE-BLENDS USED AS THE CARRIERS IN THE FORMULATIONS. THE CORRELATIONS ARE BASED ON THE AVERAGE VALUES REPORTED IN TABLES 5.2, 5.3 AND 5.4.

	Correlation coefficient		
	FPF of ED	**MMAD**	**PS of RD**
<4.5 µm	0.861	0.793	-0.882
<15 µm	0.740	0.907	-0.885
<30 µm	0.638	0.924	-0.862
d10	-0.687	-0.839	0.867
Bulk density	-0.589	-0.839	0.805
Tapped density	-0.147	0.368	-0.226
Hausner ratio	0.649	0.889	-0.866
BFE$_{Norm}$	-0.664	-0.864	0.872
DFI	-0.673	-0.784	0.870
FRI	0.578	0.825	-0.741
FE$_{Norm}$	0.748	0.800	-0.891
SE	0.413	0.431	-0.533

5.3.3.2   Partial least squares analysis of the dataset

Partial least squares analysis was developed for statistical analysis of biased data (Rajalahti *et al.* 2011). The bias can for example be highly correlated input parameters (Rajalahti *et al.* 2011). This is often the case for the carriers used in DPI formulations, because the only controlled parameter during the manufacturing process is the proportion of fines. However, the other properties of the carriers, such as flow and fluidisation characteristics, are known to change upon the addition of fines (Chapter 4). Therefore, partial least squares analysis should be well suited for analysing the current dataset.

The x-variance and R^2 values describing the PLS models for the different DPI performance measures are summarised in Table 5.7. The x-variance parameter describes the extent to which the components of the PLS model fit the underlying variation in the input parameter values. It can be seen that the PLS models established have x-variance values higher than 0.99. This means that the components capture the variance in the input data well. The R^2 value in PLS models describes the linearity between the components and the response. The R^2 values for all the models are also listed in Table 5.7. The linearity of the models is high with R^2 values between 0.92 and 0.96.

The coefficients reported by the PLS analysis describe the importance and the sign of the different input parameters in defining the components of the model (Rantanen *et al.* 2004). If the factors in the model have different units, as is the case in the current study, the standardised coefficient should be used instead. The standardised coefficients describe

how many standard deviations an output variable will change when per standard deviation increase in a predictor variable. The standardised coefficients for the different parameters describing the lactose carriers from the PLS analysis of the DPI formulation performance are summarised in Table 5.7. The standardised coefficients for the PLS analysis of FPF_{ED} are plotted in Figure 5.4. The most important parameters in the model are FRI, %<30 µm and %<4.5 µm. The standardised coefficients for these parameters were -1.88, 1.85 and 1.57 respectively. These data indicate that the fine particle delivery from a DPI formulation is governed by a combination of the proportion of fines, the presence of larger fines and the cohesive properties of the carrier.

For MMAD, the PLS model highlighted the %<15 µm as the most important parameter by far, as illustrated in Figure 5.8. The value of the standardised coefficient for this parameter was 2.75 as shown in Table 5.6. These data are in good agreement with the results of the linear regression analysis, as discussed above, and supports the theory of the larger fines acting as secondary carriers (Adi *et al.* 2009).

Figure 5.8 shows that for the pre-separator deposition, the most important parameters in the PLS model were %<30 µm, FRI and %<4.5 µm. Table 5.7 lists the values of PLS standardised coefficient for these parameters as -1.54, 1.15 and -0.93. Interestingly, the standardised coefficients for these parameters are roughly of equal magnitude but of opposite sign compared to the PLS coefficients for FPF_{ED} (Table 5.7 and Figure 5.6). This is a reassuring result, because the drug attached to the surface of the large carrier crystals will be deposited in the pre-separator and therefore will not contribute to the fine particle fraction. In contrast, the drug that has detached from the surface of the large carrier will contribute to the FPF_{ED}. Therefore, the lactose properties regulating the pre-separator deposition and the FPF_{ED} should be the same, but of opposite direction.

	Input	FPF$_{ED}$	MMAD	PS of RD
	%<4.5	1.57	-0.73	-0.93
	%<15	-0.21	2.75	0.17
	%<30	1.85	-0.25	-1.54
	d10	0.62	-0.34	-0.29
	Bulk density	0.21	-0.35	0.04
PLS	Tapped density	-0.34	0.12	0.11
Standardised	Hausner ratio	-0.13	-0.47	0.32
coefficients	BFE$_{Norm}$	-0.22	0.15	0.23
	DFI	-0.35	0.03	0.31
	FRI	-1.88	-0.62	1.15
	FE$_{Norm}$	-0.20	-0.33	0.22
	SE	0.04	-0.07	-0.10
Model	X-variance	0.9974	0.9962	0.9973
parameters	R^2	0.9632	0.9254	0.9366
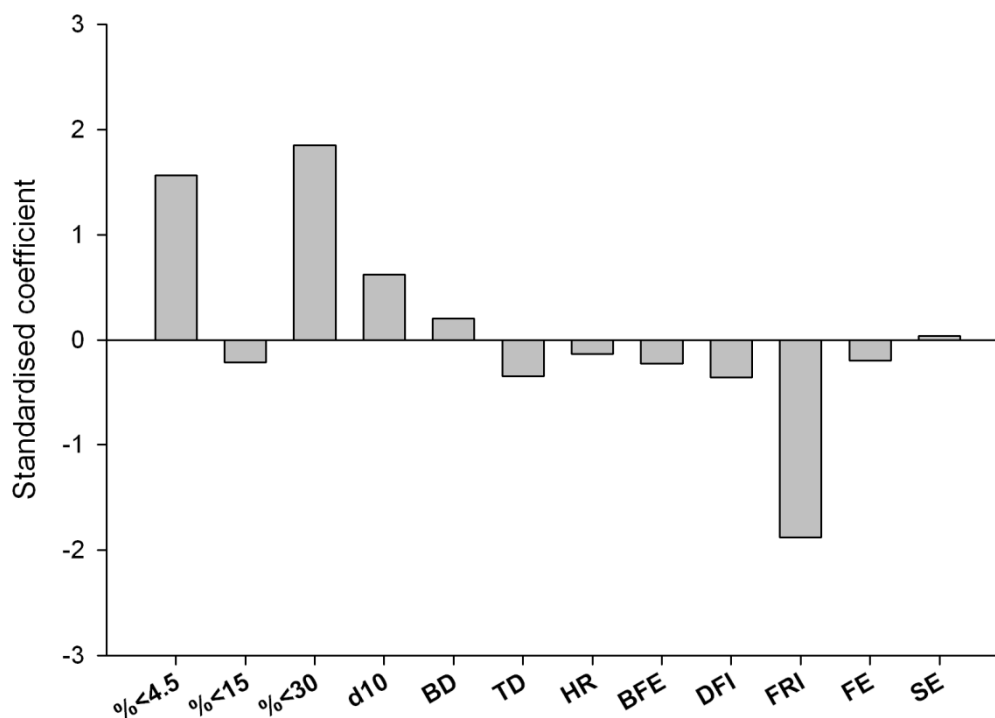
FIGURE 5.7 STANDARDISED COEFFICIENTS FOR THE DIFFERENT PARAMETERS FROM PARTIAL LEAST SQUARES ANALYSIS FOR FINE PARTICLE FRACTION OF EMITTED DOSE FOR BUDESONIDE
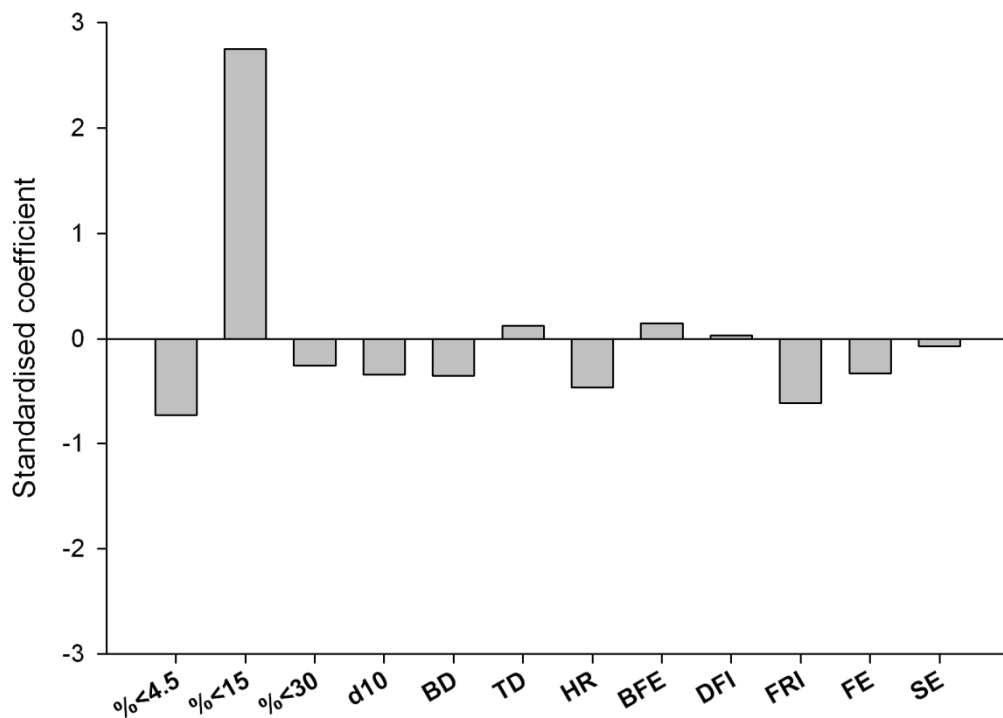
FIGURE 5.8 STANDARDISED COEFFICIENTS FOR THE DIFFERENT PARAMETERS FROM PARTIAL LEAST SQUARES ANALYSIS FOR MEAN MASS AERODYNAMIC DIAMETER OF BUDESONIDE
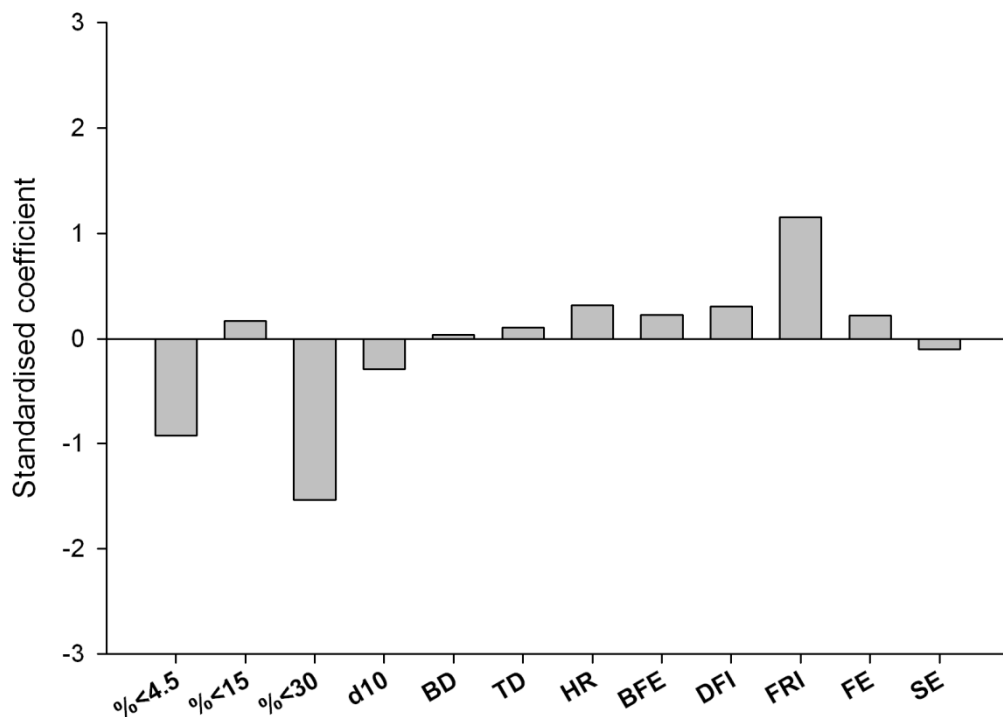
FIGURE 5.9 STANDARDISED COEFFICIENTS FOR THE DIFFERENT PARAMETERS FROM PARTIAL LEAST SQUARES ANALYSIS FOR PRE-SEPARATOR DEPOSITION OF BUDESONIDE

5.3.4　Artificial neural network analysis of the dataset

The training of the artificial neural network is of critical importance if a network with good generalisation capability is to be obtained (Basheer *et al.* 2000). Attention has to be paid so that the training data covers the range of outputs. This is because training the network is based on learning the underlying trends in data. Therefore, the network cannot perform well if it has to extrapolate data (Basheer *et al.* 2000). The measured output for the DPI performance indicators is plotted against the output predicted by the ANN in Figure 5.7. The figure shows that for all the output parameters studied here, the training set (black dots) was selected so that there is no need for extrapolating the outputs within the test (grey dots) or validation sets (circles). The graphs in Figure 5.7 also demonstrate that the networks were good at generalising data. This is because these data points are not scattered to a great extent, as discussed in the introduction of the Chapter.

Once trained, neural networks can be used for different purposes, such as forecasting, pattern classification and optimisation (Jain *et al.* 1996). In the current study, the networks were applied as a tool for understanding the mechanisms for how lactose fines govern the DPI performance. This was done by inspecting the relative importance of the different input parameters in the trained network. The importance of each of the parameters measured for the lactose carriers, in essence the weight of the connections for the parameter in the trained network, for predicting the different DPI performance attributes are summarised in Table 5.8. The relative importance of the different input parameters in the network modelling FPF_{ED} is illustrated in Figure 5.10. The proportion of fines below 4.5 µm was the most important parameter with approximately 57% connection weights deriving from this parameter. This is in an agreement with the results obtained by the statistical methods as discussed earlier in the Chapter. The proportion of fines is followed by FRI with considerably lower importance of approximately 13.6%. This result is different from the PLS model, that indicated that the proportion of fines and the FRI were equally important in determining the FPF_{ED}. As discussed in Chapter 4, FRI was not a sensitive measure for free flowing powders but was able to distinguish between cohesive powders. If the values of FRI (Table 5.3) are plotted against the %<30 µm (Table 5.2), these data points follow a single curve (graph not shown). Therefore, the possible reason for the lower significance of the FRI in the ANN model than in the PLS model is that the ANN is able to mimic the non-linearity in the data, whereas the PLS model tries to fit a linear model to data, thus resulting in a biased result (Rajalahti *et al.* 2011).
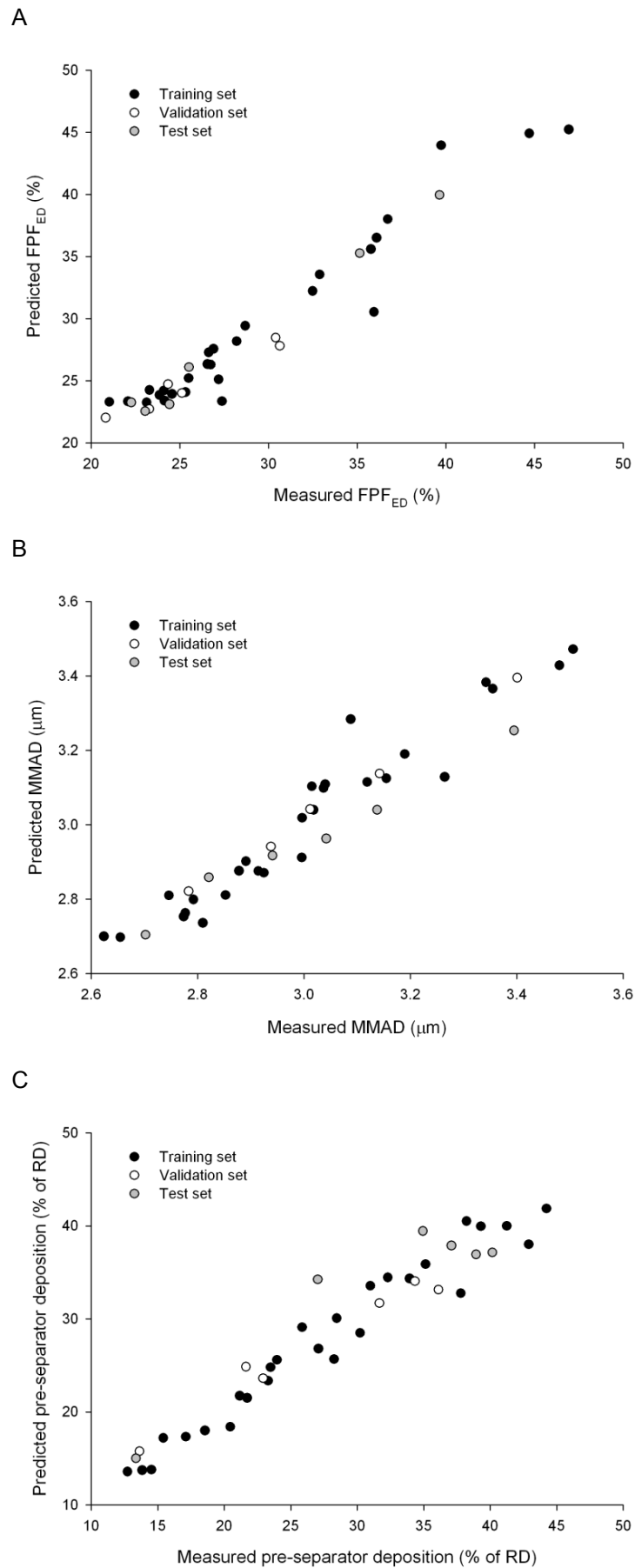
FIGURE 5.10 MEASURED VS. PREDICTED OUTPUT FOR A) FINE PARTICLE FRACTION OF EMITTED DOSE B) MEAN MASS AERODYNAMIC DIAMETER AND C) PRE-SEPARATOR DEPOSITION FOR THE DATA POINTS USED IN TRAINING (BLACK DOTS), VALIDATION (CIRCLES) AND TEST SETS (GREY DOTS)

In the network modelling the MMAD of the drug aerosolised from different formulations, the proportion of fines below 15 μm was by far the most important parameter with 76% of the connection weights in the network deriving from this parameter. This is shown in Table 5.8 and illustrated in Figure 5.11. These data indicate that although the proportion of fines <4.5 μm was the most important parameter in determining the DPI performance as defined by FPF$_{ED}$, the larger fines play a role in determining the extent of deagglomeration of the drug. Once again, this result is in agreement with the statistical analysis methods as discussed earlier in the Chapter.

Table 5.8 and Figure 5.12 demonstrate that in the network describing the drug deposition in the pre-separator, the proportion of particles finer than 4.5 μm was the most important parameter at 46% connection weight. The second most important parameter was the d10 with an importance of 19%. These data indicate it is not only the proportion of fine particle lactose that defines the pre-separator deposition, but also the size of the fines. This finding is in an agreement with the theory according to which the larger fines act as secondary carriers within DPI formulations (Adi *et al.* 2009)

Looking at the importance of the different parameters characterised for the lactose carriers as listed in Table 5.8, specific energy has a very low connection weights of less than 1% in all the models. Similarly, tapped density and Hausner ratio have low importance of less than 5% in all the networks relating to DPI performance attributes. Therefore, these properties of the lactose carriers may not have significant relevance in determining DPI performance.

TABLE 5.7 THE CONNECTION WEIGHTS FOR THE DIFFERENT INPUTS PARAMETERS IN THE NEURAL NETWORKS DESCRIBING DPI PERFORMANCE. THE NETWORKS WERE BASED ON THE AVERAGE VALUES REPORTED IN TABLES 5.2, 5.3 AND 5.4.

	Connection weights (%)		
	FPF$_{ED}$	MMAD	PS of RD
%<4.5	56.94	2.50	45.76
%<15	0.09	75.56	1.05
%<30	1.24	0.45	5.27
d10	3.64	4.82	19.17
BFE$_{Norm}$	0.57	0.08	9.05
Bulk density	6.78	1.99	7.78
Tapped density	3.75	1.56	3.45
Hausner ratio	4.91	4.45	0.43
DFI	7.90	0.37	4.21
FE$_{Norm}$	0.13	7.15	2.88
FRI	13.65	0.18	0.03
SE	0.41	0.88	0.92
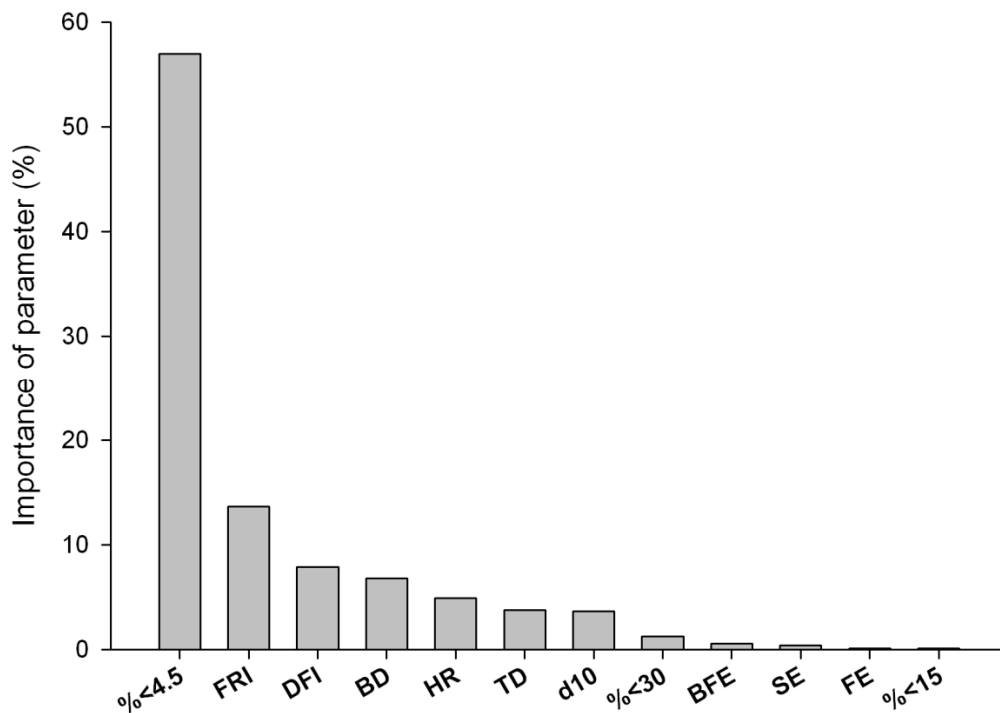
FIGURE 5.11 THE RELATIVE IMPORTANCE OF THE DIFFERENT INPUT PARAMETERS IN THE NEURAL NETWORK MODELLING FINE PARTICLE FRACTION OF EMITTED DOSE OF BUDESONIDE
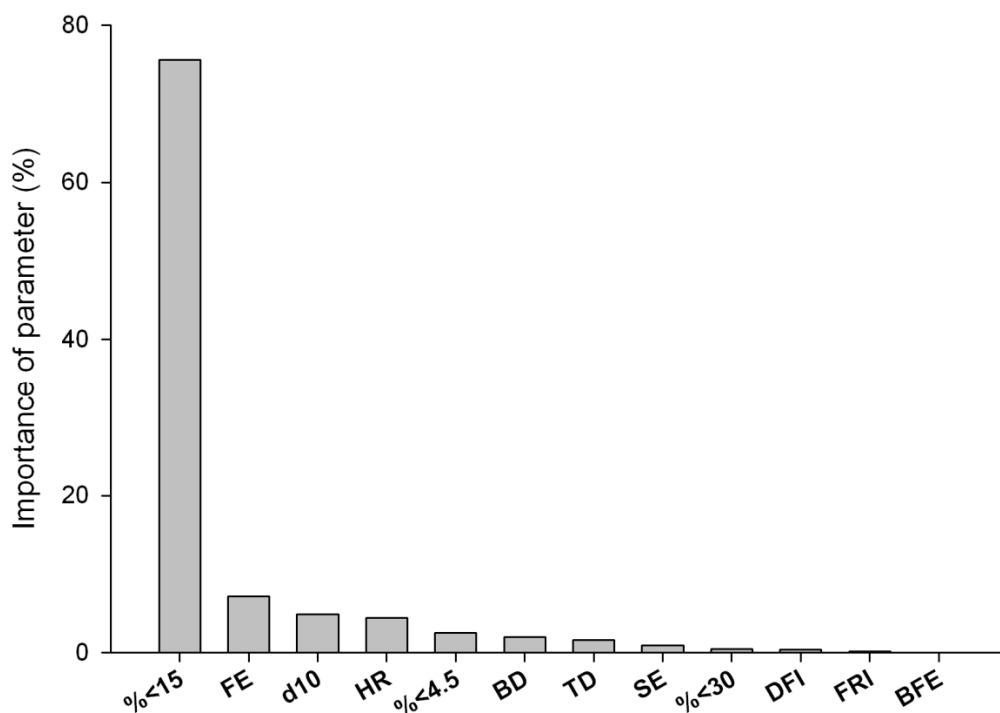
FIGURE 5.12 THE RELATIVE IMPORTANCE OF THE DIFFERENT INPUT PARAMETERS IN THE NEURAL NETWORK MODELLING MEAN MASS AERODYNAMIC DIAMETER OF BUDESONIDE
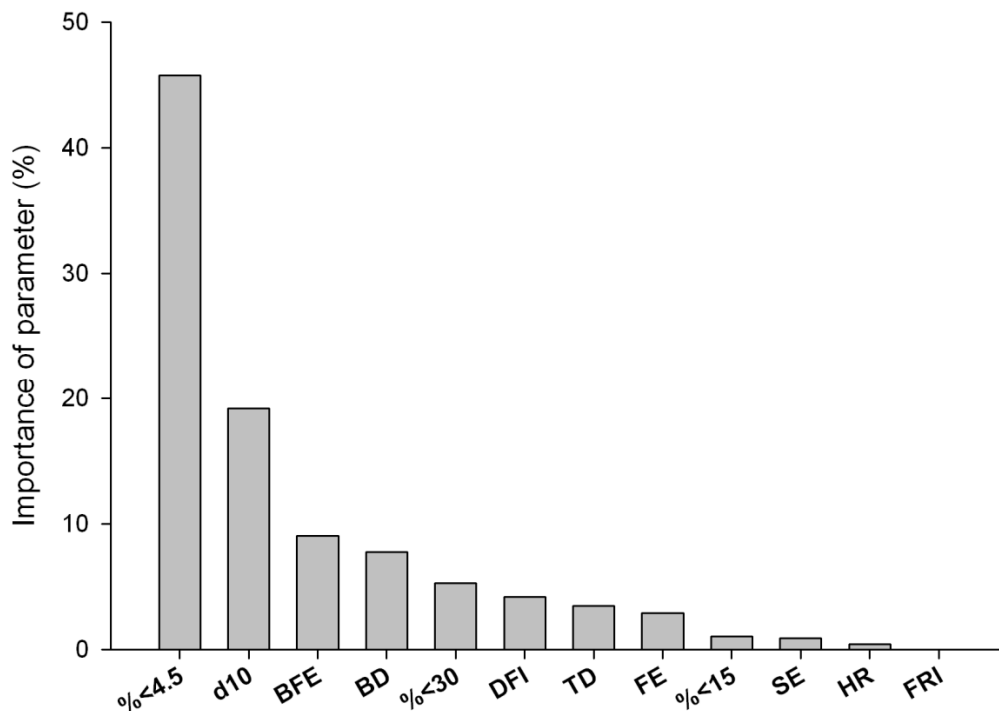
5.3.5 Mechanistic considerations for how the lactose fines govern the DPI performance

The drug that is detached from the surface of the large and intermediate carrier particles and deagglomerated will be deposited in the lower stages of the impactor and reflected in the FPF_{ED} measurements. With all the three different data analysis methods, the proportion of particles finer than 4.5 µm was one the most dominant lactose parameters in determining FPF_{ED}. These data indicate that the fine particle delivery as defined by the fine particle fraction is governed by the presence of fine particle lactose. The statistical analysis methods that are based on the assumption that the underlying data is linear and not covariant also highlighted some of the lactose flow and fluidisation properties as important in determining the FPF_{ED}. However, on the basis of data in this chapter, the only conclusion that can be made is that the presence of the fine particle lactose is essential in improving the DPI performance. No further conclusions can be drawn on the mechanisms for how these fines might improve the DPI performance.

Also the drug detachment from the carrier as defined by the pre-separator deposition was affected by the proportion of lactose fines according to all the models developed in the current study. However, some of the models also highlight the proportion of large fines

206

and the flow and fluidisation properties of the lactose carrier as relatively important parameters in determining the pre-separator deposition.

The drug de-agglomeration efficiency as measured by the MMAD on the other hand was mostly affected by the presence of the larger fine particle lactose, as the proportion of fines <30 µm produced the best R^2 value for linear correlations and the proportion of fines below 15 µm was highlighted as the single most important parameter in the PLS and ANN models for MMAD. To relate the important parameters to the drug deposition in the impactor, it has to be noted that the fine particle fraction of emitted dose used in the current study was based on fine particle mass below 5 µm collected on the impactor stages, as described in Chapter 2 of the thesis. At 90 l/min, the flow rate used in the current study, this cut-off is between NGI stages 1 and 2 (Marple *et al.* 2003b). Therefore, the drug collected on Stage 1 of the impactor will not be reflected in the FPF_{ED}. However, the material collected on Stage 1 was included in the MMAD calculation. Consequentially, it was reasoned that the MMAD described the Stage 1 deposition at least to some extent. The reason for the importance of the larger fine particle lactose in determining the MMAD is likely to be related to the fact that some of these particles with drug particles remaining attached to the surfaces of these particles may be deposited on the upper stages of the impactor. Therefore, the hypothesis of Adi *et al.* (2009) according to which the intermediate lactose fines act as secondary carriers is a viable explanation for the relationship between the presence of larger fines and the increasing MMAD.

5.4 CONCLUSIONS

The DPI performance is governed by multiple properties of the lactose carriers that often cannot be changed in a controlled way independently from each other. In this chapter, PLS and ANN analysis of the structure-function data were used in addition to linear regression to obtain more complete understanding of the lactose characteristics that govern the DPI performance. The PLS and ANN analysis of the current dataset showed that although proportion of fines is the most important parameter in determining the DPI performance, the parameter does not explain all of the variation. Therefore, simple linear correlations are not reliable for predicting the formulation performance and more comprehensive models, such as the ones applied in the current study, should be used instead.

When it comes to understanding the relationship between the lactose properties and the DPI performance, some advancements with respect to the behaviour of larger fines were

made in this chapter. The drug detachment from the large carrier particles and the deagglomeration as measured by pre-separator deposition and MMAD were seen to be regulated by the presence of the larger lactose fines. The results of the current study further confirms the role of the larger fine particle lactose acting as a secondary carrier as was suggested by Adi *et al.* (2009).

However, the role of the fine particle lactose in determining the DPI performance could not be resolved by the means of the data analysis methods used in the current study. Nevertheless, the significance of the fine particle lactose in regulating the performance was proved once again. The study represented in the following Chapter of the thesis will concentrate on understanding the significance of the fine particle lactose in regulating the *in vitro* drug deposition.

CHAPTER 6   LACTOSE CHARACTERISTICS GOVERNING THE REGIONAL DEPOSITION OF THE DRUG IN THE NEXT GENERATION IMPACTOR

6.1   INTRODUCTION

Previous studies have addressed that the fine particle lactose added to DPI formulation has to be fine enough if an improvement in the formulation performance is to be achieved (Adi *et al.* 2006; Guenette *et al.* 2009; Louey *et al.* 2003). Chapter 5 of the thesis showed that from a wide set of physical parameters describing the lactose carriers, the proportion of particles below 4.5 µm was the most important one in determining the DPI performance. Once again, this study confirmed the crucial role of the finest lactose particles in governing the DPI performance. However, the mechanism for how these fine particles of lactose alter the formulation performance has remained unclear, with a number of theories trying to explain the behaviour. It was shown in Chapter 3 of the thesis that the active sites theory (El-Sabawi *et al.* 2006; Young *et al.* 2005) is an unlikely explanation for the improved performance upon the addition of lactose fines. Similarly, Chapters 3 and 4 of the thesis showed that the increased cohesion theory (Shur *et al.* 2008a) may play a minor role in improving the DPI performance. However, this theory was not capable of universally explaining improved performance when a wide range of different carriers were investigated. The agglomerate formation theory (Lucas *et al.* 1998) has gained the strongest evidence during the investigations carried out in this thesis. Chapter 4 indicated that improved DPI performance in the presence of lactose fines was indeed related to agglomerate formation with the fine lactose particles.

As advised by the inhalation monographs of the European and US Pharmacopoeias, pharmaceutical impactors are routinely used for determining the respirable dose of the inhaled drug from different formulations. The assays often rely on dissolving the drug collected in the different parts of the impactor. The concentration of the solute is then chemically determined by means of either HPLC or UV-VIS spectrophotometry. However, these impactor data are often used solely as a performance indicator. The objective of this study is to gain a more rounded understanding of the mechanisms governing the drug deposition in the impactor in the presence of lactose fines. The goal was pursued by using complementary analytical methods alongside the *in vitro* performance analysis of DPI formulations.

The amount of drug deposited in the throat from a formulation aerosolised with different devices has previously been investigated (DeHaan *et al.* 2001). This study showed that different amounts of drug were deposited in the throat from the same formulations aerosolised using different devices. This study concluded that the drug deposition in the throat was governed by the inertia and kinetic energy of the particles exiting the device. Other studies have compared the drug deposition in the USP throat and throat casts that mimic the human oropharyngeal cavity in greater detail (Niven *et al.* 1994; Zhang *et al.* 2007). The former study showed that the amount of drug deposited in the USP throat was an overestimation of the amount of drug deposited in an induction port mimicking the human mouth and throat region (Niven *et al.* 1994). The latter study however showed that, for DPI formulations, the USP throat was as accurate an estimate of the amount of drug deposited *in vivo* in the throat as any anatomically relevant oropharyngeal cast (Zhang *et al.* 2007). Nevertheless, despite the research efforts concentrated on understanding the impact of throat geometry on the drug deposition, the impact of formulation characteristics on the drug deposition in the throat has been largely neglected in discussion of data in most studies that investigated the effect of carrier properties on the DPI performance. The only study where an attempt was made in relating the carrier properties to the throat deposition was performed by Podczeck (1998). In this study, the drug losses in the throat were attributed mainly to the aspect ratio of the large carrier particles. The study showed that less drug deposited in the throat from carriers composed of more elongated particles. It was suggested that these elongated lactose particles exhibited better aerodynamic properties. Consequentially, these particles were more likely to be carried through the USP induction port in the air stream without impacting on the walls. As a result, fewer large carrier particles with drug adhering to the surfaces were deposited in the throat thus contributing to lower drug loss in the throat.

Laser diffraction particle sizing of the aerosol emitted from the DPI device has been previously used for studying powder fluidisation and entrainment (Watling *et al.* 2010), powder de-agglomeration (Adi *et al.* 2006; Behara *et al.* 2011b; Behara *et al.* 2011c; Le *et al 2012a.* ; Zhou *et al.* 2010) and the kinetics of device emptying (Behara *et al.* 2011a). Aerosol particle sizing using laser diffraction has also been suggested as a rapid alternative for quality assurance purposes for inhalation formulations (de Boer *et al.* 2002; Marriott *et al.* 2006; Pilcer *et al.* 2008). In the study reported here, laser diffraction particle sizing of the aerosol was utilised for measuring the particle size of the plume entering and exiting the USP induction port of the Next Generation Impactor (NGI). The motivation for this was two-fold. Firstly, these experiments were expected to give information on differences in the de-agglomeration efficiency possibly related to fines content of the formulations. Secondly, the gap in the knowledge base relating drug losses in the USP

throat to the properties of the carriers containing different amounts of lactose fines could be investigated.

Pre-separator deposition is an important feature of carrier based DPI formulations and is critically important in understanding the mechanism for how the lactose fines increase performance. This is because coarse carrier particles, and any drug that remain attached to these particles upon aerosolisation of the dose, will deposit in the pre-separator. Previous studies by Guchardi *et al.* (2008) and Podczeck (1998) have demonstrated a decrease in the drug deposition in the pre-separator upon increasing fines concentration. The former of these studies concluded that the decreasing trend in the pre-separator deposition fitted with both the active site and agglomerate formation theories (Guchardi *et al.* 2008). The latter of the two studies concluded that the decrease in the proportion of drug deposited in the pre-separator was due to a smaller proportion of large carrier particles being available for the drug to adhere to (Podczeck 1998). Consequentially, agglomerates were formed between the lactose fines and the drug particles and carried through the pre-separator to the stages of the impactor. The study reported here aims to further address drug losses in the pre-separator and in understanding the relationship between carrier properties and *in vitro* drug deposition in the pre-separator.

Several studies have been made in an attempt to understand the mechanisms governing DPI performance by determining the deposition of lactose in the different parts of the impactor alongside drug determination (Guchardi *et al.* 2008; Karhu *et al.* 2000; Srichana *et al.* 1998b). These studies proved that in addition to the drug, fine lactose is deposited on the impactor stages. However, due to the limitations of traditional, solution-based analytical chemistry techniques, these studies only provided speculative evidence of agglomerate formation between lactose fines and the drug. Therefore, to study the possible co-deposition of the drug and lactose fines, there remains a need to develop a greater understanding of the fate of both fine lactose and drug and their association at the lower stages of an inertial impactor and to develop novel characterisation methods.

Early attempts in finding alternative analysis methods for materials deposited in an impactor from a DPI formulation were made by Srichana *et al.* (1998c), who used scanning electron microscopy in conjunction with X-ray microanalysis to study interactions between lactose and salbutamol sulphate particles. More recent studies have shown that Raman spectroscopy is a promising technique for studying particulate interactions in inhaled formulations. These have been mainly investigating the interactions between the different drug particles within combination pressurised metered dose (pMDI) formulations (Rogueda *et al.* 2011; Steele *et al.* 2004; Theophilus *et al.* 2006). Studies with DPI products have also been conducted using Raman spectroscopy (Kinnunen *et al.* 2009;

Šašić *et al.* 2010). Kinnunen *et al.* (2009) used Raman spectroscopy for studying the co-deposition of lactose and FP on the impactor stages from a commercial DPI formulation. Šašić *et al.* (2010) used Raman spectroscopy for investigating the particulate interactions between lactose carrier particles and two different APIs within a combination DPI. Both these studies concluded that Raman spectroscopy was a promising technique for studying the microstructure, the interaction between particles, within DPI formulations. In the current study, further developments in gaining statistically significant data were taken due to significant developments in the combination of Raman spectroscopy with microscopy imaging instrumentation. Morphologically directed Raman spectroscopy was used for characterising the physical properties and chemical composition of the material delivered to the impactor stages. This was done to obtain any evidence on drug-lactose fines agglomerate formation and co-deposition on impactor stages.

Raman spectroscopy is based on the inelastic scattering of monochromatic light upon interaction with the vibrational energy states of molecules, a phenomenon discovered by Raman and Krishnan (1928). This scattering can be divided into three different cases, as illustrated in Figure 6.1. Rayleigh scattering is the most prevalent phenomena with more than 99.999% of the incident light not interacting with the vibrational states of the molecule (Vankeirsbilck *et al.* 2002). Thus, the scattered photons have an identical frequency to the light source and produce no Raman scattering. However, some of the photons interact with the vibrational states of the molecules. The light can either excite a molecule to a higher vibrational energy state or relax the molecule to a lower vibrational energy state. As a result of these interactions, the scattered photon has either lower (Stokes scattering) or higher (anti-Stokes scattering) frequency than the light source, respectively. Due to the rarity of Stokes and anti-Stokes scattering compared to Rayleigh scattering, the Raman signal is relatively weak. However, recent advances in instrumentation have improved the sensitivity of the technique (Wartewig *et al.* 2005). Due to its non-invasive nature, Raman spectroscopy has a wide range of pharmaceutical applications. These include for example polymorph (Findlay *et al.* 1998; Gamberini *et al.* 2006), impurities (Widjaja *et al.* 2008) and counterfeit product detection (Roggo *et al.* 2010). Recently, Raman spectroscopical techniques have also been used for on-line monitoring of pharmaceutical processes thus enabling quality-by-design approaches for pharmaceutical manufacturing (De Beer *et al.* 2011).
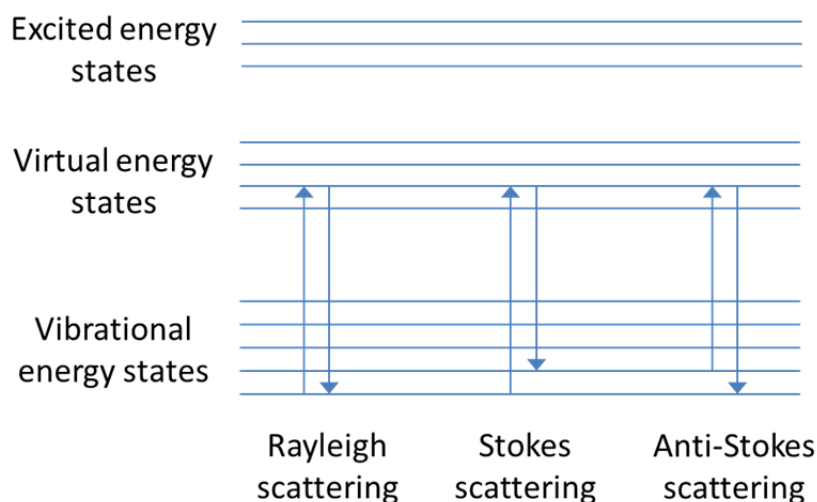
FIGURE 6.1 DIFFERENT SCATTERING PHENOMENA TAKING PLACE UPON EXCITATION OF A MOLECULE

In summary, the aim of the current study is to investigate the drug deposition in the impactor from formulations containing different amounts of lactose fines in greater detail using complementary techniques, namely aerosol particle sizing, morphological analysis and Raman spectroscopy, in parallel with *in vitro* performance assessment of the formulations. This major objective is to enhance our understanding of the mechanisms governing drug delivery from DPI formulations containing fine particle lactose. In particular, the study aims to further support that agglomerate formation between the drug and the lactose fines is the predominant mechanism for governing the DPI performance.

6.2 MATERIALS AND METHODS

The lactose pre-blends were prepared as described in Chapter 4 of the thesis. The same applies to the formulation and *in vitro* work, with the exception that a Cyclohaler device was used at a flow rate of 90l/min. The proportion of fines in the carrier blends was also characterised as described in Chapter 4.

The particle size measurements of the material exiting the device and throat were performed using the Spraytec (Malvern Instruments, Worcestershire, UK) laser diffraction instrument equipped with a 300 mm lens. The inhalation cell held in a horizontal configuration was used for sizing the material entering the throat and in a vertical configuration was used for measuring the material exiting the throat. Prior to measurements, the background scattering was recorded for a duration of 10 seconds. To ensure high enough particulate concentration at the measurement zone, the measurements were triggered once scattering of 50 units was measured at detector number 9. The particle size distributions were retrieved for a 100ms period before the

trigger condition was exceeded. Initially, measurements were performed for 5 seconds after the trigger condition had been met. However, it was observed that no powder passed through the measurement zone after approximately 1.5 seconds. Therefore, the particle size was measured for 2 seconds at a frequency of 2.5 kHz. Mie theory was applied for calculating the particle size distributions from the raw scattering data with refractive index of 1.52, imaginary refractive index of 0.01 and density of 1 applied for lactose. The refractive index of the dispersant (air) was 1. The multiple scattering correction was enabled for the analysis. The trends in particle size parameters ($d10$, $d50$, $d90$ and transmission) were inspected and averaged particle size distributions were created between time points where the plume had passed through the measurement zone.

Samples of material deposited in the pre-separator and the Stage 2 of the NGI when aerosolised at 90 l/min using the Cyclohaler were collected by placing a mirror surfaced microscope slide on the inlet of the pre-separator and underneath the nozzles on Stage 2 of the NGI.

The particles collected in the pre-separator were characterised using the Morphologi G3 automated image analysis system (Malvern Instruments, Worcestershire, UK). Episcopic bright field illumination was used for the microscopic visualisation of the particles with the light intensity calibrated at 80.0 ± 0.2 %. The 5x objective (size range 6.5 to 420 µm for shape information) lens was used for scanning the samples with the focus fixed at 0 µm and the plate tilt compensation enabled. The scan area size was set to 13 mm by 13 mm, the overlap between any two adjacent frames to 30%, the binary threshold to a grayscale value of 123 and the trash size to 10 pixels. Post analysis, any touching particles were removed by filtering out particles with values of solidities below 0.9. Before the shape analysis, particles consisting of less than 100 pixels were filtered out to remove noise from the shape distributions.

The particles deposited on Stage 2 were characterised on the Morphologi G3-ID morphologically directed Raman spectroscopy system (Malvern Instruments, Worcestershire, UK). The settings for the morphological scan were as above for the pre-separator with the following exceptions. The 50x objective lens (size range 0.5 to 40 µm for shape information) was used for the morphological analysis of the particles. The scan area was set to 4.5 mm by 4.5 mm, the overlap between adjacent frames to 40% and the binary threshold to a grayscale value of 130. Post analysis, any touching particles were removed by filtering particles with values of solidities below 0.92.

After the morphological analysis of particles deposited on Stage 2, the particles were sorted according to their size using circular equivalent (CE) diameter. All the particles

larger than 3 μm were highlighted for the Raman analysis that was performed using the Kaiser Optical Systems MK II Probe head integrated in the Morphologi G3-ID system. The XY coordinates of the particles recorded during the morphological analysis were used for locating the centre of the particles, where the Raman spectrum was acquired. The spectrum for each particle was collected using 10 seconds exposure time with excitation at a wavelength of 785 nm over the spectral range of 100 to 1825 cm^{-1} at a resolution of 4 cm^{-1}. The signal was detected using a charge coupled device (CCD) camera. The Raman spot size with the 50x objective was approximately 3 μm in diameter.

Reference spectra were recorded for lactose and budesonide. These reference spectra were used for identifying the chemical composition of the material collected on Stage 2. The identification was performed by comparing the entire spectrum for the analysed particles to the library spectra of lactose and budesonide using the Morphologi G3-ID software. The Morphologi G3-ID software was also used for allocating matching scores for lactose and budesonide for the particles analysed by comparing the similarity of the spectra of the particle to the library spectra of lactose and budesonide. A matching score of 1 indicates identical spectra and a score of 0 indicates the spectrum bears no resemblance to the library spectra at all. On the basis of the scores, the particles could be identified as pure lactose (Lactose ≥ 0.75 and budesonide < 0.450), pure budesonide (Budesonide ≥ 0.75 and lactose < 0.45) or an agglomerate of lactose and budesonide (All the remaining particles). When allocating the classification parameters for the pure substances, visual comparison of the library spectra and the spectra of the particles was used for confirming that no obvious signals of the other component was seen in the spectra. Similarly, for the particles classified as agglomerates, it was visually inspected that the characteristic signals for both the pure substances were present in the spectra.

6.3   RESULTS AND DISCUSSION

6.3.1   *In vitro* performance of the formulations

It was shown in Chapter 4 and Chapter 5 of the thesis as well as in previous studies (Guenette *et al.* 2009; Louey *et al.* 2003) that the proportion of fine lactose particles present in the carrier is an important parameter in defining the DPI performance. The fines content (%<4.5 μm) of the carriers and the *in vitro* performance of the formulations prepared with the carriers investigated in the current study are summarised in Table 6.1. Table 6.1 demonstrates that the proportion of fine particle lactose in the carriers increased from 1.3% for the LH100 to 6% for the 20 wt-% LH210 and to 23% for the 20 wt-% LH300 added to the coarse LH100 carrier. Meanwhile, the fine particle fraction of emitted dose upon the addition of 20 wt-%

LH210 and LH300 fines to LH100 increased from approximately 24 to 26 to 40% respectively.

Table 6.1 also shows that the mean mass aerodynamic diameter (MMAD) of the drug collected from the impactor stages increased simultaneously with the proportion of lactose fines and the fine particle fraction of emitted dose. The increase in the MMAD indicated that the drug was delivered to the impactor stages in larger entities upon the increase in the lactose fines content. These could either be agglomerated drug particles or agglomerates of the fine lactose and the drug particles. An increase in the value of MMAD of the drug upon the addition of lactose fines has also been previously reported by Podczeck (1998). In that study, the dependency of the MMAD on the fines content was attributed to changes in the preferred adhesion site of the drug particles (lactose fines vs. coarse lactose particles) in the presence of lactose fines.

TABLE 6.1 PROPORTION OF FINE PARTICLES IN THE CARRIER BLEND AS MEASURED BY LASER DIFFRACTION AND THE *IN VITRO* PERFORMANCE OF THE FORMULATIONS IN TERMS OF FINE PARTICLE FRACTION OF EMITTED DOSE (FPF$_{ED}$) AND THE MEAN MASS AERODYNAMIC DIAMETER (MMAD) OF THE DRUG AEROSOLISED FROM THE FORMULATIONS. THE DATA FOR % < 4.5 µM REPRESENTS AN AVERAGE OF FIVE REPEATED MEASUREMENTS. THE DATA FOR FPFED AND MMAD REPRESENTS MEAN ± STANDARD DEVIATION, N=3.

	% < 4.5 µm	FPF$_{ED}$ ± S.D. (%)	MMAD ± S.D. (µm)
LH100	1.29	24.10 ± 0.24	2.58 ± 0.02
+20% LH210	6.02	26.63 ± 0.13	3.14 ± 0.01
+20% LH300	23.04	39.74 ± 1.34	3.36 ± 0.03

The stage-by-stage deposition profiles of the drug aerosolised from the different formulations are shown in Figure 6.2 and summarised in Table 6.2. The deposition profiles show that the addition of 20 wt-% LH300 to the formulation significantly decreased the amount of drug deposited in the capsule compared to LH100 and the 20 wt-% LH210 formulations. The decrease was statistically significant (p<0.05) compared to the formulation prepared with LH100 only. Increasing trends in the device and in the mouthpiece and throat deposition were apparent upon increasing concentration of fines. Compared to the formulation prepared with LH100 only, the increase was not statistically significant for device deposition (p>0.05) but was significant for the mouthpiece and throat deposition. A decreasing trend in the pre-separator deposition was observed upon an increase in the fines content. The decrease was statistically significant (p<0.05) for both the formulations containing added fines compared to the formulation prepared with LH100 only (p<0.05). The amount of drug recovered from the pre-separator decreased from 35 to

20 and further to 10 µg upon the addition of 20 wt-% LH210 and 20 wt-% LH300, respectively. The amount of drug delivered to the impactor stages in general increased with increasing fines concentration. The increase was significant ($p < 0.05$) on all the stages for the LH300 formulations and on stages 1 and 2 for the LH210 formulation compared to the formulation containing no extrinsic lactose fines.

TABLE 6.2 THE AMOUNT OF DRUG RECOVERED FROM THE DIFFERENT PARTS OF THE NEXT GENERATION IMPACTOR FROM THE DIFFERENT FORMULATIONS. MP & T REPRESENTS THE MOUTHPIECE AND THROAT AND PS THE PRE-SEPARATOR. THE DATA REPRESENTS MEAN ± STANDARD DEVIATION, N=3.

	Amount of drug recovered from stage ± S.D. (µg)		
	LH100	+20% LH210	+20% LH300
Capsules	21.40 ± 1.18	20.30 ± 1.09	12.78 ± 0.83
Device	12.16 ± 0.74	14.23 ± 0.83	15.29 ± 0.88
MP & T	6.39 ± 0.26	11.82 ± 0.53	15.59 ± 1.31
PS	34.87 ± 1.00	20.58 ± 0.38	11.21 ± 1.25
Stage 1	1.68 ± 0.06	3.38 ± 0.08	5.59 ± 0.07
Stage 2	3.37 ± 0.10	4.78 ± 0.10	9.82 ± 0.14
Stage 3	4.01 ± 0.11	4.19 ± 0.13	7.93 ± 0.20
Stage 4	4.71 ± 0.11	3.96 ± 0.02	6.45 ± 0.25
Stage 5	1.99 ± 0.05	1.86 ± 0.13	2.50 ± 0.09
Stages 6-8	0.62 ± 0.02	0.75 ± 0.08	0.90 ± 0.03
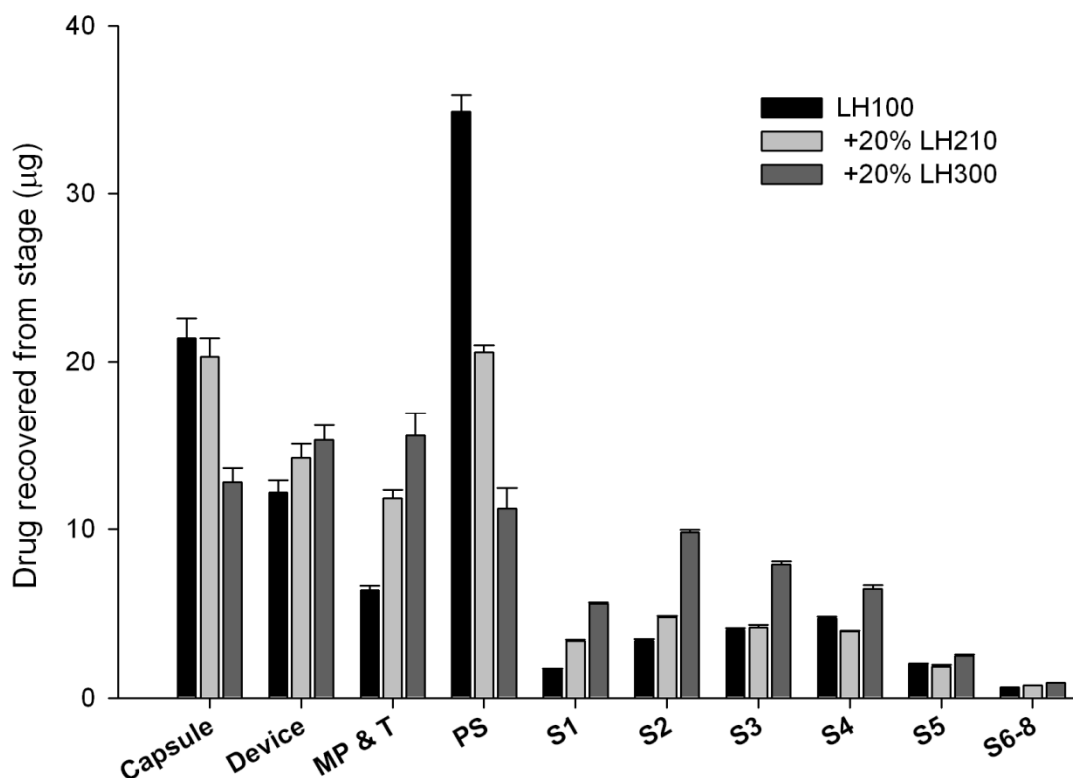
FIGURE 6.2 STAGE-BY-STAGE DEPOSITION PROFILES OF BUDESONIDE FROM THE FORMULATIONS INVESTIGATED IN THE STUDY. MP & T REPRESENTS THE MOUTHPIECE AND THROAT AND PS THE PRE-SEPARATOR. THE DATA REPRESENTS MEAN ± STANDARD DEVIATION, N=3.

6.3.2 Size of the material exiting the device

The plume exiting the device after the aerosolisation of the different formulations was characterised using laser diffraction aerosol particle sizing. The average value of d10 during device emptying and the variation in the value of d10 over this event, σ_{d10}, are summarised in Table 6.3. Additionally, the ratio between the σ_{d10} and d10 for each formulation is tabulated. These data show that the values of d10 reflect the fines content of the formulations, with LH100 formulation producing the largest and the 20 wt-% LH300 formulation the smallest d10.

A decreasing trend in σ_{d10} was observed upon increasing lactose fines concentration. To evaluate the significance of the decreasing trend for σ_{d10}, the ratio between and σ_{d10} and d10 of the formulations was calculated. It was anticipated that the decrease in σ_{d10} could be related to the measurement accuracy rather than to the formulation characteristics. If this was the case, the decrease in σ_{d10} would simply be a consequence of the decreasing value of d10, and the ratio between the two parameters would remain constant for the different formulations. Conversely, if the ratios were different for the formulations, the parameter would describe the de-agglomeration characteristics of the formulations. Table 6.3 demonstrates that the ratio between σ_{d10} and d10 varied between the different formulations with the LH100 and the 20 wt-% LH210 formulations having higher values than the 20 wt-% LH300 formulation. These data indicate that the consistency of de-agglomeration was higher for the 20 wt-% LH300 formulation than for the formulations prepared with LH100 only and with 20 wt-% LH210. These data may be indicative of the 20 wt-% LH300 formulation having a microstructure more favourable for constant de-agglomeration than the other two formulations investigated.

TABLE 6.3 THE AVERAGE d10 AND THE VARIATION IN THE VALUE OF d10 (σ_{d10}) OVER THE DEVICE EMPTYING EVENT FOR THE MATERIAL EXITING THE CYCLOHALER AND THE RATIO BETWEEN THE TWO PARAMETERS FOR THE DIFFERENT FORMULATIONS. THE DATA REPRESENTS MEAN ± STANDARD DEVIATION (S.D), N=3.

	d10 ± S.D. (µm)	σ_{d10} ± S.D. (µm)	σ_{d10}/ d10
LH100	24.58 ± 1.85	7.41 ± 0.30	0.30 ± 0.01
+20% LH210	8.16 ± 1.03	2.32 ± 0.79	0.28 ± 0.06
+20% LH300	3.00 ± 0.18	0.63 ± 0.12	0.21± 0.04

6.3.3 Throat deposition

There are numerous studies in the literature where the particle size distribution of the plume exiting the device has been characterised using a horizontal configuration for the Spraytec inhalation cell (Adi *et al.* 2006; Behara *et al.* 2011a; Behara *et al.* 2011b; Behara *et al.* 2011c; Le *et al.* 2012a; Watling *et al.* 2010; Zhou *et al.* 2010). However, to the author's knowledge, the vertical configuration of the inhalation cell has not been utilised for characterising the plume exiting the induction port of the impactor. In the current study, the particle size distributions of both the plume entering and exiting the USP throat were characterised. This was done to understand what formulation characteristics govern the drug deposition in the throat. The particle size distributions of the formulations upon entering and exiting the USP throat of the impactor are presented in Figure 6.3. For all the formulations, the particle size distributions measured after the USP throat had less fine material and more large material than the distributions measured before the throat. These data indicate qualitatively that fine material was lost in the throat.

On the basis of the distributions shown in Figure 6.3 it appeared that large material was being created as the formulations passed through the throat. However, this was practically impossible because the measurements were performed in a closed system. In addition, despite the fact that the particle size distributions are volume based, the loss of fines was still reflected in them. Thus majority of the material lost in the throat had to be fine particles. To illustrate this, the following example should be considered; if one particle of a diameter of 100 μm is lost in the throat, to have an equal contribution in the volume based distribution, 1000 particles with a diameter of 10 μm have to be lost.

To enable quantitative analysis of the amount of material deposited in throat, the particle size distributions of the formulations before the throat were normalised. To do this, an assumption that no large particles were lost in the throat had to be made. The assumption was justified due to the reasons related to the volume of particles of different sizes discussed in the preceding paragraph. Also, the results of the quantitative analysis were found to be insensitive to the assumption. To obtain a factor describing the difference in the modes of the particle size distributions, the ratios between the modes of the particle size distributions for each of the formulations before and after the throat were calculated. The size distributions of the formulations measured before throat were then multiplied by this factor. This way, particle size distributions with equal frequencies for the modes were obtained.

The normalised particle size distributions of the formulations before the throat together with the size distributions measured after the throat are presented in Figure 6.4. The

figure demonstrates that for the formulation prepared with LH100, the majority of the particles deposited in the throat were finer than approximately 50 µm. With the 20 wt-% LH210 formulation, most of the particles deposited in the throat were between 5 and 50 µm in size. However, also some particles between 50 and 100 µm were deposited in the throat from this formulation. With the 20 wt-% LH300 formulation, the particle size of material deposited in the throat was below 30 µm, although some material up to 100 µm in size was seen to deposit in the throat also from this formulation. Notably, the small population of agglomerates present in the distribution measured before the throat between 600 and 900 µm were deposited in the USP throat.

Further data analysis revealed that the amount of drug deposited in the USP throat correlated with the proportion of particles finer than 29 µm lost in the throat (R^2=0.999), as illustrated in Figure 6.5. The figure shows that the smaller the proportion of fines below 29 µm depositing in the throat, the less drug is lost in the throat. These data indicate that the drug deposition in the throat was governed by co-deposition with the lactose fines present in the formulation. This may be because of the formation of drug-fines agglomerates (20 wt-% LH300 formulation) or due to the drug adhering to the surface of the larger lactose fines present in the formulation (20 wt-% LH210 formulation). The correlation may also be partly due to higher plume density for the formulations with added fines. Consequentially, the likelihood of particles impacting on the walls of the throat is higher from the formulations with added fines. To the author's knowledge, these data relating the fines content of the lactose carrier to the drug deposition in the induction port are novel.

LH100
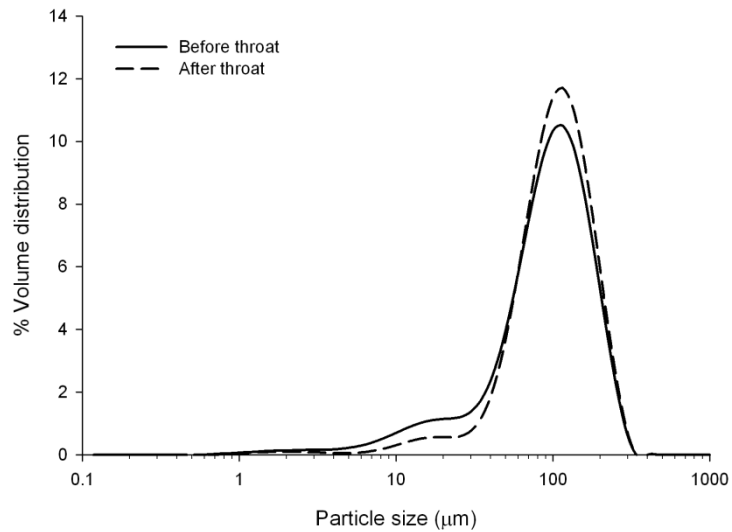
+20% LH210
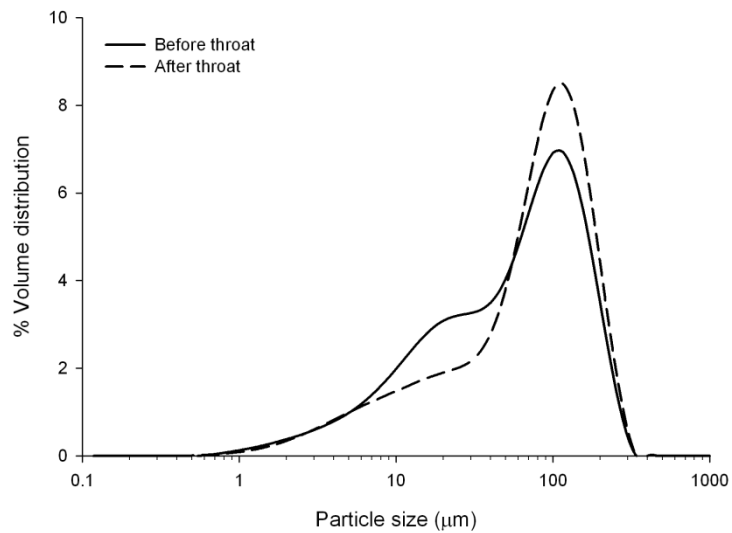
+20% LH300
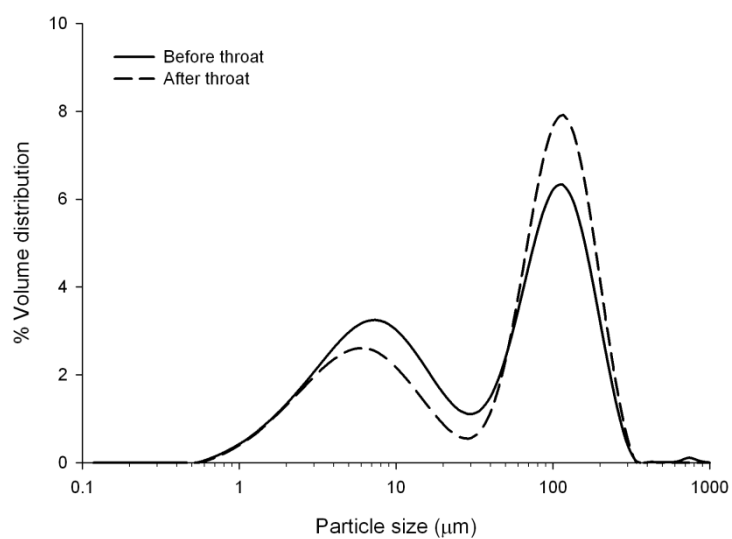
FIGURE 6.3 THE PARTICLE SIZE DISTRIBUTIONS OF MATERIAL ENTERING (SOLID LINES) AND EXITING THE THROAT (DASHED LINES) WITH LH100 (TOP), 20% LH210 (MIDDLE) AND 20% LH300 (BOTTOM) IN LH100 AS THE CARRIER. THE DATA REPRESENTS THE AVERAGE PARTICLE SIZE DISTRIBUTION OF MATERIAL PASSING THROUGH THE MEASUREMENT ZONE DURING THE DURATION OF THE MEASUREMENTS (2S).

221
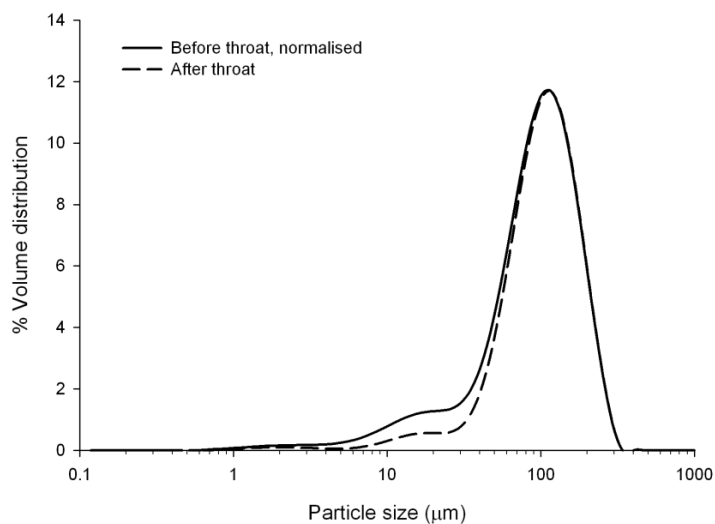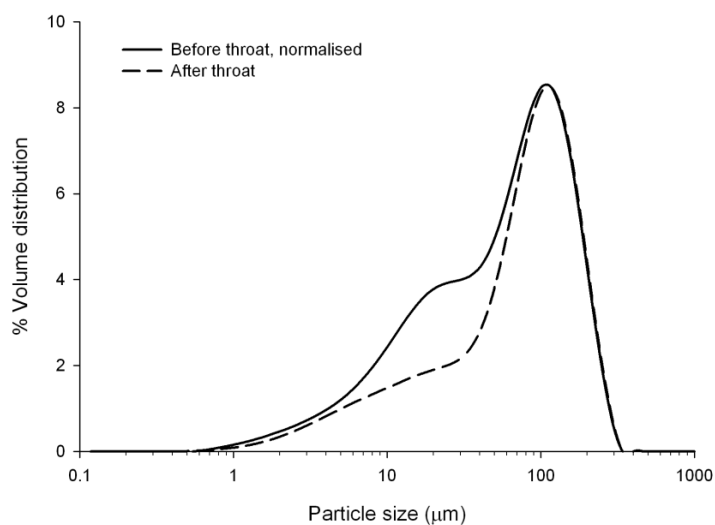
LH100
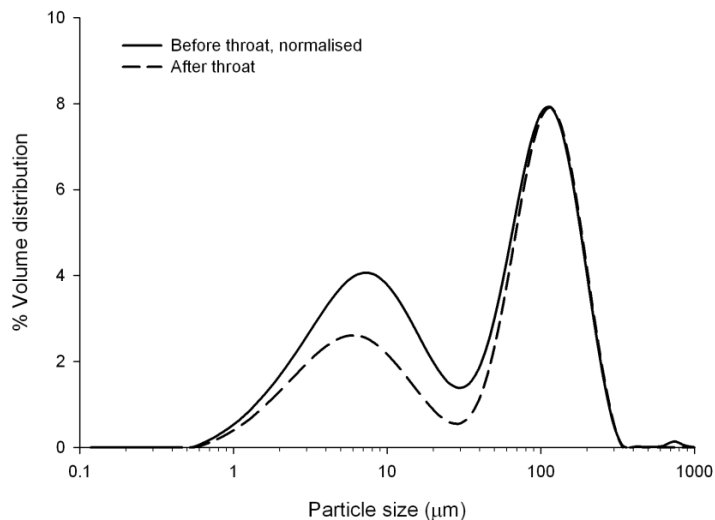
+20% LH210

+20% LH300

FIGURE 6.4 NORMALISED PARTICLE SIZE DISTRIBUTIONS OF MATERIAL ENTERING THE THROAT (SOLID LINES) AND SIZE OF THE MATERIAL EXITING THE THROAT (DASHED LINES) FOR LH100 (TOP), 20% LH210 (MIDDLE) AND 20% LH300 FORMULATIONS (BOTTOM). THE DATA REPRESENTS THE AVERAGE PARTICLE SIZE DISTRIBUTION OF MATERIAL PASSING THROUGH THE MEASUREMENT ZONE DURING THE DURATION OF THE MEASUREMENTS (2S).
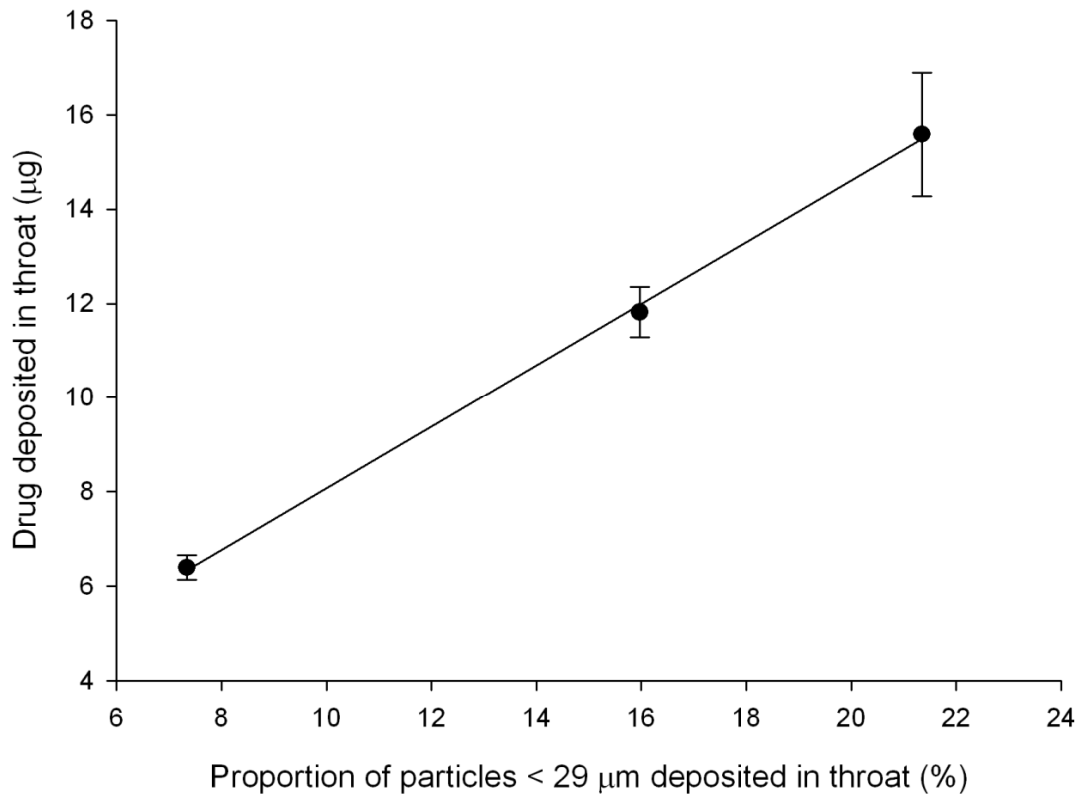
FIGURE 6.5 THE RELATIONSHIP BETWEEN THE PROPORTION OF PARTICLES DEPOSITED IN THE THROAT AND THE AMOUNT OF DRUG RECOVERED FROM THE THROAT. THE DATA FOR DRUG DEPOSITED IN THROAT REPRESENTS MEAN ± STANDARD DEVIATION. THE DATA FOR PROPORTION OF PARTICLES BELOW 29 μm IS BASED ON SINGLE MEASUREMENT. $R^2 = 0.999$

6.3.4 Pre-separator deposition

The number based particle size distributions of the material collected in the pre-separator, in terms of circular equivalent (CE) diameter, upon aerosolisation of the different formulations are summarised in Table 6.4. The d10 of the material collected in the pre-separator for all the formulations were very similar. However, this was most likely related to the limit of detection with the use of the 5x magnification optic. The formulations with added fines had a lower d50 than the LH100 formulation. In terms of d90, clear differences between the formulations were characterised with decreasing d90 upon an increase in the fines content of the formulation. The CE diameter distributions of the material collected in the pre-separator are shown in Figure 6.6. The cut-off diameter of Stage 1 of the NGI when operated at 90 l/min is 6.48 μm (Marple *et al.* 2003a). Figure 6.6 demonstrates that significant amounts of particles finer than this were collected in the pre-separator from all the formulations. Clearly, these fines can either be fine lactose or drug particles. Therefore, at least some drug loss in the pre-separator can possibly be attributed to these fine particles depositing in the pre-separator.

223

Plotting the mass of drug recovered from the pre-separator from the different formulations against the number-based d90 of the particles collected in the pre-separator resulted in a linear correlation (R^2=0.9996), as shown in Figure 6.7. These data indicate that the larger the proportion of coarse carrier crystals present in the formulation, the more drug was lost in the pre-separator. This result could be interpreted in two ways. Firstly, the advocates of the active site theory (El-Sabawi *et al.* 2006; Young *et al.* 2005) would attribute the larger proportion of drug lost in the pre-separator in the absence of lactose fines to the drug adhering to the high energy binding sites on the surface of the large carriers. The other school of thought, according to an interpretation by Podczeck (1998), would argue that the decreased drug deposition in the pre-separator in the presence of lactose fines was due to the drug being transported through the pre-separator as agglomerates with lactose fines, and thus depositing in the impactor stages rather than in the pre-separator.

Unfortunately, the pre-separator deposition data from the current study cannot provide a definitive conclusion on the mechanism governing the pre-separator deposition. However, it was shown that a large proportion of particles finer than the cut off diameter of Stage 1 (<6.48 µm) were also collected in the pre-separator from the formulation prepared with LH100. At least some of these fines are likely to be drug particles that for some reason have deposited in the pre-separator. Therefore, these data suggest that the active site theory (El-Sabawi *et al.* 2006; Young *et al.* 2005) is very unlikely to be the explanation for the decrease in the pre-separator deposition upon the addition of lactose fines.

TABLE 6.4 THE 10TH, 50TH AND 90TH PERCENTILES OF NUMBER BASED PARTICLE SIZE DISTRIBUTIONS (D10, D50 AND D90, RESPECTIVELY) OF THE MATERIAL COLLECTED IN THE PRE-SEPARATOR FROM THE DIFFERENT FORMULATIONS IN TERMS OF CIRCULAR EQUIVALENT (CE) DIAMETER. THE DATA IS BASED ON THE ANALYSIS OF 3149 (LH100), 16086 (+20% LH210) AND 12657 (+20% LH300) PARTICLES DURING A SINGLE MEASUREMENT.

	Number based CE diameter (µm)		
	d10	d50	d90
LH100	2.45	7.97	39.01
+20% LH210	2.21	3.40	20.74
+20% LH300	2.29	3.77	9.61
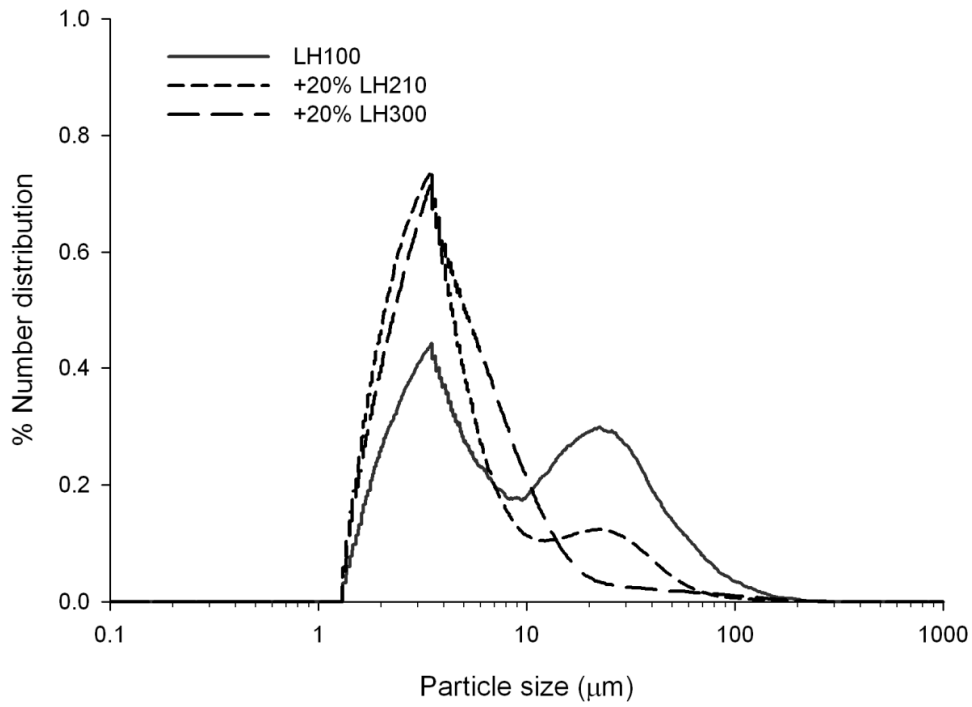
FIGURE 6.6 NUMBER-BASED CIRCULAR EQUIVALENT (CE) DIAMETER DISTRIBUTIONS OF MATERIAL COLLECTED IN THE PRE-SEPARATOR FROM THE DIFFERENT FORMULATIONS. THE DATA REPRESENTS THE SIZE DISTRIBUTION OF 3149 (LH100), 16086 (+20% LH210) AND 12657 (+20% LH300) PARTICLES ANALYSED DURING A SINGLE MEASUREMENT.
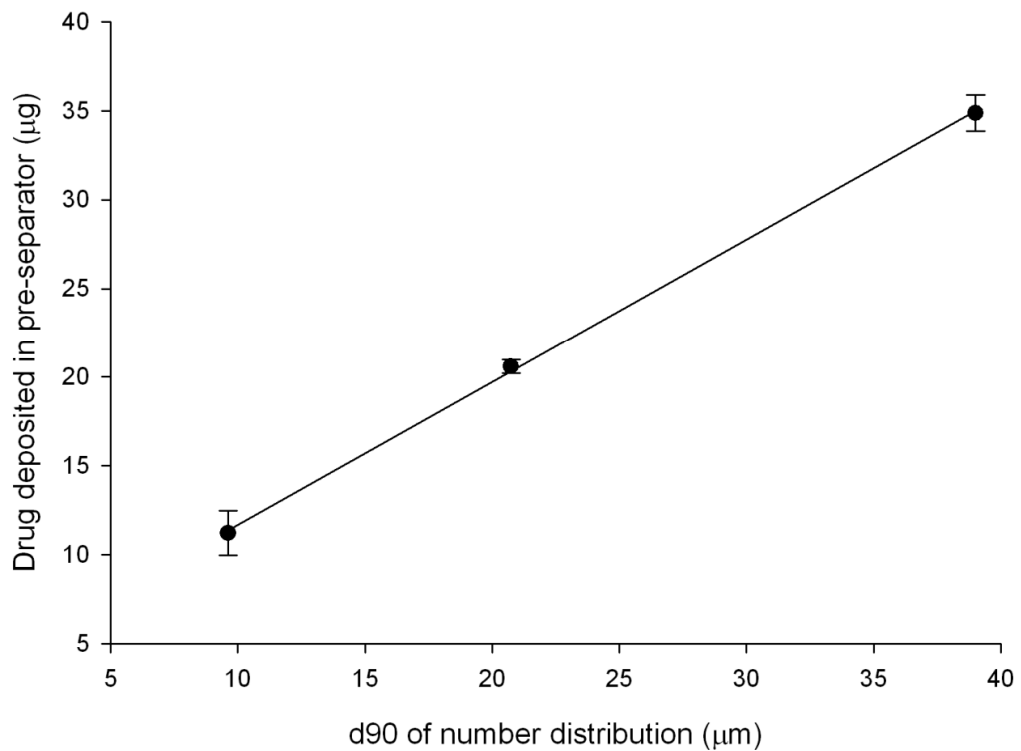
FIGURE 6.7 RELATIONSHIP BETWEEN THE NUMBER-BASED d90 OF THE CIRCULAR EQUIVALENT DIAMETER OF THE CARRIER AND THE AMOUNT OF DRUG DEPOSITED IN THE PRE-SEPARATOR. D90 IS BASED ON THE DISTRIBUTIONS REPORTED IN FIGURE 6.6. THE AMOUNT OF DRUG DEPOSITED IN THE PRE-SEPARATOR IS MEAN ± STANDARD DEVIATION, N=3. R^2=0.9996

6.3.5   Stage 2 deposition

The number-based and volume-converted CE diameter distributions of the material collected from the NGI Stage 2 from the different formulations are summarised in Table 6.5. The table shows that, in number terms, a slight increase in the value of d10 was seen as the fines content of the formulations was increased. The cut-off diameter (the mean diameter of the material collected on the stage) of Stage 2 when the NGI is operated at 90 l/min is 3.61µm (Marple *et al.* 2003a).

Table 6.5 shows that the number based values of d50 measured for the formulations were close to this. Values of d50 did not exhibit a clear trend related to the fines content of the formulations. In terms of d90, an increase was apparent as the fines content was increased. The increasing particle size in the upper end of the distributions as the fines content was increased is clearly visible in Figure 6.8, where the number-based CE diameter distributions of the material collected on Stage 2 from the different formulations are presented.

Table 6.5 and Figure 6.9, where the volume converted CE diameter distributions of the material collected on Stage 2 are shown, indicate that, in volume terms, the increase in the particle size in the upper end of the distributions was even more pronounced. These data suggest the material collected on Stage 2 became increasingly agglomerated upon increasing lactose fines content of the formulation.

The particle shape of the material collected from Stage 2 is summarised in Table 6.5 in terms of mean high sensitivity (HS) circularity and convexity values for the different formulations. For both shape descriptors, a decreasing trend in the mean values was seen as the lactose fines concentration of the formulations was increased. Following the definition of these shape parameters (Willen 2008), the higher the value of the parameters, the more compact the shape of a particle. It is also known that agglomerates often exhibit less compact shape than primary particles (Huck 2007). Therefore, the decreasing trend in the particle shape descriptors upon the addition of fines indicated a simultaneous increase in the presence of agglomerates. The increasing degree of agglomeration in the presence of lactose fines as indicated by the larger particle size and less compact shape in the formulations was also reflected in MMAD of the drug collected from the formulations, as was shown in Table 6.1.

TABLE 6.5 NUMBER-BASED AND VOLUME-CONVERTED CIRCULAR EQUIVALENT (CE) DIAMETER DISTRIBUTIONS AND THE MEAN VALUES OF HIGH SENSITIVITY (HS) CIRCULARITY AND CONVEXITY OF THE MATERIAL COLLECTED ON STAGE 2 OF THE NEXT GENERATION IMPACTOR FROM THE DIFFERENT FORMULATIONS. THE DATA IS BASED ON ANALYSIS OF 7406 (LH100), 18361 (+20% LH210) AND 21551 (+20% LH300) PARTICLES DURING A SINGLE MEASUREMENT.

|	Number based particle size (µm)			Volume converted particle size (µm)			Particle shape Mean values	
	d10	d50	d90	d10	d50	d90	HS Circularity	Convexity
LH100	1.56	3.84	5.77	3.68	5.35	8.06	0.859	0.986
+20% LH210	1.72	3.62	6.14	3.60	5.98	9.48	0.846	0.983
+20% LH300	1.86	3.94	6.72	3.95	6.53	10.4	0.824	0.980
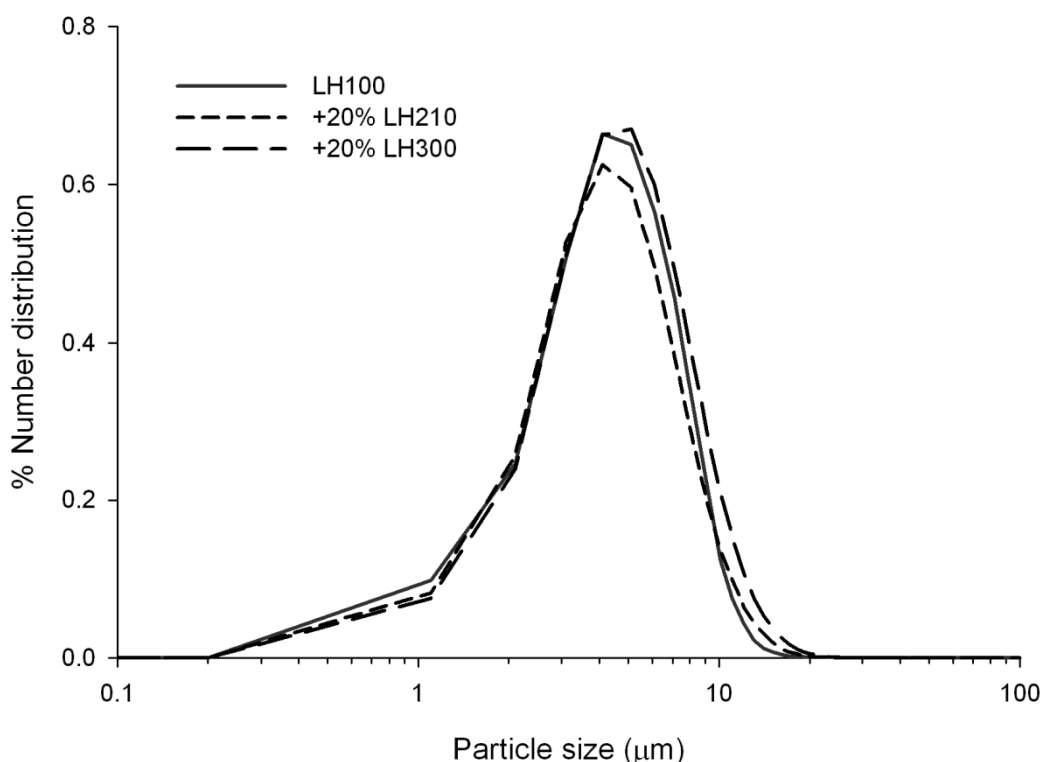
FIGURE 6.8 NUMBER-BASED CIRCULAR EQUIVALENT (CE) DIAMETER DISTRIBUTIONS OF MATERIAL COLLECTED ON STAGE 2 OF THE NGI FROM THE DIFFERENT FORMULATIONS. THE DISTRIBUTIONS REPRESENTED ARE BASED ON ANALYSIS OF 7406 (LH100), 18361 (+20% LH210) AND 21551 (+20% LH300) PARTICLES.
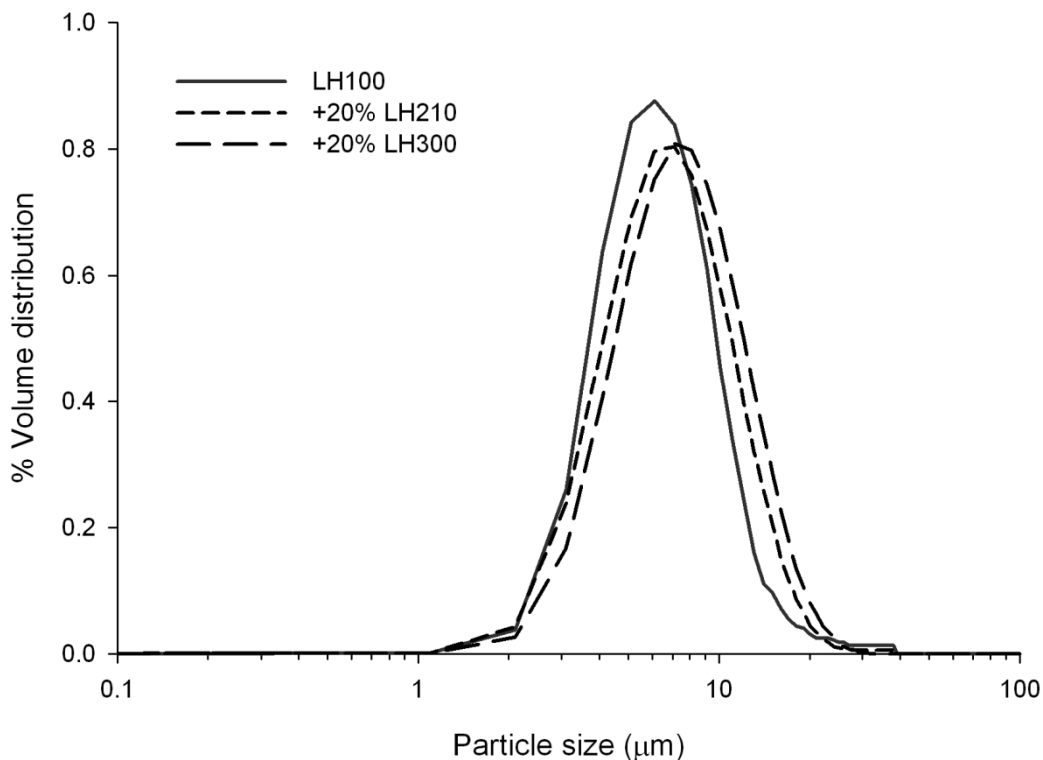
FIGURE 6.9 VOLUME-CONVERTED CIRCULAR EQUIVALENT (CE) DIAMETER DISTRIBUTIONS OF MATERIAL COLLECTED ON STAGE 2 OF THE NGI FROM THE DIFFERENT FORMULATIONS. THE DISTRIBUTIONS ARE BASED ON THE SAME DATA AS THE DISTRIBUTIONS SHOWN IN FIGURE 6.8.

The chemical composition of the material collected on Stage 2 was studied by Raman spectroscopy. The library spectrum of lactose is shown in Figure 6.10. Susi *et al.* (1974) reported the Raman spectra of α-lactose monohydrate in the crystalline state. The authors pointed out that lactose molecule has a low symmetry. Consequentially, the Raman spectrum of lactose exhibits 129 different vibrational modes. Due to the complexity of the spectra, the study did not present a detailed analysis of the different signals. However, the study concluded that the strong signals between 300 and 500 cm^{-1} were due to the different vibrations related to the glycosidic bond linking the galactose and glucose rings of the molecule. In the current study, these vibrations were used for visually distinguishing lactose from budesonide. Since the study by Susi *et al.*, at least two studies have utilised Raman spectroscopy for characterising the polymorphic forms of lactose (Kirk *et al.* 2007; Murphy *et al.* 2005). The Raman spectra of lactose used in the current study as shown in Figure 6.10 is typical for α-lactose monohydrate, as reported in all three studies referred to here.

The library Raman spectrum for budesonide is presented in Figure 6.11. The Raman spectrum of budesonide exhibited a very strong signal at a wavenumber of 1656 cm^{-1}. This signal was used for distinguishing budesonide from lactose during visual inspection

228

of the spectra. This signal has been attributed to the stretching vibration of C=C bond in the aromatic ring of the steroid backbone of the molecule (Ali *et al.* 2007) The same study also attributed the weak signal at 1721 cm^{-1} to the stretching vibration of the C=O bond of the aromatic ring, and the signals at 1627 and 1602 cm^{-1} to the asymmetric ring vibrations of the aromatic C=C and C=O bonds (Ali *et al.* 2007).
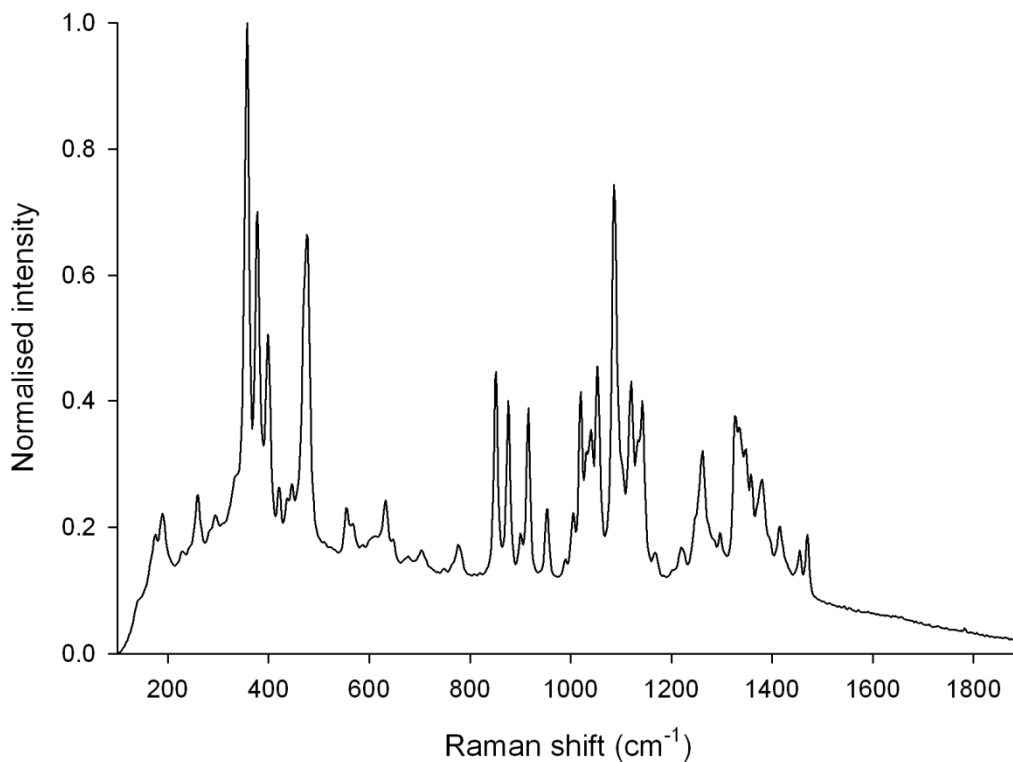
FIGURE 6.10 LIBRARY RAMAN SPECTRUM OF α-LACTOSE MONOHYDRATE
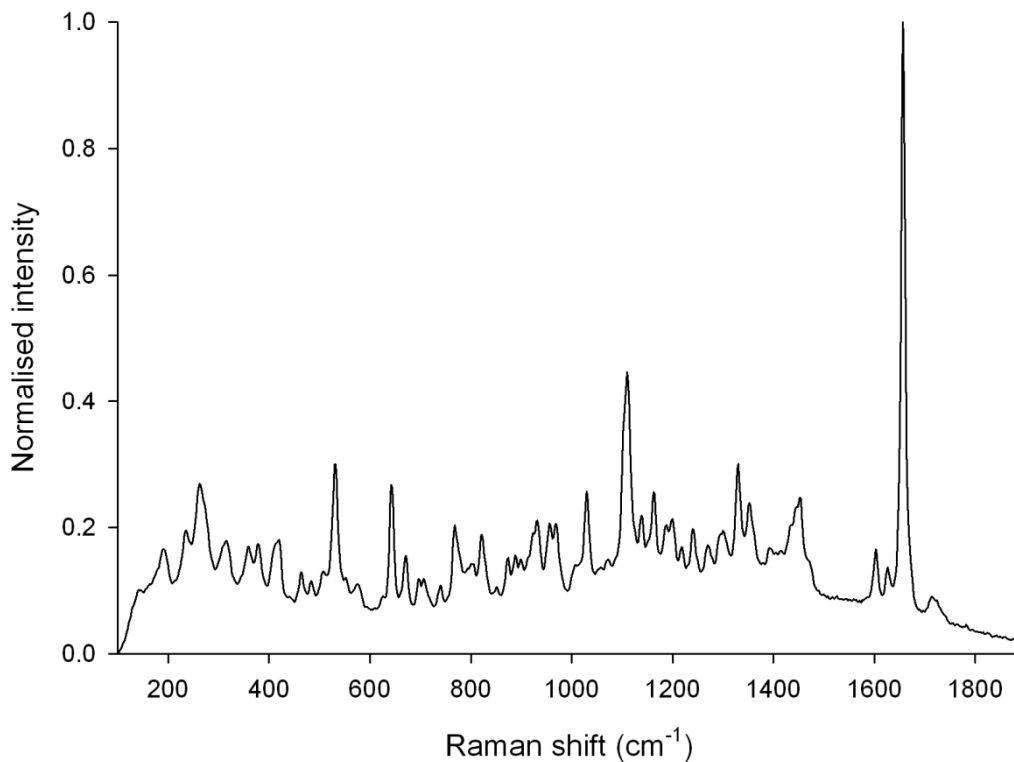
FIGURE 6.11 LIBRARY RAMAN SPECTRUM OF BUDESONIDE

A 50x magnification field of view photomicrograph of material deposited on Stage 2 from the 20 wt-% LH300 formulation is presented in Figure 6.12. The photomicrograph clearly demonstrates that both primary and agglomerated particles were collected on Stage 2. Raman spectroscopical characterisation enabled the analysis of the chemical components forming these agglomerates. The Raman spectrum of the highlighted particle is displayed on the top right of Figure 6.12 and the library spectra of lactose and budesonide below that. The characteristic, strong signal of budesonide at 1656 cm^{-1} is present in the spectrum of the highlighted particle. Also the characteristic signal for lactose between the wavenumbers of 300 and 500 cm^{-1} is exhibited in the spectrum of the highlighted particle. The matching scores for the library spectra as allocated by the Morphologi G3-ID software for this particle were 0.681 for lactose and 0.635 for budesonide. Therefore, on the basis of matching scores and the visual inspection of the Raman spectrum, the highlighted particle could be characterised as an agglomerate of lactose and budesonide. Similarly, pure particles of lactose and budesonide could be characterised based on their Raman spectrum. This way, the chemical composition of approximately 1200 particles collected on Stage 2 were characterised for each of the formulations.
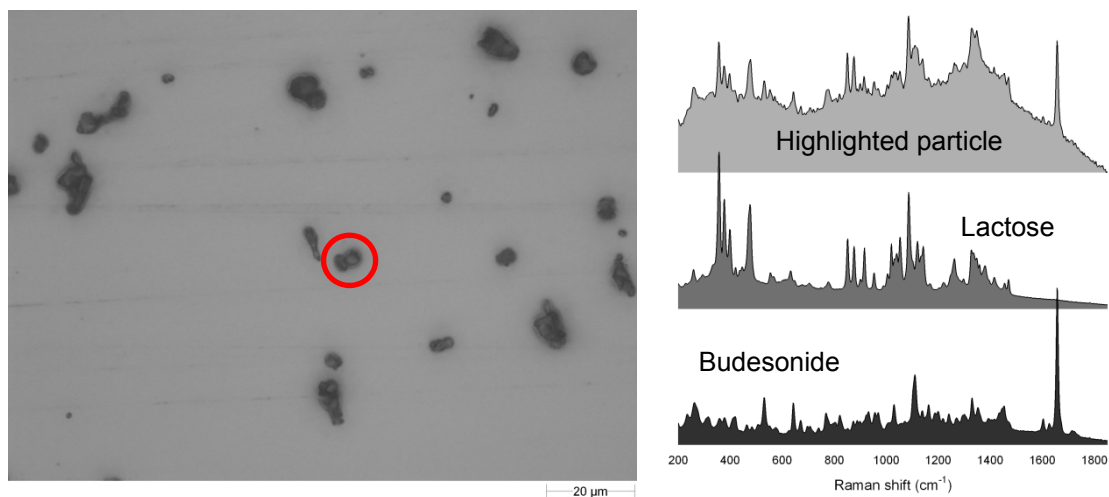
FIGURE 6.12 A 50X MAGNIFICATION FIELD OF VIEW PHOTOMICROGRAPH OF PARTICLES DEPOSITED ON STAGE 2 OF THE NGI, THE RAMAN SPECTRA OF THE HIGHLIGHTED PARTICLE AND THE LIBRARY SPECTRA OF α-LACTOSE MONOHYDRATE AND BUDESONIDE

Following the Raman spectroscopic fingerprinting of the particles collected on Stage 2, a classification was set up according to whether the material was lactose, budesonide or an agglomerate of the two components. Proportions of the different chemical species in the different formulations are summarised in Table 6.6 and presented in Figure 6.13. These data show that, even for the formulation prepared with LH100 only, nearly 40% of the particles delivered to the impactor Stage 2 were lactose. With added lactose fines, the proportion of lactose delivered to the Stage 2 was even higher at approximately 80%. These data are in an agreement with previous studies, where it was reported that fine particle lactose is indeed delivered to the impactor stages (Guchardi *et al.* 2008; Karhu *et al.* 2000; Srichana *et al.* 1998b).

Figure 6.13 and Table 6.6 demonstrate that the majority, nearly half of the particles, on Stage 2 from the LH100 only formulation were single particles or multiplets of budesonide. In contrast, the proportion of pure budesonide in the formulations with added lactose fines was very low, with 10% for the LH210 formulation and 6% for the LH300 formulation characterised as pure budesonide.

Analysing the amounts of lactose and the drug particles delivered to the different parts of the impactor is straightforward by different chemical assays. However, when these techniques are used, addressing the possible presence of drug-lactose fine agglomerates is impossible. Using Raman spectroscopy for analysing the chemical composition of the particles collected on the impactor stages enables studying the possible agglomerate formation between two chemically different species. A previous study used Raman spectroscopy for qualitatively assessing the chemical composition of material deposited on the impactor stages (Kinnunen *et al.* 2009). The results showed co-deposition of

231

lactose and drug took place. The next step was taken in the current study by quantifying the proportions of drug-lactose agglomerates delivered to the impactor stage. Table 6.6 and Figure 6.13 show, that the proportion of agglomerates of the drug and the lactose fines remained similar for all the formulations, with the proportion varying between 11.5 and 17%.

TABLE 6.6 PROPORTIONS OF BUDESONIDE, LACTOSE AND AGGLOMERATES OF THE TWO SPECIES DEPOSITED ON STAGE 2 OF THE NGI FROM THE DIFFERENT FORMULATIONS. THE DATA ARE BASED ON RAMAN ANALYSIS OF 1353 (LH100), 1095 (+20% LH210) AND 1156 (+20% LH300) PARTICLES COLLECTED.

	Lactose (%)	Budesonide (%)	Agglomerates (%)
LH100	37.4	48.8	13.8
+20% LH210	79.0	9.5	11.5
+20% LH300	77.3	5.7	17.0
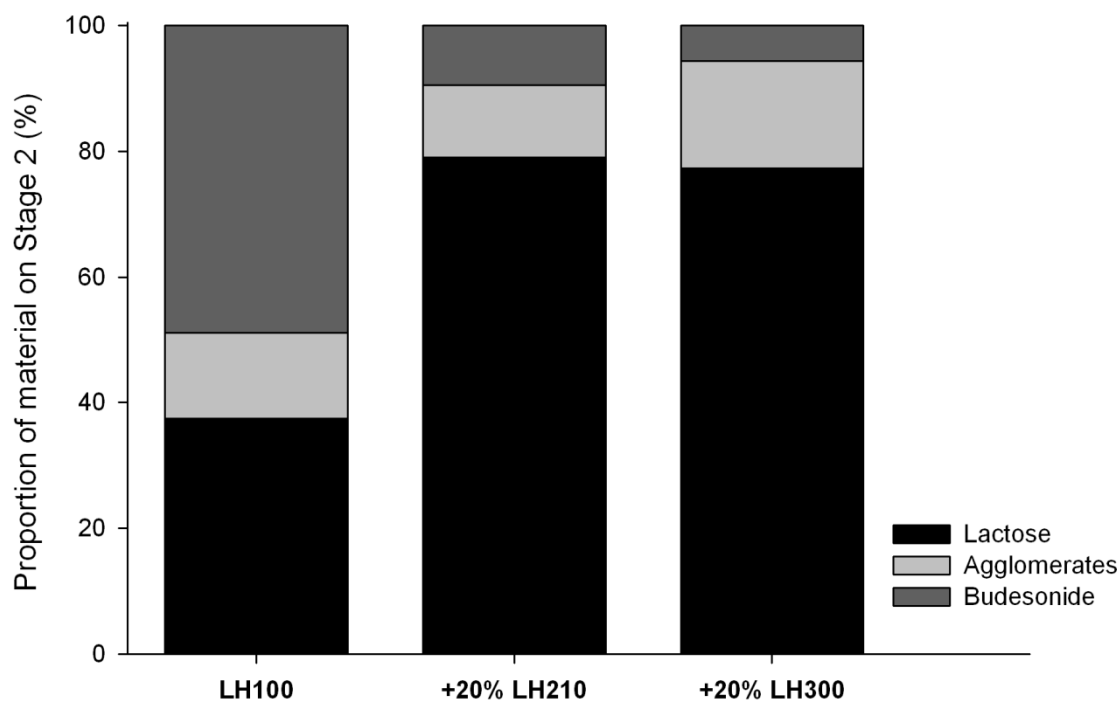
FIGURE 6.13 PROPORTIONS OF PURE LACTOSE AND BUDESONIDE AND THE AGGLOMERATES OF THE TWO COMPONENTS ON STAGE 2 OF THE NGI FROM THE DIFFERENT FORMULATIONS AS CHARACTERISED BY THE RAMAN FINGERPRINT OF THE PARTICLES

To understand the underlying mechanisms for how the lactose fines alter the DPI performance, further analysis relating the *in vitro* deposition of the drug to the proportion of drug delivered to Stage 2 either as pure budesonide or agglomerates was performed. These data are summarised in Table 6.7. The total proportion of budesonide containing species (pure budesonide and agglomerates) was approximately 63% for the LH100 only formulation and approximately 20% for the formulations containing added lactose fines.

Because the proportions of agglomerates and pure budesonide of the budesonide containing species were known (Table 6.6), the amounts of budesonide in agglomerates and as pure budesonide could be quantified. This analysis revealed that interestingly, as shown in Table 6.7, the mass of the drug delivered to the Stage 2 of the impactor as pure budesonide remained constant from all the formulations. Meanwhile, the mass of budesonide delivered to the Stage 2 as agglomerates increased as the lactose fines content of the formulation was increased. For the 20% LH210 formulation the mass of budesonide in agglomerates was approximately four times as high as for the LH100 formulation. For the 20% LH300 formulation, the mass of budesonide in agglomerates on Stage 2 was tenfold compared to the LH100 only formulation. These data show that agglomerate formation takes place upon the addition of lactose fines and consequentially, an improvement in the DPI performance is achieved. These results demonstrate that lactose fines have to be fine enough to be co-deposited in the impactor stages with the drug if an improvement in formulation performance is to be gained. Therefore, these results also explain why only the finest fractions of lactose fines are efficient in improving the DPI performance, as has been previously reported (Guenette *et al.* 2009; Louey *et al.* 2003)

TABLE 6.7 THE MEAN ± STANDARD DEVIATION (N=3) AMOUNT OF BUDESONIDE RECOVERED FROM STAGE 2 OF THE NGI, TOTAL PROPORTION OF SPECIES CONTAINING BUDESONIDE OF THE PARTICLES ANALYSED BY RAMAN FOR EACH OF THE FORMULATIONS AND THE AMOUNT OF PURE BUDESONIDE AND BUDESONIDE IN AGGLOMERATES ON STAGE 2 BASED ON THE RAMAN ANALYSIS.

	Budesonide on Stage 2 ± S.D. (µg)	Total budesonide (%)	Budesonide in agglomerates (µg)	Pure budesonide (µg)
LH100	3.37 ± 0.10	62.6	0.7	2.6
+20% LH210	4.78 ± 0.10	21.0	2.6	2.2
+20% LH300	9.82 ± 0.14	22.7	7.4	2.4

6.4 CONCLUSIONS

The current study aimed to create a holistic picture of the mechanisms governing the regional drug deposition in the impactor by complementing the *in vitro* performance assessment of the formulations by using alternative analytical techniques in parallel with the *in vitro* analysis. The results from the complementary analytical techniques were successfully related to the *in vitro* deposition characteristics of drug from DPI formulations containing different concentrations of lactose fines.

The study demonstrated that the drug deposition in the USP induction port of the impactor was related to loss of fine particles in the throat. This was attributed to the drug depositing in the throat as agglomerates with the fine particle lactose. Also, the higher plume density in the presence of lactose fines may contribute to the higher drug losses in throat in the presence of fine particle lactose. The drug losses in the pre-separator were demonstrated to be related to the proportion of large carrier particles present in the formulation. However, large proportions of fine particles were also collected in the pre-separator. Therefore, evidence for the active site theory in governing the DPI performance in the presence of lactose fines (El-Sabawi *et al.* 2006; Young *et al.* 2005) is still very limited.

Agglomerate formation and deposition in the impactor stages upon the increasing fines content was demonstrated with both the *in vitro* and the complimentary analysis techniques. *In vitro* analysis established an increasing trend in MMAD upon the increase in the lactose fines content of the carrier. Morphological analysis demonstrated increasing particle size and less compact shape upon increasing lactose fines content indicating agglomerate formation. However, these analysis methods gave no information on the components forming the agglomerates. By means of Raman spectroscopy, proportions of pure budesonide and lactose and the agglomerates of the two materials delivered to Stage 2 could be quantified. Combining the results of the Raman and *in vitro* analysis revealed that the amount of pure drug delivered to the impactor Stage 2 remained constant from all the formulations. However, the amount of drug delivered to the Stage 2 as agglomerates increased drastically upon the increase in the fines content of the carrier.

The results of this study demonstrated that agglomerate formation between the drug and the lactose fines may be the dominant mechanism in how lactose fines improve DPI performance. The more fines were available within the carrier, the more drug was agglomerated with them and consequentially delivered to the impactor stage. The results also shed light on the question of why only the finest lactose fines are efficient in improving the DPI performance. This is because the lactose fines have to be fine enough to be co-deposited in the impactor with the drug particles. As a consequence, the results of the study highlighted why the proportion of fine particles present in the carrier is such a popular tool for predicting the DPI performance amongst formulators.

CHAPTER 7 GENERAL CONCLUSIONS AND FUTURE WORK

7.1 ON THE PROCESS HISTORY OF THE LACTOSE FINES

The role of lactose fines in improving dry powder inhaler performance was investigated during the current PhD project. Lactose fines with different process histories (milled and micronised) were used during the studies. It was seen that the micronised fines were very efficient in improving the DPI performance whereas milled fines had a less of an impact. These findings were attributed to the greater proportion of fine particle lactose (%<4.5 µm) present in the carrier blends prepared with the micronised fines. However, although not necessarily playing a significant role in improving the performance, addition of milled fines to DPI formulations may still provide the carrier blend with properties useful for the manufacturing process. For example, addition of milled fines may increase the cohesion of the carrier blend, and consequentially formulation, such that automated capsule filling equipment can be used during manufacturing.

7.2 ON THE ROLE OF LACTOSE FINES IN IMPROVING DPI PERFORMANCE

The main aim of the project was to determine the mechanism by which the fines improved the DPI performance. In Chapter 3 it was shown that the active sites theory is not likely to explain the improved DPI performance upon the addition of lactose fines. Chapter 4 indicated that the addition of lactose fines, independent of the process history, increased the cohesion of the carrier blends. However, this increase did not necessarily correspond to an improved DPI performance. Therefore, the increased cohesion theory is unlikely to be the sole explanation for the improved DPI performance in the presence of fine particle lactose.

On the basis of SEM images, the improvement in the formulation performance was seen to correlate with agglomerate formation, either with drug only (Chapter 3) or between lactose fines and the drug (Chapter 4). In Chapter 6, further evidence for the agglomerate formation, and consequential drug-lactose co-deposition within the impactor was seen. The extent of co-deposition was quantified and it was shown that the more fine lactose particles were available, the more agglomerates of the drug and the lactose fines were deposited on the impactor stage 2. Therefore, the current thesis indicates that the drug-fines agglomeration theory is the most likely explanation for the improved DPI performance in the presence of lactose fines.

7.3 ON THE PARAMETERS DESCRIBING THE LACTOSE PROPERTIES IN PREDICTING THE DPI PERFORMANCE

The project also aimed to develop a universal model for predicting DPI performance on the basis of lactose properties, independent of the process history of the lactose. Linear correlations between lactose properties and DPI performance have been reported in the literature. However, it was shown in Chapter 4 that, when a diverse and large enough set of carriers is used, simple, universal, linear correlations between the carrier properties and the DPI performance are non-existent.

In Chapter 5, statistical methods and artificial neural networks were applied for modelling the importance of different lactose properties in determining DPI performance in terms of fine particle fraction of emitted dose, mean mass aerodynamic diameter and the proportion of drug recovered in the pre-separator. It was shown that the proportion of fine particle lactose (%<4.5 µm) was the most important parameter for the networks modelling fine particle fraction of emitted dose and the proportion of drug deposited in the pre-separator. However, this parameter only explained 57 and 45% of the variation in the data, respectively. For MMAD, the proportion of lactose particles finer than 15 µm explained approximately 75% of the variation. Therefore, other parameters, such as powder flow and fluidisation characteristics, although of less significance, are also important in capturing the variations in DPI performance. This finding most likely derives from the co-linear characteristics of lactose carriers, that on the other hand stem from the limited control over lactose properties during manufacturing process involving for example milling, sieving and air classification steps to control particle size post crystallisation.

7.4 FUTURE WORK

Micronised fines were seen to be efficient in improving DPI performance whereas milled fines had less influence. However, although the milled fines had very little influence on the performance, these fines still increased the cohesion of the carrier blends. Currently, micronised fines are not used in commercial products due to a short shelf life of half a year. Therefore, future work should involve developing more stable lactose fines with a particle size distribution similar to micronised fines and testing whether these engineered fines would still be effective in improving the DPI performance. The studies in the current thesis were conducted using capsule based devices. It would also be interesting to see whether similar trends would be observed with blister based devices, for which the deagglomeration mechanisms may significantly differ from capsule based devices.

REFERENCES

Adi, H., I. Larson, H. Chiou, P. Young, D. Traini and P. Stewart (2006). Agglomerate Strength and Dispersion of Salmeterol Xinafoate from Powder Mixtures for Inhalation. Pharmaceutical Research 23(11): 2556-2565.

Adi, H., I. Larson and P. J. Stewart (2009). Influence of the polydispersity of the added fine lactose on the dispersion of salmeterol xinafoate from mixtures for inhalation. European Journal of Pharmaceutical Sciences 36: 265–274.

Agatonovic-Kustrin, S. and R. Beresford (2000). Basic concepts of artificial neural network (ANN) modeling and its application in pharmaceutical research. Journal of Pharmaceutical and Biomedical Analysis 22(5): 717-727.

Agusti, A. G. N. (2005). COPD, a multicomponent disease: implications for management. Respiratory Medicine 99(6): 670-682.

Aitkin, M. and R. Foxall (2003). Statistical modelling of artificial neural networks using the multi-layer perceptron. Statistics and Computing 13(3): 227-239.

Alavi, S. and B. Caussat (2005). Experimental study on fluidization of micronic powders. Powder Technology 157(1-3): 114-120.

Ali, H. R. H., H. G. M. Edwards, J. Kendrick, T. Munshi and I. J. Scowen (2007). Vibrational spectroscopic study of budesonide. Journal of Raman Spectroscopy 38(7): 903-908.

Al-Showair, R. A. M., W. Y. Tarsin, K. H. Assi, S. B. Pearson and H. Chrystyn (2007). Can all patients with COPD use the correct inhalation flow with all inhalers and does training help? Respiratory Medicine 101(11): 2395-2401.

Ariyananda, P. L., J. E. Agnew and S. W. Clarke (1996). Aerosol delivery systems for bronchial asthma. Postgraduate Medical Journal 72(845): 151-156.

Bailey, A. G. (1984). Electrostatic phenomena during powder handling. Powder Technology 37(1): 71-85.

Baldrick, P. and D.G. Bamford (1997). A Toxicological Review of Lactose to Support Clinical Administration by Inhalation. Food and Chemical Toxicology 35: 719-733.

Barmpalexis, P., K. Kachrimanis and E. Georgarakis (2011). Solid dispersions in the development of a nimodipine floating tablet formulation and optimization by artificial neural networks and genetic programming. European Journal of Pharmaceutics and Biopharmaceutics 77(1): 122-131.

Basheer, I. A. and M. Hajmeer (2000). Artificial neural networks: fundamentals, computing, design, and application. Journal of Microbiological Methods 43(1): 3-31.

Begat, P., D. A. V. Morton, J. N. Staniforth and R. Price (2004a). The Cohesive-Adhesive Balances in Dry Powder Inhaler Formulations II: Influence on Fine Particle Delivery Characteristics. Pharmaceutical Research 21(10): 1826-1833.

Begat, P., D. A. V. Morton, J. N. Staniforth and R. Price (2004b). The Cohesive-Adhesive Balances in Dry Powder Inhaler Formulations I: Direct Quantification by Atomic Force Microscopy. Pharmaceutical Research 21(9): 1591-1597.

Begat, P., R. Price, H. Harris, D. A. V. Morton and J. N. Staniforth (2005). The influence of force control agents on the cohesive-adhesive balance in dry powder inhaler formulations. KONA 23: 109-120.

Behara, S. R. B., P. Kippax, I. Larson, D. A. V. Morton and P. Stewart (2011a). Kinetics of emitted mass - A study with three dry powder inhaler devices. Chemical Engineering Science 66(21): 5284-5292.

Behara, S. R. B., P. Kippax, M. P. McIntosh, D. A. V. Morton, I. Larson and P. Stewart (2011b). Structural influence of cohesive mixtures of salbutamol sulphate and lactose on aerosolisation and de-agglomeration behaviour under dynamic conditions. European Journal of Pharmaceutical Sciences 42(3): 210-219.

Behara, S. R. B., I. Larson, P. Kippax, D. A. V. Morton and P. Stewart (2011c). The kinetics of cohesive powder de-agglomeration from three inhaler devices. International Journal of Pharmaceutics 421(1): 72-81.

Bell, J. H., P. S. Hartley and J. S. G. Cox (1971). Dry powder aerosols I: A new powder inhalation device. Journal of Pharmaceutical Sciences 60(10): 1559-1564.

Benitez, J. M., J. L. Castro and I. Requena (1997). Are artificial neural networks black boxes? Neural Networks, IEEE Transactions on 8(5): 1156-1164.

Bharadwaj, R., W. R. Ketterhagen and B. C. Hancock (2010). Discrete element simulation study of a Freeman powder rheometer. Chemical Engineering Science 65(21): 5747-5756.

Bika, D. G., M. Gentzler and J. N. Michaels (2001). Mechanical properties of agglomerates. Powder Technology 117(1-2): 98-112.

Boerefijn, R., Z. Ning and M. Ghadiri (1998). Disintegration of weak lactose agglomerates for inhalation applications. International Journal of Pharmaceutics 172(1-2): 199-209.

Boshhiha, A. M. and N. A. Urbanetz (2009). Influence of carrier surface fines on dry powder inhalation formulations. Drug Development and Industrial Pharmacy 35(8): 904-916.

Broadhead, J., S. K. Edmond Rouan and C. T. Rhodes (1995). Dry-powder inhalers: evaluation of testing methodology and effect of inhaler design. Pharmaceutica Acta Helvetiae 70(2): 125-131.

Brown, R. (1828). A brief account of microscopical observations on the particles contained on pollen of plants and on the general existence of active molecules in organic and inorganic bodies. Edinburgh New Philosophical Journal: 358-371.

Cai, F. S. and C. P. Yu (1988). Inertial and interceptional deposition of spherical particles and fibers in a bifurcating airway. Journal of Aerosol Science 19(6): 679-688.

Carman, P. C. (1956). Flow of gases through porous media, Butterworths Scientific Publications.

Carr, R. L. (1965). Classifying flow properties of solids. Chemical Engineering 72: 69-72.

Carvalho, T. C., J. I. Peters and R. O. Williams (2011). Influence of particle size on regional lung deposition - What evidence is there? International Journal of Pharmaceutics 406(1-2): 1-10.

Castellanos, A. (2005). The relationship between attractive interparticle forces and bulk behaviour in dry and uncharged fine powders. Advances in Physics 54(4): 263 - 376.

Cazzola, M., C. Donner and N. A. Hanania (2007). One hundred years of respiratory medicine chronic obstructive pulmonary disease (COPD). Respiratory Medicine 101(6): 1049-1065.

Clark, A. R. and A. M. Hollingworth (1993). The Relationship Between Powder Inhaler Resistance and Peak Inspiratory Conditions in Healthy Volunteers - Implications for In Vitro Testing. Journal of Aerosol Medicine 6(2): 99-110.

Clydesdale, G., J. R. Kevin, B. T. Gillian and J. W. G. David (1997). Modeling the crystal morphology of α-lactose monohydrate. Journal of Pharmaceutical Sciences 86(1): 135-141.

Dalby, R. and J. Suman (2003). Inhalation therapy: technological milestones in asthma treatment. Advanced Drug Delivery Reviews 55(7): 779-791.

De Beer, T., A. Burggraeve, M. Fonteyne, L. Saerens, J. P. Remon and C. Vervaet (2011). Near infrared and Raman spectroscopy for the in-process monitoring of pharmaceutical production processes. International Journal of Pharmaceutics 417(1–2): 32-47.

de Boer, A. H., D. Gjaltema, P. Hagedoorn, M. Schaller, W. Witt and H. W. Frijlink (2002). Design and application of a new modular adapter for laser diffraction characterization of inhalation aerosols. International Journal of Pharmaceutics 249(1–2): 233-245.

de Boer, A. H., P. Hagedoorn, D. Gjaltema, J. Goede, K. D. Kussendrager and H. W. Frijlink (2003). Air classifier technology (ACT) in dry powder inhalation Part 2. The effect of lactose carrier surface properties on the drug-to-carrier interaction in adhesive mixtures for inhalation. International Journal of Pharmaceutics 260(2): 201-216.

de Boer, A. H., B. H. J. Dickhoff, P. Hagedoorn, D. Gjaltema, J. Goede, D. Lambregts and H. W. Frijlink (2005). A critical evaluation of the relevant parameters for drug redispersion from adhesive mixtures during inhalation. International Journal of Pharmaceutics 294(1-2): 173-184.

de Boer, A. H., H. K. Chan and R. Price (2012). A critical view on lactose-based drug formulation and device studies for dry powder inhalation: Which are relevant and what interactions to expect? Advanced Drug Delivery Reviews 64(3): 257-274.

DeHaan, W. H. and W. H. Finlay (2001). In vitro monodisperse aerosol deposition in a mouth and throat with six different inhalation devices. Journal of Aerosol Medicine, Deposition, Clearance and Effects in the Lung 14(3): 361-367.

DeHaan, W. H. and W. H. Finlay (2004). Predicting extrathoracic deposition from dry powder inhalers. Journal of Aerosol Science 35(3): 309-331

de Matas, M., Q. Shao, M. F. Biddiscombe, S. Meah, H. Chrystyn and O. S. Usmani (2010). Predicting the clinical effect of a short acting bronchodilator in individual patients using artificial neural networks. European Journal of Pharmaceutical Sciences 41(5): 707-715.

de Matas, M., Q. Shao, C. H. Richardson and H. Chrystyn (2008). Evaluation of in vitro in vivo correlations for dry powder inhaler delivery using artificial neural networks. European Journal of Pharmaceutical Sciences 33(1): 80-90.

Delebarre, A., J.-M. Morales and L. Ramos (2004). Influence of the bed mass on its fluidization characteristics. Chemical Engineering Journal 98(1-2): 81-88.

DFEPharma (2011). "The custom-made solutions of DFE Pharma Inhalation." Retrieved 18/11/2011, from http://www.dfepharma.com/en/Excipients/Inhalation/Respitose-SV010.aspx#tab-downloads.

Dhumal, R. S., S. V. Biradar, A. R. Paradkar and P. York (2008). Ultrasound Assisted Engineering of Lactose Crystals. Pharmaceutical Research 25(12): 2835-2844.

Dickhoff, B. H. J., M. J. H. Ellison, A. H. de Boer and H. W. Frijlink (2002). The effect of budesonide particle mass on drug particle detachment from carrier crystals in adhesive mixtures during inhalation. European Journal of Pharmaceutics and Biopharmaceutics 54(2): 245-248.

Dickhoff, B. H. J., A. H. de Boer, D. Lambregts and H. W. Frijlink (2005). The interaction between carrier rugosity and carrier payload, and its effect on drug particle redispersion from adhesive mixtures during inhalation. European Journal of Pharmaceutics and Biopharmaceutics 59(1): 197-205.

Dickhoff, B. H. J., A. H. de Boer, D. Lambregts and H. W. Frijlink (2006). The effect of carrier surface treatment on drug particle detachment from crystalline carriers in adhesive mixtures for inhalation. International Journal of Pharmaceutics 327(1-2): 17-25.

Dolovich, M. B. and R. Dhand (2011). Aerosol drug delivery: developments in device design and clinical use. The Lancet 377(9770): 1032-1045.

Donovan, M. J. and H. D. C. Smyth (2010). Influence of size and surface roughness of large lactose carrier particles in dry powder inhaler formulations. International Journal of Pharmaceutics 402(1-2): 1-9.

Edge, S., A. Kibbe and K. D. Kussendrager (2006). Lactose, monohydrate. Handbook of Pharmaceutical Excipients, Fifth edition. Edited by R. C. Rowe, P. J. Sheskey and S. C. Owen. London, Pharmaceutical Press: 389-395.

Edwards, A. M. and A. Chambers (1989). Comparison of a lactose-free formulation of sodium cromoglycate and sodium cromoglycate plus lactose in the treatment of asthma. Current Medical Research and Opinion 11(5): 283-292.

Egermann, H. and N. A. Orr (1983). Ordered mixtures - interactive mixtures. Powder Technology 36(1): 117-118.

El-Sabawi, D., S. Edge, R. Price and P. M. Young (2006). Continued investigation into the influence of loaded dose on the performance of dry powder inhalers: Surface smoothing effects. Drug Development and Industrial Pharmacy 32(10): 1135-1138.

Emery, E., J. Oliver, T. Pugsley, J. Sharma and J. Zhou (2009). Flowability of moist pharmaceutical powders. Powder Technology 189(3): 409-415.

European Medicines Agency (2007). European Pharmacopoeia 6.0. Inhalation monograph

Fanta, C. H. (2009). Drug therapy: Asthma. New England Journal of Medicine 360(10): 1002-1014.

FDA (2004). Guidance for industry: PAT - A framework for innovative pharmaceutical development, manufacturing and quality assurance. US Department of Health and Human Services.

FDA (2006). Guidance for Industry: Quality systems approach to pharmaceutical GCMP Regulations. US Department of Health and Human Services.

Findlay, W. P. and D. E. Bugay (1998). Utilization of Fourier transform-Raman spectroscopy for the study of pharmaceutical crystal forms. Journal of Pharmaceutical and Biomedical Analysis 16(6): 921-930.

Freeman, R. (2007). Measuring the flow properties of consolidated, conditioned and aerated powders -- A comparative study using a powder rheometer and a rotational shear cell. Powder Technology 174(1-2): 25-33.

Gac, J., T. R. Sosnowski and L. Gradon (2008). Turbulent flow energy for aerosolization of powder particles. Journal of Aerosol Science 39(2): 113-126.

Gamberini, M. C., C. Baraldi, A. Tinti, C. Rustichelli, V. Ferioli and G. Gamberini (2006). Solid state characterization of chloramphenicol palmitate. Raman spectroscopy applied to pharmaceutical polymorphs. Journal of Molecular Structure 785(1–3): 216-224.

Ganderton, D., (1992). The generation of respirable clouds from coarse powder aggregates. Journal of Biopharmaceutical Sciences 3: 101-105.

Ganderton, D. (1997).General factors influencing drug delivery to the lung. Respiratory Medicine 91(Supplement 1): 13-16.

Ganderton, D. and N. M. Kassem (1991). Aerosol Carriers. International patent number WO/1991/011179.

Geldart, D. (1973). Types of Gas Fluidization. Powder Technology 7: 285-292.

Geldart, D. and J. Baeyens (1985). The design of distributors for gas-fluidized beds. Powder Technology 42(1): 67-78.

Geldart, D., E. C. Abdullah and A. Verlinden (2007). Characterisation of dry powders. Symposium on Powder Science and Technology - Powders and Sintered Material, Albi, France, Elsevier Science Sa.

Goldstein, J., D. E. Newbury, P. Echlin, D. C. Joy, A. D. Romig, C. E. Lyman, C. Fiori and E. Lifshin (1992). Scanning electron microscopy and x-ray microanalysis. New York, Plenum Publishers.

Graham, C., J. R. Kevin, B. T. Gillian and J. W. G. David (1997). Modeling the crystal morphology of alpha-lactose monohydrate. Journal of Pharmaceutical Sciences 86(1): 135-141.

Grey, R. O. and J. K. Beddow (1969). On the Hausner Ratio and its relationship to some properties of metal powders. Powder Technology 2(6): 323-326.

Guchardi, R., M. Frei, E. John and J. S. Kaerger (2008). Influence of fine lactose and magnesium stearate on low dose dry powder inhaler formulations. International Journal of Pharmaceutics 348(1-2): 10-17.

Guenette, E., A. Barrett, D. Kraus, R. Brody, L. Harding and G. Magee (2009). Understanding the effect of lactose particle size on the properties of DPI formulations using experimental design. International Journal of Pharmaceutics 380(1-2): 80-88.

Gänzle, M. G., G. Haase and P. Jelen (2008). Lactose: Crystallization, hydrolysis and value-added derivatives. International Dairy Journal 18(7): 685-694.

Hamishehkar, H., J. Emami, A. R. Najafabadi, K. Gilani, M. Minaiyan, H. Mandavi and A. Nokhodchi (2010). Influence of carrier particle size, carrier ratio and addition of fine ternary particles on the dry powder inhalation performance of insulin-loaded PLGA microcapsules. Powder Technology 201(3): 289-295.

Hanania, N. A., N. Ambrosino, P. Calverley, M. Cazzola, C. F. Donner and B. Make (2005). Treatments for COPD. Respiratory Medicine 99, Supplement 2: S28-S40.

Harjunen, P., V.-P. Lehto, K. Martimo, E. Suihko, T. Lankinen, P. Paronen and K. Järvinen (2002). Lactose modifications enhance its drug performance in the novel multiple dose Taifun® DPI. European Journal of Pharmaceutical Sciences 16(4-5): 313-321.

Harjunen, P., T. Lankinen, H. Salonen, V.-P. Lehto and K. Järvinen (2003). Effects of carriers and storage of formulation on the lung deposition of a hydrophobic and hydrophilic drug from a DPI. International Journal of Pharmaceutics 263(1-2): 151-163.

Harnby, N. (2000). An engineering view of pharmaceutical powder mixing. Pharmaceutical Science & Technology Today 3(9): 303-309.

Hausner, H. H. (1967). Friction conditions in a mass of metal powder. International Journal of Powder Metallurgy 3(7): 7-13.

Heinrich, M. J., R. N. Sidney and P. B. Robert (1996). The Physics of Granular Materials. Physics Today 49(4): 32-38.

Hersey, J. A. (1975). Ordered Mixing: A New Concept in Powder Mixing Practice. Powder Technology 11: 41--44.

Heyder, J. (2004). Deposition of Inhaled Particles in the Human Respiratory Tract and Consequences for Regional Targeting in Respiratory Drug Delivery. Proceedings of the American Thoracic Society 1(4): 315-320.

Hino, T., T. Serigano, H. Yamamoto, H. Takeuchi, T. Niwa and Y. Kawashima (1998). Particle design of Wogon extract dry powder for inhalation aerosols with granulation method. International Journal of Pharmaceutics 168(1): 59-68.

Ho, R., A. S. Muresan, G. A. Hebbink and J. Y. Y. Heng (2010). Influence of fines on the surface energy heterogeneity of lactose for pulmonary drug delivery. International Journal of Pharmaceutics 388(1-2): 88-94.

Holdich, R. G. (2002). Fundamentals of Particle Technology Shepshed, Midland Information Technology and Publishing.

Hooton, J. C., M. D. Jones and R. Price (2006). Predicting the Behavior of Novel Sugar Carriers for Dry Powder Inhaler Formulations via the Use of a Cohesive–Adhesive Force Balance Approach. Journal of Pharmaceutical Sciences 95(6): 1288-1297.

Horio, M. (2010). Fluidization science, its development and future. Particuology 8(6): 514-524.

Huck, D. (2007). Image Analysis Coupled with Classification – A Powerful Combination for the Study of Agglomeration. Powder 19(1): 42-44.

Hyde, D. M., Q. Hamid and C. G. Irvin (2009). Anatomy, pathology, and physiology of the tracheobronchial tree: Emphasis on the distal airways. Journal of Allergy and Clinical Immunology 124(6, Supplement): S72-S77.

Ikegami, K., Y. Kawashima, H. Takeuchi, H. Yamamoto, D.-I. Momose, N. Saito and N. Isshiki (2000). In vitro inhalation behavior of spherically agglomerated steroid particles with carrier lactose. Advanced Powder Technology 11(3): 323-332.

Ilie, M., E. A. Matida and W. H. Finlay (2008). Asymmetrical aerosol deposition in an idealized mouth with a DPI mouthpiece inlet. Aerosol Science and Technology 42(1): 10-17.

Islam, N., P. Stewart, I. Larson and P. Hartley (2004). Lactose Surface Modification by Decantation: Are Drug-Fine Lactose Ratios the Key to Better Dispersion of Salmeterol Xinafoate from Lactose-Interactive Mixtures? Pharmaceutical Research 21(3): 492-499.

Jain, A. K., M. Jianchang and K. M. Mohiuddin (1996). Artificial neural networks: a tutorial. Computer 29(3): 31-44.

Jones, M. D., J. C. Hooton, M. L. Dawson, A. R. Ferrie and R. Price (2008). An Investigation into the Dispersion Mechanisms of Ternary Dry Powder Inhaler Formulations by the Quantification of Interparticulate Forces. Pharmaceutical Research 25(2): 337-348.

Jones, M. D., J. G. F. Santo, B. Yakub, M. Dennison, H. Master and G. Buckton (2010). The relationship between drug concentration, mixing time, blending order and ternary dry powder inhalation performance. International Journal of Pharmaceutics 391(1-2): 137-147.

Kachrimanis, K., V. Karamyan and S. Malamataris (2003). Artificial neural networks (ANNs) and modeling of powder flow. International Journal of Pharmaceutics 250(1): 13-23.

Kaialy, W., A. Alhalaweh, S. P. Velaga and A. Nokhodchi (2011). Effect of carrier particle shape on dry powder inhaler performance. International Journal of Pharmaceutics(1): 12-23.

Kaialy, W., M. Ticehurst and A. Nokhodchi (2012a). Dry powder inhalers: Mechanistic evaluation of lactose formulations containing salbutamol sulphate. International Journal of Pharmaceutics 423(2): 184-194.

Kaialy, W., G. P. Martin, H. Larhrib, M. D. Ticehurst, E. Kolosionek and A. Nokhodchi (2012b). The influence of physical properties and morphology of crystallised lactose on delivery of salbutamol sulphate from dry powder inhalers. Colloids and Surfaces B: Biointerfaces 89(0): 29-39.

Karhu, M., J. Kuikka, T. Kauppinen, K. Bergström and M. Vidgren (2000). Pulmonary deposition of lactose carriers used in inhalation powders. International Journal of Pharmaceutics 196(1): 95-103.

Karner, S. and N. A. Urbanetz (2011). The impact of electrostatic charge in pharmaceutical powders with specific focus on inhalation-powders. Journal of Aerosol Science 42(6): 428-445.

Kawashima, Y., T. Serigano, T. Hino, H. Yamamoto and H. Takeuchi (1998). Effect of surface morphology of carrier lactose on dry powder inhalation property of pranlukast hydrate. International Journal of Pharmaceutics 172(1-2): 179-188.

Keller, M. (1999). Innovations and perspectives of metered dose inhalers in pulmonary drug delivery. International Journal of Pharmaceutics 186(1): 81-90.

Kinnunen, H., J. Shur, G. A. Hebbink, A. S. Muresan, S. Edge and R. Price (2009). Spectroscopic Investigations into the Structure of Carrier-Based Dry Powder Inhaler Formulations Drug Delivery to the Lungs 20, Edinburgh, The Aerosol Society.

Kirk, J. H., S. E. Dann and C. G. Blatchford (2007). Lactose: A definitive guide to polymorph determination. International Journal of Pharmaceutics 334: 103–114.

Kokhanovsky, A. A. and R. Weichert (2001). Multiple Light Scattering in Laser Particle Sizing. Applied Optics 40(9): 1507-1513.

Krantz, M., H. Zhang and J. Zhu (2009). Characterization of powder flow: Static and dynamic testing. Powder Technology 194(3): 239-245.

Kwauk, M., J. Li and D. Liu (2000). Particulate and aggregative fluidization - 50 years in retrospect. Powder Technology 111(1-2): 3-18.

Labiris, N. R. and M. B. Dolovich (2003). Pulmonary drug delivery. Part II: The role of inhalant delivery devices and drug formulations in therapeutic effectiveness of aerosolized medications. British Journal of Clinical Pharmacology 56(6): 600-612.

Larhrib, H., G. P. Martin, C. Marriott and D. Prime (2003a). The influence of carrier and drug morphology on drug delivery from dry powder formulations. International Journal of Pharmaceutics 257(1-2): 283-296.

Larhrib, H., G. P. Martin, D. Prime and C. Marriott (2003b). Characterisation and deposition studies of engineered lactose crystals with potential for use as a carrier for aerosolised salbutamol sulfate from dry powder inhalers. European Journal of Pharmaceutical Sciences 19(4): 211-221.

Larhrib, H., X. M. Zeng, G. P. Martin, C. Marriott and J. Pritchard (1999). The use of different grades of lactose as a carrier for aerosolised salbutamol sulphate. International Journal of Pharmaceutics 191: 1-14.

Le, V. N. P., E. Robins and M. P. Flament (2010). Air permeability of powder: A potential tool for Dry Powder Inhaler formulation development. European Journal of Pharmaceutics and Biopharmaceutics 76(3): 464-469.

Le, V. N. P., E. Robins and M. P. Flament (2012a). Agglomerate behaviour of fluticasone propionate within dry powder inhaler formulations. European Journal of Pharmaceutics and Biopharmaceutics 80(3): 596-603.

Le, V. N. P., H. Bierend, E. Robins, H. Steckel and M. P. Flament (2012b). Influence of the lactose grade within dry powder formulations of fluticasone propionate and terbutaline sulphate. International Journal of Pharmaceutics 422(1–2): 75-82.

Le, V. N. P., T. H. Hoang Thi, E. Robins and M. P. Flament (2012c). In vitro evaluation of powders for inhalation: The effect of drug concentration on particle detachment. International Journal of Pharmaceutics 424(1–2): 44-49.

Lipworth, B. J. (1996). Pharmacokinetics of inhaled drugs. British Journal of Clinical Pharmacolology 42(6): 697-705.

Loezos, P. N., P. Costamagna and S. Sundaresan (2002). The role of contact stresses and wall friction on fluidization. Chemical Engineering Science 57(24): 5123-5141.

Longest, P. W., M. Hindle, S. Das Choudhuri and J. Xi (2008). Comparison of ambient and spray aerosol deposition in a standard induction port and more realistic mouth-throat geometry. Journal of Aerosol Science 39(7): 572-591.

Louey, M., D., P. Mulvaney and P. Stewart (2001). Characterisation of adhesional properties of lactose carriers using atomic force microscopy. Journal of Pharmaceutical and Biomedical Analysis 25: 559-567.

Louey, M., D. and P. J. Stewart (2002). Particle Interactions Involved in Aerosol Dispersion of Ternary Interactive Mixtures. Pharmaceutical Research 19(10): 1524-1531.

Louey, M., D., S. Razia and P. J. Stewart (2003). Influence of physico-chemical carrier properties on the in vitro aerosol deposition from interactive mixtures. International Journal of Pharmaceutics 252: 87–98.

Lough, W. J. and I. W. Wainer (1995). High Performance Liquid Chromatography: Fundamental Principles and Practice. Glasgow, Blackie Academic & Professional.

Lucas, P., K. Anderson and J. N. Staniforth (1998). Protein deposition from dry powder inhalers: Fine particle multiplets as performance modifiers. Pharmaceutical Research 15(4): 562-569.

Marple, V. A., B. A. Olson and N. C. Miller (1995). A Low-Loss Cascade Impactor with Stage Collection Cups: Calibration and Pharmaceutical Inhaler Applications. Aerosol Science and Technology 22(1): 124-134.

Marple, V. A., D. L. Roberts, F. J. Romay, N. C. Miller, K. G. Truman, M. Van Oort, B. Olsson, M. J. Holroyd, J. P. Mitchell and D. Hochrainer (2003a). Next Generation Pharmaceutical Impactor (A New Impactor for Pharmaceutical Inhaler Testing). Part I: Design. Journal of Aerosol Medicine 16(3): 283-299.

Marple, V. A., B. A. Olson, K. Santhanakrishnan, J. P. Mitchell, S. C. Murray and B. L. Hudson-Curtis (2003b). Next Generation Pharmaceutical Impactor (A New Impactor for Pharmaceutical Inhaler Testing). Part II: Archival Calibration. Journal of Aerosol Medicine 16(3): 301-324.

Marriott, C., H. B. MacRitchie, X.-M. Zeng and G. P. Martin (2006). Development of a laser diffraction method for the determination of the particle size of aerosolised powder formulations. International Journal of Pharmaceutics 326(1–2): 39-49.

McDonald, K. J. and G. P. Martin (2000). Transition to CFC-free metered dose inhalers — into the new millennium. International Journal of Pharmaceutics 201(1): 89-107.

Mendyk, A. and R. Jachowicz (2005). Neural network as a decision support system in the development of pharmaceutical formulation--focus on solid dispersions. Expert Systems with Applications 28(2): 285-294.

Mishra, B. K. and C. Thornton (2001). Impact breakage of particle agglomerates. International Journal of Mineral Processing 61(4): 225-239.

Mohammadi, M. S. and N. Harnby (1997). Bulk density modelling as a means of typifying the microstructure and flow characteristics of cohesive powders. Powder Technology 92(1): 1-8.

Molerus, O. (1982). Interpretation of Geldart's type A, B, C and D powders by taking into account interparticle cohesion forces. Powder Technology 33(1): 81-87.

Mueannoom, W., A. Srisongphan, K. M. G. Taylor, S. Hauschild and S. Gaisford (2012). Thermal ink-jet spray freeze-drying for preparation of excipient-free salbutamol sulphate for inhalation. European Journal of Pharmaceutics and Biopharmaceutics 80(1): 149-155.

Muresan, A. S. and G. A. Hebbink (2009). Dry powder inhalers: modelling dose dependent Fine Particle Dose data is a useful tool in understanding the DPI functionality. Drug Delivery to the Lungs 20, Edinburgh, The Aerosol Society.

Murphy, B. M., S. W. Prescott and I. Larson (2005). Measurement of lactose crystallinity using Raman spectroscopy. Journal of Pharmaceutical and Biomedical Analysis 38(1): 186-190.

Narang, A. S., V. M. Rao and K. S. Raghavan (2009). Chapter 6 - Excipient Compatibility. Developing Solid Oral Dosage Forms. Edited by Q. Yihong, C. Yisheng, G. Z. Z. Geoffet. San Diego, Academic Press**:** 125-145.

Newell, R. L. M. (2003). Anatomy of the Post-laryngeal Airways, Lungs and Diaphragm. Surgery (Oxford) 21(3): 57-61.

Newton, R. G. (1982). Scattering theory of waves and particles. New York, Springer-Verlag New York, Inc.

Nichols, G., S. Byard, M. J. Bloxham, J. Botterill, N. J. Dawson, A. Dennis, V. Diart, N. C. North and J. D. Sherwood (2002). A review of the terms agglomerate and aggregate with a recommendation for nomenclature used in powder and particle characterization. Journal of Pharmaceutical Sciences 91(10): 2103-2109.

Niven, R. W., F. D. Lott, A. Y. Ip, K. D. Somaratne and M. Kearney (1994). Development and use of an in vitro system to evaluate inhaler devices. International Journal of Pharmaceutics 101(1-2): 81-87.

Nolan, L. M., L. Tajber, B. F. McDonald, A. S. Barham, O. I. Corrigan and A. M. Healy (2009). Excipient-free nanoporous microparticles of budesonide for pulmonary delivery. European Journal of Pharmaceutical Sciences 37(5): 593-602.

Ojha, R. P., P. A. Lemieux, P. K. Dixon, A. J. Liu and D. J. Durian (2004). Statistical mechanics of a gas-fluidized particle. Nature 427(6974): 521-523.

Olsson, B. O. and L. Asking (1994). A Model for the Effect of Inhalation Device Flow Resistance on the Peak Inspiratory Flow Rate and Its Application in Pharmaceutical Testing. Journal of Aerosol Medicine 7(2): 201-204.

Ooi, J., D. Traini, S. Hoe, W. Wong and P. M. Young (2011). Does carrier size matter? A fundamental study of drug aerosolisation from carrier based dry powder inhalation systems. International Journal of Pharmaceutics 413(1-2): 1-9.

Parker, A. (2009). Functionality of excipients in medicinal products. Chimica Oggi/ Chemistry Today 27(5): 5-7.

Patton, J. S., C. S. Fishburn and J. G. Weers (2004). The Lungs as a Portal of Entry for Systemic Drug Delivery. Proceedings of the American Thoracic Society 1(4): 338-344.

Patton, J. S. and P. R. Byron (2007). Inhaling medicines: delivering drugs to the body through the lungs. Nature Reviews in Drug Discovery 6(1): 67-74.

Pifferi, G., P. Santoro and M. Pedrani (1999). Quality and functionality of excipients. Il Farmaco 54(1–2): 1-14.

Pilcer, G., F. Vanderbist and K. Amighi (2008). Correlations between cascade impactor analysis and laser diffraction techniques for the determination of the particle size of aerosolised powder formulations. International Journal of Pharmaceutics 358(1-2): 75-81.

Pilcer, G. and K. Amighi (2011). Formulation strategy and use of excipients in pulmonary drug delivery. International Journal of Pharmaceutics 392(1-2): 1-19.

Pilcer, G., N. Wauthoz and K. Amighi (2012). Lactose characteristics and the generation of the aerosol. Advanced Drug Delivery Reviews 64(3): 233-256.

Pitchayajittipong, C., R. Price, J. Shur, J. S. Kaerger and S. Edge (2010). Characterisation and functionality of inhalation anhydrous lactose. International Journal of Pharmaceutics 390(2): 134-141.

Podczeck, F. (1998). The relationship between physical properties of lactose monohydrate and the aerodynamic behaviour of adhered drug particles. International Journal of Pharmaceutics 160: 119–130.

Podczeck, F. (1999). The Influence of Particle Size Distribution and Surface Roughness of Carrier Particles on the in vitro Properties of Dry Powder Inhalation. Aerosol Science and Technology 31(4): 301-321.

Rajalahti, T. and O. M. Kvalheim (2011). Multivariate data analysis in pharmaceutics: A tutorial review. International Journal of Pharmaceutics 417(1–2): 280-290.

Raman, C. V. and K. S. Krishnan (1928). A New type of secondary radiation. Nature 121(31st of March): 501-502.

Rantanen, J., H. Wikström, R. Turner and L. S. Taylor (2004). Use of In-Line Near-Infrared Spectroscopy in Combination with Chemometrics for Improved Understanding of Pharmaceutical Processes. Analytical Chemistry 77(2): 556-563.

Raula, J., A. Lähde and E. I. Kauppinen (2009). Aerosolization behavior of carrier-free l-leucine coated salbutamol sulphate powders. International Journal of Pharmaceutics 365(1-2): 18-25.

Rietema, K. (1984). Powders, what are they? Powder Technology 37(1): 5-23.

Robertson, D. L. N., J. N. Staniforth and B. J. Meakin (1996). The influence of (Pseudo)polymorphic forms of lactose on dry powder inhaler performance. European Journal of Pharmaceutical Sciences 4, Supplement 1(0): S179.

Roggo, Y., K. Degardin and P. Margot (2010). Identification of pharmaceutical tablets by Raman spectroscopy and chemometrics. Talanta 81(3): 988-995.

Rogueda, P. G. A., R. Price, T. Smith, P. M. Young and D. Traini (2011). Particle synergy and aerosol performance in non-aqueous liquid of two combinations metered dose inhalation formulations: An AFM and Raman investigation. Journal of Colloid and Interface Science 361(2): 649-655.

Saleem, I., H. Smyth and M. Telko (2008). Prediction of dry powder inhaler formulation performance from surface energetics and blending dynamics. Drug Development and Industrial Pharmacy 34(9): 1002-1010.

Sanders, M. (2007). Inhalation therapy: an historical review. Primary Care Respiratory Journal 16(2): 71-81.

Šašić, S. and L. Harding (2010). Global illumination Raman chemical imaging of a combination of two drug molecules in a dry powder inhaler formulation. Analytical Methods 2(10): 1528-1535.

Schmidt, A., S. Zidowitz, A. Kriete, T. Denhard, S. Krass and H.-O. Peitgen (2004). A digital reference model of the human bronchial tree. Computerized Medical Imaging and Graphics 28(4): 203-211.

Schulze, D. (2010). "Flow Properties of Powders and Bulk Solids." Retrieved 26/12/2011, from http://www.dietmar-schulze.de/grdle1.pdf.

Schulze, D. and A. Wittmaier (2003). Flow Properties of Highly Dispersed Powders at Very Small Consolidation Stresses. Chemical Engineering & Technology 26(2): 133-137.

Schwedes, J. and D. Schulze (1990). Measurement of flow properties of bulk solids. Powder Technology 61(1): 59-68.

Seville, J. P. K., C. D. Willett and P. C. Knight (2000). Interparticle forces in fluidisation: a review. Powder Technology 113(3): 261-268.

Shah, R. B., M. A. Tawakkul and M. A. Khan (2008). Comparative evaluation of flow for pharmaceutical powders and granules. AAPS PharmSciTech 9(1): 250-258.

Shaw, P. E. (1917). Experiments on Tribo-Electricity. I. The Tribo-Electric Series. Proceedings of the Royal Society of London. Series A, Containing Papers of a Mathematical and Physical Character 94(656): 16-33.

Shur, J., H. Harris, M. D. Jones, J. S. Kaerger and R. Price (2008). The role of fines in the modification of the fluidization and dispersion mechanism within dry powder inhaler formulations. Pharmaceutical Research 25(7): 1931-1940.

Shur, J. and R. Price (2008b). Fine tuning DPI formulas. Manufacturing chemist. June 2008.

Smith, I. J. and M. Parry-Billings (2003). The inhalers of the future? A review of dry powder devices on the market today. Pulmonary Pharmacology & Therapeutics 16(2): 79-95.

Srichana, T., G. P. Martin and C. Marriott (1998a). Dry powder inhalers: The influence of device resistance and powder formulation on drug and lactose deposition in vitro. European Journal of Pharmaceutical Sciences 7: 73–80.

Srichana, T., G. P. Martin and C. Marriott (1998b). On the relationship between drug and carrier deposition from dry powder inhalers in vitro. International Journal of Pharmaceutics 167: 13–23.

Srichana, T., A. Brain, G. P. Martin and C. Marriott (1998c). The determination of drug-carrier interactions in dry powder inhaler formulations. Journal of Aerosol Science 29, Supplement 2: S757-S758.

Staniforth, J. N. (2000). Carrier particles for use in dry powder inhalers. International patent number 6153224

Steckel, H. and B. W. Müller (1997).In vitro evaluation of dry powder inhalers I: drug deposition of commonly used devices. International Journal of Pharmaceutics 154(1): 19-29.

Steckel, H. and H. G. Brandes (2004a). A novel spray-drying technique to produce low density particles for pulmonary delivery. International Journal of Pharmaceutics 278(1): 187-195.

Steckel, H., P. Markefka, H. te Wierik and R. Kammelar (2004b). Functionality testing of inhalation grade lactose. European Journal of Pharmaceutics and Biopharmaceutics 57: 495–505.

Steckel, H., P. Markefka, H. te Wierik and R. Kammelar (2006). Effect of milling and sieving on functionality of dry powder inhalation products. International Journal of Pharmaceutics 309(1-2): 51-59.

Steele, D., P. Young, R. Price, T. Smith, S. Edge and D. Lewis (2004). The potential use of raman mapping to investigate in vitro deposition of combination pressurized metered-dose inhalers. The AAPS Journal 6(4): 41-44.

Stevens, J. J. W. M. and J. G. Jones (1995). Functional anatomy and pathophysiology of the upper airway. Baillière's Clinical Anaesthesiology 9(2): 213-234.

Subero, J. and M. Ghadiri (2001). Breakage patterns of agglomerates. Powder Technology 120(3): 232-243.

Susi, H. and J. S. Ard (1974). Laser-raman spectra of lactose. Carbohydrate Research 37(2): 351-354.

Svozil, D., V. Kvasnicka and J. Pospichal (1997). Introduction to multi-layer feed-forward neural networks. Chemometrics and Intelligent Laboratory Systems 39(1): 43-62.

Takayama, K., J. Takahara, M. Fujikawa, H. Ichikawa and T. Nagai (1999). Formula optimization based on artificial neural networks in transdermal drug delivery. Journal of Controlled Release 62(1–2): 161-170.

Tay, T., S. Das and P. Stewart (2010). Magnesium stearate increases salbutamol sulphate dispersion: What is the mechanism? International Journal of Pharmaceutics 383(1–2): 62-69.

Tee, S. K., C. Marriott, X. M. Zeng and G. P. Martin (2000). The use of different sugars as fine and coarse carriers for aerosolised salbutamol sulphate. International Journal of Pharmaceutics 208: 111–123.

Telko, M. J. and A. J. Hickey (2005). Dry Powder Inhaler Formulation. Respiratory Care 50(9): 1209-1227.

Thalberg, K., D. Lindholm and A. Axelsson (2004). Comparison of different flowability tests for powders for inhalation. Powder Technology 146(3): 206-213.

Theophilus, A., A. Moore, D. Prime, S. Rossomanno, B. Whitcher and H. Chrystyn (2006). Co-deposition of salmeterol and fluticasone propionate by a combination inhaler. International Journal of Pharmaceutics 313(1–2): 14-22.

Thoren, P., A. Wallin, P. J. Whitehead and T. Sandström (2001). The effect of different concentrations of lactose powder on the airway function of adult asthmatics. Respiratory Medicine 95(11): 870-875.

Tobyn, M., J. Staniforth, D. Morton, Q. Harmer and M. E. Newton (2004). Active and intelligent inhaler device development. International Journal of Pharmaceutics 277: 31-37.

Tong, H. H. Y., B. Y. Shekunov, P. York and A. H. L. Chow (2006). Predicting the Aerosol Performance of Dry Powder Inhalation Formulations by Interparticulate Interaction Analysis using Inverse Gas Chromatography. Journal of Pharmaceutical Sciences 95(1): 228-233.

Traini, D., P. M. Young, F. Thielmann and M. Acharya (2008). The Influence of Lactose Pseudopolymorphic Form on Salbutamol Sulfate-Lactose Interactions in DPI Formulations. Drug Development and Industrial Pharmacy 34(9): 992-1001.

Tsuda, A., F. S. Henry and J. P. Butler (2008). Gas and aerosol mixing in the acinus. Respiratory Physiology & Neurobiology 163(1–3): 139-149.

Tuley, R., J. Shrimpton, M. D. Jones, R. Price, M. Palmer and D. Prime (2008). Experimental observations of dry powder inhaler dose fluidisation. International Journal of Pharmaceutics 358: 238–247.

Valderrama, J. O. (2010). The legacy of Johannes Diderik van der Waals, a hundred years after his Nobel Prize for physics. The Journal of Supercritical Fluids 55(2): 415-420.

Valverde, J. M., A. Ramos, A. Castellanos and P. K. Watson (1998). The tensile strength of cohesive powders and its relationship to consolidation, free volume and cohesivity. Powder Technology 97: 237-245.

Valverde, J. M., A. Castellanos, A. Ramos, T. Perez Alberto, A. Morgan Michael and P. K. Watson (2000). An automated apparatus for measuring the tensile strength and compressibility of fine cohesive powders. Review of Scientific Instruments 71(7): 2791-2795.

Valverde, J. M., A. Castellanos and M. A. S. Quintanilla (2003). The memory of granular materials. Contemporary Physics 44(5): 389 – 399.

Vankeirsbilck, T., A. Vercauteren, W. Baeyens, G. Van der Weken, F. Verpoort, G. Vergote and J. P. Remon (2002). Applications of Raman spectroscopy in pharmaceutical analysis. Trends in Analytical Chemistry 21(12): 869-877.

Visser, J. (1989). Van der Waals and other cohesive forces affecting powder fluidization. Powder Technology 58(1): 1-10.

Voss, A. and W. H. Finlay (2002). Deagglomeration of dry powder pharmaceutical aerosols. International Journal of Pharmaceutics 248(1-2): 39-50.

Wang, X. S. and M. J. Rhodes (2004). Mechanistic study of defluidization by numerical simulation. Chemical Engineering Science 59(1): 215-222.

Wartewig, S. and R. H. H. Neubert (2005). Pharmaceutical applications of Mid-IR and Raman spectroscopy. Advanced Drug Delivery Reviews 57(8): 1144-1170.

Watling, C. P., J. A. Elliott and R. E. Cameron (2010). Entrainment of lactose inhalation powders: A study using laser diffraction. European Journal of Pharmaceutical Sciences 40(4): 352-358.

Weber, M. W. and C. M. Hrenya (2006). Square-well model for cohesion in fluidized beds. Chemical Engineering Science 61(14): 4511-4527.

Weibel, E. R., B. Sapoval and M. Filoche (2005). Design of peripheral airways for efficient gas exchange. Respiratory Physiology & Neurobiology 148(1–2): 3-21.

Welte, T. and D. A. Groneberg (2006). Asthma and COPD. Experimental and Toxicologic Pathology 57, Supplement 2(0): 35-40.

WHO. (2012). "Asthma, Fact sheet No 307, May 2011." Retrieved 11/02/2012, from http://www.who.int/mediacentre/factsheets/fs307/en/index.html.

Widjaja, E. and R. K. H. Seah (2008). Application of Raman microscopy and band-target entropy minimization to identify minor components in model pharmaceutical tablets. Journal of Pharmaceutical and Biomedical Analysis 46(2): 274-281.

William, M. (2003). COPD: causes and pathology. Medicine 31(12): 71-75.

Williams, J. C. (1968). The mixing of dry powders. Powder Technology 2(1): 13-20.

Wright, P. C. and J. A. Raper (1998). Examination of dispersed liquid-phase three-phase fluidized beds Part 1. Non-porous, uniform particle systems. Powder Technology 97(3): 208-226.

Willen, U. (2008). Automation in image analysis for particle size and shape measurement. G.I.T. Laboratory Journal 7-8: 34-36

Wright, P. C. and J. A. Raper (1998). Examination of dispersed liquid-phase three-phase fluidized beds Part 1. Non-porous, uniform particle systems. Powder Technology 97(3): 208-226.

Xu, Z., H. M. Mansour, T. Mulder, R. McLean, J. Langridge and A. J. Hickey (2010). Dry powder aerosols generated by standardized entrainment tubes from drug blends with lactose monohydrate: 1. Albuterol sulfate and disodium cromoglycate. Journal of Pharmaceutical Sciences 99(8): 3398-3414.

Young, P. A., S. Edge, D. Traini, M. D. Jones, R. Price, D. El-Sabawi, C. Urry and C. Smith (2005). The influence of dose on the performance of dry powder inhalation systems. International Journal of Pharmaceutics 296(1-2): 26-33.

Young, P. M., P. Kwok, H. Adi, H. K. Chan and D. Traini (2009). Lactose Composite Carriers for Respiratory Delivery. Pharmaceutical Research 26(4): 802-810.

Young, P. M., O. Wood, J. Ooi and D. Traini (2011). The influence of drug loading on formulation structure and aerosol performance in carrier based dry powder inhalers. International Journal of Pharmaceutics 416(1): 129-135.

Zeng, X. M., G. P. Martin, S.-K. Tee and C. Marriott (1998).The role of fine particle lactose on the dispersion and deaggregation of salbutamol sulphate in an air stream in vitro. International Journal of Pharmaceutics 176: 99-110.

Zeng, X. M., G. P. Martin, S.-K. Tee, A. A. Ghoush and C. Marriott (1999). Effects of particle size and adding sequence of fine lactose on the deposition of salbutamol sulphate from a dry powder formulation. International Journal of Pharmaceutics 182 133–144.

Zeng, X. M., G. P. Martin, C. Marriott and J. Pritchard (2000a). The influence of carrier morphology on drug delivery by dry powder inhalers. International Journal of Pharmaceutics 200: 93-106.

Zeng, X. M., K. H. Pandhal and G. P. Martin (2000b).The influence of lactose carrier on the content homogeneity and dispersibility of beclomethasone dipropionate from dry powder aerosols. International Journal of Pharmaceutics 197(1-2): 41-52.

Zeng, X. M., G. P. Martin and C. Marriott (2001a). Particulate interactions in dry powder formulations for inhalation, Taylor & Francis, London.

Zeng, X. M., G. P. Martin, C. Marriott and J. Pritchard (2001b). Lactose as a Carrier in Dry Powder Formulations: The Infuence of Surface Characteristics on Drug Delivery. Journal of Pharmaceutical Sciences 90(9).

Zeng, X. M., G. P. Martin, C. Marriott and J. Pritchard (2001c).The use of lactose recrystallised from carbopol gels as a carrier for aerosolised salbutamol sulphate. European Journal of Pharmaceutics and Biopharmaceutics 51(1): 55-62.

Zhang, Y., K. Gilbertson and W. H. Finlay (2007). In Vivo-In Vitro Comparison of Deposition in Three Mouth-Throat Models with Qvar® and Turbuhaler® Inhalers. Journal of Aerosol Medicine 20(3): 227-235.

Zhou, T. and H. Li (1999). Effects of adding different size particles on fluidization of cohesive particles. Powder Technology 102(3): 215-220.

Zhou, Q. T., B. Armstrong, I. Larson, P. J. Stewart and D. A. V. Morton (2010). Understanding the influence of powder flowability, fluidization and de-agglomeration characteristics on the aerosolization of pharmaceutical model powders. European Journal of Pharmaceutical Sciences 40(5): 412-421.

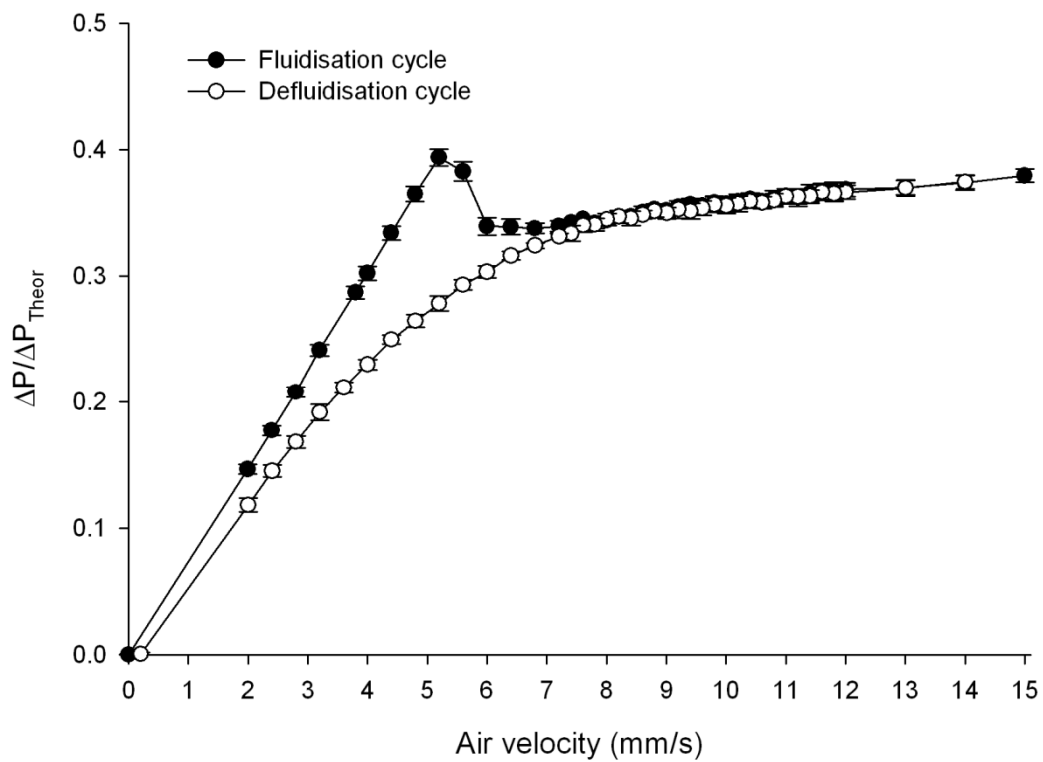# APPENDIX I   FLUIDISATION-DEFLUIDISATION CURVES OF THE FLUTICASONE PROPIONATE FORMULATIONS STUDIED IN CHAPTER 3
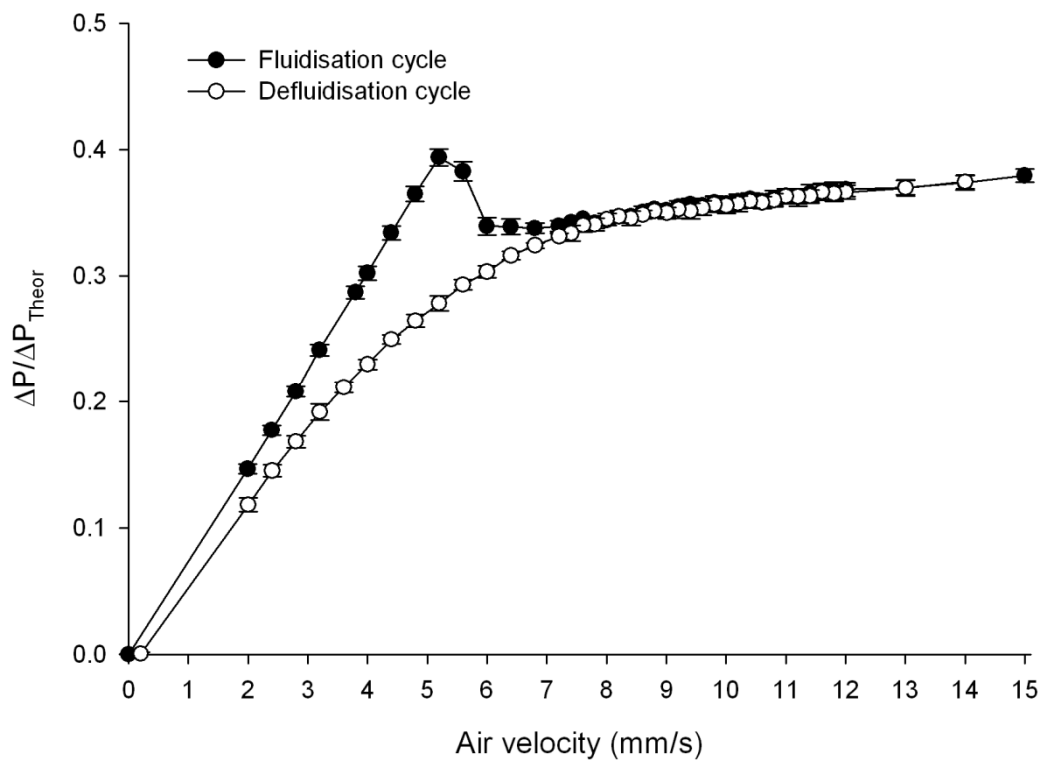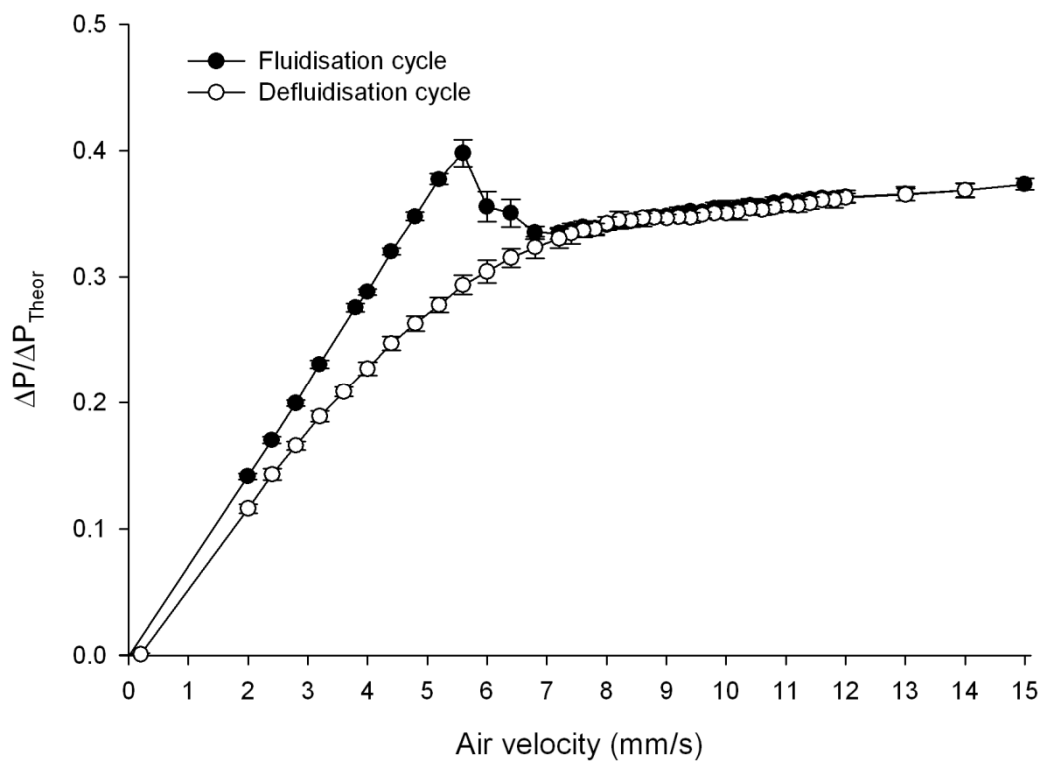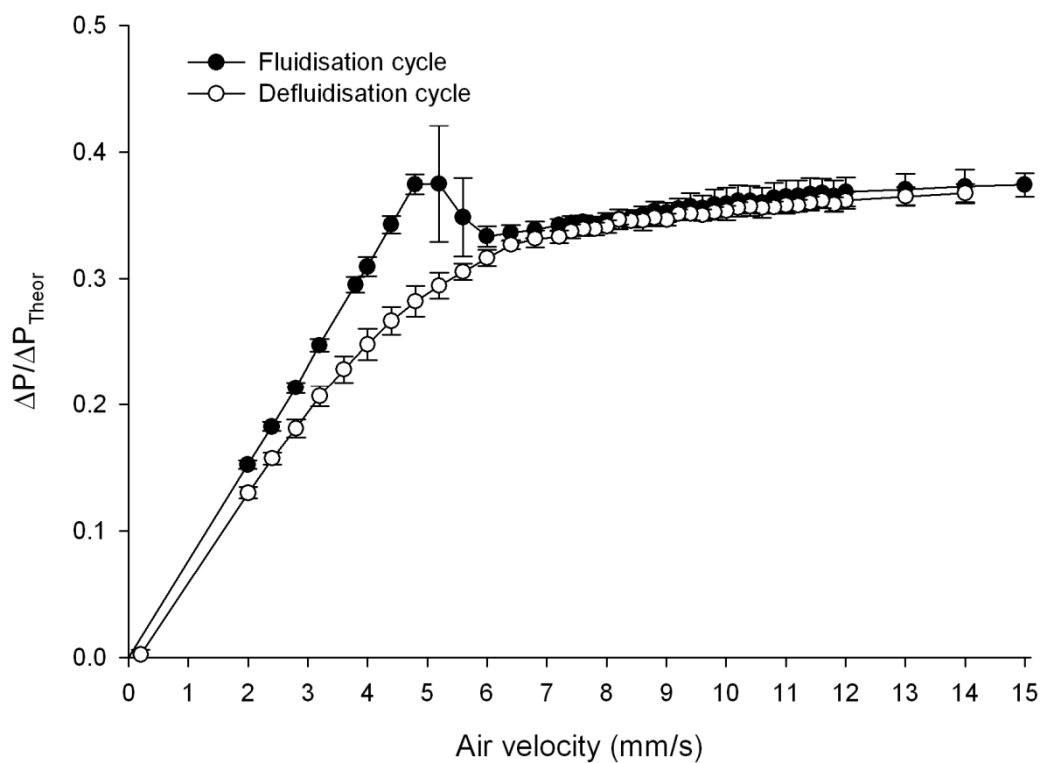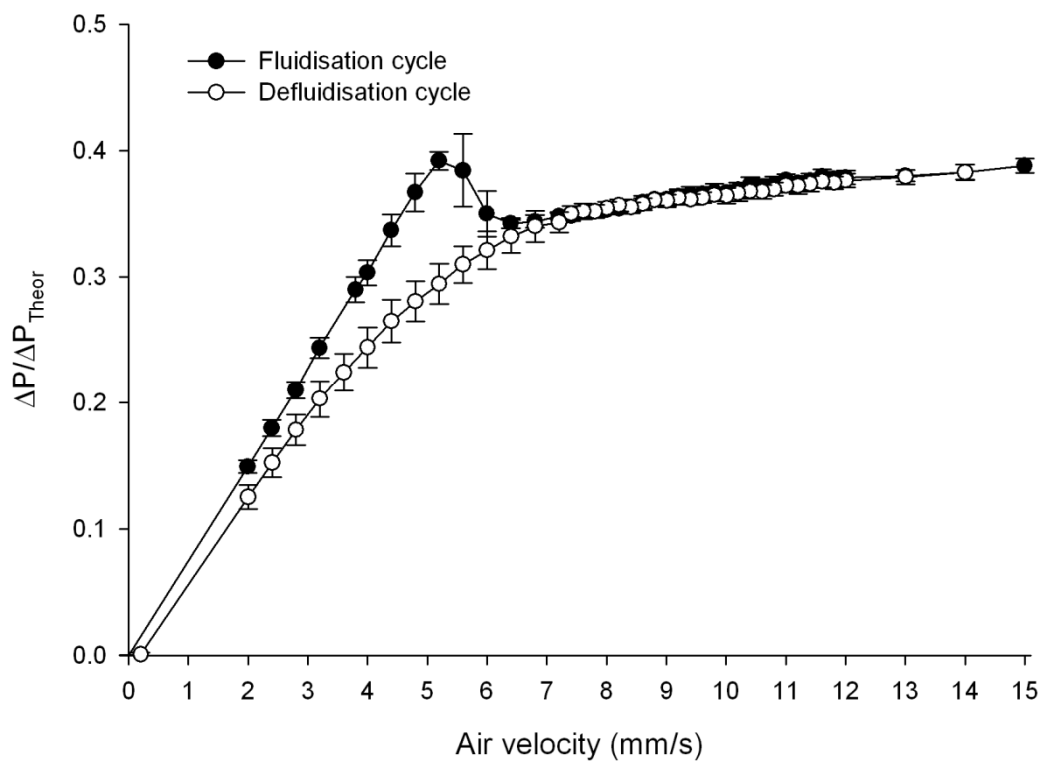
LH100
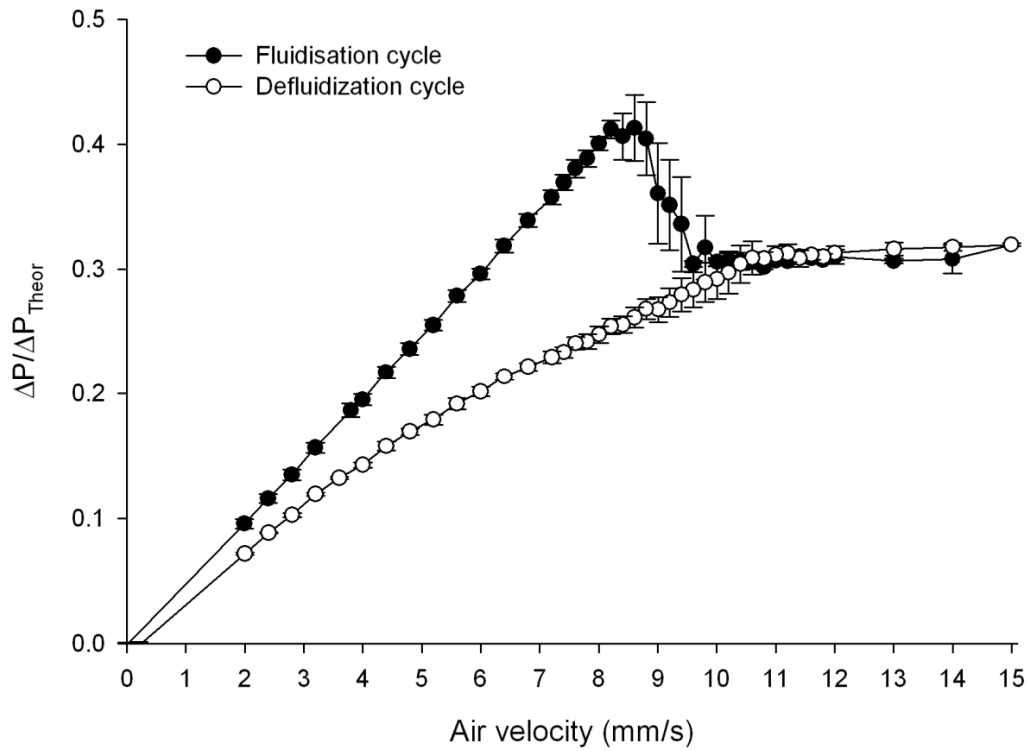
0.02% FP in LH100
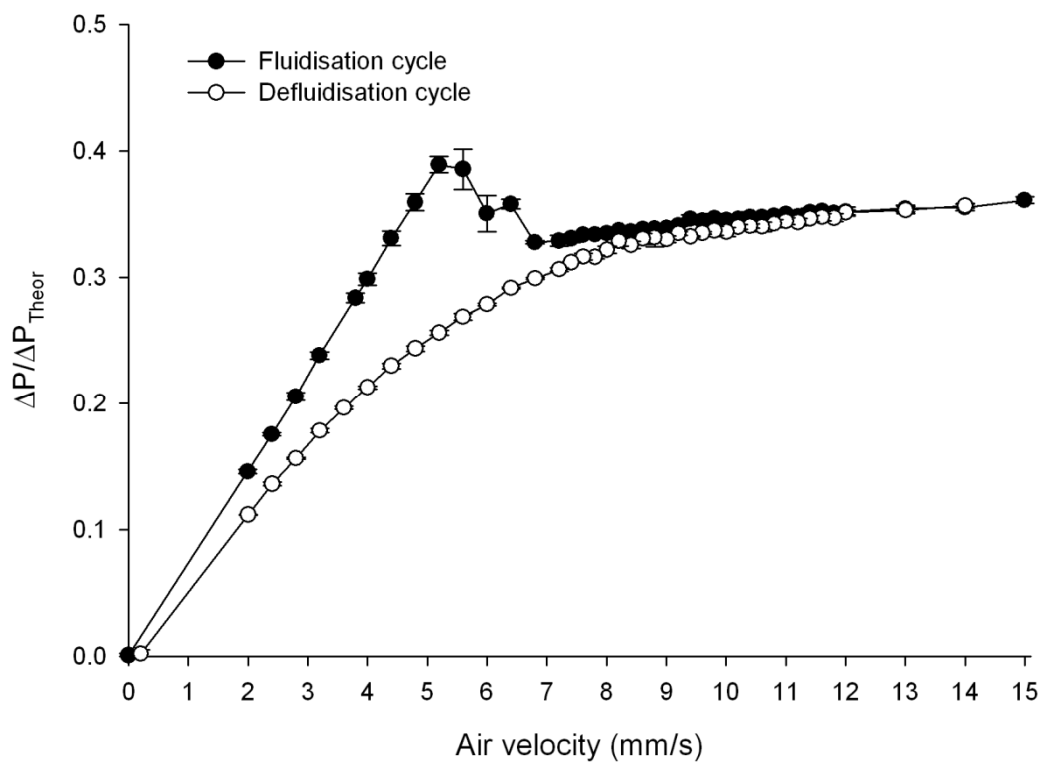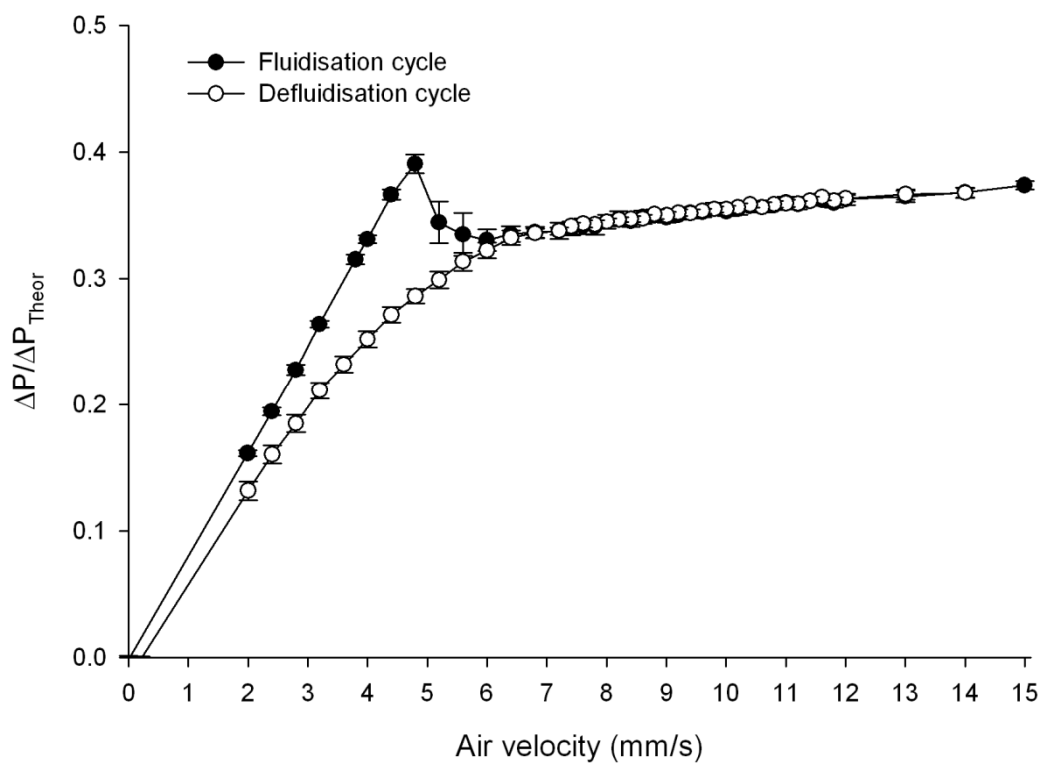
0.05% FP in LH100

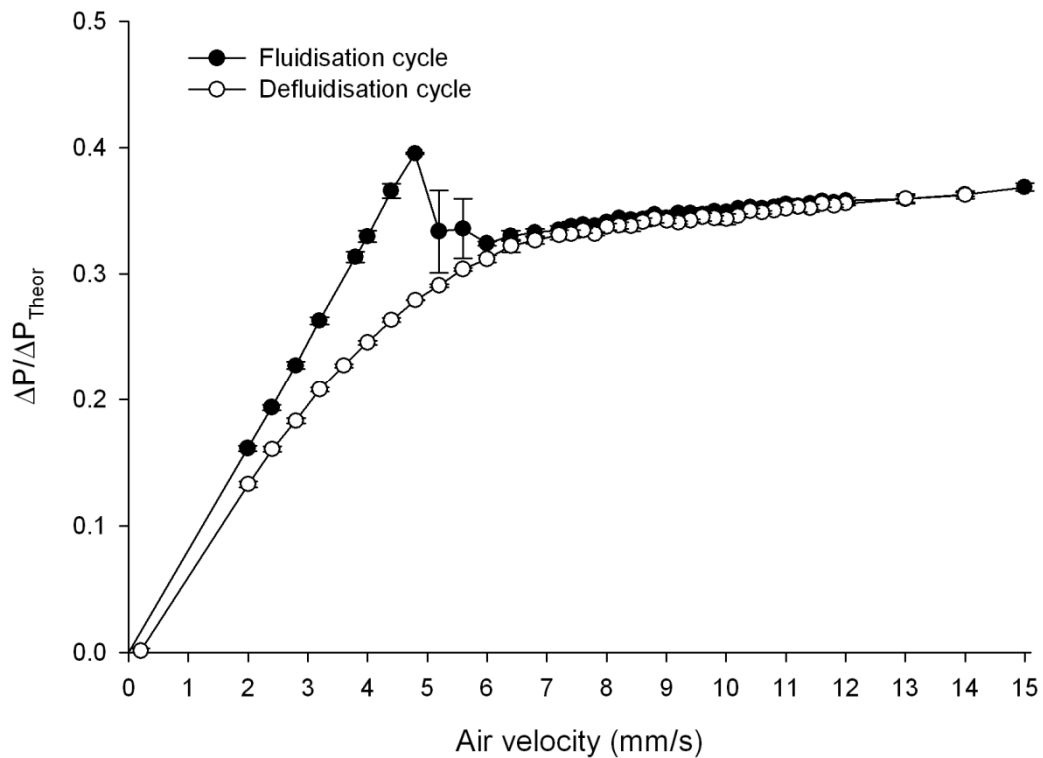
0.08% FP in LH100

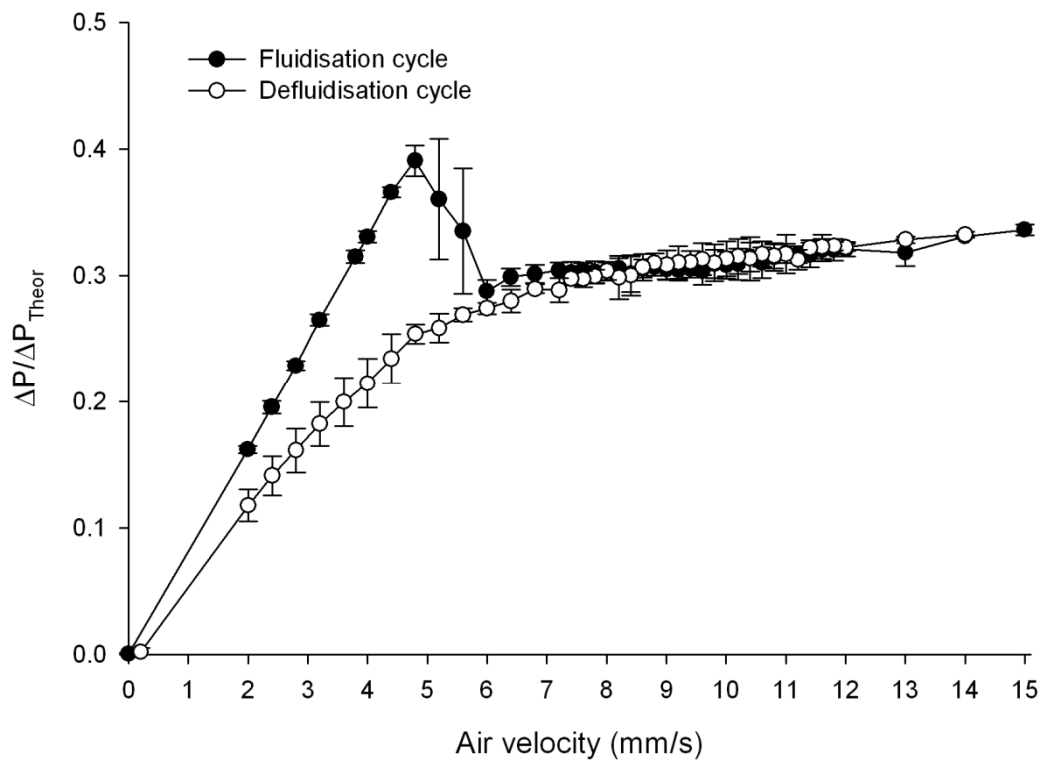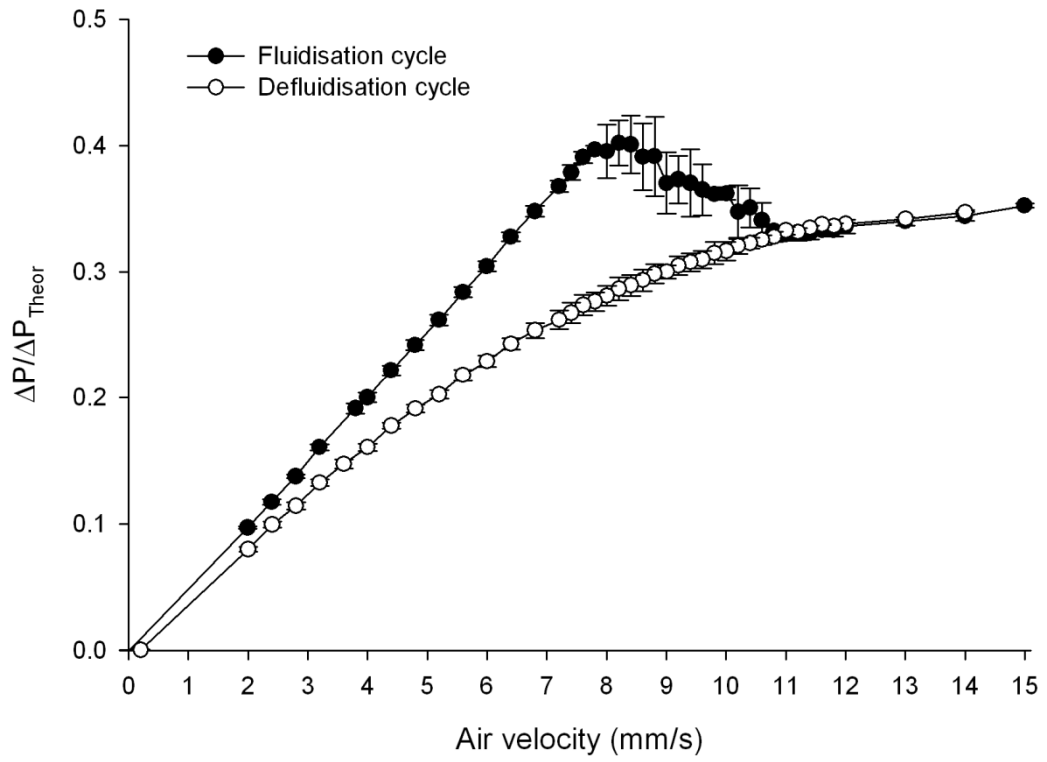**0.10% FP in LH100**

0.15% FP in LH100

0.20% FP in LH100

0.40% FP in LH100

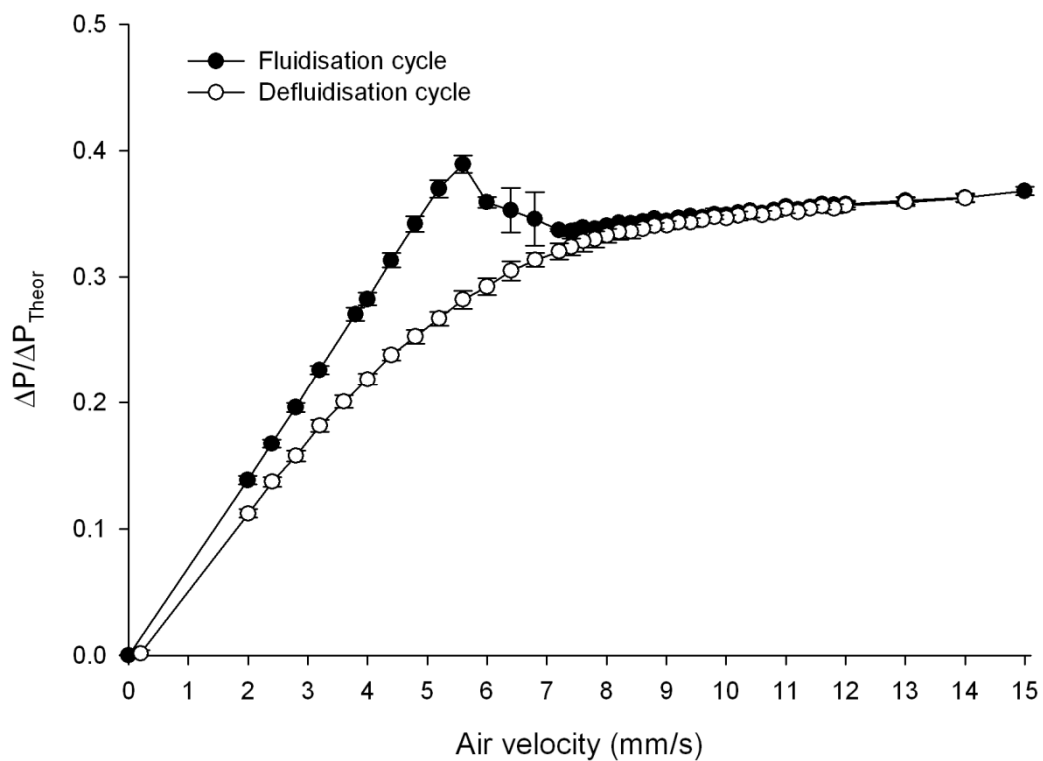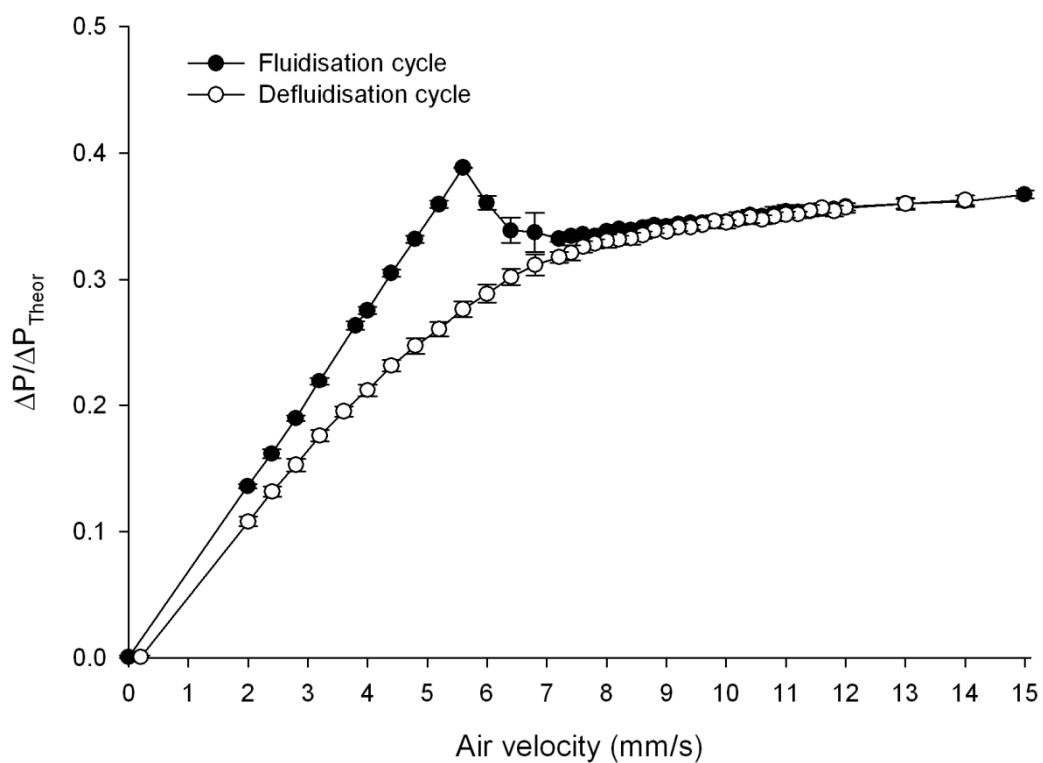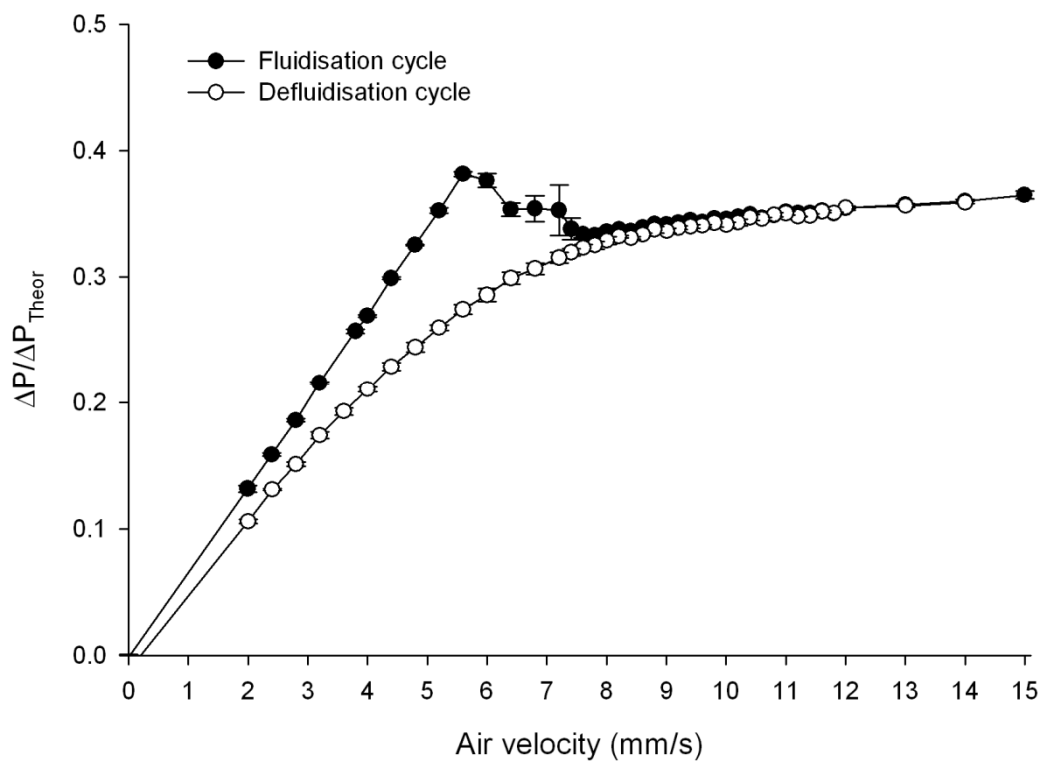## 1.00% FP in LH100

2.00% FP in LH100

SV010
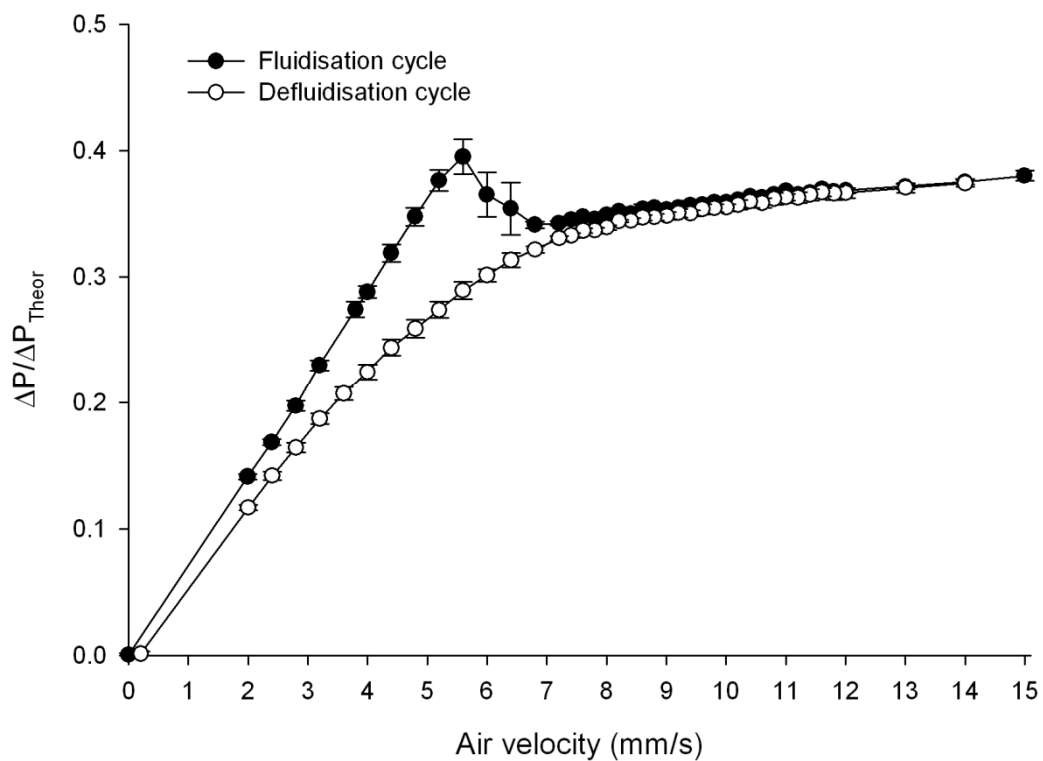

0.02% FP in SV010
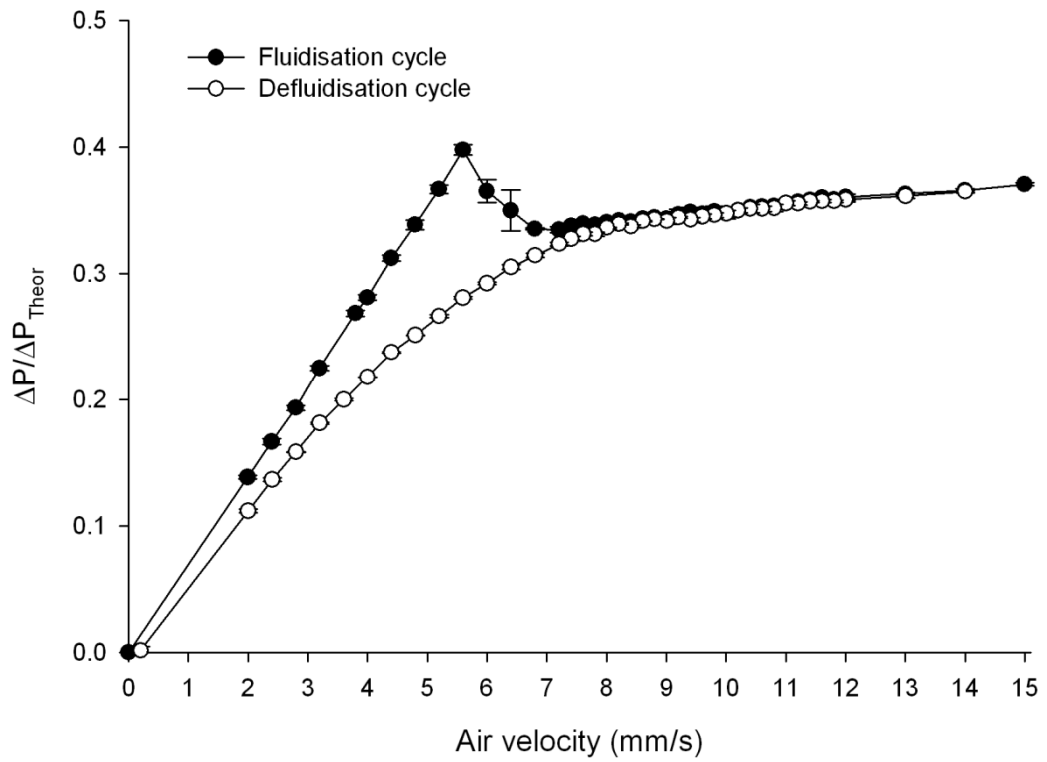
0.05% FP in SV010

0.08% FP in SV010

0.10% FP in SV010

0.20% FP in SV010
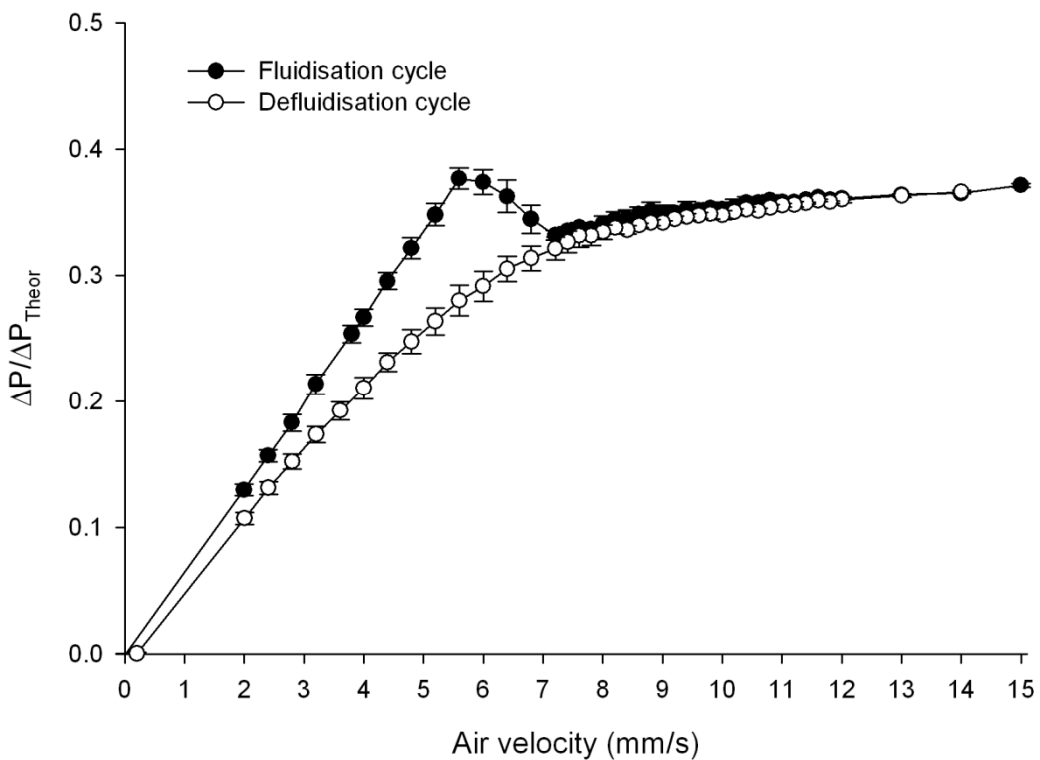
0.30% FP in SV010

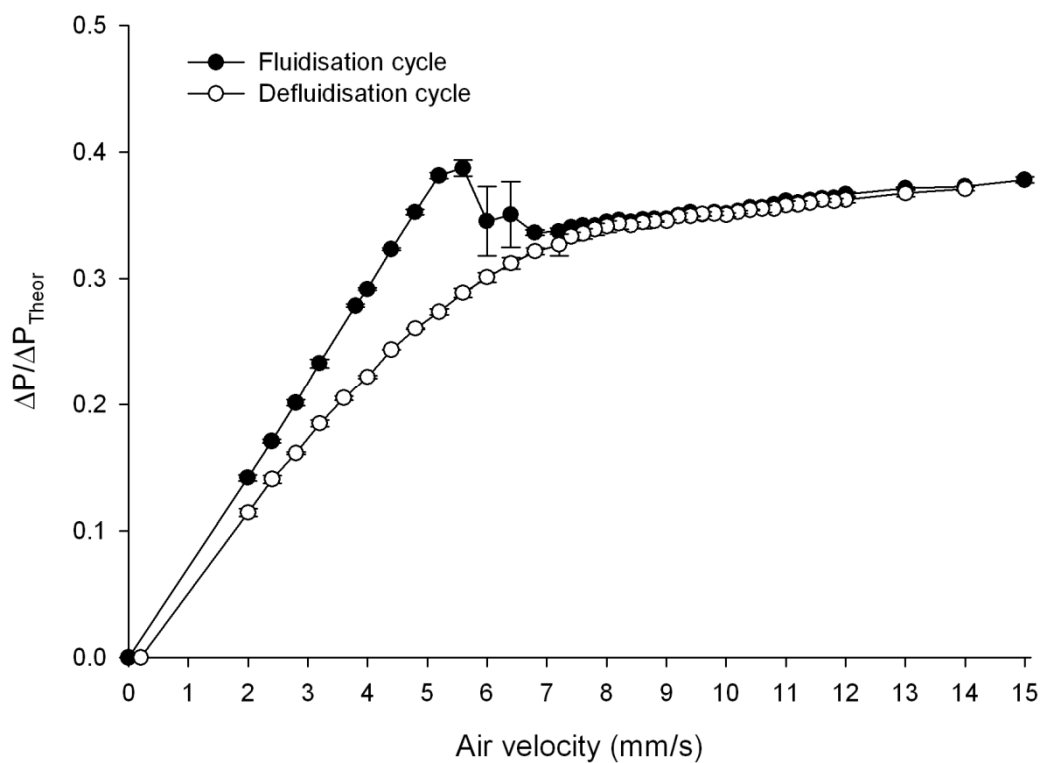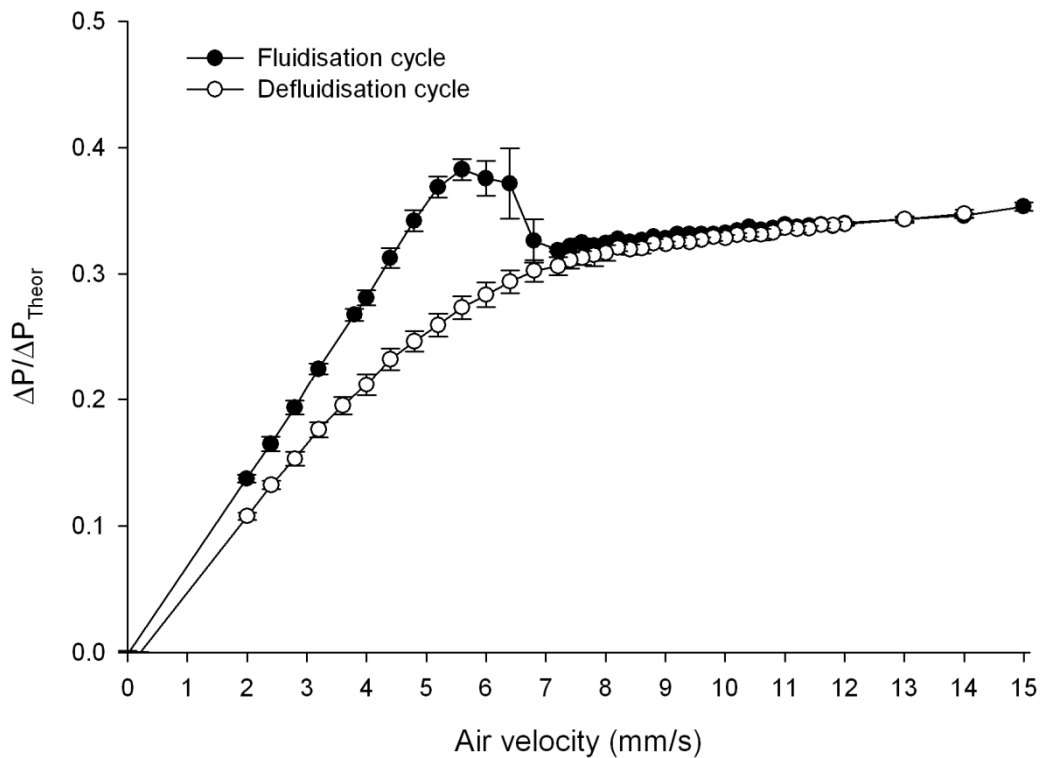**0.40% FP in SV010**

1.00% FP in SV010

2.00% FP in SV010

X